Investigations on Particles Dispersed Latent Heat Thermal Energy Storage System for Solar Water Heaters

THESIS

Submitted in partial fulfilment
of the requirements for the degree of
DOCTOR OF PHILOSOPHY

By

Jegadheeswaran S

Under the Supervision of

Dr. Sanjay D. Pohekar

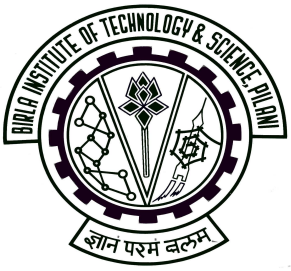

BIRLA INSTITUTE OF TECHNOLOGY AND SCIENCE
PILANI (RAJASTHAN)

2012

CERTIFICATE

BIRLA INSTITUTE OF TECHNOLOGY AND SCIENCE
PILANI (RAJASTHAN)

This is to certify that the thesis entitled **'Investigations on Particles Dispersed Latent Heat Thermal Energy Storage System for Solar Water Heaters '** and submitted by **Jegadheeswaran S** ID No **2007PHXF448P** for award of Ph.D. Degree of the institute, embodies original work done by him under my supervision.

Signature in full of the Supervisor: ----------

Name in capital block letters: **Dr. SANJAY D. POHEKAR**

Designation: **PROFESSOR, TOLANI MARITIME INSTITUTE, PUNE**

Date: April, 2012

Dedicated to

My father, (Late) A. Selvaraj,

My mother, S. Angayammal

and

All my teachers, in particular,

Prof. Michael N. Kumar,

who taught me

Computational Fluid Dynamics

ACKNOWLEDGEMENTS

I am indebted to my supervisor Dr. S.D. Pohekar, Professor, Tolani Maritime Institute, Pune, for constructive suggestions, continued support and encouragement without which, it would have not been possible to produce this thesis.

I am very much grateful to the management of Tolani Maritime Institute, Pune, for funding and providing all the necessary facilities to complete this research work. It is my privilege to thank Dr. B. K. Saxena, Principal, Tolani Maritime Institute, Pune, for his timely approval of all the projects and invaluable guidance. My special thanks to Capt. R. K. Razdan, Provost, Tolani Maritime Institute, Pune, for his encouraging support during the research period.

I would like to sincerely thank Dr. B.N. Jain, Vice Chancellor, Birla Institute of Technology and Science, Pilani, for giving me an opportunity to do research. I also thank Dr. L.K. Maheshwari, Professor Emirates and Advisor to Chancellor, BITS, Pilani and Dr. Ravi Prakash, Former Dean, R&C Division, BITS, Pilani and Vice Chancellor, Jaypee University of Information technology, Waknaghat, for their continued support. I take this opportunity to acknowledge the help received from Dr. Asis Das, Dean, R&C Division, BITS, Pilani, Members of Doctoral Advisory Committee, Members of Doctoral Research Committee and Nucleas members of R&C Division, BITS, Pilani.

My special thanks to Dr. T. Kousksou, University of Pau, France and his research group for giving me opportunities to have collaborative works with them. Dr. Kousksou's constructive suggestions helped me a great deal in refining this work. Throughout the period of research, Dr. N. Lakshmi Narasimhan, SSN College of Engineering, Chennai, had been instrumental by transferring his extensive knowledge in the field of phase change research. He deserves special thanks. I wish to extend my thanks to Dr. Vijaykumar Boratti, University of Mysore, for devoting his valuable time to read the manuscripts carefully and his inputs are gratefully acknowledged. I would also like acknowledge the inputs received from Dr. Pablo Dolado, University of Zaragoza, Spain.

I take this opportunity to thank Dr. Ashish Lele, Polymers and Advanced Materials Laboratory, National Chemical Laboratory, Pune and Dr. Neelima S. Iyer,

Physical Chemical Division, National Chemical Laboratory, Pune, who were kind enough to test the samples at NCL. My gratitude goes to, Dr. D.S. Bhatkhande, Head of the Department, Chemical Engineering, Vishwakarma Institute of Technology, Pune, for permitting me to avail the lab facilities at VIT. I am also grateful to Prof. S. R. Kulkarni, Department of Chemical Engineering, VIT, Pune, for his guidance and assistance while carrying out experiments.

My Sincere thanks to Dr. D.D. Mundhra, Examination Controller, TMI, Pune, for his keen interest in my success and creating a lively and supportive environment while I was working for the examination related matters so that my focus was not diverted from research. It is my pleasure to acknowledge the help received at different stages from all my colleagues particularly, Prof. I.K. Basu, Dr. S. Kanungo, Col. G. P. Krishnamurthy (retd), Prof. N. K. Joshi, Dr. N. D. Junnarkar, Prof. S. Dasgupta, Prof. N. K. Mishra, Prof. D. Dave, Mr. Md. Ayaz Khan and Mr. Praveen Vaidya of TMI, Pune and Mr. Ravi Reosekar, BITS- Pilani, Pune centre. I wish to acknowledge the support received from Mr. P.R. Deshmukh, Mr. M.S. Masani, Mr. P.R. Deshponde and Mr. A.L. Pawar during the experimental trials. I also appreciate the assistance provided by Mr. J. Wallace and Ms. Unnati N.Chaudhari, TMI, Pune, in developing the computer codes.

I would also place on records my thanks to the chief editors and anonymous reviewers of Renewable and Sustainable Energy Reviews, International Journal of Energy and Environment, Journal of Renewable and Sustainable Energy, CLEAN-Soil Air Water, Solar Energy Cells and Solar Materials and Energy Procedia, whose timely and scholarly reviews have helped in bringing best out of this research.

Special thanks must go to my wife M.Geethapriya for her continued support, patience and understanding throughout the research period. Without doubt she deserves a special mention as she had to handle family concerns on her own. Last, but not the least, I appreciate the understanding of my son J. Ajay and daughter J. Srinidhi as they had to miss their father for most of the time.

Jegadheeswaran S

ABSTRACT

The enormous potential of solar energy has made it very attractive for space heating/cooling, green house heating, cooking, hot water production, etc. Due to time gap between availability of solar energy and need, energy storage is emphasized to ensure continuous and efficient supply. Phase change material (PCM) based latent heat thermal storage (LHTS) systems offer a challenging option to be employed as an effective energy storage and retrieval device. Although LHTS systems offer high energy density and transfer energy under isothermal conditions, the poor thermal conductivity (usually 0.1-0.6 W/m.K) of PCMs drastically affects the thermal performance of the systems, which in turn limits their practical application. This necessitates the employment of performance enhancement techniques for LHTS system. The addition of high conductivity particles is proposed as one of the promising performance enhancement techniques for LHTS.

The purpose of the present study is to investigate the performance enhancement of a shell and tube storage unit applicable to solar water heaters due to the addition of two versions of high conductivity particles, i.e. nano size and micro size copper particles. The identified PCMs were paraffin wax, from organic group and hydrated salt, from inorganic group. The thermo-physical properties of nano particles composites were evaluated employing analytical relations and those of micro particles composites were experimentally obtained using *Temperature-History* technique. To explore the heat transfer characteristics of composite PCMs, numerical models were developed and the numerical study involves both charging and discharging modes. The solidification process of nano particles composites was simulated ignoring the natural convection in the liquid PCM, whereas the same during melting was included through effective thermal conductivity which was evaluated as a function of Rayleigh number (Ra). In case of micro particles composites, the numerical model also features a transport equation for particle flux. The enthalpy based two dimensional-transient equations were solved using FLUENT- a commercial computational fluid dynamics (CFD) code. In addition, exergy models were developed to demonstrate the effect of particle dispersion on exergy performance of LHTS systems. The numerical models were validated by comparing the numerical results with literature / own experimental results.

The thermal behavior and exergy performance in terms of exergy efficiency and total exergy stored/recovered of particles dispersed PCM units are compared with those of pure PCM unit. Although both the charging and discharging times could be reduced by the addition particles, the reduction is more significant during discharging process. The heat transfer performance of pure PCM system is consistently enhanced by particles right through the discharging process. On the other hand, the enhancement could be observed only during the earlier stages of charging process. The comparison of effects of micro and nano size particles reveals that micro particles are superior to nano particles in enhancing the heat transfer performance during discharging. At the same time micro size particles are found to be hampering the charging heat transfer performance of pure PCM to a greater extent than encountered with nano size particles. When it comes to exergy performance, both the nano and micro size particles help in increasing the exergy efficiency of pure PCM system during discharging. Also, the exergy recovered from composites are higher as compared to that of pure PCM. On both the accounts, again the micro particles are better than the nano particles. However, opposite trend is shown by micro particles during charging. In any case, it is found that hydrated salt composites exhibit better exergy efficiency than paraffin wax composites due to their enhanced thermal performance. However, the former cannot be stated as better choice because of its inability to store /recover more exergy.

Different Reynolds numbers (i.e. Re = 500-10000) are considered in the numerical trials to investigate the influence of mass flow rate of heat transfer fluid (HTF) on the performance of the system. The results reveal that the role of HTF mass flow rate in increasing the overall thermal performance of LHTS unit is insignificant. On the other hand, variation in HTF inlet temperature is seen influential. The LHTS systems produce better heat transfer performance when the difference between HTF inlet temperature and melting temperature of PCM is higher. However, the exergy performance is found to be superior when HTF inlet temperature condition is such that the temperature difference is lower.

TABLE OF CONTENTS

TABLE OF CONTENTS

TABLE OF CONTENTS

TABLE OF CONTENTS

TABLE OF CONTENTS

List of Figures

List of Figures

List of Figures

List of Figures

List of Figures

List of Figures

List of Tables

List of Tables

Nomenclature

a	Particle diameter, m
A	Coefficient in Equation (4.24)
b	Tube wall thickness, m
Bi	Biot number
c	Constant in Equation (3.6)
C	Mushy zone constant
c_p	Specific heat, J/kg.K
e	Particle volume fraction
Ex	Total exergy stored/recovered, J
$\dot{E}x$	Exergy rate, W
f_l	Liquid fraction
g	Gravitational acceleration, m/s^2
h	Sensible enthalpy, J/kg or Heat transfer coefficient, $W/m^2.K$
H	Latent heat enthalpy, J/kg
k	Thermal conductivity, W/m.K
k_{eff}	Effective thermal conductivity, W/m.K
K_c	Constant in Equation (4.16)
K_μ	Constant in Equation (4.17)
L	Length, m
$\dot{m}$	Mass flow rate of HTF, kg/s
M	Mass, kg
n	Constant in Equation (3.6)
N_s	Entropy generation number
P	Pressure, Pa

Q	Total energy recovered, J
$\dot{Q}$	Instantaneous heat transfer rate, W
r	Radial co-ordinate, m
R	Gas constant, J/kg.K
Ra	Rayleigh number
Re	Reynolds number
R_i	Tube radius, m
R_o	Shell radius, m
S	Entropy, J/K or Source term
Ste	Stefan number
t	Time, s
T	Temperature, ^{o}C or K
T_{atm}	Atmospheric temperature, ^{o}C or K
T_m	Melting temperature, ^{o}C or K
u	velocity component in x-direction, m/s
V	Velocity vector, m/s
x	Axial co-ordinate, m

Greek letters

α	Thermal diffusivity, m^2/s
β	Coefficient of volume expansion, 1/K
ε	Computational constant in Equation (4.25)
ρ	Density, kg/m^3
λ	Latent heat of fusion, J/kg
μ	Dynamic viscosity, kg/m.s
$\dot{\gamma}$	Strain rate, 1/s

η	Energy efficiency
ψ	Exergy efficiency
Γ	Diffusive coefficient
$\forall$	Volume, m^3

Subscripts

char	Charging or melting process
dis	Discharging or solidification process
f, final	Final state
HTF	Heat transfer fluid
in	Inlet
init	Initial state
l	Liquid PCM
m	PCM-particle mixture
out	Outlet
overall	Cycle
p	Particle
PCM	Phase change material
ref	reference state
s	Solid PCM
w	Wall

Chapter 1: Introduction

The increasing gap between the global demand and supply of energy is becoming a major threat as well as a challenge for the engineering community to fulfill the needs of the energy hungry society. The utilization of conventional energy sources is becoming a greater concern due to the rapid depletion of sources and the environmental issues arising from increasing CO_2 emissions. This prompted us to look for renewable energy sources such as solar, wind, geothermal, tidal etc., These renewable energy sources are given greater importance owing to abundant availability and sustainability. The enormous potential of solar energy has made it very attractive for space heating and cooling, green house heating, cooking, hot water production etc., However, the application of solar thermal energy may not be efficient and economical, if not properly managed. The major problem in managing energy from the above-mentioned source is the time gap between availability and need. Similar kind of problem arises while recovering energy from waste and tapping excess energy from various hot exit streams. The storage of thermal energy has been emphasized as an attractive solution for such kind of problems on energy management and conservation, in both industrial and domestic sectors.

1.1 Thermal energy storage

Energy storage is used to bridge the time lag between the availability of energy and the requirement for energy. Although solar thermal energy is abundant, it is available only during the day time and it is also unpredictable as it is intermittent in nature. There is, thus, a marked need for the storage of energy or another product of the solar process, if the solar energy is to meet energy needs. This bridging of time lag is evident as the cases like solar energy heat pumps, combined heat and electricity producing systems use low tariff night electricity.

The storage of thermal energy is also required in heat recovery systems, where the availability of waste heat and utilization of the same may not match each other. Here the energy storage device is used to extract the energy, which would have lost along with the exhaust. Similarly, regenerative energy sources can be utilized

effectively only in combination with heat storage units. Heat storage units can reduce the number of fuel burner cycles, thereby leading to a substantial reduction in pollutant emissions (50% of the emissions of CO and hydrocarbon CxHy are produced during burner's starting phases) and fuel consumption. The operation of heat generation units can thus be regulated effectively by the integration of a heat storage unit into the system. Solid fuel boilers in combination with heat storage units can have an extended life time i.e. the connected electrical energy is lower, allowing the use of a smaller heat pump, thus saving heat and investment cost. Furthermore, losses during the heat pump-startup and shutdown phases are minimized.

Hence, it is clear that thermal energy storage enhances the overall efficiency of large energy producing units through load leveling, decreases energy demand through the use of waste heat recovery and allows alternative sources of energy to be utilized very effectively. Energy storage devices can be used to reduce the consumption of energy in industrial and commercial establishments through the usage of waste heat recovery systems and renewable energy storage systems. In short, thermal storage can be regarded as a thermal battery (Demirbas, 2006).

In general, the thermal energy from the source can be transferred to a storage medium in where it is transformed into an internal energy. Thus, the energy is stored in the form of thermo-chemical heat, sensible heat, latent heat, or combination of sensible and latent heat. Accordingly, thermal energy storage systems are broadly classified into the following categories

- Thermo- chemical storage system
- Sensible thermal energy storage system
- Phase change / Latent heat thermal energy storage system

1.1.1 Thermo-chemical storage systems

Thermal energy can be stored as chemical bond energy. Energy can be used to drive an energy-consuming (endothermic) reaction and energy can be withdrawn from the same by reversing the energy releasing (exothermic) reaction. In general, completely reversible chemical reactions and attainment of equilibrium temperature form the basis of chemical storage systems. Such reactions may be either homogeneous gas locations or heterogeneous solid-gas or liquid-gas reactions.

1.1.2 Sensible heat thermal energy storage systems

In this class, the thermal energy is stored in the form of sensible heat of fluids or solids. During the energy storage/recovery process, the medium encounters a change in internal energy without a change of phase. Thus, energy is stored by increasing the temperature of medium and it can be retrieved by decreasing the temperature. Thermal energy content depends upon the heat capacity of the medium and among the commonly used materials such as water, iron, aluminium, concrete, rock, brick etc., water has the highest value. However, other materials posses very low values.

1.1.3 Latent heat thermal energy storage systems

As the name implies, in latent heat thermal storage (LHTS) systems, energy is stored in the form of latent heat, which may also be accompanied by sensible heat. The absorbed/released heat can be in the form of latent heat. The phase transformations are generally solid-liquid, liquid-gas, solid-gas and solid-solid. Among all, liquid-gas and solid-gas phase transformations have high latent heat fusion. However, these materials undergo large change in volume during the phase transition, which makes the design of container, complex and impractical. Hence, the potential application of storage systems involving these materials is ruled out. Although the solid-solid phase change is free from the problems associated with the container design, the economical viability of this class suffers from smaller latent heat value. The solid-liquid phase transformation is proved to be better option than others as the volume change during phase change is not more than 10% despite having a lower latent heat value than liquid-gas or solid-gas cases.

The material which undergoes phase change during energy storage or retrieval is called phase change material (PCM). The PCM stores heat by undergoing a change of phase from solid to the liquid phase/state, and releases this heat by reversing back to the solid state (freezing), except in the case of cold thermal storage applications. In cold energy storage applications, energy is stored during freezing of the PCM while retrieved during the melting process. When a solid is heated, its temperature continues to rise until its melting temperature is reached. As more heat is added, its temperature remains constant at melting temperature but it begins to undergo a phase transition to

the liquid state. No increase in temperature will occur until the melting process is completed. The heat per unit mass absorbed by and stored in the medium during the phase transition is termed as latent heat.

Among the three types of thermal energy storage systems, LHTS system is more effective and attractive. This is mainly due to its ability to store higher energy per unit volume, which results in large space savings. Hence, the use of latent heat storage is ideally suited where space is at a premium. The comparison between sensible and latent heat storage mediums for a stored energy of 1,000 MJ in terms of required mass and volume can be seen from Table 1.1.

Table 1.1 Comparison of various thermal storage for a stored energy of 1,000 MJ

Material	Type of Heat Storage	Mass (kg)	Volume (m^3)
Rock (Solid)	Sensible	67,000	30
Water (liquid)	Sensible	16,000	16
PCM (organic)	Latent	5300	6.6
PCM (Inorganic)	Latent	4350	2.7

(Source: Hasnain, 1998)

In spite of several relative advantages, the rate of phase change process (melting / solidification of PCM) has not been up to the expected level and thus, the large scale utilization of LHTS units, remains unsuccessful. Therefore, to tackle the above-mentioned drawbacks, it becomes necessary to improve the thermal performance of the LHTS units employing PCMs. The various techniques adopted for enhancing the thermal performance of the LHTS units are enumerated below:

- Using extended surfaces (Zhang and Faghri, 1996, Velraj *et al*, 1997, Liu *et al*, 2005, Devahastin and Pitakusuriyarat, 2006, Reddy, 2007 and Gharebaghi and Sezai , 2008)
- Employing multiple PCM's method (Wang *et al*, 2001, Cui *et al*, 2003, Fang, 2007, Michels and Pitz-Paal, 2007, Seeniraj and Narasimhan, 2008 and Adine and El-Qarnia, 2009)

- Thermal conductivity enhancement (Seeniraj, 2002, Fukai *et al*, 2003 and Kim and Drzal, 2009)
- Micro-encapsulation of PCM (Schossig *et al*, 2005, Smith *et al*, 2006, Hawlader *et al*, 2006, Ozonur *et al*, 2006, Cabeza *et al*, 2007 and Alkan *et al*, 2009)

A comprehensive review on the implementation of heat transfer enhancement techniques in different configurations of LHTS systems has been given in Chapter 2.

1.1.3.1 Phase change materials and applications

The employment of any PCM for energy storage may be useful, if the following thermophysical, chemical and kinectic properties are accomplished by the PCM (Sharma *et al*, 2009).

- High latent heat of fusion, high specific heat and high thermal conductivity
- Congruent melting
- Small volume change
- The phase change must be reversible over a very large number of cycles without serious degradation
- Must be harmless (non-toxic, non inflammable, non combustible and non corrosive)
- No supercooling
- High rate of crystal growth

It is quite difficult to find a material possessing all the above characteristic qualities. So a trade-off approach is necessary in the selection of candidate heat storage material.

The PCMs are generally divided into three groups: organic, inorganic and eutectics. Organic compounds include paraffins (alkanes) and non-paraffins (fatty acids, esters, alcohols and glycols). Inorganic group comprises of salt hydrates and metallic materials. Eutectics are mixtures of two or more components and formed to lower the temperature of phase change to below the normal melting points of any one of the components forming the mixture.

Most widely studied PCMs are paraffin waxes, hydrated salts and fatty acids. Paraffin waxes are chemically stable and available commercially. However, the latent

heat of fusion of paraffins (≈ 200 kJ/kg) is only half of that of hydrated salts. Hydrated salts are much cheaper than paraffins, but suffer from supercooling effect during melting. Moreover, they pose corrosion problems with metals. Fatty acids posses similar characteristics of paraffins, but they are two to three times expensive than paraffins. For comprehensive details of variety of PCMs and their properties, readers are referred to the recent review articles by Zalba *et al.* (2003), Farid *et al.* (2004), Sharma and Sagara (2005), Kenisarin and Mahkamoy (2007) and Kenisarin (2010).

Table 1.2 Suitable phase change temperature ranges for various applications

Phase change temperature (^{o}C)	Applications
-20 to -10	Process and storeroom cooling, food freezing
2 to 15	Cold storage in air conditioning systems
20 to 60	Solar energy storage (water heater, green house and space heating, solar drier etc.,), electronic devices cooling, building applications
80 to 120	Heat storage in vapor absorption cooling systems, waster heat recovery applications
>150	High temperature storage in solar thermal power plants

Several application areas have been identified for the potential employment of PCMs. They are,

- Solar thermal power plant (Laing *et al*, 2010, Bayon *et al*, 2010 and Gil *et al*, 2010)
- Thermal management of photovoltaics (Hasan, 2010, Huang *et al*, 2011 and Malvi *et al*, 2011)
- Thermal management of portable electronic devices (Jaworski, 2011, Wang and Yang, 2011 and Yang and Wang, 2012)
- Thermal comfort in buildings (Ceron *et al*, 2011, Kuznik *et al*, 2011 and Chan, 2011)

- Exhaust waste heat recovery and preheating in IC engines (Vasiliev *et al*, 2000, Gumus, 2009 and Pandiyarajan *et al*, 2011)
- Cold thermal energy storage in refrigerators/air conditioners (Azzouz *et al*, 2009, Parameshwaran *et al*, 2010 and Cheng *et al*, 2011)
- Thermal comfort regulation of textile clothing (Mondal, 2008, Salaun *et al*, 2010 and Sanchez *et al*, 2010)

The above list is just indicative, not exhaustive. For any application, the selection of appropriate PCM should be mainly based on the phase transition temperature. A large number of PCMs with wide range of melting temperature has been investigated for different applications. He (2004) and Agyenim (2010) have listed the ranges of phase transition temperatures for various applications and summary is presented in Table 1.2.

1.1.3.2 Performance assessment of LHTS systems

The employment of LHTS units for energy storage/retrieval can be realized only if the performance of the unit is known. The performance assessment of any LHTS system requires thorough knowledge about the thermal behavior of the PCM that is employed. Mathematical modeling of thermal and fluid flow systems continues to be attractive as it allows carrying out investigations on large scale in less time and requires low expenditure.

Phase change problems are examples of what are closely referred to as moving boundary problems. The existence of a moving boundary generally means that the problem does not admit a simple closed form analytical solution and accordingly much research has focused on approximate solution techniques. In general, phase change problems involve a transient, non-linear phenomenon with a moving liquid-solid interface whose position is unknown a priori and also flow problems associated with heat transfer fluid (HTF). In addition, the two phases of PCM may have different properties and configuration of the LHTS unit may differ with the applications. Substantial number of numerical based studies on LHTS units employing enhancement techniques and on their performance measurement is available in literature. Verma *et al.* (2008) and Dutil *et al.* (2011) have provided **e**xcellent reviews on issues related to numerical modeling of LHTS systems. The numerical

formulations widely implemented so far are enthalpy method and effective heat capacity method.

In the enthalpy method, the enthalpy which is a function of temperature is considered as a dependent variable along with temperature. Thus, the enthalpy based conduction equation is valid for both solid and liquid phases. Besides, it is valid for solid-liquid interface. Therefore, there is no need to track the interface which makes this formulation attractive (Ozisik, 1994). In the effective heat capacity method, the heat capacity of the PCM during phase change process (effective heat capacity) is introduced. The effective heat capacity is directly proportional to the stored/released energy during the phase change and the specific heat. Therefore, with effective heat capacity it is also possible to describe the non-isothermal phase change in the PCM. For the details of these two formulations, readers are referred to Date (1992) for enthalpy method and Lamberg (2003) for effective heat capacity method. Besides these two formulations, Yingqiu *et al.* (1999) have proposed another method called alternate thermal resistance method.

Once the thermal behavior is known, the performance of LHTS units can be evaluated through two approaches. They are:

1. By applying energy conservation principle (based on first law of thermodynamics)
2. By applying exergy principle (based on second law of thermodynamics)

The effective handling of performance evaluation of LHTS unit would result in optimized system for the application of interest. However, the analysis based on first law of thermodynamics is employed to identify the ways to improve the quantity of heat stored/recovered. At this point, it is important to mention the popular quote by Bejan (1978) which is

> *"the primary purpose of a thermal energy storage system is not, as the name implies, to store the energy, rather, to store useful work".*

From this perspective, it can be stated that first law based analysis i.e. energy analysis becomes inadequate as information on usefulness of energy cannot be obtained. The quality or usefulness of energy can be appreciated only through exergy analysis.

1.2 Objectives

From the view of above mentioned points, the objectives of the present work are drawn as follows:

i. To investigate the effect of addition of high conductivity micro particles/nano-particles on the heat transfer characteristics of pure PCM;

ii. To investigate the performance enhancement of shell and tube LHTS module due to the addition of high conductivity materials under different design and operating conditions using numerical models;

iii. To gauge the relative role of micro size conductivity particles in comparison with nano size particles in enhancing the thermal and exergy performance of LHTS systems;

iv. To develop numerical models describing the melting and solidification processes of PCM-micro particles mixture/ PCM-nano particles mixture;

v. To develop second law based (exergy) model to assess the performance of shell and tube LHTS module applicable to solar water heaters;

vi. To evaluate the thermophysical properties of PCM-high conductivity nano- particles mixture analytically;

vii. To prepare mixtures of organic PCM and high conductivity micro metal particles / inorganic PCM and micro high conductivity metal particles;

viii. To evaluate the thermophysical properties of PCM-high conductivity micro particles mixture experimentally;

1.3 Scope and limitations

The present work seeks to investigate majorly the performance enhancement of LHTS units applicable to solar water heaters due to dispersion of high conductivity particles. Numerical models are developed to simulate the melting and solidification processes of nano/micro particles added PCMs and are validated. Hence, the presented computational techniques are expected to provide guidelines for modeling of thermal behavior of particles-PCM composites in any application. Techniques concerning the evaluation of thermophysical properties of PCMs are comprehensively discussed and this facilitates the choice of appropriate technique for any new PCM.

The particular focus of this work is exergy based approach for performance assessment of LHTS units in order to explore the impact of particles addition on exergy performance. Suitable exergy models for melting and solidification processes are presented for the same. The outcomes of this investigation provide detailed information of both positive and adverse effects of nano/micro particles on the heat transfer and exergy performances of conventional PCMs. This presentation provides the opportunity for a detailed examination of all aspects of particles dispersion in PCMs.

This work is also intended to examine the influences of operating conditions like temperature and mass flow rate of HTF on the performance of particle dispersed PCM. However, the effect of geometrical parameters of the unit is not included. Although entropy generation based second law analysis is discussed in Chapter 2, the present work involves only evaluation of exergy parameters rather than entropy generation number.

The effective thermal conductivity model employed is found to be good enough to simulate the natural convection in the liquid PCM during melting. Since the said model only mimics the natural convection effect, the real pattern of liquid flow cannot be visualized. This, of course, is beyond the scope of this work.

1.4 Organization of the thesis

The presentation of the thesis is structured in the following sequence. Chapter 1 discusses the basic aspects of LHTS systems, in order to give the background of the topic.

Chapter 2 reviews the issues related to performance enhancement techniques for LHTS systems and exergy analysis. The review is presented by revisiting the related reported works. Subsequently, the gap in the existing research is identified and reported.

Chapter 3 briefs the analytical method of evaluating the thermophysical properties of nano metal particles based PCM composites and computational techniques adopted for analyzing the exergy performance of those composites. The validity and limitations of the theoretical methods are also highlighted.

Chapter 4 begins with experimental evaluation of thermophysical properties of micro particles based PCM composites. The subsequent sections focus on numerical investigation of exergy performance of micro particles-PCM composites. This chapter also includes the details of experimental test rig built in house for the validity of numerical model.

Chapter 5 is devoted for presenting the results of the present investigations. In view of examining the validity of numerical results, stringent comparisons between numerical results and experimental results obtained in the present work / reported in the literature are presented in the beginning of the chapter. The results are presented in the form of heat transfer characteristics and exergy parameters. The comparison of heat transfer as well as exergy performances of two selected PCMs (an organic and an inorganic) is also reported. The logical reasons for the obtained results are comprehensively discussed at appropriate places.

2.1 Heat transfer enhancement

Although conventional PCMs offer high energy density, slower rates of melting and solidification limit the potential applications of LHTS systems in practical systems. This is due to the fact that all the conventional PCMs –both organic and inorganic possess very low thermal conductivity ranging from 0.1-0.6 W/m.K. Table 2.1 lists thermal conductivity values along with latent heat values for few PCMs, which are identified as widely investigated by researchers so far.

Table 2.1 Thermal conductivity and latent heat of selected PCMs

Name of the PCM	Thermal conductivity (W/m.K)	Latent Heat of fusion (kJ/kg)
Organics		
n-Octadecane	0.35 (solid) and 0.149 (liquid)	245
n-Docosane	0.22	194.6
Paraffin wax	0.514 (solid) and 0.224 (liquid)	251
Caprylic acid	0.149	149
Capric acid	0.153	153
Inorganics		
KNO_3	0.5	266
$NaNO_3$	0.5	172
$MgCl_2.6H_2O$	0.694 (solid) and 0.57 (liquid)	168.6
$CaCl_2.6H_2O$	1.088 (solid) and 0.54 (liquid)	190.8
Inorganic Eutectics		
58.7%$Mg(NO_3).6H_2O$-41.3%$MgCl_2.6H_2O$	0.678 (solid) and 0.51 (liquid)	132
66.6%Urea-33.4%NH_4Br	0.682 (solid) and 0.331 (liquid)	161

(Source: Zalba *et al.* (2003), Farid *et al.* (2004), Sharma and Sagara (2005) and Pincemin *et al.* (2008a))

The thermal conductivity of conventional PCMs can be enhanced by employing high conductivity materials. However, it is important to understand that whether the presence of high conductivity materials in the PCM does really give the appreciable heat transfer enhancement or not. Because the governing heat transfer mechanisms may be different for different phase change processes (melting and solidification). The

proceeding discussions deal with heat transfer mechanisms and role of high conductivity materials in determining the modes of heat transfer during melting and solidification separately.

2.1.1. Melting

During melting, heat is transferred to the PCM first by conduction and later by natural convection. This is because the solid region moves away from the heat transfer surface and the thickness of the liquid region increases near the heat transfer surface. Since thermal conductivity of liquid PCM is less than that of solid PCM, the heat transfer by conduction almost becomes negligible as the melting process continues. The further melting is mostly by natural convection due to the density gradient that exists within the liquid PCM.

Lamberg and Siren (2003) investigated melting in a semi-infinite PCM storage, with an internal fin. The analytical model consists of the well-known Newmann solution, which assumes that the heat is transferred only by conduction and natural convection can be negligible. It is found that though Newmann solution is exact solution, it underestimates the location of the melt front. Lamberg *et al.* (2004) conducted numerical study on melting of PCM in a rectangular enclosure with and without the natural convection effect and the results were compared with experimental results. It was observed from the results that when the natural convection effect was ignored, the PCM took double the time of actually it takes in reality to reach the maximum temperature.

Stritih (2004) traced the interface location during melting of PCM in a rectangular storage through experimental work. Only at the beginning of melting process, the conduction based analytical results showed good agreement with experimental results. Once melting began, the experimental interface location was much ahead of that one obtained from analytical calculation.

Zhang *et al.* (1993) experimentally studied the melting of n-octadecane, which was discretely heated at a constant rate from one side of an enclosure. During the melting process, the temperature in the upper region of the liquid was found to be higher than that in the lower region. Moreover, the discrete heat sources had nearly the same temperatures at the early stage of the process and as the melting process

progressed, the surface temperatures became different, increasing from top to bottom. This indicates that the early stage of heat transfer is conduction controlled and the further heat transfer was convection dominated. Natural convection dominated melting process in rectangular cavity with an isothermal wall is also reported by Gong *et al.* (1999). Jellouli *et al.* (2007) have shown the convection dominated melting in rectangular enclosure even heated from below.

Like in rectangular enclosure, natural convection has also been found as dominant heat transfer mechanism in cylindrical and spherical enclosures. Ng *et al.* (1998) investigated the melting of PCM stored in a horizontal cylindrical annulus heated isothermally from inside. The natural convection was modeled by Boussinesq approximation. The results showed recirculation cells which are representations of natural convection flow in the liquid PCM. Regin *et al.* (2006) analyzed the melting behavior of paraffin wax encapsulated in a cylindrical capsule surrounded by hot water. The experimental results showed the influence of natural convection on the melting process as the process occurred axisymmetrically, i.e. melting in top region was much faster than that in bottom region. Moreover, better agreement between numerical results and experimental results could be achieved only after including the natural convection in the numerical modeling.

Jones *et al.* (2006) conducted experimental and numerical study on melting of PCM in cylinder heated from side vertical wall. Digital photographs, which were taken during the melting process, revealed that only in earlier stages of melting, the melt layer thickness was uniform along the vertical direction (conduction dominated). As the time elapsed, the melt layer thickness began to vary along the vertical direction. This is the indication of convection dominated melting. The shapes of the melt front at different times are similar to that of observed in rectangular enclosures. Akgun *et al.* (2007) observed similar kind of heat transfer during the experimental work on melting of paraffin in a tube in shell configuration, which was oriented vertically. When the PCM was heated from inner wall, the molten PCM extended radially outward and the molten region established a conical shape. Very recently, Shmuli et al. (2010) have shown that the shape of the solid PCM in vertical cylinder changes to conical and shrinks from top to bottom during melting due to natural convection. Convection controlled melting is also simulated in two interesting

configurations by Khillarkar *et al.* (2000). Square external tube with a circular inner tube and circular external tube with a square inner tube were the configurations taken for the investigation.

Though spherical system provides largest volume per unit surface area, only limited study could be found their application in LHTS systems. However, a detailed experimental study by Bahrami (1990) provides the details of phase change process in spheres. Although the solid-liquid interface was flat in the beginning of melting, in very short period it assumed a dome-like shape and remained unchanged till the end of melting. This is an indication of more melting at the upper portion of the spherical container. More at the upper portion is due to the fact that the solid sinks to the bottom as the solid PCM is heavier than the liquid PCM. Hence, solid PCM is in contact with the lower wall of the sphere through out the melting process. This is termed as unconstrained melting by Tan (2008). It is also reported that the melting at the top portion was still mainly due to natural convection as the natural convection cells were observed during the entire melting process. The experimental study by Tan (2008) was also extended to constrained melting in which the solid PCM was held to prevent it from sinking down to the bottom. The asymmetric melting was more pronounced in constrained melting. The digital images revealed that the melting front took oval shaped pattern during the melting due to the existence of natural convection cells at the top and bottom halves of the sphere. However, faster melting was observed at the top portion as stronger natural convection prevailed at top. Similarly, the melting process in spheres was found to be asymmetric by Ettouney *et al.* (2005). Due to temperature gradient, hotter melt at the base of the sphere could rise upward and loses part of heat to the cooler melt and solid PCM. As a result, natural convection was initiated and started diminishing the role of conduction.

From these studies, it is clear that during the melting process, the heat transfer is dominated by natural convection. The domination of natural convection during melting of PCM in various geometries of LHTS has been illustrated in Figure 2.1. As it can be seen, due to natural convection more melting takes place in the top portion of all types of geometries. However, when top wall of the rectangular system is used as heated wall, then melting would be dominated by conduction for longer period of time. This has been revealed by Lacroix and Benmadda (1998) as the isotherms

obtained were parallel to the heated top wall. The temperature gradient was found in the negative y-direction and thus condition became stable. Even the existence of buoyancy driven flows in the molten PCM could be noticed, they were found to be relatively weak. Because of the absence of natural convection, in the top wall heating system, the melting process took more time (approximately double) as compared to bottom wall heating. Similarly only conduction dominated melting process was observed by Ettouney *et al.* (2004), when the HTF was allowed to flow downward in a vertical shell and tube configuration. Hence, the role of natural convection in the melting process can be ruled out in a rectangular module with top wall heating. However, if the system with top wall heating is coupled with environment i.e. the bottom wall is not at adiabatic condition, then natural circulation in the liquid phase could be expected (Pinelli and Piva, 2003). The melting of PCM in a vertical cylinder (since it was a two dimensional formulation, the resulting system is nothing but rectangular cavity) from the top was investigated by Pinelli *et al.* (2000). Although the results of conduction based numerical study could show good agreement with experimental results, considerable difference was observed at advanced stages of melting. In the extended study on the same configuration by Pinelli and Piva (2003), natural convection was accounted for. The numerical results showed significant quantitative improvement in the agreement with experimental data. This indicates that natural convection exists even in top wall heating system, as the system is coupled with environment. Therefore, if high conductivity materials are added into PCM, then the presence of those should not necessarily be for improving the conduction rate, but more importantly for improving the natural convection process.

2.1.2 Solidification

Contrary to melting process, solidification is dominated by conduction. During solidification natural convection exists only in the beginning and as the time goes the effect of natural convection becomes almost zero as compared to the effect of conduction (Lamberg, 2006).

Stritih (2004) compared the analytical results [conduction based] of solidification process in a rectangular storage unit with experimental results and obtained a good agreement between two. The natural convection was found to be 10

times lower than that in case of melting process. Ettouney *et al.* (2005) studied the solidification in a shell and tube heat exchanger and found the solidification isotherms were almost parallel to the heat transfer surface as the solidified layers took the same shape of the heat transfer surface. Hence, natural convection effects were found to be negligible whether the direction flow of HTF was upward or downward. Ettouney *et al.* (2004) found higher heat transfer coefficient during melting than that of during solidification, for same HTF temperature and HTF velocity in a fixed size of spherical storage. It indicates that melting was governed by natural convection where as it is not so in case of solidification.

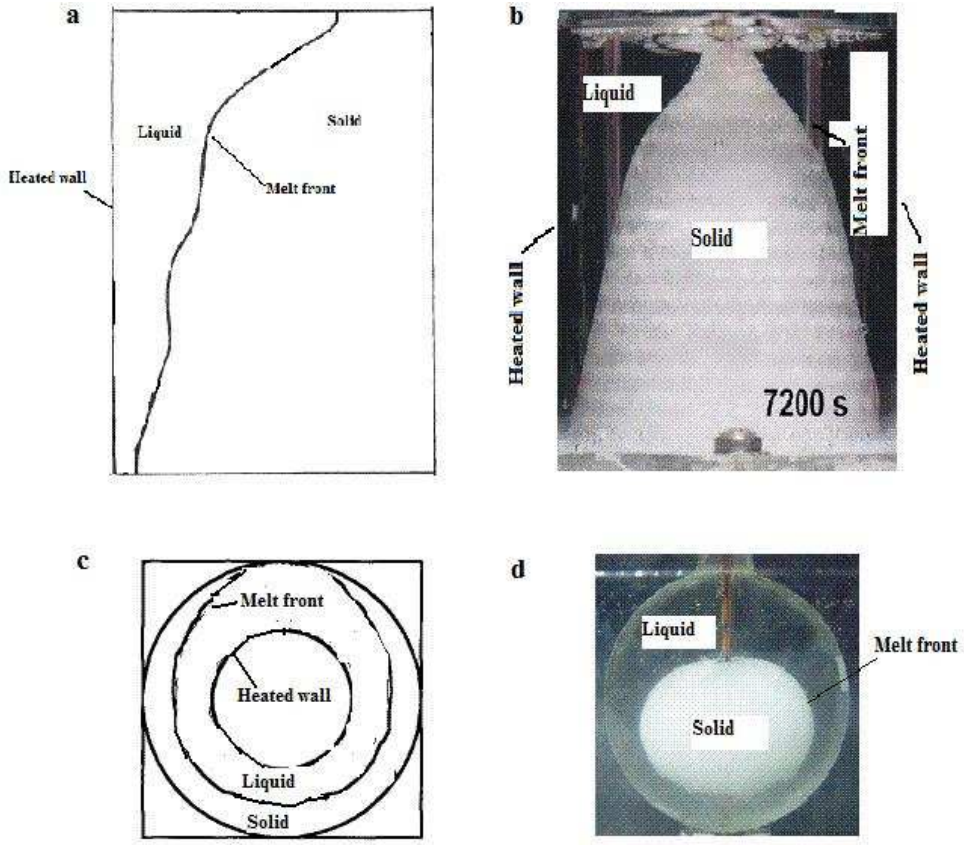

Figure 2.1 Natural convection dominated melting process: (a) rectangular system (Zhang *et al,* 1993); (b) cylindrical system (Jones *et al,* 2006); (c) cylindrical annulus (Ng *et al,* 1998); (d) spherical system (Tan, 2008)

These studies prove that in all configurations of LHTS, natural convection exists in the liquid PCM only at earlier stages of solidification and diminishes rapidly as the solidification progresses, which means the further process becomes conduction dominated. Therefore, if high conductivity particles are to be employed to enhance the

solidification rate, then the sole purpose is to improve upon the conduction heat transfer.

2.1.3. Thermal conductivity enhancement

The use of high conductivity materials to enhance the thermal conductivity of conventional PCMs has been dealt with in different ways by researchers, which can be summarized as follows:

- Impregnation of high conductivity porous material with the PCM
- Dispersion of high conductivity particles in the PCM
- Placing of metal structures in the PCM
- Use of high conductivity, low density materials

2.1.3.1 Impregnation of porous materials

Porous structure may be either metal matrices made of aluminum, copper etc., or naturally available porous material such as graphite. As far as metal matrices are concerned, recently Fiedler *et al.* (2008) have found that copper matrices give approximately 80% increase in effective thermal conductivity as compared to that of aluminum matrices. Mesalhy *et al.* (2005) have reported that the performance enhancement is dependent on both porosity and thermal conductivity of the matrix. All though for all porosity values higher melting rates were observed, decrease in porosity resulted in decrease in enhancement. Since low porosity values lead to higher effective thermal conductivity, theoretically there should be increase in performance enhancement. However, low porosity matrix dampens the motion of liquid PCM and thus natural convection within the liquid PCM. The results of this numerical study have proved this point as conductionlike temperature profiles and streamlines were observed with lower porosity values. Krishnan *et al.* (2005) and Krishnan *et al.* (2007) obtained similar results from the numerical study on melting process in a rectangular enclosure filled with metal foam impregnated with PCM. In case of composite PCM, due to the restricted convective flow, the melt volume fraction at steady state was lower than that of pure PCM case despite a substantial decrease in response time of the system. Hence, it can be concluded that the porous matrix should possess not only high thermal conductivity but also high porosity for highest possible performance

enhancement. However, Shiina and Inagaki (2008) have shown that the porosity should be optimum which is higher for low heat transfer coefficient and vice versa.

Graphite is known for its high thermal conductivity, high electrical conductivity and high absorbability. The thermal conductivity of graphite varies from 24 W/mK to 470 W/mK (Mehling *et al*, 2000). According to Haillot *et al.* (2008), the thermal conductivity of PCM (0.2-1 W/mK) can be intensified by a factor of 5-100 depending upon the density of graphite added into the PCM. Cabeza *et al.* (2006) have found that using PCM-graphite compound is the best option in applications like thermally stratified storage tank. The cheapest form of graphite is natural graphite flakes, which are composed of dense staked graphite layers. However, it is found that expanded graphite (EG) can be a better choice as it is of better absorbability due to high porosity. Generally EG can be prepared from natural graphite through chemical oxidation in the presence of concentrated sulphuric/nitric acid/mixture of sulphuric and nitric acids and followed by drying up process in oven and finally by rapid heating in a furnace. Sari and Karaipekli (2007) investigated thermal conductivity enhancement and storage enhancement due to the addition of EG in a paraffin based LHTS system. The results showed that the thermal conductivity can be increased by increasing the mass fraction of EG. Hence, a significant reduction in melting time (about 32%) was observed when from-stable composite PCM (no liquid PCM leakage) was used in the LHTS system. However, the increase in mass fraction resulted in decrease in latent heat value and thus, reduced storage capacity. The optimum mass fraction was taken as 10% as this form-stable composite PCM possessed about four times higher thermal conductivity than that of pure paraffin with small decrease in latent heat value. Zhong *et al.* (2010) have also reported that composite PCM formed with graphite foam possesses reduced latent heat as compared to pure PCM and hence, the authors have proposed a composite with large pore size (filled with more paraffin) and thicker ligament of graphite foam. On contrary to other's results, Yin *et al.* (2008) have reported that the thermal conductivity of EG/paraffin composite steadily increased only up to the EG mass fraction value of 6.25. Beyond this value thermal conductivity started decreasing. The presence of some lacunas and gases in the loose structure of composite PCM with high EG mass fraction has been cited as reason the reduction in thermal conductivity.

This indicates that composite should be prepared with appropriate mass fraction of graphite in such way the lacunas and gases are not present in the pores.

Recently, Kim and Drzal (2009) used exfoliated graphite nanoplatelets (XGnP) to form graphite/paraffin composite. The XGnP, which are of less than 10 nm thick, and 15 μm average diameter can be obtained by pulverizing the EG using an ultrasonic processor. The results showed strong relation between mass percentage of XGnP and thermal conductivity. The continuous increase in thermal conductivity was observed up to the highest studied mass fraction of 7%. Besides, with all XGnP mass fractions, the latent heat values very closely matched with those of pure paraffin. In case of XGnP composite, since the high surface area of XGnP presented good dispersion in the PCM, there was no decrease in the latent heat. Hence, it can be stated that XGnP is more effective than EG as it enhances thermal conductivity with out reducing the storage capacity of pure PCM.

The use of graphite to improve the thermal conductivity of PCM is not only limited to low melting point PCMs such as paraffin, but also proposed for high melting point PCMs such as salts or eutectic mixtures (Pincemin *et al,* 2008a). Generally composite PCMs are made by mixing the graphites with molten PCM. Pincemin *et al*. (2008b) prepared eutectic salt/graphite composite by cold compression method. In cold compression method, after mixing the solid PCM with graphite powder physically, the mixture was compressed at room temperature. Due to the compression most of the porosity was removed resulted in a monolithic composite. This kind of composite can easily be shaped as per the geometry of the storage system. The composite obtained from cold compression method possessed anisotropic characteristics because of rearrangement of graphite layer orthogonally to the compression axis. The thermal conductivity measurement showed that radial thermal conductivity was much higher than that of axial one. For the same graphite quantity, the thermal conductivity of cold compressed composite was higher by two times as compared to that of composite obtained by mixing of graphite with molten PCM. Nevertheless, cold compressed composites were not found to be form-stable one due to the presence of impurities and mechanical stresses.

Pincemin *et al*. (2008a) used graphite powders of different particle sizes to prepare the composite with eutectic salt. The thermal conductivity was found to be

dependent not only on graphite amount but also on particle size. It is suggested that for higher graphite amount, larger particle size should be preferred and vice versa for better conductive network. As far as storage capacity is concerned, smallest particle size led to larger capacity when the graphite quantity was more. For smaller graphite content, the effect of particle size was not pronounced. The results also revealed that there was a decrease in phase change temperature variation due to the addition of graphite i.e. the composite PCM possessed almost a congruent melting point. This is obviously an additional benefit as it would lead to more or less isothermal operation. The different types of graphites used by the researchers to make composite PCMs are shown in Figure 2.2.

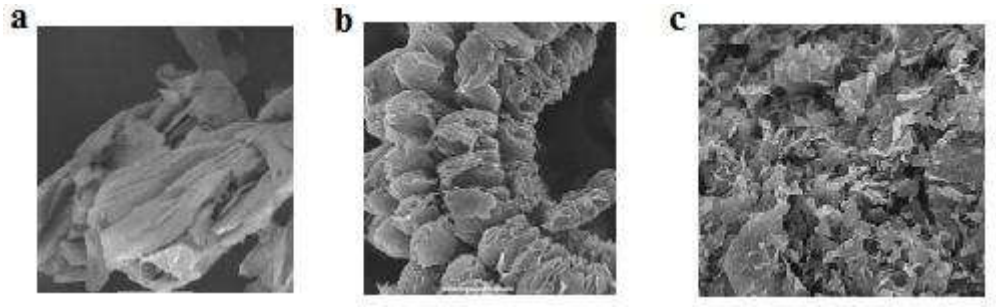

Figure 2.2 Types of graphite

2.1.3.2 Dispersion of high conductivity particles in the PCM

Using graphite made composite PCMs has been proven as efficient and successful way in enhancing the performance of LHTS systems. However, graphite composites can be prepared only through various mechanical/chemical processes like heat treatment, drying, mixing, grinding/compression etc., which are time and energy consuming processes. Moreover, Elgafy and Lafdi (2005) have reported that the porosity of graphite is very crucial in deciding the effectiveness of the composites. If graphite of small mean pore size is used, then there may be decrease in latent heat value as small mean pore size hinders the molecular motion and thus very difficult to impregnate the porous media with the PCM. On the other hand, increasing pore size reduces the capillary force resulting in leakage of liquid PCM. Since the high conductivity metal particles are free from these shortcomings, dispersion of high conductivity particles into the PCM is relatively simpler technique to enhance the

thermal conductivity of PCM.

Mettawee and Assassa (2007) carried out experiments to investigate the enhancement in the performance of PCM based solar collector due to the dispersion of micro aluminum particles. Due to increase in thermal conductivity, the charging time was decreased by 60% as compared to that of pure PCM. The effect was more pronounced during discharging, as the conduction dominated solidification presented more homogeneous process. To evaluate the overall benefit of embedding aluminum particles, the mean daily efficiency was calculated. The mean daily efficiency is defined as the ratio between heat gained by water during discharging and total incoming solar radiation during charging. For all mass flow rates of water, the highest mean daily efficiency obtained was 94% with composite PCM, where as with pure PCM it was only 55%. Although the performance enhancement due to particle addition is reported, the effect of adding the particles on the storage capacity has not been discussed in the paper.

Khodadadi and Hosseinizadeh (2007) have reported that the latent heat of PCM would decrease as the mass fraction of embedded particles is increased. They simulated the solidification of nanofluid [water+nano copper particles] in a square storage model. At earlier stages there was not much increase in the speed of the interface due to the addition of particles. As the time elapsed, the effect was more pronounced as the interface was at more advanced locations in case of higher mass fractions. This resulted in considerable reduction in overall solidification time. Recently, Wang *et al.* (2009) investigated the effect of addition of β –aluminum nitride and observed significant enhancement due to the addition of β –aluminum nitride despite the fact that it also resulted in reduced storage capacity.

Besides copper and aluminum particles, silver has also been tried to obtain composite PCM. Zeng *et al.* (2007) prepared a composite made of 1-tetradecanol and silver nano particles. Apart from increasing thermal conductivity, silver particles brought in additional benefit as there was no strong reaction between silver and organic PCM. The thermal stability of the composite was almost same as that of pure PCM whereas the phase change temperature of the composite was found to be slightly lesser than that of pure PCM. Although it is reported that latent heat decreases with increase in mass fraction of particles (Khodadadi and Hosseinizadeh, 2007 and Zeng

et al, 2007), no attempt has been made in those studies to investigate the outcomes of different particles mass fraction. The effect of particle mass fraction has been extensively studied by Seeniraj *et al.* (2002) with a shell and tube arrangement. The increase in particle fraction reduces the volume occupied by the PCM. This leads to decrease in the amount of heat stored, even though higher heat transfer rate could be achieved. Therefore, it is important to determine the optimum particle fraction, so that maximum heat transfer rate with minimum loss in latent heat storage capacity can be achieved. For the determination of optimum particle mass fraction, Seeniraj *et al.* (2002) calculated ratio of cumulative energy stored with particles and to that without particles. The results revealed the existence of optimum particle fraction at which highest ratio of cumulative energy stored was observed. As a matter of fact, at any given conditions there was a range of optimum particle fraction and it is suggested to choose lower value in the band to ensure high mass of PCM and thus more amount of energy stored. The analysis further indicated that the optimum mass fraction for maximum energy stored depended upon the particle thermal conductivity and maximum allowable radius for interface location. For higher values of particle thermal conductivity, the optimum mass fraction was also higher. Similarly, increase in optimum mass fraction was observed with increase in maximum allowable radius for interface. The maximum allowable radius for interface is determined by the dimensions of LHTS unit. Hence, an appropriate combination of particle thermal conductivity and particle mass fraction is quiet important when the conductivity particles are to be dispersed in the PCM to enhance the performance of the unit.

2.1.3.3 Placing of metal structures

Placing of metal structures into the PCM has also been addressed as one of the thermal conductivity enhancement techniques by few researchers. Velraj *et al.* (1999) placed thin walled hollow cylindrical steel structures into paraffin stored in a cylindrical LHTS system. This structure is named as lesser rings (Figure 2.3a). The results indicated considerable reduction in solidification time due to the addition of lesser rings. The time for complete solidification with lesser rings was approximately $1/9^{th}$ of that without lesser rings, whereas with longitudinal fins, the time for complete solidification was around $1/4^{th}$ of that without fins. However, the above-mentioned

reduction in solidification time could be achieved only with lesser rings occupying 20% of total volume as against fins occupying just 7% of total volume. This clearly shows that to get the same reduction in solidification time, more volume of lesser rings are required as compared to that of fins. It is also reported that the enhancement factor due to lesser rings depends upon the diameter of the cylindrical module, where as in case of fins, it remains almost constant for a fixed number of fins irrespective of diameter of the module. This proves that lesser rings are more effective than fins in larger storage systems.

This statement is not only valid for lesser rings, but also for other types of metal structures according to Ettouney *et al.* (2004). In a double pipe arrangement, stainless steel balls combined with stainless steel screens (Figure 2.3b) were placed inside the PCM to increase the melting rate. The results revealed the fact that enhancement due to metal balls cum screens purely dependent on diameter and number of balls. Increasing diameter and number of balls resulted in increase in enhancement and the enhancement factor of up to 3 could be achieved. As mentioned earlier, in smaller systems the enhancement factor may be limited. This has also been proved by Ettouney *et al.* (2006). The study was carried out to investigate the effect of steel balls inserted into the PCM stored in small spherical module (Figure 2.3c). Both melting and solidification processes were analyzed. The results showed only 15 % reduction in melting and solidification times due to the addition of balls. This is obviously much smaller than that in larger systems.

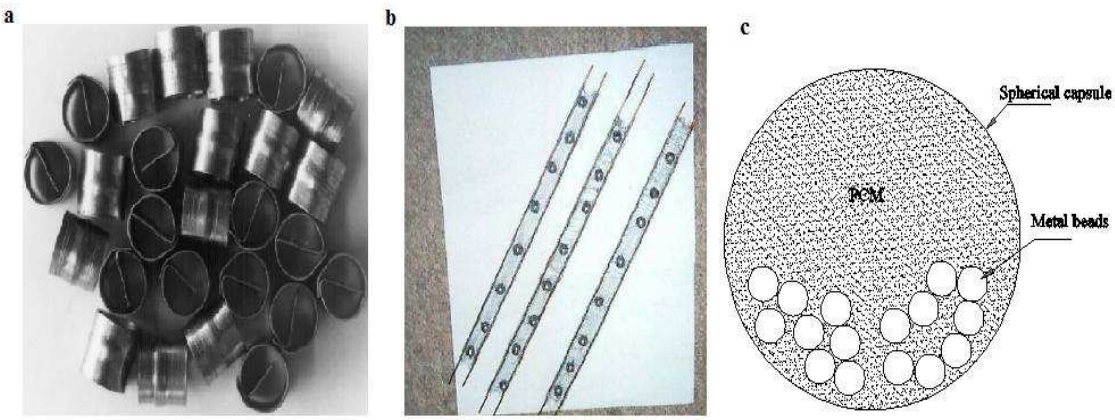

Figure 2.3 Types metal structures: (a) lesser rings [49]; (b) metal balls combined with metal screens (Ettouney *et al*, 2004); (c) metal beads (Ettouney *et al*, 2006)

2.1.3.4 Use of high conductivity and low density materials

Due to relatively high density, the metal particles/metal structures may settle on the bottom surface of the container and add considerable weight to the system. Since the densities of carbon fibers are relatively lower than those of metals and the thermal conductivities are almost equal to that of aluminium and copper, these can be better alternatives to enhance the thermal performance of LHTS systems. Moreover, carbon fibers possess high corrosive resistance and hence compatible with most of the PCMs.

Elgafy and Lafdi (2005) prepared a composite by adding carbon nano fibers into paraffin wax using shear mixing and melting. The thermal conductivity of the composite was found to be increasing almost linearly with increase in mass fraction of nano fiber. As a result, high solidification rate was observed. There was also no reduction in the storage capacity due to the additives as the output power increased linearly with increase in fiber mass fraction. The study was extended to investigate the effect of surface characteristics of fibers on solidification rate and found higher transfer rate with surface treated fibers than that with fibers of untreated surface. The study has also revealed the importance of uniform distribution of fibers in the PCM to obtain further enhancement in the performance. Frusteri et al. (2005) have insisted the homogeneity of composite for better enhancement.

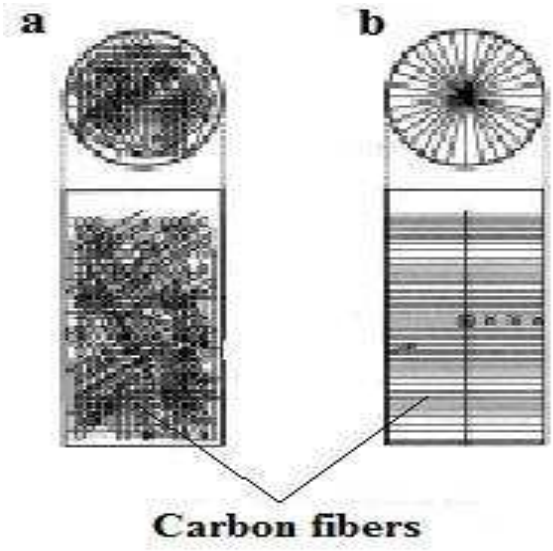

Figure 2.4 Distribution of carbon fibers in cylindrical capsule (Fukai *et al*, 2000).: (a) random distribution; (b) brush type

The importance of uniform distribution of carbon fibers has also been reported by Fukai *et al.* (2000). In a cylindrical capsule, carbon fibers were either randomly distributed or used as brushes (Figure 2.4). The effective thermal conductivity with brush type was found to be three times higher than that with random type. This is because in brush type the fibers were distributed uniformly in such a way all the fibers were arranged in radial direction, which was the heat flow direction. For lower mass fraction of fibers, the randomly distributed arrangement could not present higher melting rate than that with pure paraffin, even though the effective thermal conductivity of former is greater than that of latter. This is due to the loss in natural convection in case of randomly distributed arrangement. On the other hand, the loss in natural convection could not affect the higher melting rate in case of brush type. This shows that the fibers should be arranged in such a way that they are oriented in the direction of heat flow.

The superiority of brush type arrangement also in shell tube arrangement is proved by Fukai *et al.* (2003). They could achieve 30% and 20 % higher solidification rate and melting rate respectively with 1% mass fraction carbon brush type fibers as compared to those with pure PCM. Hamada *et al.* (2003) compared the fiber brush with fiber chips. The experiments were conducted for melting process and results revealed that fiber chips resulted in higher thermal resistance near the heat transfer tube and thus the over all heat transfer rate was lower than that for fiber brush type. According to Fukai *et al.* (2002), when carbon fiber brushes are used around heat transfer tube, then there was a critical diameter for the brush. When the diameter of the brush was increased beyond a value at which the brushes cross the heat transfer tubes, there was no further improvement in thermal response. This was due to the fact that beyond this critical diameter, the thermal resistance between fibers and the tube surface was higher.

Hamada *et al.* (2005) have also discussed the critical diameter of carbon fiber brushes. It is stated that if brush diameter is too large, then the fibers leaving the heat transfer surface form a region where the density of fibers is low. This low density region would prevent the further improvement in heat transfer rate. Hence it is important to make sure that there is no low-density fiber region to get maximum benefit out of carbon fibers.

According to Hamada and Fukai (2005), carbon fiber brushes could effectively reduce the cost and space. The investigated LHTS unit without carbon brushes needed relatively bigger size to produce the required thermal output than that of LHTS with 0.8 volume fraction of carbon fiber brushes. On the other hand, for the same thermal output the cost of latter was only 75% of that of former. As mentioned earlier, there exists thermal contact resistance between carbon fiber brush and heat transfer surface. This may affect the heat transfer enhancement especially when the volume fraction of fiber is less. Very recently, Nakaso *et al.* (2008) have proposed a new technique of using carbon fibers. They used carbon fiber cloths in place of carbon fiber brushes. The cloths made of carbon fibers were highly stretched over the heat transfer surface from end to end of the tubes (Figure 2.5). It is reported that these cloths with high surface density can act as fins. The results showed that fiber cloths of 0.42% volume fraction presented the same thermal performance of fiber brushes of 0.75% volume fraction. It is clear that low volume /mass fraction is desirable as reduction in storage capacity due to the additives would be negligible.

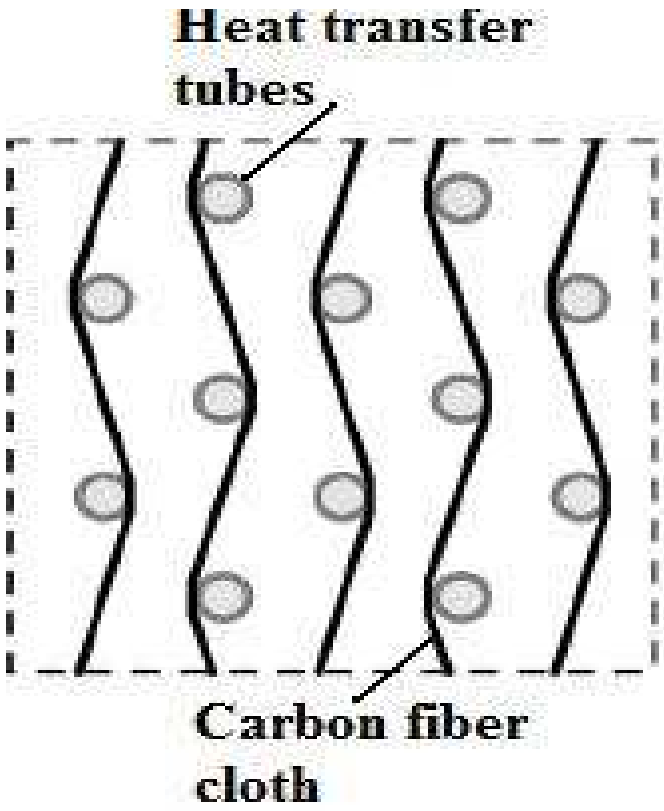

Figure 2.5 Carbon fiber cloths stretched over heat transfer tube (Nakaso *et al*, 2008)

The review on thermal conductivity enhancement methods has revealed that the phase change rate (melting/solidification) can be increased considerably by adding high conductivity substances. According to Fan and Khodadadi (2011), the additives of various forms like metal structures, graphite foams, carbon brushes etc., are nothing but fixed, stationary inserts. Hence, it is clear that the fixed, stationary inserts would weaken the buoyancy driven natural convection in the liquid PCM. On the other hand, the particles dispersed PCMs would be a free-form, fluid-like composites and are expected enhance the natural convection too. However, Ho and Gao (2009) have reported that the viscosity of particle dispersed PCM is higher than that of pure one and increase in viscosity is far greater than that of thermal conductivity. This may dampen out the natural convection during melting. Moreover, the relatively high density metal particles may settle on the bottom surface of the container especially during melting. If the settlement of particles occurs at a reasonable rate, then the role of particles in enhancing the effective thermal conductivity would become insignificant. All the reported works (except the one by Mettawee and Assassa, 2007) are numerical based and the settlement of particles is ignored in the modeling for simplicity. This is not addressed even by Mettawee and Assassa (2007) in their experimental investigations. Hence, the exact role of particle dispersion in enhancing the thermal performance of LHTS is not yet clear. This prompts the need for investigation of settlement of particles to come to a concrete conclusion on the role of particle dispersion in enhancing the thermal performance of LHTS.

2.2 Performance analysis of LHTS systems

The performance of a thermal system can be evaluated through a well known parameter, efficiency or effectiveness. As far as LHTS systems are concerned, the efficiency is nothing but a measure of how effectively the heat or cold energy is stored or recovered. In other words, it indicates how much heat or cold that could not be stored or recovered. Hence, the efficiency of LHTS can be determined as charging efficiency or discharge efficiency or overall (complete cycle) efficiency.

Many investigators carried out calculation of efficiency or a similar parameter of LHTS units employed for different applications. El Qarnia (2009) calculated the storage efficiency of LHTS used for solar water heater. The efficiency is expressed as

a ratio between the latent heat stored in the PCM and the total solar radiation. Higher mass flow rates of heat transfer fluid (HTF) and more number of tubes used in the heat exchanger resulted in maximum storage efficiency. In the similar way, Kaygusuz (2003) has computed the storage efficiency of LHTS unit of a solar heat pump. It is reported that stored heat and storage efficiency of LHTS were found to be increasing with increase in mass flow rate of HTF. In addition to that, the effect of inlet temperature of HTF on the storage capacity was studied and the effect is reported as less significant. Pandiyarajan *et al.* (2010) employed shell and tube LHTS for diesel engine to recover exhaust gas waste heat. The charging rate and charging efficiency were higher at higher loads, which indicate that exhaust gas, i.e., the HTF should be at higher temperature for better performance of LHTS unit.

Seeniraj *et al.* (2002) investigated the thermal performance of shell and tube LHTS unit employed for space based power generation. The thermal performance was studied using a quantity which is the ratio between the total heat stored and the maximum latent heat that can be stored. The results have once again proved that higher mass flow rates of HTF and smaller size unit would lead to high storage performance. Although Canbazoglu *et al.* (2005) have not calculated the efficiency, the total heat (sensible + latent heat) that can be stored in the PCM was calculated to compare the storage capacity of various hydrated salts. The LHTS unit taken up for the study is the one integrated with solar water heaters.

In some applications, the performance of LHTS system must be known during discharging period rather than during charging period. Gumus (2009) has designed a LHTS unit for preheating of internal combustion engines at cold conditions. Hence, the efficiency was calculated during discharging process which is expressed as ratio of energy gained by engine components and total heat stored in the unit. It is found that the discharge efficiency of the unit increases with time and the unit could produce a maximum efficiency of 57.5%, which is obviously at the end of the discharging process.

Devahastin and Pitakusuriyarat (2006) proposed a shell and tube LHTS unit for drying food products like sweet potato. In this case, performance during the heat recovery process by the HTF is obviously more important. Hence, the authors calculated the rate of extractable energy from the unit using the temperature

difference between the inlet and outlet of the HTF. It is also reported that the extractable energy per unit mass flow rate of HTF decreases as the velocity of HTF increases. The rate of heat recovered from the unit is taken as a performance parameter also by Mettawee and Assassa (2006). The heat recovered was calculated from the heat gained by the HTF. The effect of mass flow rate on the heat recovery was found to similar to that reported in the other works.

The calculation of efficiency during both charging and discharging processes but separately can also be found in some works. Kaizawa *et al.* (2008) have used heat storage ratio and heat release ratio as performance parameters. The heat storage ratio is given as,

$$\frac{\text{Total energy stored in the unit}}{\text{Maximum storage capacity of the unit}}$$

Similarly, the heat release ratio is expressed as,

$$\frac{\text{Total energy released by the unit}}{\text{Maximum storage capacity of the unit}}$$

The heat stored and released are calculated from the heat absorbed and released respectively by the HTF. The maximum heat storage capacity takes into account the sensible and latent heat capacity of the PCM. The results show that both the performance ratios increase with increase of mass flow rate of HTF at all times.

Mawire and McPherson (2008) have defined charging and discharge efficiencies separately for a LHTS unit proposed for solar cookers as follows:

$$\eta_{char} = \left[\frac{\text{Total energy stored in the unit}}{\text{Total energy supplied by the HTF}} \right],$$

$$\eta_{dis} = \left[\frac{\text{Total energy absorbed by the HTF}}{\text{Total energy stored in the unit}} \right]$$

However, the results of these efficiencies are not reported, as the objective of the work was limited to development of control techniques for control problems.

The complete cycle or overall efficiency of the system has also been used by some researchers. Mettawee and Assassa (2007) have defined mean daily efficiency

for a LHTS integrated with a solar collector which is used for hot water production. The mean daily efficiency considers total heat absorbed by HTF and total incoming radiation as output and input respectively. Exactly in the similar way, Sharma *et al.* (2005) have calculated a performance parameter to represent the overall performance of a LHTS of solar cooker. However, the effect of operating/design parameters on the efficiency is not discussed in these papers.

From the summary given above, one may think that detailed information on system efficiency or capacity either during charging and discharging separately or during the complete working cycle along with the influence of various operating/design parameters are explored. Subsequently, the explored information would enable the designer to develop an optimum system. However, the performance of LHTS units is assessed using only energy balance in these studies. This procedure, in fact, is based on first law of thermodynamics and generally employed to identify the ways to improve the quantity of heat stored/recovered. However, energy analysis does not reflect the quality of energy stored/recovered. Hence, an 'optimized LHTS unit' based on energy analysis is not necessarily an optimum system. This inadequacy can be overcome, if an analysis based on second law of thermodynamics is carried out for LHTS units. This is because the degradation of energy stored/recovered is very much appreciated only in the second law analysis.

Rosen *et al.* (1999) have reported that energy analysis is complicated and confusing when it comes to cold thermal storage systems those correspond to one employed for building cooling. This is because only heat flows are taken into account rather than cold flows, in energy analysis. On the other hand, second law based analysis can treat both heat and cold which is out of equilibrium with the environment, as a valuable commodity. Hence, second law analysis is inherently the better option than energy analysis especially in case of cold thermal storage systems. In general, when it comes to renewable energy sources, exergy analysis is very useful tool as exergy is a way to sustainable development (Hepbasli, 2008). Moreover, a thermoecomomics analysis of a thermal system is necessarily based on second law analysis in order to obtain feasible design and operating conditions. This is because only second law analysis correctly reflects the economic value of the storage operation (Rosen, 2001).

Thermoeconomics analysis combines second law analysis and engineering economics. Since the second law analysis takes into account the true potential of energy, estimation of cost and subsequent optimization of the system can be realized through thermoeconomics. In the scope of energy storage systems, investigations using thermoeconomics methods have been reported by Badar and Zubair (1993), Badar and Zubair (1995), Al-Naglah (1997), Zubair (1999), Demirel and Ozturk (2006), Demirel (2007) and Kim (2010).

2.2.1. Second law analysis-thermodynamic concepts

The second law of thermodynamics is very distinct from the first law as it introduces new concepts of exergy and entropy. Hence, the analysis based on the second law of thermodynamics needs to be established with a clear understanding of these concepts. This section overviews the concepts of exergy and entropy and their roles in the second law based analysis.

2.2.1.1 Exergy

Unlike first law of thermodynamics, second law of thermodynamics quantifies the quality of energy. The quality of energy is gauged from the state of system in relation to the surrounding conditions. This quality or usefulness of energy is termed as “exergy”. Many more equivalent terms like availability, available energy, essergy, work capability, utilizable energy etc., can be found in literature. However, Kaygusuz and Ayhan (1993) have reported that use of the term exergy should be encouraged, as it was agreed at the *“Fourth International Symposium on Second Law Analysis of Thermal System”* held at Rome, Italy in 1987. Moreover, the term exergy is more commonly employed than others. Hence, in this paper, we are confined to the term exergy.

Exergy is defined as maximum quantity of work that can be produced by a system as it comes to equilibrium with surrounding. A system can carry exergy only if it is not in equilibrium with surrounding and the exergy becomes more and more as the system deviates more and more from surrounding. Once the equilibrium is attained then exergy becomes zero. This means exergy cannot be conserved, but can be consumed or destroyed. This statement highlights the reason why energy is getting

degraded. It is clear from the abovementioned points that the degradation of energy is automatically accounted for in the analysis, if it is second law (exergy) based analysis.

2.2.1.2. Entropy

The association between entropy and second law of thermodynamics is well known as the latter is often called law of entropy. Moreover, as we have seen before, unlike energy, exergy cannot be conserved, rather is destroyed. However, exergy can be conserved, if the process takes place in a reversible manner. It is well known that all real processes are irreversible and hence, the irreversibilities associated with the process can be stated as responsible for the exergy destruction. The exergy analysis is not only concerned with exergy, but also with exergy destruction. This means that it is also necessary to know that to what extent exergy can be destroyed in order to quantify the true potential of the system/process. This is where the concept of entropy becomes more useful.

Entropy here is used as a measure of irreversibility. This is explained as follows. Any process which is irreversible is accompanied by energy degradation and when the equilibrium is attained, the exergy content reaches zero value. At the same time, the irreversible process is also accompanied by increase in entropy which reaches a maximum when the system comes in equilibrium with surrounding. Thus, all irreversible processes proceed in the direction of increase in entropy and decrease in exergy. This highlights the relation between exergy and entropy. In actual system, entropy is always generated and exergy is destroyed. Hence, the destroyed exergy must be proportional to generated entropy. As standard entropy relations are much easier to deal with, the generated entropy is included in the exergy analysis to explore the destroyed exergy quantity.

2.2.1.3. Second law efficiency

First law based efficiency can be stated as the ratio of energy output and energy input. In practical thermal systems the energy output is less than energy input because of energy loss. Hence, efficiency can be improved only by reducing losses. However, the losses do not reflect the degradation of energy. To LHTS units, this is of more important, which can be explained as follows:

The efficiency of a well insulated LHTS unit during the cycle (comprises of melting and solidification processes) can be defined as the ratio between total energy recovered during solidification and total energy stored during melting. Since the latent heats of both melting and solidification are the same, the efficiency of the LHTS unit becomes 100%. Due to the adiabatic condition, no energy loss can occur. Nevertheless, energy would be destroyed due to internal irrerversibilities. Even if the realistic condition of non-adiabatic is included in the analysis, the energy efficiency cannot reflect the destroyed quantity as it measures only energy loss due to infiltration. On the other hand, the second law or exergy efficiency which takes into account the exergy, can identify and quantify both the destroyed quantity as well as lost quantity. Due to this reason, the exergy efficiency is found to be less in LHTS systems when compared to energy efficiency (Venkataramayya and Ramesh, 1998, Rosen *et al*, 1999, Sari and Kaygusuz, 2000, Ozturk, 2005, Koca *et al*, 2008, Kousksou *et al*, 2008, Erek and Dincer, 2009 and MacPee and Dincer, 2009).

The second law or exergy efficiency of a thermal system is thus, defined as the ratio of exergy output and exergy input. For a given quantity of exergy, the output exergy is less due to exergy destruction. As we know exergy destruction is due to irrerversibilities. Thus, exergy efficiency (ψ) is a measure of irrerversibilities and is defined as,

$$\psi = 1 - \left[\frac{\text{Exergy destroyed}}{\text{Exergy input}} \right]$$

As already mentioned, the more exergy is destroyed the more is the generated entropy. Hence, the ratio of destroyed exergy and exergy input can be replaced by a factor called entropy generation number (N_s). This implies that,

$$\psi = 1 - N_s \tag{2.1}$$

Equation (2.1) shows that the system performance can be improved by minimizing the entropy generation number. The entropy minimization is taken as an important criterion in the thermal system optimization (Bejan, 1996).

The above discussions clear that exergy and entropy are closely associated with each other and the second law analysis revolves around these two. A comprehensive discussion on exergy and entropy is presented by Dincer and Cengel (2001).

2.2.2. Exergy analysis of LHTS systems

In general, exergy analysis is based on the thermodynamic concepts associated with second law of thermodynamics along with conservations principles of mass and energy. Hence, exergy analysis provides the information on how to use energy to perform a specific task (Badescu, 2007). This section presents the exergy methodologies i.e. methods of evaluation of exergy based performance parameters applicable to LHTS systems.

2.2.2.1. Exergy efficiency

Rosen (1992) has pointed out that though energy based efficiencies for thermal energy storage systems are reasonable and widely applied, more meaningful efficiencies are defined based on exergy. The exergy efficiency is evaluated by establishing the exergy analysis and subsequently, the system can be optimized in such a way that the exergy efficiency of the system is maximum possible. Similar to energy efficiency, the exergy efficiency is expressed for charging period and discharging period separately or for the complete cycle.

During charging mode, the HTF transfers the exergy to PCM and part of the exergy is stored in the PCM. Hence, the exergy stored is considered as desired output in the definition of exergy efficiency. Accordingly, the exergy efficiency is expressed as given by Watanabe and Kanzawa (1995),

$$\psi_{char} = \frac{\text{Exergy stored in the PCM}}{\text{Exergy supplied by the HTF}}$$

Since in LHTS systems the heat transfer is time dependent, it is also important to evaluate the exergy efficiency at different times during melting. This prompts to define the exergy efficiency in terms of exergy rate. So,

$$\psi_{char} = \frac{\text{Rate of exergy stored in the PCM}}{\text{Rate of exergy supplied by the HTF}}$$

However, Rosen and Dincer (2003) have reported that the power input to handle the HTF (pump work) must be accounted for in the exergy efficiency evaluation. The authors have demonstrated that the difference between the exergy efficiency which

neglects the pump power and that of considering pump work is significant. Moreover, this difference is more pronounced in case of exergy efficiency than in case of energy efficiency. An expression for exergy efficiency considering the pump work can be found in (Ozturk, 2005) and the same is given below:

$$\psi_{char} = \frac{\text{Rate of exergy stored in the PCM}}{\text{Rate of exergy supplied by the HTF + Power input to compressor or pump}}$$

In the above expressions, the exergy supplied by HTF is nothing but the change in flow exergy of HTF during heat transfer with PCM. The change in flow exergy can be calculated by using the difference between the inlet and outlet temperatures of HTF along with the environment temperature. Hence, the exergy efficiency indicates the amount of exergy stored from the supplied exergy during the heat transfer. The maximum exergy that can be supplied by the HTF, however, is not considered here and hence, the maximum possible exergy storage capacity of LHTS system cannot be obtained. This deficit can be overcome by evaluating the exergy efficiency as defined by Gong and Majumdar (1996a) and the same is given as,

$$\psi_{char} = \frac{\text{Rate of exergy stored in the PCM}}{\text{Exergy rate possesed by the HTF before contact with PCM}}$$

Similar expression is also reported by Demirel and Ozturk (2006). It is clear from the expression that this form of exergy efficiency takes into account the temperature at which the exergy is available for storing as it uses the difference between the inlet temperature of HTF and environment temperature rather than the difference between the inlet and outlet temperatures of HTF. Thus, it obviously provides the information on how much maximum exergy that can be stored from the maximum available potential work.

Similar expressions can be obtained also for discharging (solidification) mode. In the discharging mode, the exergy output is the exergy gained by the HTF which is the change of flow exergy of HTF. On the other hand, the exergy input is exergy available with the PCM. Hence, the following expression can be given for the exergy efficiency of the system during the discharging process (Watanabe and Kanzawa, 1995).

$$\psi_{dis} = \frac{\text{Exergy gained by the HTF}}{\text{Initial exergy available with the PCM}}$$

This expression provides the total exergy extracted by the HTF from the maximum available exergy with the PCM. From the perspective of time dependent operation, the exergy efficiency can be defined as (Gong and Majumdar, 1996a and Venkataramayya and Ramesh, 1998),

$$\psi_{dis} = \frac{\text{Rate of exergy gained by the HTF}}{\text{Rate of exergy released by the PCM}}$$

One can identify the variation of exergy efficiency with respect to time during discharging process from the above expression.

The operation of thermal energy storage systems is inherently a cycle comprises of energy storage process followed by energy removal process. The analysis may lead to serious errors, if this cyclic nature is not accounted for i.e. analyzing either charging or discharging alone (Krane, 1987). Although the author has highlighted this point with reference to sensible heat storage systems, it is felt that the same is applicable to LHTS systems too. This is demonstrated by Bellecci and Conti (1994) as they could minimize the errors arising from the latter approach by switching over to the former. The study focused on LHTS integrated solar assisted heat engine, nevertheless the overall exergy efficiency calculation is recommended for all applications involving LHTS units. This can also be justified from the results of Gong and Majumdar (1996a). The authors have proved that analysis considering charging alone underpredicts the exergy efficiency significantly. Hence, the calculation of overall cycle exergy efficiency becomes necessary. The evaluation of exergy efficiency can readily be done from the exergy efficiencies of charging and discharging processes. The required expression is as follows (Venkataramayya and Ramesh, 1998),

$$\psi_{overall} = \psi_{char} \cdot \psi_{dis} \tag{2.2}$$

Alternatively, the overall efficiency is given as (Sari and Kaygusuz, 2004),

$$\psi_{overall} = \frac{\text{Exergy extracted from the PCM by the HTF during discharging}}{\text{Exergy input to the PCM during charging}}$$

It is evident from the above discussions that the several forms of exergy efficiencies are developed and used by the investigators. Nevertheless, the evaluation of overall exergy efficiency is proved to be better approach than limiting to charging or discharging modes alone.

2.2.2.2. Exergy evaluation

Demirel and Ozturk (2006) have employed the following expression for the rate of exergy supplied by HTF during charging period.

$$\dot{E}x_{input} = \dot{m}_{HTF} c_{p,HTF} \left[\left(T_{HTF,in} - T_{HTF,out} \right) - T_{atm} \ln\left(\frac{T_{HTF,in}}{T_{HTF,out}} \right) \right] \tag{2.3a}$$

Equation (2.3a) expresses exergy input as the change in flow exergy of HTF as a result of heat transfer. However, as stated earlier, the exergy input can be the exergy content of HTF. The exergy content of the HTF is the minimum useful energy obtainable as it reaches to the state of environment. Therefore, the rate of exergy input can be expressed as,

$$\dot{E}x_{input} = \dot{m}_{HTF} c_{HTF} \left[\left(T_{HTF,in} - T_{atm} \right) - T_{atm} \ln\left(\frac{T_{HTF,in}}{T_{atm}} \right) \right] \tag{2.3b}$$

As it is known, the total exergy input to the PCM during any time interval can be readily obtained by the time integration of the relevant expressions.

During the charging mode of operation, the exergy stored at any time instant is computed from the instantaneous heat transfer rate. The instantaneous heat transfer rate (Q) can be obtained by establishing the energy balance i.e.

Heat gained by PCM = Heat trasnferred by HTF

Thus,

$$\dot{Q} = \dot{m}_{HTF} c_{p,HTF} \left(T_{HTF,in} - T_{HTF,out} \right) \tag{2.4}$$

Now, the rate of exergy stored in PCM is given as,

$$\dot{E}x_{stored} = \dot{Q} \left[1 - \left(\frac{T_{atm}}{T_{PCM}} \right) \right] \tag{2.5a}$$

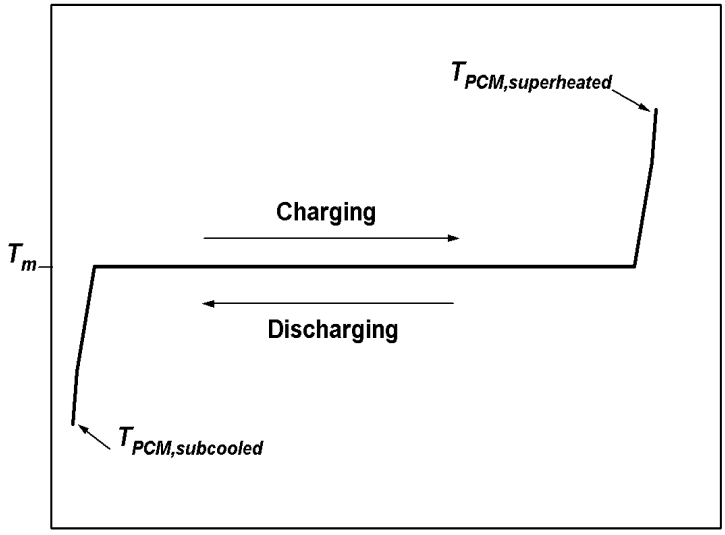

Figure 2.6 Temperature profile of PCM during phase change with sensible heating/cooling

The temperature of the PCM (T_{PCM}) is taken as its melting temperature by Gong and Majumdar (1996a), as the PCM is assumed to be at its melting temperature right through the melting process. This means the sensible heat of PCM is neglected. However, Farid and Kanzawa (1989) have stated that in practical LHTS systems, the sensible heat contributes considerably to the total heat. This is because the PCM is subjected to sensible heating prior to melting and subcooling after solidification. As shown in Figure 2.6, the beginning of charging process is at its subcooled solid temperature and the charging is terminated when the PCM reaches a superheated temperature. In this case, the temperature of PCM is computed as the average of initial and final temperatures of PCM (Demirel and Ozturk, 2006). However, this is simply an approximation as its fails to take into account the instantaneous temperatures of PCM. Moreover, at any time, the temperature of PCM is different at different locations because of the continuous movement of solid/liquid interface as the time progresses. Due to this fact, it becomes necessary to consider the temperature variation in the PCM. Hence, it is suggested to evaluate the T_{PCM} as the average of several temperature values measured/calculated at any instant at different locations. The energy balance used to obtain Equation (2.4) assumes that there is no heat loss from the system during the heat transfer i.e. the system is perfectly insulated. Following this, the exergy balance can be arrived as,

Exergy input = Exergy output + Exergy destroyed

The exergy efficiency based on the above exergy balance can reflect only the destroyed exergy due to internal irreversibilities. According to Erek and Dincer (2009), the heat loss/heat gain is the primary parameter in thermal behavior of the system and both the energy and exergy efficiencies depend on the heat loss/heat gain. From this perspective, the energy balance for charging process may be established as follows in order to include the effect of heat loss/heat gain.

Energy transferred by HTF = Energy gained by PCM + Energy lost to the surrounding

Subsequently, the exergy balance is written as,

Exergy associated with HTF = Exergy stored + Exergy destroyed + Exergy lost to the surrounding

Hence, the rate of exergy stored is computed from the expression given below:

$$\dot{E}x_{stored} = \dot{Q}\left[1-\left(\frac{T_{atm}}{T_{PCM}}\right)\right] - \dot{Q}_{loss}\left[1-\left(\frac{T_{atm}}{T_{PCM}}\right)\right] \tag{2.5b}$$

The total exergy stored in PCM during charging can be readily obtained by performing time integration of Equation (2.5b). However, it requires the computation of heat loss to the surrounding. An alternate form, simpler than the time integrated form of Equation (2.5b) can be found in (MacPee and Dincer, 2009) as,

$$\begin{aligned} Ex_{stored} = {} & M\lambda\left[1-\left(\frac{T_{atm}}{T_m}\right)\right] + Mc_{p,PCM,s}\left[\left(T_m - T_{PCM,init}\right) - T_{atm}\ln\left(\frac{T_m}{T_{PCM,init}}\right)\right] \\ & + Mc_{p,PCM,l}\left[\left(T_{PCM,final} - T_m\right) - T_{atm}\ln\left(\frac{T_{PCM,final}}{T_m}\right)\right] \end{aligned} \tag{2.6}$$

The first term on the right hand side of Equation (2.6) is the exergy stored during melting and the second and third terms indicate exergy stored during sensible heating before and after the melting respectively. Equation (2.6) is not only simpler but also more direct and appropriate as it also includes exergy stored during sensible heat transfer before and after phase change process.

Similarly, the more appropriate form of exergy balance for discharging process would be,

$$\text{Exergy of PCM} + \text{Exergy gain from surrounding} = \text{Exergy gained by HTF} + \text{Exergy destroyed}$$

The exergy balance for a typical LHTS system is illustrated in Figure 2.7. Based on exergy balance, the corresponding exergy expressions for discharging process can be obtained in the similar way corresponds to the charging process.

2.2.2.3. Entropy generation

The exergy efficiency computed in terms of exergy output and exergy input, for instance, exergy stored in the PCM and exergy supplied by the HTF provides the information on how much exergy is destroyed. Since this class of expressions does not stress the calculation of exergy destruction, one may not be able to identify the reasons for exergy destruction. In other words, since the exergy destruction is due to the internal irreversibilities, no information on when and where the irreversibilities occur can be obtained. In the process of optimization, however, it is the irreversibilities that are to be identified so that an attempt to reduce the same can be made. The difference between reversible and irreversible process is described quantitatively by the amount of entropy generation. Thus, the entropy generation is the direct measure of internal irreversibility or exergy destroyed. The optimum system can now be developed in which the entropy generation is minimal. In fact Bejan (1996) has stated that optimization of a system through entropy generation minimization is distinct from that of through exergy analysis. This is basically because the exergy analysis deals with only thermodynamics where as to calculate and minimize entropy generation one needs to use heat transfer and fluid mechanics principles along with thermodynamics.

For LHTS systems, during charging or discharging process, the net entropy generation (S_{gen}) is written as (Strub and Bedecarrats, 1999, Strub and Bedecarrats, 2000 and Kousksou *et al*, 2007),

$$S_{gen} = S_{flow} + \Delta S_{PCM} + \Delta S_{HTF} \tag{2.7a}$$

where S_{flow} is the entropy transfer due to the heat transfer between PCM and HTF during any time interval. The second and third terms on the right hand side of

Equation (2.7a) correspond to the entropy variations in the PCM and HTF respectively.

In Equation (2.7a), the entropy variation of heat transfer surface (wall) is neglected. To include the same, Erek and Dincer (2008) have suggested an expression for entropy variation, which further includes the entropy generation due to the interaction of system with the environment ($S_{heat\ loss/gain}$). The general form of the expression applicable to both charging and discharging processes can be,

$$S_{gen} = S_{flow} + \Delta S_{PCM} + \Delta S_{HTF} + \Delta S_{wall} \pm \left(\frac{Q_{loss} \text{ or } Q_{gain}}{T_o} \right) \qquad (2.7b)$$

In Equation (2.7b), the positive and negative signs stand for Q_{loss} and Q_{gain} respectively.

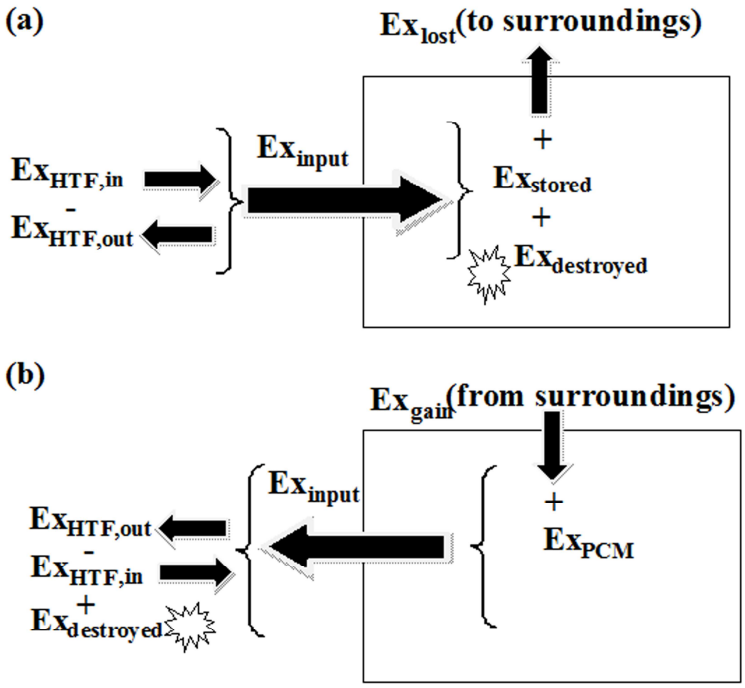

Figure 2.7 Exergy balance for a typical LHTS system (a) during charging (b) during discharging

The thermal storage is necessary under the following two circumstances:

- Heat source is available excessive than the demand, so the excessive energy would be stored
- Heat source is available but there is no demand, thus, entire energy is to be stored

In the former case, after the storage, the HTF is used in the application. Therefore, there will be no entropy generation due to the difference between HTF outlet temperature and surrounding temperature. On the other hand, the latter case requires discharge of HTF into the atmosphere. Due to this, there exits an entropy generation and the same has to be included in the net entropy generation. Thus,

$$S_{gen} = S_{flow} + \Delta S_{PCM} + \Delta S_{HTF} + \Delta S_{wall} \pm \left(\frac{Q_{loss} or\, Q_{gain}}{T_o} \right) + \Delta S_{atm} \qquad (2.7c)$$

The last term on the right hand side of Equation (7c) denotes the entropy generation due to the discharge of HTF into the atmosphere. In case of discharging process, HTF will always be used in the application after the energy recovery from the LHTS unit. Hence, ΔS_{envn} is always eliminated for discharging. The terms on the right hand side of Equation (2.7c) are given by the following Equations.

$$S_{flow} = \dot{m}_{HTF} c_{p,HTF} \int_0^t \ln\left(\frac{T_{HTF,out}}{T_{HTF,in}} \right) dt \qquad (2.8a)$$

Equation (2.8a), however, ignores the pressure drop irreversibilities due to the flow of HTF. According to Charach (1993), the pressure drop irreversibilities are significant especially when the heat transfer area is higher. To include the same, Kousksou *et al*. (2008) have proposed the following expression.

$$S_{flow} = \dot{m}_{HTF} c_{p,HTF} \int_0^t \ln\left(\frac{T_{HTF,out}}{T_{HTF,in}} \right) dt + \dot{m}_{HTF} R \int_0^t \ln\left(\frac{P_{HTF,in}}{P_{HTF,out}} \right) dt \qquad (2.8b)$$

The second term on the right hand side of Equation (2.8b) presents the pressure drop irreversibilities. However, the HTF is assumed to be an ideal gas, which may not be valid in case of liquids. MacPee and Dincer (2009) have stated that the entropy generation due to the pressure drop irreversibilities is the entropy generation due to viscous dissipation. Accordingly, Equation (2.8b) can be modified as,

$$S_{flow} = \dot{m}_{HTF} c_{p,HTF} \int_0^t \ln\left(\frac{T_{HTF,out}}{T_{HTF,in}} \right) dt + \frac{\dot{m}_{HTF} \Delta t \left(P_{HTF,in} - P_{HTF,out} \right)}{\rho_{HTF} T_{HTF}} \qquad (2.8c)$$

where T_{HTF} is the average of initial and final temperatures of HTF and he second term

on the right hand side of Equation (2.8c) is the entropy generation due to the pressure drop irreversibilities.

Now, we address the computation of entropy variation in the PCM. El-Dessouky and Al-Juwayhel (1997) have assumed that during the phase change process, the specific Gibbs free energies for solid and liquid phases are same at the melting point. This implies that,

$$h_{PCM,s} - T_m S_{PCM,s} = h_{PCM,l} - T_m S_{PCM,l} \tag{2.9a}$$

Thus,

$$\Delta S_{PCM} = \frac{h_{PCM,s} - h_{PCM,l}}{T_m} = \frac{M\lambda}{T_m} \tag{2.9b}$$

Equation (2.9b) is valid only if the temperature of PCM is equal to its melting point throughout the phase change. For a process in which sensible heat transfer is involved, the expression should take the following form (Kousksou *et al*, 2007).

$$\Delta S_{PCM} = \rho_{PCM,l}\lambda\forall_{PCM}\int_0^t f(t)dt + \rho_{PCM}c_{p,PCM}\forall_{PCM}\int_0^t \ln\left(\frac{T_{PCM}(t)}{T_{PCM}(t=0)}\right)dt \tag{2.9c}$$

The first term on the right hand side of Equation (2.9c) denotes the entropy variation in the PCM due to phase change and the second term denotes the entropy variation in the PCM due to sensible heating/cooling.

Similarly, the entropy variation in HTF and wall can be written respectively,

$$\Delta S_{HTF} = \rho_{HTF}c_{p,HTF}\forall_{HTF}\int_0^t \ln\left(\frac{T_{HTF}(t)}{T_{HTF}(t=0)}\right)dt \tag{2.10}$$

$$\Delta S_{w} = \rho_{w}c_{p,w}\forall_{w}\int_0^t \ln\left(\frac{T_{w}(t)}{T_{w}(t=0)}\right)dt \tag{2.11}$$

The literature review reveals that none of the works considered all the terms appearing in Equation (2.7c) together, for the calculation of net entropy generation. However, it is recommended that all the terms appearing in the Equation (2.7c) need to be considered as each term contributes significantly to the net entropy generation.

Once the entropy generation is known, the destroyed exergy ($Ex_{destroyed}$) can be obtained from the well known *Gousy-Stodala theorem* (Bejan, 1996), which is in the

following mathematical form,

$$Ex_{destroyed} = T_{atm} S_{gen} \tag{2.12}$$

Then the exergy efficiency becomes,

$$\psi = 1 - \left[\frac{T_{atm} S_{gen}}{Ex_{input}} \right] \tag{2.13}$$

As stated earlier, the ratio of destroyed exergy ($T_o S_{gen}$) and exergy input can be replaced by entropy generation number and the expression for exergy efficiency takes the form given in Equation (2.1). It is clear from Equation (2.1) that the system achieves the maximum efficiency if entropy generation number becomes zero. In other words, the system operates in complete reversible manner and thus, no exergy is destroyed. This ideal condition is possible only if the overall number of transfer units becomes infinite and pressure drop is zero (El-Dessouky and Al-Juwayhel, 1997). This highlights the importance of entropy generation number in optimization of the system.

2.2.3. Exergy analysis with heat transfer enhancement techniques

The enhancement due to employment of all proposed methods except multiple PCMs method is invariably assessed only through energy analysis. Even for multiple PCMs method, the exergy techniques are employed only by few investigators (Watanabe and Kanzawa, 1995, Gong and Mujumdar, 1996a, Domanski and Fellah, 1996, Gong and Mujumdar, 1996b, Gong, 1996 and Kousksou et al, 2007). Recently, Bi *et al.* (2010) have noticed that properly controlled uniform phase change rate would result in optimal operating characteristic of LHTS system i.e. minimum entropy generation. Moreover, poor heat transfer rate from HTF to PCM during charging process results in relatively high temperature HTF at exit. Adebiyi (1991) has shown that significant exergy loss would occur, if HTF exits the system at a rather high temperature for a long time during the storage process. This exergy loss can be expected to be less if heat transfer enhancement techniques are employed.

As stated earlier, high conductivity additives may lead to loss of storage capacity of pure PCM as the mass of PCM decreases. Therefore, it is important to estimate the optimum mass/volume fraction of additives. It can be stated that the

optimization of mass/volume fraction of additives should not be from storage point of view alone. This is because the additives of any form are expected to contribute to the total entropy generation. Moreover, the addition of high conductivity materials has direct impact on natural convection during the melting process. According to Charach and Zemel (1992), the entropy generation is expected to be higher for convection processes due to faster interface motion. Since no work is reported on exergy analysis of system with high conductivity additives, it is not yet clear how the additives enhance the exergy performance of LHTS systems.

2.3 Gap in existing research

From the literature review the following can be drawn as gaps in the existing research.

- Many organic and inorganic compounds have been used as energy storage medium for LHTS systems. However, none of works has compared the organic and inorganic PCMs possessing similar properties under the same conditions.
- Only a limited number of works is reported on dispersion of high conductivity particles, although a large number of studies have focused on other performance enhancement techniques.
- Almost all the investigations concerning high conductivity particles have suggested only nano size particles for improving the heat transfer characteristics of PCMs. Although nano particles seem to be potential candidate in this perspective, they are very expensive. On the other hand, the cheaper version of high conductivity particles, i.e. micro size particles have not yet been tried. Hence, the relative role of micro conductivity particles in enhancing the heat transfer performance of PCM is unknown.
- The literature review also reveals that the effect of reduced latent value due to the addition of particles on the energy stored/recovered is not comprehensively investigated. However, the study on effect of high conductivity particles on the performance of LHTS becomes more realistic, if the reduced latent value is included in the analysis.

- A study based on exergy analysis would be a better option for the complete evaluation of enhancement in performance under the influence of possible enhancement techniques. To the best of the author's knowledge exergy analysis is carried out only for multiple PCMs technique and no exergy work is reported for high conductivity particle dispersed system.

Chapter 3: Performance analysis of nano-particles dispersed LHTS system

This chapter presents the methodology employed for evaluating the performance enhancement due to the dispersion of high conductivity nano-particles in the PCM using exergy analysis.

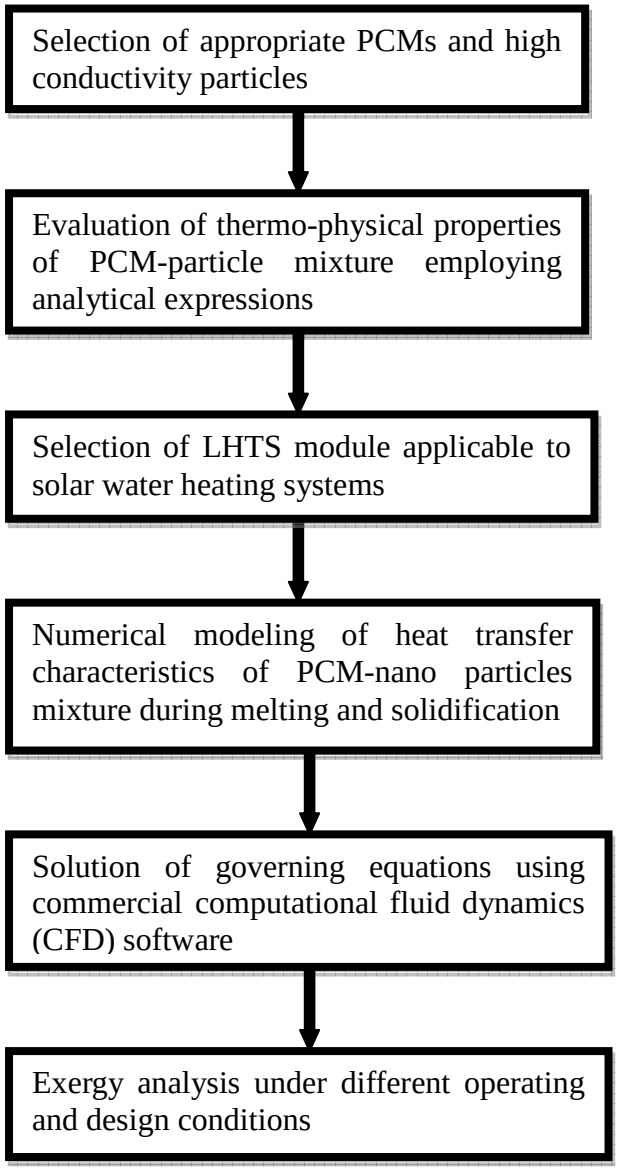

Figure 3.1 Methodology- performance analysis of nano particles dispersed LHTS system

The selection of PCMs and high conductivity particles along with the thermo-physical properties are given in the beginning section of this chapter. This is followed by a section describing analytical procedure for evaluating the thermo-physical properties of the nano-particles dispersed PCMs. The next section focuses on the numerical modeling describing the heat transfer characteristics of PCM during melting and solidification processes and the development of numerical solution techniques. The subsequent section describes the exergy model employed for the performance evaluation. Figure 3.1 summarizes the scheme of performance analysis.

3.1 Selection of materials

3.1.1 Selection of PCMs

The main criterion for the selection of PCM is its melting temperature. It is obvious that the melting temperature of PCM should be less than the operating temperature system used in any application. Since the LHTS system proposed in this work is the one that corresponds to the solar water heating system, the melting temperature can be in the range of 55-65^{o} C. The PCMs those can undergo phase change at this temperature range can be employed if the other criteria which are discussed in Chapter 1, are also satisfied, although it is hard to find such a PCM. However, some of the important qualities like high latent heat capacity, low subcooling, non-toxicity, non-flammability, thermal and chemical stability etc. can be realized by using additives and nucleating agents. Accordingly, a PCM product specially prepared for the solar water heating applications by Pluss Polymers, India (www.thermalstorage.in/plussproducts.html), has been chosen for this study. The PCM selected (HS58) is a mixture of inorganic hydrated salts, additives and nucleating agents. In fact, hydrated salts are more attractive due to their higher latent heat values and relatively high thermal conductivity as compared to organic PCMs.

For the sake of comparative study, it is also felt that using an organic PCM would be more appropriate. The most widely studied organic PCM is paraffin wax. Since pure paraffin waxes are very expensive, only technical grade paraffin waxes are generally employed. Technical grade paraffin waxes are commercially available,

however, they are expensive than salt hydrates. Paraffins are having melting temperatures ranging from 23 to 67 ^{o} C. From the view of required melting point, the preferred paraffin in this work is the one with melting temperature 55 – 59 ^{o} C, available from RUBITHERM, Germany (www.rubitherm.com).

The thermo-physical properties of HS 58 and paraffin wax, as provided by the manufacturer are presented in Table 3.1.

Table 3.1 Thermo-physical properties of PCMs

Properties	HS-58	Paraffin wax
Melting temperature (^{o}C)	57-58	55-59
Latent heat of fusion (kJ/kg)	250	178
Thermal conductivity (W/m.K)	0.65 (solid),	0.2 (solid)
	0.40 (liquid)	0.109 (liquid)
Density (kg/m^3)	1400 (solid),	910 (solid),
	1290 (liquid)	777 (liquid)
Specific heat (kJ/kg.K)	2.500	2.100
Dynamic viscosity (kg/m.s)	0.031*	0.0273
Coefficient of volume expansion (1/K)	0.00095	0.000815

**Measured at National Chemical Laboratory, Pune.*

3.1.2 Selection of high conductivity particles

Since the objective of dispersion of particle into the PCM is to enhance the thermal conductivity, the particles selected should possess highest possible thermal conductivity. Among the high conductivity particles like silver, nickel, gold, alumina, copper, aluminum etc, copper and aluminum are less expensive and easily available. As far as cost is concerned, there is not much difference between copper and aluminum. However, the thermal conductivity of copper is significantly higher than that of aluminum. Hence, copper particles are preferred over aluminum in this work. Table 3.2 lists the thermo-physical properties of copper, which are used for the analytical evaluation of properties of composite PCMs.

In recent years, there has been growing interest in the preparation of nano fluids for various heat transfer applications. A nano fluid is a low conductivity liquid containing high conductivity solid particles of nano size (1nm=10^{-9} m). Due to the enhancement in the thermal conductivity, the nano fluids show much improved thermal performance (Eastman *et al.* 2004 and Jang and Choi, 2007). However, the nanoparticles are not economically viable at present, for instance, the cost of nanoparticles is roughly 25 times of that of micro size (1µm=10^{-6} m) particles of same material. This is due to mainly the processing cost. Hence, no experimental attempt is made to investigate the thermal performance of nano copper particles dispersed LHTS systems.

Table 3.2 Thermo-physical properties of copper

Properties	Values
Thermal conductivity (W/m.K)	400
Density (kg/m^3)	8954
Specific heat (kJ/kg.K)	0.383

3.2 Evaluation of thermo-physical properties of PCM-nano particles mixtures

As the heat transfer characteristics of PCM are mainly governed by the thermo-physical properties of the PCM, prior knowledge of the same is at most important to predict the thermal performance of LHTS system either numerically or experimentally. The identified thermo-physical properties which to be known priori, are,

- density (ρ),
- specific heat (c_p),
- latent heat (λ)
- dynamic viscosity (μ)
- thermal conductivity (k)
- coefficient of volume expansion (β)

Wide range of PCMs, whether organic or inorganic, commercial or non-commercial are extensively characterized and reported in the literature. However, when it comes to composite PCMs, especially PCM with high conductivity metal particles, no data on their properties could be found in literature. Hence, the evaluation the thermo-physical properties should be the first step towards the investigation. Even for pure PCMs, it is better to verify the data provided by the manufacturer as they may not be as accurate as the manufacturer's claim (Tyagi and Buddhi, 2007).

3.2.1 Analytical procedure

When high conductivity nano particles are added into the PCM, the thermo-physical properties of the mixture are a combination of the properties of the particles and the PCM. This indicates that the addition of particles causes significant change in the properties of PCM-particle mixture depending on the quantity of particles added. In other words, the properties of mixture should be evaluated as a function of volume fraction of particles in the mixture. This can be done through analytical procedure and the relevant analytical expressions are as follows:

The properties such as density, specific heat and latent heat can be evaluated by applying mass and energy balance principles. The resulting expressions for density, specific heat and latent heat respectively, are given below as proposed by Goel *et al.* (1994),

$$\rho_m = (1-e)\rho_{PCM} + e\rho_p \tag{3.1}$$

$$c_{p_m} = \frac{(1-e)(\rho c_p)_{PCM} + e(\rho c_p)_p}{\rho_m} \tag{3.2}$$

$$\lambda_m = \frac{(1-e)(\rho\lambda)_{PCM}}{\rho_m} \tag{3.3}$$

with e being the volume fraction of particles dispersed and subscripts m, PCM, p correspond to PCM-particle mix, pure PCM and particles respectively.

From Equation (3.1), it is clear that the increase in density of PCM –particle

composite due to the addition of particles (densities of common metal particles such as copper, aluminum etc., are generally much higher than that of available PCMs) is accounted for and hence, effect of increased density on the buoyancy driven flow during the melting process can be observed. On the other hand, metal particles posses lesser specific heat capacity as compared to pure PCM and have no latent heat capacity. Hence, both specific heat and latent heat values of mixture are expected to less than those of pure PCM (Equations (3.2) and (3.3)).This enables us to comprehend the effect of particle addition on the storage/release capacity of LHTS system.

Along with density, dynamic viscosity of liquid PCM is also very critical in controlling the buoyancy driven flow during the melting process. Again the dynamic viscosity of the PCM-particle mix is dependent only on the volume fraction of particles. Thus, the dynamic viscosity of PCM-particle mix can be given by the following relation (Vand, 1945).

$$\mu_m = \frac{\mu_{PCM}}{(1-e)^{2.5}} \tag{3.4}$$

The major objective of adding high conductivity particles is to enhance the molecular thermal conductivity of PCM. Hence, the thermal conductivity of mixture is expected to increase monotonically with increase in particle volume fraction. Accordingly, the expression for thermal conductivity of PCM-particle mix, which is called Maxwell's equation, is written as (Maxwell, 1954 and Siegel, 1977),

$$k_m = k_{PCM}\left[\frac{k_p + 2k_{PCM} - 2e(k_{PCM} - k_p)}{k_p + 2k_{PCM} + e(k_{PCM} - k_p)}\right] \tag{3.5}$$

As far as coefficient of volume expansion of mixture is concerned, no analytical expression is proposed in the literature. Hence, the particles may not have any effect and the value of pure PCM may be considered for PCM-particle mixture too.

3.2.2 Validity of analytical expressions

Inherently, all the above expressions are valid only if the particles are dispersed

homogeneously and remain in suspension. The homogeneity of the mixture and the suspension stability of particles in the liquid PCM can be realized through emulsification technique. In emulsification process, particles are coated with surfactants before mixing with liquid PCM using ultrasonicators. The details of emulsification technique are given in Chapter 4. Recently, Wang *et al.* (2010) demonstrated that the paraffin-nano copper composites prepared through this technique are homogeneous and stable even after 24 hours. Hence, the settlement of particles may not be an issue and the above written expressions are applicable.

Although Equations (3.1) through (3.3) are valid for even micro size ($1\mu m=10^{-6}$ m) particles, Equation (3.4) is valid only for nano size particles. Moreover, the maximum particle volume fraction should not exceed 0.2, as Equation (3.4) is not applicable for high dense mixtures. Moreover, as mentioned earlier, reduction of storage capacity works against utilization of high fractions of particles. Therefore, to disperse more than 20% of particles into the base PCM is neither practical and is, frankly, nor worthwhile investigating.

The Maxwell's equation (Equation (3.4)) used for thermal conductivity, is valid only if following conditions are satisfied.

- the dispersed particles are spherical in shape (the commercially available nano scale metal particles are generally of spherical shape and thus, this condition can easily be satisfied)
- no interaction between the particles
- the interfacial resistance between the particle and liquid is insignificant
- no irregular movement of the particles

The interaction between the particles is seen as aggregation between each other to form chain structures (Murshed *et al*, 2005). This means that the particles cannot be considered to be isolated from each other as they may form a percolated network. The formation of such networks obviously results in more heat transfer through conduction mode. Although Maxwell equation does not take into account the enhancement in thermal conductivity due to particle aggregation, the same is still valid under certain circumstances. Firstly, the particle aggregation is found to be occurring only at higher volume fraction of particles. Secondly, the effect of particle

aggregation on effective thermal conductivity is significant only when the thermal conductivities of suspended particles and the media are comparable. This is proved by Heine *et al*. (2006) as their experimental results could show good agreement with the data predicted by Maxwell's equation when,

- the maximum volume fraction of particles is limited to approximately 0.2.
- the ratio of thermal conductivity of particles and fluid is sufficiently high (conductivity ratio >> 1)

As mentioned already, the work deals with maximum volume fraction of 0.2 and the ratio of thermal conductivity of particles and PCM is around 1000-2000. Hence, it is very reasonable to ignore the particle interactions and the Maxwell's equation is applicable.

The liquid molecules close to the interface between solid particles and surrounding liquid are believed to be more organized and this effect is known as liquid layering. The liquid layering effect results in enhanced thermal conductivity as the organized liquid layers can act as a bridge for heat transfer across the interface (Choi *et al*, 2001). On the other hand, since the nature of heat conduction in nano materials and the liquid is generally not same, there exists interfacial thermal resistance at the solid-liquid interface. The existence of interfacial thermal resistance is reported by Xue *et al*. (2004) and thus, there is a question mark over the role of liquid layering effect in enhancing thermal conductivity. This implies that it is not yet clear whether interfacial thermal resistance is positive or negative and thus, it is appropriate to ignore the same.

The mixture thermal conductivity is believed to be function of not only particle volume fraction but also of particle size. This is because the Brownian-induced motion of the nano particles is also a potential contributor to the mixture thermal conductivity. The Brownian motion is nothing but the irregular movement of the particles caused by the random collisions of the surrounding liquid molecules. The Brownian motion of the particles may lead to enhanced heat transfer in two ways. Firstly, the diffusion mode heat transport among the particles can be expected to be higher due the particles collision. Secondly, the convection of the liquid may be triggered by this Brownian motion. The enhancement in thermal diffusivity and

convection obviously results in increased thermal conductivity. Since the Brownian motion should be estimated using the particle size, the effective thermal conductivity should be expressed in terms of both particle volume fraction and particle size. This clears that the particle size plays an important role in modeling of Brownian motion (Jang and Choi, 2007) to evaluate the mixture thermal conductivity. However, Fan and Wang (2011) have recently reported that there is still a lack of agreement regarding the role of Brownian motion as the thermal diffusivity of particles is much lower than that of liquid and the convective velocity of liquid cannot be same as Brownian velocity of particles. Hence, it is decided to ignore the Brownian motion in the formulation.

Table 3.3 Comparison of mixture thermal conductivity values obtained from Maxwell's expression with experimental values of Ho and Gao (2009)

Mixture composition	Thermal conductivity (W/m.K)	
	Experimental	Maxwell's model
Paraffin- Alumina (5 % weight)	0.1343	0.134
Paraffin- Alumina (10 % weight)	0.1385	0.1379

All the aforementioned points clearly justify the employment of Maxwell's equation. Furthermore, Cherkasova (2009) has reported that considerable experimental evidences are available in the literature for the validity of the Maxwell model. At the same time, the suspected error in the results due to this simplification was verified in the present work by comparing the results of Maxwell's expression with the experimental results of Ho and Gao (2009). The comparison is presented in Table 3.3. Ho and Gao (2009) prepared paraffin composites with various fractions of alumina nano particles and the thermal conductivities of composites were experimentally measured by Decagaon devices KD2 thermal analyzer. Table 3.3 reveals that the results of Maxwell's expression agree reasonably well with experimental results. Although there are deviations, it is felt that the extent of agreement is sufficient enough to continue with Maxwell's expression in this comparative study.

3.3 Physical model of LHTS unit

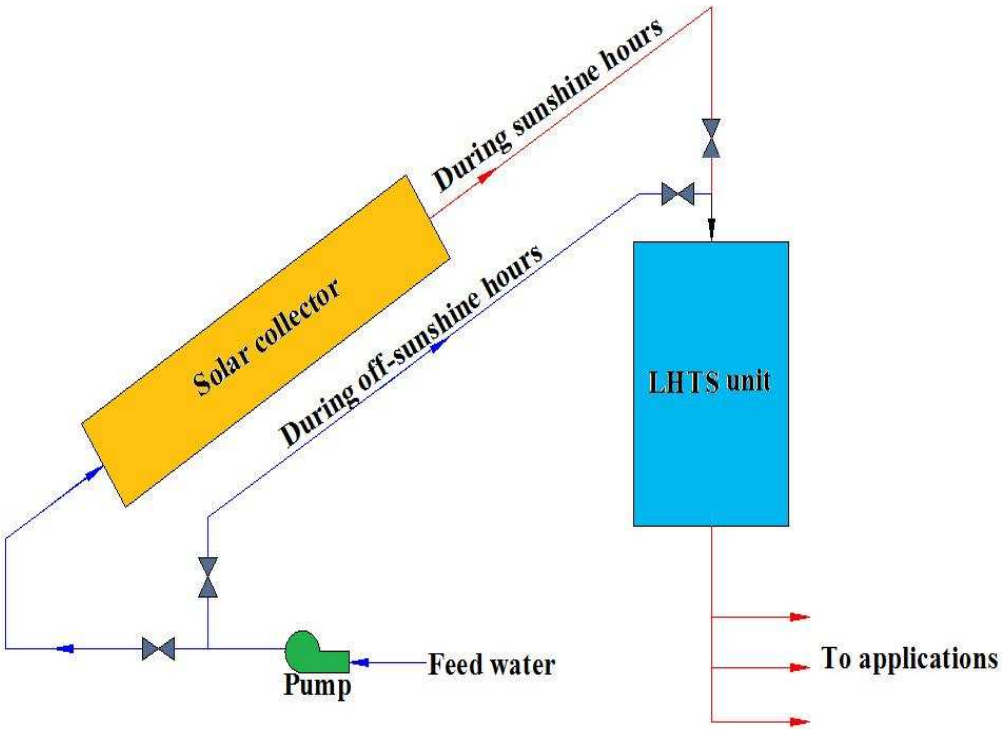

Figure 3.2 Schematic of solar water heating system with LHTS unit

As mentioned earlier, the investigated LHTS unit is associated with the solar water heating systems. The schematic of LHTS unit incorporated solar water heating system is shown in Figure 3.2. The objective of employing LHTS unit for any solar thermal applications is to store excess solar energy available during sunshine hours which can be retrieved in the absence of solar radiation. During sunshine period, the hot water coming out of solar collector passes through the insulated LHTS unit, before getting utilized by the consumers. The hot water exchanges the heat along the way and the heat conveyed by the water leads to melting of PCM loaded and hence, heat is partly stored. When the solar radiation is not available (i.e. off sun shine period), the cold water is pumped through the LHTS unit. This time the cold water gains energy as the liquid PCM solidifies and releases the heat. The water coming out of LHTS unit thus becomes hot, which ensures continuous supply of hot water even in the evening hours.

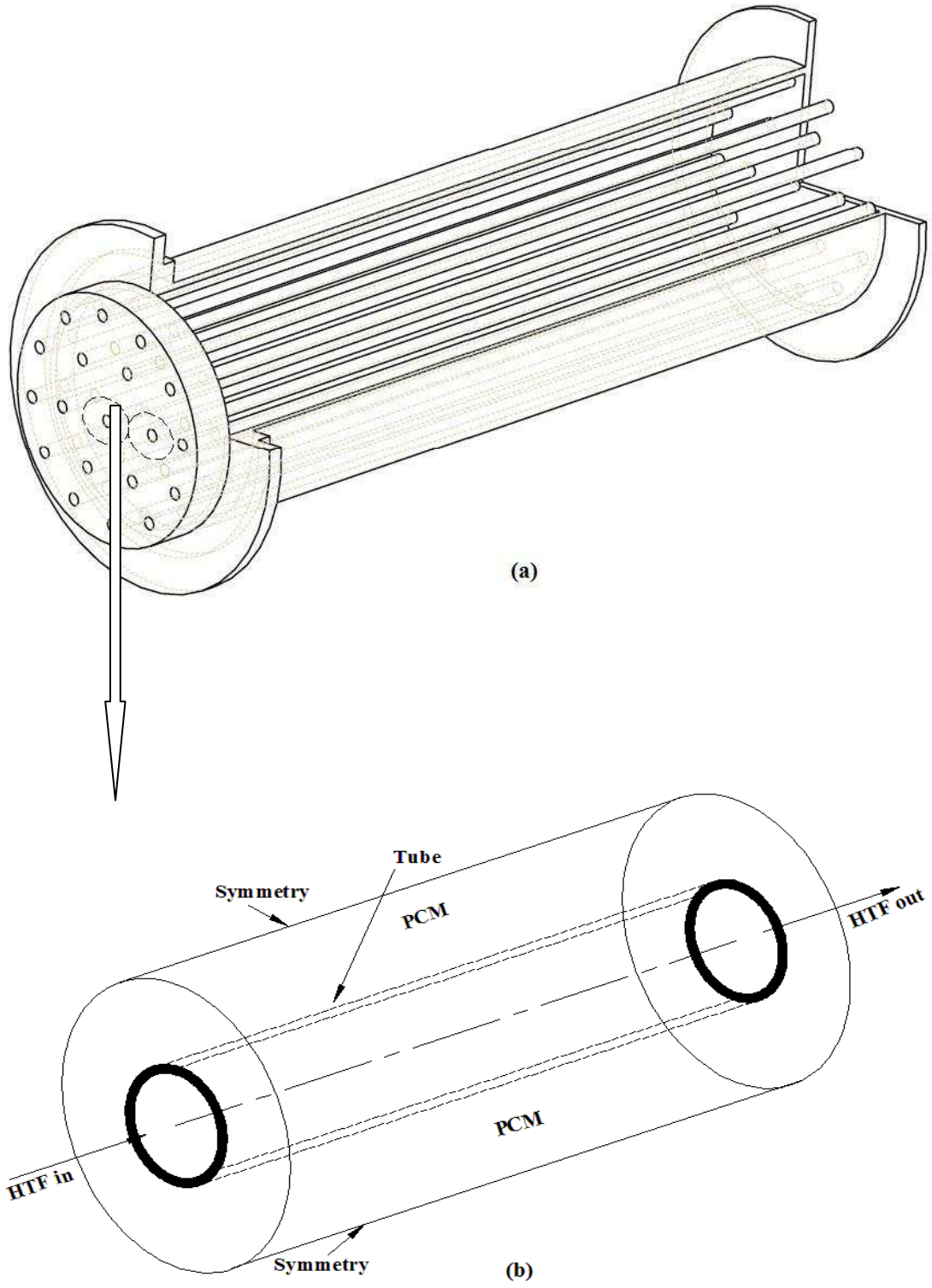

Figure 3.3 Configuration of LHTS unit (a) A typical shell and tube heat exchanger (b) Single tube arrangement considered for analysis

From the above, it is clear that the LHTS unit is necessarily a heat exchanger in the solar water heating loop. The configuration of heat exchanger thus plays very important role in improving the overall performance. The performance of different types of heat exchangers used as LHTS units has been investigated by many researchers. For the recent review on various kinds of heat exchangers proposed by researchers, the readers are referred to Sharma *et al.* (2009). Among these shell and tube / concentric double pipe heat exchangers have been proved as high efficient for minimum volume (Lacroix , 1993). It is obvious that solar energy storage requires a high efficient, minimum volume system. From this perspective, shell and tube heat exchanger is most attractive device as a LHTS unit and such a device has been chosen in this study.

The shell and tube heat exchanger generally consists of a bank of tubes arranged in a particular pattern inside a coaxial cylinder. The proposed shell and tube LHTS module is shown in Figure 3.3a. In such a module, the PCM is stored in the insulated shell and the tubes carry the HTF (hot/cold water). Since symmetry can be assumed to prevail around each single tube, the present analysis is restricted to a single tube configuration, which is given in Figure 3.3b.

3.4 Heat transfer characteristics of PCM-nano particles composites

For the comparative performance analysis between pure PCM and thermal conductivity enhanced composites under different operating and design conditions, performing experimentation is very time consuming and not cost effective. On the other hand, numerical methods are attractive in simulating parametric studies involving heat transfer and fluid flow as they are powerful, flexible and possible with almost at no cost.

As far as analysis of LHTS systems is concerned, the problem involves two kinds which are strongly coupled; the phase change process of PCM is the one and the second is convective heat transfer associated with the HTF. The mathematical model, thus, comprises of system of conservative governing equations that describe the heat transfer and fluid flow characteristics of the unit. Since the phase change heat transfer mechanisms of melting and solidification processes are not same, the mathematical

formulation of melting is different from that of solidification. The numerical procedure adopted here is described in the following sections.

3.4.1 Mathematical formulation of melting of PCM

Although the unit can be oriented vertically or horizontally, the vertical orientation is considered to ensure the axisymmetric phase change around the inner tube. Because of the axisymmetric phase change process, only one half of the physical model with axis as symmetry line is sufficient for computational analysis. All the physical boundaries along with the axis are adiabatic boundaries. Since the variation of bulk temperature of HTF in the direction perpendicular to radial and axial directions is negligible, the phase distribution of PCM in the third direction would be essentially same. This allows performing only two dimensional simulations, which of course would be computationally economical without compromising on accuracy in the results. The two dimensional computational domain is presented in Figure 3.4. In all the numerical trails the dimensions of the unit were kept constant and are given in Table 3.4.

As shown in Figure 3.4, the insulated shell is loaded with either PCM or PCM-particles mixture in solid phase and during storage, the HTF, i.e. hot water enters from the top at a temperature (T_{in}), which is higher than the melting temperature of PCM. The HTF inlet temperature is maintained constant throughout the charging process. This ensures continuous melting of PCM, which is initially at ambient temperature, i.e. in sub cooled solid state. The numerical transient analysis is carried out until entire PCM melts.

Table 3.4 Dimensions of LHTS unit

Parameters	Values (m)
R_i	0.015
R_o	0.07
L	1
b	0.001

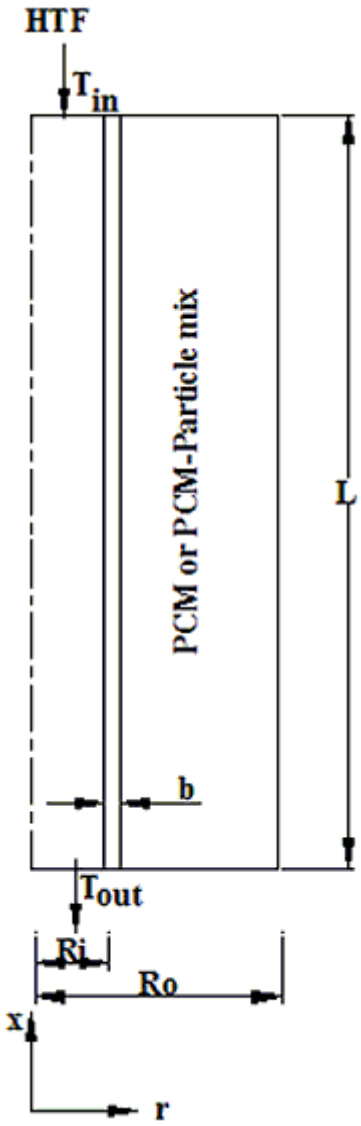

Figure 3.4 Computational model of LHTS unit

3.4.1.1 Assumptions

From the perspective of validity of the analytical procedure adopted to evaluate the mixture thermal conductivity, the assumptions related to dispersed particles are summarized as follows:

- The dispersed copper particles are of spherical in shape and having diameters less than 50 nm
- The PCM – particles composites with any particle volume fraction are

homogeneous and the particles in the mixture remain in suspension all the time

- The maximum particle volume fraction in the mixture is limited to 0.2
- Brownian motion of the particles is weak in nature

In addition to the above, the following assumptions / statements are also made in the present study to enable the mathematical modeling of the LHTS unit:

- Physical properties of the PCM in both liquid and solid phase are constant and however, may be different for different phases
- As the length of the tube is large compared to its diameter, thermal entrance effects are neglected in the HTF. The flow of HTF is either laminar or turbulent and fully developed
- No settlement of particles on the bottom surface due to density effects
- The particles are in local thermodynamic equilibrium with the surrounding PCM

3.4.1.2 Governing equations

Regardless of configuration of system, the melting of PCM is dominated by natural convection in the liquid PCM. To couple natural convection and melting, Shatikian *et al.* (2005) and Shatikian *et al.* (2008) have considered the density of liquid PCM as a function of temperature. Alternatively, natural convection can be modeled by the well known Boussinesq approximation. This model assumes the density as a constant value in all solved equations, except in momentum equations. In other words, the density variation is considered only for the buoyancy term in the momentum equations. Boussinesq approximation has been successfully applied for melting problems by Reddy (2007) and Khodadadi and Hosseinizadeh (2007). Nevertheless, both the models require the solution of momentum equations and thus, are expected to be computationally expensive. In fact, Shatikian *et al.* (2005) stated that such a model requires large computational time even for smaller system like a rectangular domain of 10 mm x 2.6 mm. This clears that a larger system like the one considered in this study, would require more computational time.

This complexity can be overcome by replacing the molecular thermal

conductivity of liquid PCM (k_l) with an effective thermal conductivity for liquid PCM (k_{eff}) in the energy equation, to include the effect of natural convection (Incropera *et al.* 2007). The effective thermal conductivity is introduced to approximate the combined effect of conduction and natural convection. In brief, the model assumes that the fluid (liquid PCM) is stationary, but the fictitious stationary fluid transfers the same amount of heat as the actual moving fluid. This implies that the natural convection is mimicked and combined with conduction through the introduction of effective thermal conductivity. Recently, the effective thermal conductivity has been applied by Xia *et al.* (2010) for packed bed system, in which the PCM is filled in number of spherical containers. The same model is also employed for investigating the melting of PCM in vertical/horizontal cylinders by Farid *et al.* (1989) and Adine and El-Qarnia (2009). From these works, it can be seen that the effective thermal conductivity is a reasonable approximation for including the effect of natural convection during melting. Since this model assumes that the liquid PCM remains stationary throughout the melting process, there is no need to solve continuity and momentum equations.

Following the works of Farid *et al.* (1989), Adine and El-Qarnia (2009) and Xia *et al.* (2010), the effective thermal conductivity can be expressed by the empirical relation,

$$k_{eff} = k_l c \mathrm{Ra}^n \tag{3.6}$$

where c and n are the constants (0.18 and 0.25 respectively) and Ra is the Rayleigh number, which is given as,

$$\mathrm{Ra} = \frac{\rho^2 c_p \mathrm{g} \beta L^3 (T_w - T_m)}{\mu k} \tag{3.6a}$$

where g is the gravitational acceleration (m/s^2), β is the volume expansion coefficient of PCM (1/K), L is the length of tube (m), T_w and T_m are the temperature of tube wall and melting temperature of PCM (K) respectively.

Since the effective thermal conductivity is defined as a function of Rayleigh number, the natural convection is taken into account without momentum equation.

During melting, at any time, the domain consists of solid and liquid portions. Hence, the effective thermal conductivity can be defined only for liquid PCM and the molecular thermal conductivity is used for solid PCM.

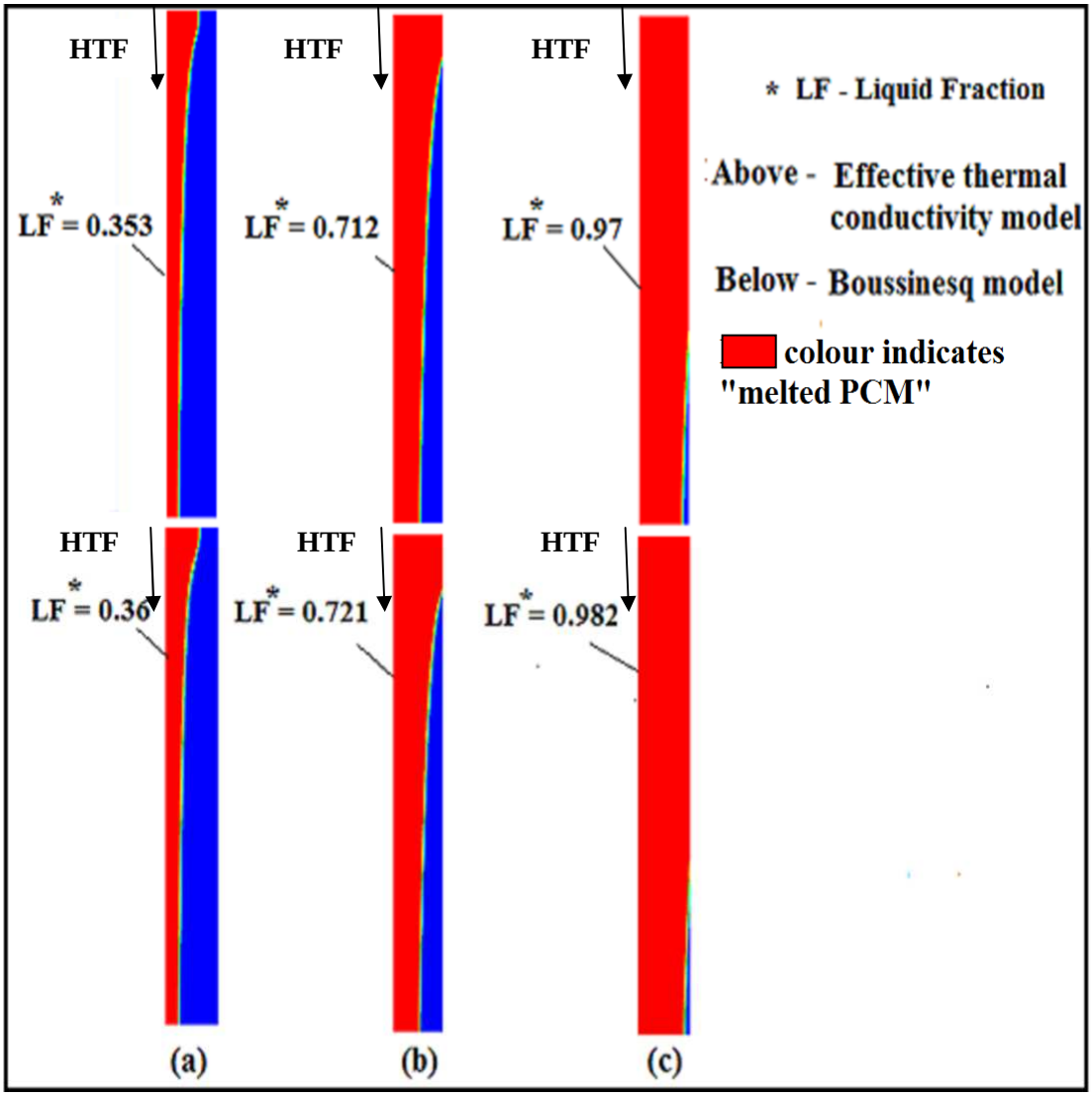

Figure 3.5 Interface locations during melting of pure PCM (a) at t = 100 mins (b) at t = 194 mins (c) at t = 294 mins

As mentioned earlier, the effective thermal conductivity model is computationally inexpensive without comprising on the accuracy of the results. To verify the computational inexpensiveness and accuracy of effective thermal conductivity model, the melting of pure PCM (paraffin wax) was simulated first by employing Boussinesq model and then by effective thermal conductivity model. The

transient simulation was performed with a time step of 0.1 s. It is found that during the simulations with Boussinesq model, each time step required around 100 iterations for convergence of solution. On the other hand, effective thermal conductivity model required only 10-15 iterations under the same conditions. At the same time, the locations of solid/liquid interface at different times obtained from both the models were found to be almost same. This can be seen from Figure 3.5. Although the effective thermal conductivity model slightly under predicts the interface locations, the deviations seem to be insignificant. Hence, the effective thermal conductivity model is employed for this analysis.

Due to the natural convection in the liquid PCM, the top portion of the PCM would melt at faster rate and thus, the solid-liquid interface cannot be flatter one at any time during melting. As it can be seen from Figure 3.5, the effective thermal conductivity model is also able to reflect the same, despite not having considered the liquid motion. On the other hand, the interface during solidification would remain parallel to the heat transfer surface at all times because of the domination of conduction right through the solidification. The representative results of tracked interface locations during melting as well solidification can be found in Appendix I.

When effective thermal conductivity model is applicable, the transient melting of PCM in a two dimensional system is governed by only energy equation:

$$\frac{\partial}{\partial t}(\rho H) = \frac{\partial}{\partial x}(k\frac{\partial T}{\partial x}) + \frac{\partial}{\partial r}\left(k\frac{\partial T}{\partial r}\right) \tag{3.7}$$

where H is the enthalpy of PCM (J/kg), T is the temperature (K), t is the time (s), x and r are the axial and radial co-ordinates(m) respectively. Although the system is cylindrical, the two dimensional geometry can be approximated as rectangular and hence, energy equation is given in Cartesian co-ordinates.

In order to account for the phase change of PCM and for the closure of the formulation, additional equations are required. As a matter of fact, these additional equations establish relationships of enthalpy with temperature and of enthalpy with liquid fraction (f_l). The liquid fraction is a quantity associated with each cell in the domain, which indicates the fraction of the cell volume that is in liquid form.

The enthalpy of the material is computed as the sum of the sensible enthalpy, *h*, and the enthalpy change due to phase change, ΔH.

$$H=h+\Delta H \tag{3.8a}$$

The sensible enthalpy and enthalpy change appeared are expressed respectively, as follows,

$$h = h_{ref} + \int_{T_{ref}}^{T} c_p \, dT$$

$$\Delta H = f_l \lambda \tag{3.8b}$$

Since both the selected PCMs undergo phase change processes over a range of temperatures $T_s < T < T_l$, the liquid fraction can be given as,

$$f_l = 0, \qquad T < T_s$$

$$f_l = 1, \qquad T > T_l$$

$$f_l = \frac{T - T_s}{T_l - T_s}, \qquad T_s < T < T_l \tag{3.9}$$

where T_s is the solidus temperature (K) and T_l is the liquidus temperature (K).

The above described formulation is called enthalpy-porosity formulation-an approach proposed by Voller and Swaminathan (1991), for modeling the solidification/melting process. This technique treats enthalpy rather than temperature as the main dependent variable in the energy equation. The enthalpy formulation for heat-diffusion moving boundary problems is a weak formulation, which is similar to the one used for the heat equation for finite element methods and eliminates explicit reference to the moving boundary. The absence of explicit reference to the moving boundary makes the formulation particularly attractive in numerical schemes where otherwise, one of the main difficulties is tracking the moving boundary. Hence, in this technique, the solid/liquid interface is not tracked explicitly. Instead, the liquid fraction is computed at each iteration, based on an enthalpy balance. The liquid fraction value is associated

with each cell in the PCM computational domain and the computed liquid fraction indicates the volume of any cell that in the liquid form. Initially each cell is in solid state and liquid fraction is zero. As the melting process progresses, the cells in which the material is not yet fully melted, form mushy zone. The mushy zone is a region which is modeled as a pseudo porous medium, in which the porosity or liquid fraction lies between 0 and 1. When the material has fully melted in a cell, the porosity becomes one.

As far as HTF is concerned, the enthalpy formulation is not applicable, as there is no phase change heat transfer. On the other hand, the heat transfer which involves HTF is a forced convective one due to the continuous flow of HTF in downward direction. Hence, the governing equations, which describe the heat transfer characteristics of HTF should comprise of conservative equations for mass, momentum and energy. Accordingly the respective equations are written in tensor notion as follows:

Mass conservation or continuity equation

$$\frac{\partial \rho}{\partial t} + \nabla.(\rho V) = 0 \tag{3.10}$$

where V is the velocity of HTF (m/s).

Momentum equation

$$\frac{\partial (\rho V)}{\partial t} + \nabla.(\rho VV) = -\nabla P + \mu \nabla^2 V + \rho g \tag{3.11a}$$

where P is the pressure (Pa).

This form of momentum equation is valid as long as the flow remains laminar. In this work, it is also decided to investigate the effect of mass flow rate of HTF on the performance of LHTS system. Hence, the simulations are required to be performed with both the laminar and turbulent flow conditions. In case of turbulent flow, the momentum equation should be modified in order to take into account the effect of

turbulent fluctuations. Accordingly, the modified momentum equation for turbulent flow can be written as,

$$\frac{\partial(\rho V)}{\partial t} + \nabla.(\rho VV) = -\nabla P + \mu\nabla^2 V + \nabla(-\rho\overline{V}\overline{V}) + \rho g \qquad (3.11b)$$

where $\nabla(-\rho\overline{V}\overline{V})$ - Reynolds time averaged turbulent shear stress

Since the modified momentum equation contains additional unknown variable, i.e. Reynolds time averaged turbulent shear stress, additional set of equations are required to determine this variable in terms of known quantities. The formulation of such additional set of equations is called turbulent model and the standard *turbulence kinetic energy - rate of dissipation of turbulence kinetic energy* model is employed in this work. This model is a semi-empirical model based on model transport equations for the turbulence kinetic energy and its dissipation rate. The model transport equation for turbulence kinetic energy is derived from the exact equation, while the model transport equation for turbulence kinetic energy dissipation rate is obtained through physical reasoning and bears little resemblance to its mathematically exact counterpart. The details of the model can be found elsewhere (Versteeg and Malalasekera, 1995).

Energy equation

$$\frac{\partial T}{\partial t} + V\nabla T = \alpha\left(\nabla^2 T\right) \qquad (3.12)$$

where α is the thermal diffusivity (m^2/s).

3.4.1.3 Initial and boundary conditions

Initial conditions

$T = T_{in} > T_l$; $\quad 0 \le x \le L$, $0 \le r \le R_i$;

$T = T_{ref} < T_s$; $\quad 0 \le x \le L$, $R_i \le r \le R_o$;

Boundary conditions

$$T = T_{in} > T_l \ , V_r = V_{in} , V_x = 0; \qquad x = L, 0 \le r \le R_i \ , \ t > 0;$$

At the outlet of the tube, the boundary condition called outflow boundary, is applied. This boundary condition assumes that the diffusion fluxes in the direction normal to the exit plane are zero. i.e;

$$\frac{\partial T}{\partial x} = 0, \frac{\partial V}{\partial x} = 0; \qquad x = 0, 0 \le r \le R_i , t > 0;$$

The walls of the shell as well as the axis of the tube are adiabatic boundaries. i.e;

$$\frac{\partial T}{\partial x} = 0, \frac{\partial T}{\partial r} = 0, V_x = 0, V_r = 0; \qquad 0 \le x \le L, r = R_o , t \ge 0;$$

$$\frac{\partial T}{\partial x} = 0, \frac{\partial T}{\partial r} = 0, V_x = 0, V_r = 0; \qquad x = L, (R_i + b) \le r \le R_o , t \ge 0;$$

$$\frac{\partial T}{\partial x} = 0, \frac{\partial T}{\partial r} = 0, V_x = 0, V_r = 0; \qquad x = 0, (R_i + b) \le r \le R_o , t \ge 0;$$

$$\frac{\partial T}{\partial x} = 0, \frac{\partial T}{\partial r} = 0, V_x = 0, V_r = 0; \qquad 0 \le x \le L, r = 0, t \ge 0;$$

3.4.2 Numerical solution of melting problem

For numerical solution of governing equations, the general purpose, commercial computational fluid dynamics (CFD) code, called FLUENT 6.2.36 is adopted. FLUENT is a state-of-the-art computer program for modeling fluid flow and heat transfer even in complex geometries. In FLUENT code, the solution of governing equations is based on finite volume method. The code uses an iterative procedure in which the phase change rate is linearized as truncated Taylor series and then the old iteration values are used to compute the linear term. The modeling of axisymmetric geometry shown in Figure 3.4, and generation of mesh are realized using GAMBIT, which is the preprocessor in the FLUENT package. The computational mesh is

created using quadrilateral elements with uniform grid spacing in *x* and *r* directions. For the optimization of grid spacing, numerical trials involving pure PCM were performed with coarse and finer meshes, i.e. grid spacing ranging from 0.1 to 0.001. The obtained instantaneous heat fluxes and liquid fraction at different time instants with various grid sizes are compared in Table 3.5. From the comparison it is clear that a grid spacing of 0.0015 seems to be the optimum one as further decrease does not result in any notable differences in the results.

Table 3.5 Instantaneous heat flux and liquid fraction values with various grid sizes (Pure PCM, Re=500, T_{in} = 340 K)

Time (h) ↓	Heat flux (W)				Liquid fraction			
Grid size →	0.1	0.01	0.0015	0.001	0.1	0.01	0.0015	0.001
1	767	778	791	791.2	0.15	0.18	0.20	0.201
2	699	713	725	725.3	0.302	0.37	0.43	0.432
3	606	628	645	645.2	0.54	0.59	0.66	0.662
4	491	502	517	517.2	0.71	0.784	0.85	0.853
5	269	286	304	304.3	0.84	0.878	0.98	0.982

To carry out transient analysis, the time step size of 0.1 s is selected. This is the sufficient enough smallest time step as increase in time step led to convergence difficulties. On the other hand, further decrease, i.e. to 0.5 could not make any difference in the results. The difference between liquid fraction values obtained with time step size of 0.1 and that of obtained with 0.5 was found to be in the range of 0.1-0.2 %.

For the convergence of the solution, convergence criterion of 10^{-5} for continuity and momentum equations and 10^{-6} for energy equations are fixed. To improve the rate of convergence, under relaxation factor is introduced and the optimum under relaxation factor for liquid fraction update is found to be 0.7. The solution controls

used in this analysis are:

- *SIMPLE* algorithm for Pressure-Velocity coupling
- *Standard scheme* (pressure equation) and *Second order upwind scheme* (momentum and energy equations) as discretization schemes

As mentioned earlier, k and k_{eff} are used for solid PCM and liquid PCM respectively. To allow the solver to perform this, a user- defined function (UDF) written in "C" language is compiled in FLUENT, which can be found in Appendix II. The UDF is used to define the thermal conductivity of PCM in any cell and at each iteration, as either k_s or k_{eff} depending upon the temperature of the cell. i.e.

$k = k_s$, if $T<T_m$;

$k = k_{eff,}$ if $T \geq T_m$;

The other properties of PCM and HTF are set as constant values.

3.4.3 Mathematical formulation of solidification of PCM

During energy retrieval, the liquid PCM is allowed to solidify and thus, energy stored in the PCM can be transferred to the cold water. To analyze the cyclic process of storage and retrieval, the solidification of liquid PCM obtained after the complete melting is to be investigated. This indicates that the final condition of liquid PCM after melting is to be taken as the initial condition for the solidification.

It should be mentioned that the temperature of liquid PCM after complete melting would not be same everywhere in the domain. Moreover, the same would be different for different cases of pure PCM or PCM-particle composites under various operating conditions. In such a situation, it is worth investigating the different cases under same uniform initial condition rather than applying different initial conditions as the former would yield fair comparison. Hence, for all cases the same uniform initial temperature is considered. However, the geometry and dimensions of the unit are kept same as the one used for investigation of melting.

Initially, the insulated shell of the unit contains either PCM or PCM-particles mixture in liquid phase. The temperature of the PCM is uniform everywhere in the domain and is equal to either liquidus temperature or more than that, i.e. either in

saturated or superheated state. To initiate the solidification, the cold water is allowed to flow through the tube from the top at a temperature (T_{in}), which is lower than the solidus temperature of PCM. The HTF inlet temperature is maintained constant throughout the charging process. This ensures continuous solidification of PCM. The numerical transient analysis is carried out until entire PCM solidifies.

3.4.3.1 Governing equations

Unlike melting, solidification is dominated by conduction and the influence of natural convection is proven to be insignificant. Hence, the natural convection does not need to be coupled while modeling the solidification phase change. In the absence of natural convection, the effective thermal conductivity is not required and thus, the conventional molecular thermal conductivity for liquid PCM is valid at all times.

The energy equation for solidification is same as given for melting (Equation (3.7)). Since the enthalpy-porosity formulation described earlier is applicable to any phase change process, during solidification too, the enthalpy is computed as a function of liquid fraction (Equations (3.8a) and (3.8b)). Initially, liquid fraction of all computational cells is taken as one and at each iteration, liquid fraction of any cell is updated depending on its temperature employing Equation (3.9). Once the material in the cell completely solidifies, the liquid fraction becomes zero.

For HTF, the governing equations take the same forms of Equations (3.10) - (3.12).

3.4.3.2 Initial and boundary conditions

Initial conditions

$T = T_{in} < T_s$; $\quad 0 \le x \le L$, $0 \le r \le R_i$;

$T \ge T_l$; $\quad 0 \le x \le L$, $R_i \le r \le R_o$;

Boundary conditions

Inlet boundary $T = T_{in} < T_s$, $V_r = V_{in}$, $V_x = 0$; $\quad x = L$, $0 \le r \le R_i$, $t > 0$;

Outlet boundary $\frac{\partial T}{\partial x}=0, \frac{\partial V}{\partial x}=0; \qquad x=0, 0\le r\le R_i, t>0;$

Walls of shell and tube axis

$$\frac{\partial T}{\partial x}=0, \frac{\partial T}{\partial r}=0, V_x=0, V_r=0; \qquad 0\le x\le L, r=R_o, t\ge 0;$$

$$\frac{\partial T}{\partial x}=0, \frac{\partial T}{\partial r}=0, V_x=0, V_r=0; \qquad x=L, (R_i+b)\le r\le R_o, t\ge 0;$$

$$\frac{\partial T}{\partial x}=0, \frac{\partial T}{\partial r}=0, V_x=0, V_r=0; \qquad x=0, (R_i+b)\le r\le R_o, t\ge 0;$$

$$\frac{\partial T}{\partial x}=0, \frac{\partial T}{\partial r}=0, V_x=0, V_r=0; \qquad 0\le x\le L, r=0, t\ge 0;$$

3.4.4 Numerical solution of solidification problem

Since the conservative equations governing PCM solidification and HTF flow, are same except the effective thermal conductivity relation, similar solution procedure is adopted for solidification too. This means that the mesh size, time step size, under relaxation factor, scheme for pressure-velocity coupling, and discretization schemes are same as those used for melting process. However, the solution is initialized by setting temperature of PCM either equal or higher than its liquidus temperature and the temperature of HTF less than PCM's solidus temperature.

Although effective thermal conductivity model is not applicable, an UDF is still required for thermal conductivity. This is to define different thermal conductivity values for solid and liquid PCMs as follows.

$k = k_s$, if $T<T_m$;

$k = k_l$, if $T\ge T_m$;

3.5 Exergy analysis

The solution of the governing equations leads to the results in terms of instantaneous heat transfer rate, liquid fraction/solidified fraction of PCM and HTF outlet temperature at all times during charging or discharging. These values can subsequently be used to assess the performance enhancement due to particle dispersion. The performance of a thermal system can be evaluated through a well known parameter, efficiency or effectiveness. As far as LHTS systems are concerned, the efficiency is nothing but a measure of how effectively the heat or cold energy is stored or recovered. In other words, it indicates how much heat or cold that could not be stored or recovered. However, the present system studied is assumed as an adiabatic and hence, the heat released by HTF is completely absorbed by PCM during charging and vice versa during discharging. As a result, the efficiency of the system becomes unity all the time. Hence, the calculation of energy efficiency is not sufficient to design more efficient system by reducing the internal inefficiencies (irreversibilities). This is where the exergy analysis is more useful. In the present work, the following procedure is employed for the exergy analysis.

3.5.1 Exergy analysis of charging process

During the charging period, the rate of exergy transferred by the HTF at any instant is expressed as,

$$\dot{E}x_{HTF} = \dot{m}c_{p,HTF}\left[\left(T_{in} - T_{out}\right) - T_{atm}\ln\left(\frac{T_{in}}{T_{out}}\right)\right] \tag{3.13}$$

where $\dot{m}$ is the HTF mass flow rate (kg/s), T_{in} and T_{out} are the HTF temperatures at inlet and outlet respectively (K) and T_{atm} is the atmospheric temperature (K).

The rate of exergy stored in the PCM can be written as follows,

$$\dot{E}x_{PCM} = \dot{Q}\left[1 - \frac{T_{atm}}{T_{PCM}}\right] \tag{3.14}$$

where $\dot{Q}$ is the heat transfer rate and T_{PCM} is the temperature of PCM (K).

At any instant, T_{PCM} is not same everywhere. Hence, it was determined by averaging the nodal values.

Now the exergy efficiency of the system can be calculated using Equations (3.13) and (3.14) and is given as,

$$\psi = \frac{\dot{E}x_{PCM}}{\dot{E}x_{HTF}} \tag{3.15}$$

The effect of reduced latent heat due to particle dispersion can be investigated using the ratio of total energy stored with and without particles ($Q_{e>0}$ and $Q_{e=0}$ respectively) after complete melting.

$$\frac{Q_{e>o}}{Q_{e=0}} \tag{3.16}$$

However, this ratio doesn't consider the quality of energy stored as it ignores the temperature at which the energy is stored. Hence, similar to the ratio given above, a ratio of total exergy stored with and without particles ($Ex_{e>0}$ and $Ex_{e=0}$ respectively) after complete melting is calculated.

$$\frac{Ex_{e>0}}{Ex_{e=0}} \tag{3.17}$$

The total energy/exergy stored can be calculated by integrating the heat transfer rate/stored exergy rate values numerically using Simpon's 1/3 rd rule.

3.5.2 Exergy analysis of discharging process

During the discharging period, the PCM in the unit transfers the heat to HTF. Then the rate of exergy transferred by the PCM at any instant is expressed by the following equation,

$$\dot{E}x_{PCM} = -\dot{Q}\left[1 - \frac{T_{atm}}{T_{PCM}}\right] \tag{3.18}$$

The rate of exergy recovered by HTF can be written as follows,

$$\dot{E}x_{HTF} = \dot{m}c_{p,HTF}\left[\left(T_{out} - T_{in}\right) - T_{atm}\ln\left(\frac{T_{out}}{T_{in}}\right)\right] \tag{3.19}$$

The exergy efficiency for the discharging process is the ratio of exergy recovery rate by HTF to the transferred exergy rate by PCM, i.e. it is the inverse of the charging process,

$$\psi = \frac{\dot{E}x_{HTF}}{\dot{E}x_{PCM}} \tag{3.20}$$

To study the effect of reduced latent heat value on the discharging performance, similar ratios given in Equation (3.16) and (3.17), which are the ratio of total energy/exergy recovered with and without particles after complete solidification, are calculated.

$$\frac{Q_{e>o}}{Q_{e=0}} \tag{3.21}$$

$$\frac{Ex_{e>0}}{Ex_{e=0}} \tag{3.22}$$

Again numerical integration through Simpon's 1/3 rd rule, is applied to calculate total energy/exergy recovered from heat transfer rate/recovered exergy rate values.

Chapter 4: Performance analysis of micro-particles dispersed LHTS system

This chapter presents the methodology employed for evaluating the performance enhancement due to the dispersion of high conductivity micro particles in the PCM. The configuration and geometrical properties of the LHTS module, PCM and high conductivity particles are kept same as employed for nano-particles system. However, the behavior of micro particles in the PCM is not same as that of nano particles in PCM and hence, the characterization procedure as well as numerical model would be different.

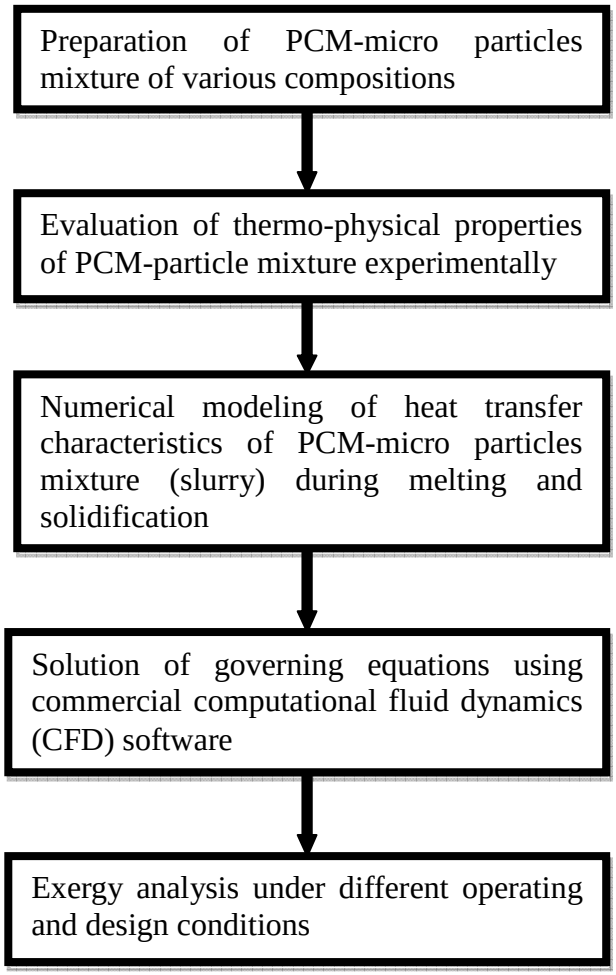

Figure 4.1 Methodology- performance analysis of micro particles dispersed LHTS system

This chapter begins with a section that describes the techniques employed for the preparation of PCM-micro particles composites. The next section presents the experimental procedure for the characterization of prepared composites. The final section explores the details of numerical analysis of heat transfer performance of PCM- micro particles composites. Since the exergy model, the details of which is briefed in Chapter 3 is also applicable here, the same is not repeated. Figure 4.1 summarizes the methodology of the performance evaluation of PCM-micro particles system.

4.1 Preparation of PCM-micro particles composites

The well prepared mixture of PCM and particles would be the key in achieving significant enhancement in the thermal performance of LHTS unit employing composites. Hence, the preparation of composite is one of the critical steps in this work. A well prepared composite must primarily satisfy the following:

- Particles should be thoroughly and homogeneously dispersed in the PCM.
- The dispersed particles should remain in suspension in the liquid PCM all the time.

While preparing emulsions, microemulsions, colloids and foams, their stability is given vital importance to ensure the right composition and success of the final products. In view of this, surfactants are being widely used in all chemical industries involving the products like detergents, cosmetics, pharmaceutics, paints, fibres, ceramics etc. (Tadros, 1991, Schramm *et al*. 2003 and Tadros, 2005). Surfactants are surface active substances, which act at the interface between two phases to reduce the surface tension (Vaisman *et al.* 2006). This characteristic of surfactants can be used to enhance the physical as well as the kinetic stability of the solid particles dispersed in the liquid. Hence, as a first step, i.e. prior to dispersing the copper particles, the same were coated with a surfactant, namely, sodium acetate. The ratio of copper particles to the surfactant was 3:1 by mass. The micro copper particles were prepared out of copper rods (99.9% purity) using simple filing technique. The size of the prepared particles was measured with electron microscope and the average size was found to be 250 µm. A representative image of particles obtained from micrograph is shown in Figure 4.2.

Figure 4.2 Micrograph of sample copper particles employed

Figure 4.3 Probe type ultrasonicator

The surfactant coated copper particles were then, dispersed into the liquid PCM. To enhance the dispersion and the homogeneous nature of the resulting composite, the following procedure was adopted.

While dispersing the particles, the liquid PCM in the mixing container was thoroughly stirred for about 15 minutes using a magnetic stirrer. The magnetic stirrer was integrated with the thermostat controlled heater, however, could be separately operated. After the stirring process, the mixture was treated with ultrasonic disruptor for more than one hour. Ultrasonication is very effective and well established method among all the physical methods used for homogeneous particle dispersion in the liquid (Challis *et al.* 2005, Lu *et al*. 2005 and Schramm *et al*. 2005). When the high intensity ultrasonic waves are induced in the liquid, the propagation of waves results in cavitation in the liquid (due to alternating high pressure and low pressure cycles). This ultrasonic cavitation produces very high velocity liquid jets (up to 1000 km/hr) and they exert high pressure between the dispersed particles in the cavity, which in turn separate them from each other (deagglomeration). Moreover, the size of the small particles may also be reduced as they are accelerated with the liquid jets and colloid at high speeds.

For ultrasonication, the probe type sonicator was used. The photograph the probe type sonicator along with magnetic stirrer and thermostat controlled heater is presented in Figure 4.3. The amplitude and frequency of ultrasonic waves were set as 50 % and 50 Hz respectively during the sonication.

The above stated procedure was employed to prepare the composites of both paraffin-copper and hydrated salt-copper with various volume fractions of copper particles. The volume fractions of copper particles in the each composite were 5%, 10%, 15% and 20%.

4.2 Evaluation of thermo-physical properties of PCM-micro particles mixtures

The analytical expressions used to calculate the density and specific heat of PCM- particles composites (Equations (3.1) and (3.2) respectively) are applicable regardless of the size of the particles as the equations satisfy mass and energy balances. On the other hand, the expressions correspond to latent heat, thermal

conductivity and viscosity are developed only for nano particles. The viscosity of composites containing micro particles can still be calculated analytically using alternate expressions such as Mori-Ototake equation (Ozilgen, 2011) and Krieger equation (Krieger, 1972). However, no analytical expressions could be traced in literature for latent heat and thermal conductivity of PCM-micro particles composites. Hence these properties are evaluated experimentally in this investigation. Since the physical evaluation of latent heat facilitates the calculation of specific heats too, the same are arrived experimentally.

4.2.1 Experimental procedure

For the measurement of thermo-physical properties of PCM, the most commonly used methods are drop calorimetry (DC), differential thermal analysis (DTA) and differential scanning calorimetry (DSC) methods. The outlines of these methods are given below:

DC- measures the enthalpy of the sample as a function of temperature by dropping the temperature from higher value to lower one.

DTA – measures the difference in the temperatures of the sample and a reference which undergo identical thermal cycles.

DSC - measures the difference in the heat required as a function of temperature to raise the temperature of the samples and a reference.

Based on DC, DTA and DSC methods, the required test apparatuses and measurement techniques are well developed over the years. Recently, Kuznik *et al.* (2011) have reviewed the details of DTA and DSC methods applicable to PCMs. The practical implementation of the DC, DTA and DSC methods for the characterization of PCMs can be found from the works reported by Marcus *et al.* (2003)-DA, Buddhi *et al.* (1987)-DTA, Kouskou *et al.* (2010) and Pokhrel *et al.* (2010)-DSC. Although DTA and DSC methods are regarded as fairly accurate ones, these methods are also known for various shortcomings. They are:

- The sample PCM to be tested should be of very small size (1-10mg). However, the properties of bulk PCM would be different from those of sample. Especially, when it comes to PCM composites, the heterogeneous of additives cannot be accounted for, if the sample size is

very small. Moreover, the small sample size cannot reflect the degree of supercooling of the PCM as the small container would show higher degree of supercooling.

- Due to the small sample size, the phase change process cannot be visualized. Especially, the volume expansion of liquid PCM, which is critical for the computation of effective thermal conductivity during melting, cannot be observed.
- The related experimental units are complicated and expensive.
- These methods cannot measure the properties of several samples simultaneously.
- Thermal conductivity values cannot be obtained.

In view of the above mentioned facts, the present work employs, a simple and cost effective method, namely *Temperature –History* method for the measurement of all the thermo-physical properties of pure PCM/PCM-particle mixtures. The *Temperature –History* method was originally developed by Yinping *et al.* (1999) and is subsequently improved by various researchers.

4.2.1.1 Principle of Temperature –History method for measurement of specific heats and latent heat

The latent heat of PCM and specific heats of both solid and liquid PCMs can be evaluated from the cooling characteristics of liquid PCM. The cooling characteristics of liquid PCM to be obtained in the form of temperature *Vs* time plot. This is the reason why this method is known as *Temperature –History* method. To plot the *T-History* curve of PCM, the following procedure is required.

The liquid PCM which is at a higher and uniform temperature than its melting point ($T_{init} < T_m$), in a test tube is suddenly exposed to an atmosphere. Since the atmosphere temperature is below the melting point of PCM (though atmosphere temperature is time dependent), the liquid PCM starts cooling and subsequently freezing would occur. The measurement of temperature of PCM at every small time interval would enable to plot the *T-History* curve. Typical *T-History* curves of PCMs are presented in Figure 4.4.

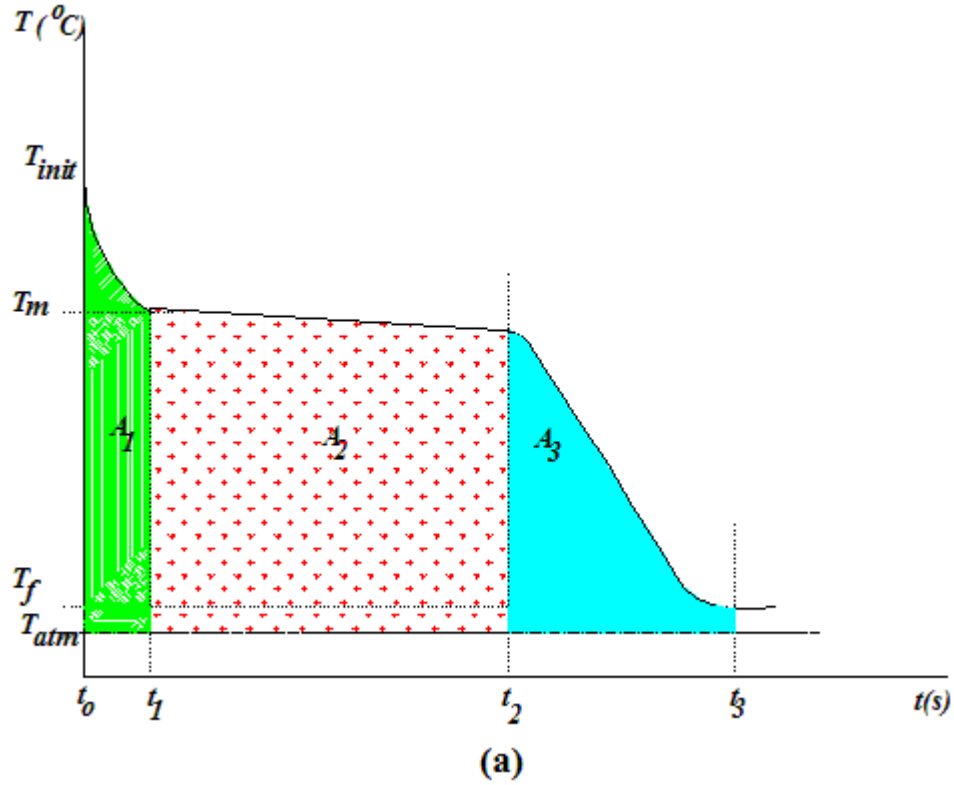

(a)

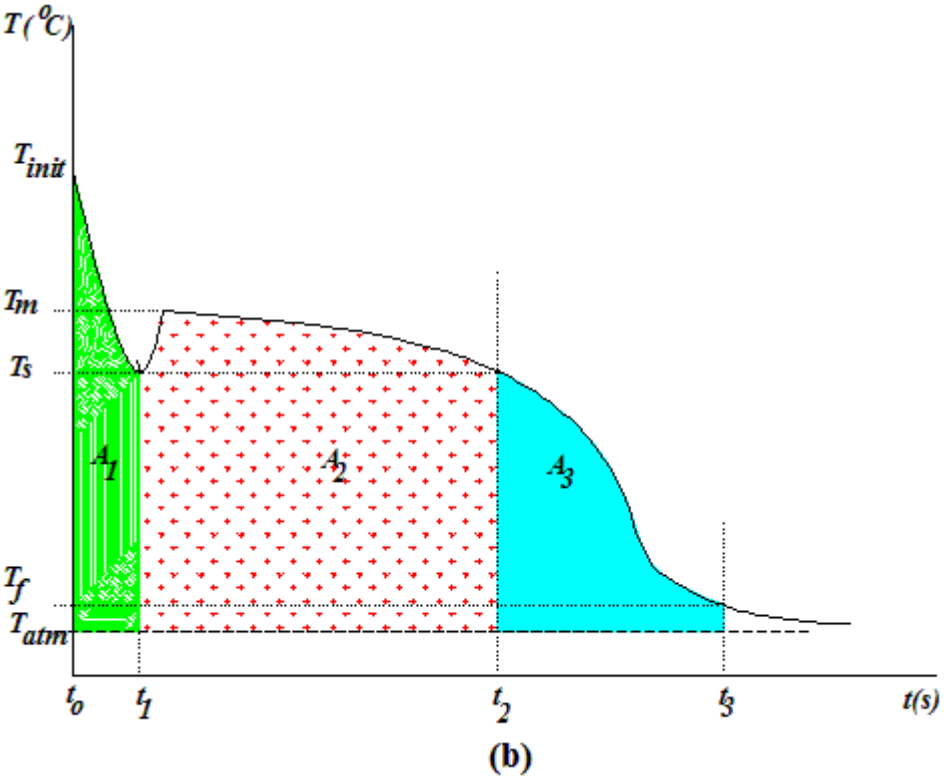

(b)

Figure 4.4 Typical *T-History* curves of PCMs (a) without supercooling (b) with supercooling

From the Figure, it is clear that the *T-History* may have supercooling portion before the phase change (solidification) process. Nevertheless, the plot of any PCM (with or without supercooling) can be divided into three regions as shown in Figure 4.4. These regions/areas are regarded as,

A_1- area below the liquid sensible cooling curve

A_2- area below the phase change curve

A_3- area below the solid sensible cooling curve

Table 4.1 Details of areas of the PCM *T-History* curve

Area	Period	Description
A_1	Liquid sensible cooling	Integral of temperature difference *Vs* time between t_o and t_1
A_2	Phase change	Integral of temperature difference *Vs* time between t_1 and t_2
A_3	Solid sensible cooling	Integral of temperature difference *Vs* time between t_2 and t_3

The corresponding time periods are given as t_o-t_1, t_1-t_2 and t_2-t_3, respectively. Hence, each area can be mathematically expressed as,

$$A_1 = \int_{t_0}^{t_1} (T_{PCM} - T_{atm})dt \tag{4.1a}$$

$$A_2 = \int_{t_1}^{t_2} (T_{PCM} - T_{atm})dt \tag{4.1b}$$

$$A_1 = \int_{t_2}^{t_3} (T_{PCM} - T_{atm})dt \tag{4.1c}$$

Where, T_{PCM} and T_{atm} are temperatures of PCM and atmosphere respectively.

Table 4.1 presents the details of three areas of the *T-History* curve. Hence, the division of areas requires the selection of t_1 and t_2 i.e. the starting and end points of solidification process. If supercooling occurs, t_1 and t_2 can be chosen by using the release temperature of supercooling as the boundary between latent heat and solid sensible heat range as per the original method proposed by Yinping *et al.* (1999). Accordingly, the temperature ranges of the three periods are,

- Liquid sensible cooling T_{init}- T_s
- Phase change T_m-T_s
- Solid sensible cooling T_s- T_f

In this case, the selection of t_1 is straight forward as the release temperature (T_s) is starting point of solidification. However, the same has no relation with the end of solidification. This is because the supercooling phenomenon depends on various parameters like volume, purity, cooling speed, nature of cooling surface etc., This means the supercooling is not a thermophysical property of PCM.

To overcome the lack of accuracy that arises due to above mentioned approximation, Hong *et al.* (2003) and Hong *et al.* (2004) have proposed an alternative technique to choose t_2. In this technique, an inflection point is used to indicate the end of solidification process. The inflection point is the one at which the first derivative of *T-History* curve becomes minimum. This can be justified by the fact that the temperature of PCM remains constant or decreases gradually during phase change, but decreases exponentially once the phase change is completed. Hence, the use of inflection point is much more accurate and easier to employ whether the solidification takes place at constant temperature or with change in temperature. Moreover, if solidification occurs without supercooling, then it becomes almost impossible to choose the end point of solidification without the use of inflection point. This prompts us to use the inflection point for the selection of t_1 and t_2 in the present work. The use of infection point is illustrated in Figure 4.5. The corresponding temperature is T_i. Based on inflection point, the temperature ranges of the three periods are modified as,

- Liquid sensible cooling T_{init}-T_s
- Phase change T_m-T_i
- Solid sensible cooling T_i-T_f

The cooling of PCM can be termed as a conduction problem that involves surface convection effects. Hence, the Biot number (Bi = $hR / 2k$, where h is the heat transfer coefficient of air outside the tube, R is the radius of tube and k is the thermal conductivity of PCM*)* plays an important role. In such problems, if the condition of Bi < 0.1 is satisfied, then the temperature distribution can be assumed as uniform and it allows employing the lumped capacitance method.

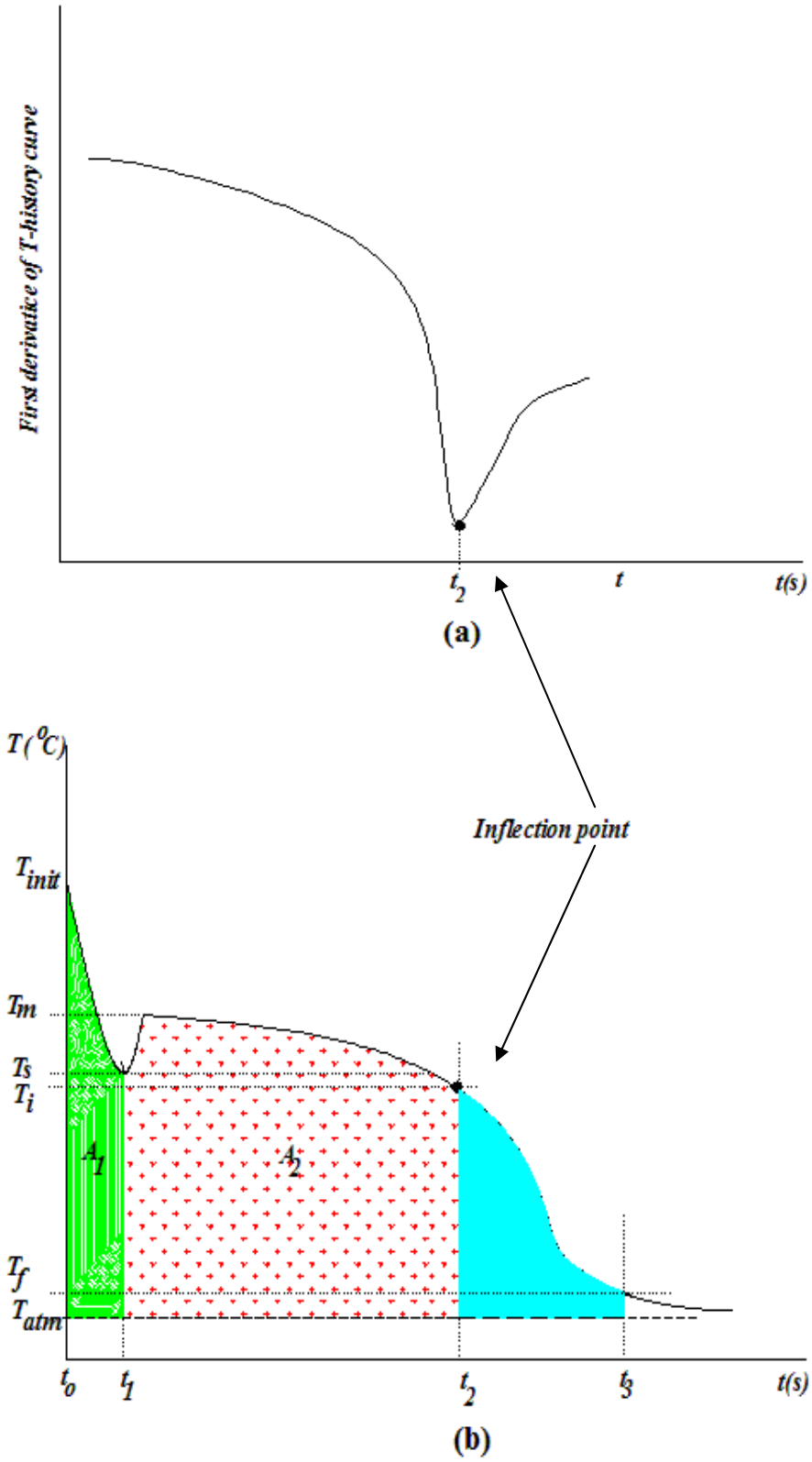

Figure 4.5 Use of inflection point (a) first derivative of *T-history* curve giving inflection point (b) inflection point on *T-history* curve

To satisfy the above condition, the tube of very smaller diameter as compared to the length has been chosen in the work (i.e inner diameter = 13 mm, length = 155 mm). These dimensions along with surrounding atmosphere would keep Bi lower and hence, error associated with the employment of lumped capacitance method would be negligible.

When lumped capacitance method is applicable, the energy balance can be formulated as follows:

for the liquid sensible cooling period during $t_o \le t \le t_1$, we have,

$$\left(m_{t,p}c_{p,t} + m_{PCM}c_{p,l}\right)\left(T_{init} - T_s\right) = hA_t A_1 \tag{4.2}$$

where $m_{t,p}$ and $c_{p,t}$ are the mass of tube contacting with PCM and the specific heat of tube material respectively, m_{PCM} and $c_{p,l}$ are the mass of PCM and the specific heat of liquid PCM respectively and A_t is the heat transfer area of the tube contacting with PCM.

For the latent heat (phase change) period during $t_1 \le t \le t_2$ the energy balance is given as,

$$m_{PCM}\,\lambda = hA_t A_2 \tag{4.3}$$

The above equation is valid only if phase change takes place at constant temperature. However, most of the PCMs available in the market including the one considered in this work undergo phase change with change in temperature. Hence, it is appropriate to include the sensible heat of PCM along with the sensible heat of tube in the energy equation. Thus, we have,

$$\left(m_{t,p}c_{p,t} + m_{PCM}\left(\frac{c_{p,l} + c_{p,s}}{2}\right)\right)\left(T_m - T_i\right) + m_{PCM}\lambda = hA_t A_2 \tag{4.4}$$

where $c_{p,s}$ is the specific heat solid PCM.

Similarly, for the solid sensible cooling period which takes place during $t_2 \le t \le t_3$, the corresponding energy equation is,

$$\left(m_{t,p}c_{p,t} + m_{PCM}c_{p,s}\right)\left(T_i - T_f\right) = hA_t A_3 \tag{4.5}$$

where T_f is the final temperature which is taken as a reference.

Hence, three equations are obtained for the three stages of PCM cooling. Along

with PCM, another tube containing distilled water (reference fluid) at the same temperature of PCM is also exposed to the same atmosphere. In the similar manner, the *T-History* curve of distilled water (Figure 4.6) can be obtained. Now the *T-History* curve of distilled water can also be divided into three portions using the same temperature ranges used for PCM. For distilled water too, the lumped heat capacitance method is applicable as Bi < 0.1, the energy equations during the above mentioned time intervals can be given as follows:

$$\left(m_{t,w}c_{p,t} + m_w c_{p,w}\right)\left(T_{init} - T_s\right) = hA_t' A_1' \ , \quad t_o' \le t \le t_2' \tag{4.6}$$

$$\left(m_{t,w}c_{p,t} + m_w c_{p,w}\right)\left(T_m - T_i\right) = hA_t' A_2' \ , \quad t_1' \le t \le t_3' \tag{4.7}$$

$$\left(m_{t,w}c_{p,t} + m_w c_{p,w}\right)\left(T_i - T_f\right) = hA_t' A_3' \ , \quad t_3' \le t \le t_4' \tag{4.8}$$

where $m_{t,w}$ is the mass of tube contacting with water, m_w and $c_{p,w}$ are the mass of water and the specific heat of water respectively and A_t' is the heat transfer area of the tube contacting with PCM. The areas A_1', A_2' and A_3' are expressed as,

$$A_1' = \int_{t_0'}^{t_2'} (T_w - T_{atm})dt \tag{4.9a}$$

$$A_2' = \int_{t_1'}^{t_3'} (T_w - T_{atm})dt \tag{4.9b}$$

$$A_3' = \int_{t_3'}^{t_4'} (T_w - T_{atm})dt \tag{4.9c}$$

The details of above mentioned areas can be seen in Table 4.2.

Finally, simple mathematical manipulation of Equations (4.2) through (4.8) results in expressions for liquid and solid specific heats and latent heat of PCM. They are,

$$c_{p,l} = \frac{m_{t,w}c_{p,t} + m_w c_{p,w}}{m_{PCM}} \frac{A_t}{A_t'} \frac{A_1}{A_1'} - \frac{m_{t,p}}{m_{PCM}} c_{p,t} \tag{4.10}$$

$$c_{p,s} = \frac{m_{t,w}c_{p,t} + m_w c_{p,w}}{m_{PCM}} \frac{A_t}{A_t'} \frac{A_3}{A_3'} - \frac{m_{t,p}}{m_{PCM}} c_{p,t} \tag{4.11}$$

$$\lambda = \frac{m_{t,w}c_{p,t} + m_w c_{p,w}}{m_{PCM}} \frac{A_t}{A_t'} \frac{A_2}{A_2'} (T_m - T_i) - \left(\frac{m_{t,p}}{m_{PCM}} c_{p,t} + \left(\frac{c_{p,l} + c_{p,s}}{2} \right) \right) (T_m - T_i) \tag{4.12}$$

Table 4.2 Details of areas of the reference fluid *T-History* curve

Area	Temperature difference	Description
A_1'	T_{init}-T_s	Integral of temperature difference *Vs* time between t_o' and t_2'
A_2'	T_m-T_i	Integral of temperature difference *Vs* time between t_1' and t_3'
A_3'	T_i-T_f	Integral of temperature difference *Vs* time between t_3' and t_4'

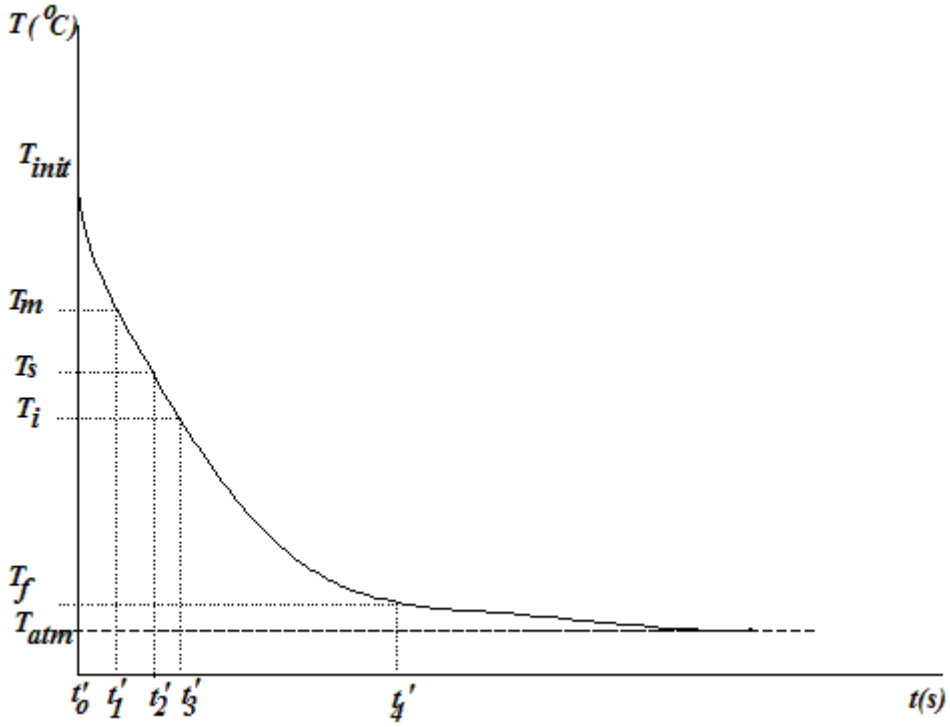

Figure 4.6 Typical *T-History* curve of reference fluid (distilled water)

4.2.1.2 Other modifications of T-History method - not considered in the present work

As mentioned earlier, some more modifications to original *T-History* method can also be found in the literature. The summary of those modifications is given below. For more details of the same, readers are referred to the corresponding papers.

Marin *et al.* (2003) have suggested using enthalpy-temperature relation instead of temperature-time relation. The enthalpy-temperature curves can be obtained using enthalpy concept and its relationship with temperature during small variations of temperature. Recently, this idea has been successfully implemented by Rady *et al.* (2010). This modification is suggested mainly to determine the specific heats as functions of temperature and to overcome the difficulty in determining the solid – liquid phases. However, the variation of specific heats with temperature is generally very minimum and considering constant specific heat values is a reasonable approximation in the numerical modeling. As far as the difficulty in determining the solid – liquid phases is concerned, as mentioned earlier, it can be overcome by using inflection point.

The other modification is related to orientation of the test tube. According to that, the test tubes containing PCM should be placed horizontally instead of vertically to minimize the gravity effects i.e. natural convection effects. This idea is proposed by Zalba *et al*. (2005). However, Peck *et al.* (2006) have stated that the volume difference between the inner wall of tube and PCM in the horizontal set up results in complex calculations to the heat transfer coefficient and area of the vapour layer. Hence, the horizontal set up requires an additional tube, which to be installed vertically. This obviously eliminates the simplicity and convenience of using original set up. The natural convection in the liquid PCM occurs only after the thermal boundary layer thickness becomes the same order of magnitude as the thickness of the molten layer (Bejan, 1989 and Bejan, 2004). This means the thickness of the molten layer is to be considerable as compared to the height of the system for the buoyancy driven flow. In case of smaller diameter tube, the thickness of the molten layer would not be sufficient for the buoyancy driven flow even after complete melting of PCM and thus, onset of natural convection cannot be expected. Hence, the vertical orientation of a tube of smaller diameter-height ratio would not lead to error in the

measurement.

The other notable modification is the one by Kravvarities *et al.* (2010). The modification is with reference to the measurement processing. For the calculation of properties, the original method considers a given temperature of PCM at a time and the time at which the reference fluid reaches the same temperature of PCM. This is referred as use of time delay between PCM and reference fluid. On the other hand, Kravvarities *et al.* (2010)'s method uses the thermal delay (temperature difference) between PCM and reference fluid at a same given time. There are few advantages of this improvement like reduced processing time, reduced no of equations etc, are listed. However, this method results in only the effective thermal capacity rather the specific heats and latent heat values.

In general, the results obtained in the present work (without the above listed modifications) for pure PCM, have shown good agreement with the data provided by the manufacturer. Hence, these modifications are not considered in the present work.

4.2.1.3 Measurement of thermal conductivities

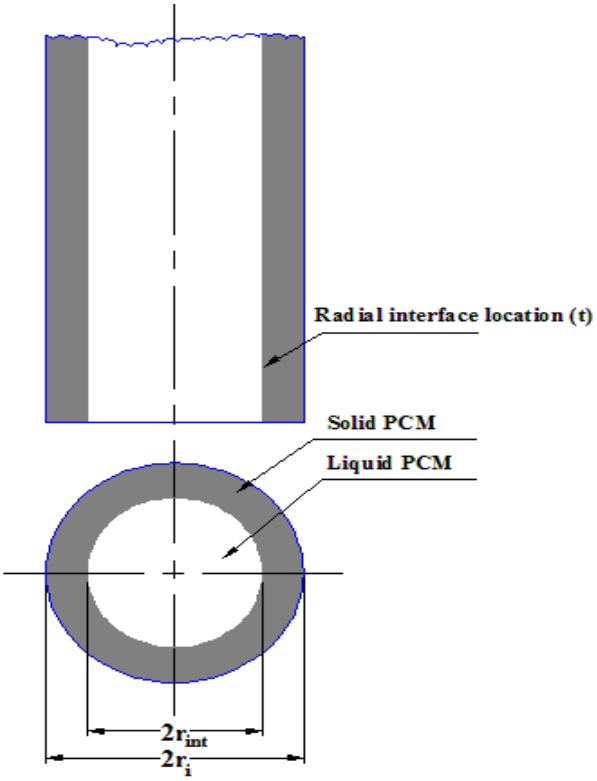

Figure 4.7 One dimensional inward solidification of PCM in a long tube of length/diameter > 10

The experimental set up required for measuring thermal conductivity is almost the same that can be used for measuring specific heats and latent heat values.

To measure the thermal conductivity of solid PCM, the liquid PCM is to be allowed to solidify completely. If the test tube contains molten PCM is suddenly put into the water which is at a temperature lower than the melting temperature of PCM, solidification can be initiated. Because of smaller diameter to height ratio, the lumped capacitance method is applicable here also. Hence, the heat transfer from PCM to water during solidification is one dimensional and the one dimensional transient heat diffusion equation for cylindrical geometry (referring to Figure 4.7) can be written as,

$$\frac{k_s}{\rho c_{p,s}} \frac{1}{r} \frac{\partial}{\partial r}\left(r \frac{\partial T}{\partial r} \right) = \frac{\partial T}{\partial t} \qquad r_{\text{int}} \le r \le r_i, \quad t > 0 \tag{4.13}$$

The initial and boundary conditions are respectively,

$$k_s \left. \frac{\partial T}{\partial r} \right|_{r=r_i} = h_w \left(T_w - T\left(r_i, t\right) \right) \qquad t > 0$$

$$T\left(r_{\text{int}} = r_i\right) = T_m \qquad t = 0$$

where r_i is the radius of tube, r_{int} is the radius of interface, h_w is the water side heat transfer coefficient, and T_w is the temperature of water bath.

At all instants, the conditions for solid/liquid interface are,

$$r_{\text{int}} = r_i \qquad t = 0$$

$$\frac{k_s}{\rho_s \lambda} \left. \frac{\partial T}{\partial r} \right|_{r=r_{\text{int}}} = \frac{\partial r_{\text{int}}}{\partial t}$$

Now Equation (4.13) along with initial and boundary conditions can be solved using perturbation method. The solution procedure of perturbation method can be found elsewhere (Huang and Shih, 1975, Parang *et al.* 1990). Although Huang and Shih (1975) have stated that the perturbation solution is not valid at the end of phase change, Song (1981) has demonstrated that the solution is still valid at the end of phase change, if the first order term of time is chosen. Accordingly, the resulting equation for thermal conductivity of solid PCM is given as,

$$k_s = \frac{[1+\text{Ste}]}{4\left[\frac{t_f(T_m - T_w)}{\rho_s r_i^{\,2}\lambda} - \frac{1}{h_w r_i}\right]} \tag{4.14a}$$

where, Ste is the Stefan number = $\frac{c_p(T_m - T_w)}{\lambda}$ and t_f is the time taken for complete solidification.

The above equation can further be simplified by neglecting the term, $\frac{1}{h_w r_i}$ as Yinping *et al.* (1999) have stated that,

$$\frac{t_f(T_m - T_w)}{\rho_s r_i^{\,2}\lambda} >> \frac{1}{h_w r_i}$$

Thus, we have,

$$k_s = \frac{[1+\text{Ste}]}{4\left[\frac{t_f(T_m - T_w)}{\rho_s r_i^{\,2}\lambda}\right]} \tag{4.14b}$$

To obtain the thermal conductivity of liquid PCM, the tube containing solid PCM is dipped into a hot water bath, which is at a temperature higher than the melting point of PCM. Once the time taken for the complete melting (t_m) is known, the expression for thermal conductivity of liquid PCM can be arrived following a similar procedure described above.

$$k_l = \frac{[1+\text{Ste}]}{4\left[\frac{t_m(T_w - T_m)}{\rho_l r_i^{\,2}\lambda}\right]} \tag{4.15}$$

In fact, Equations (4.14a) and (4.15) are obtained by neglecting second order term of the perturbation expansion. However, the error in the calculated values would be less significant i.e. < 5%, if the following conditions are satisfied.

- Bi < 0.1 - This is to ensure the one dimensional heat transfer
- Ste < 0.5 - This is because Ste is taken as the smaller perturbation parameter in the perturbation method and the variables (temperature, interface location and time) are expanded as powers in terms of

Ste (Caldwell and Kwan, 2003 and Caldwell and Kwan, 2009)

As mentioned earlier, employing a tube of smaller diameter to height ratio satisfies the condition, Bi < 0.1. To satisfy the condition Ste < 0.5, the difference between the melting temperature of PCM and the temperature of water bath should be chosen in accordance with the specific heat values and latent heat of PCM. In case of composite PCM (PCM with particles), the temperature difference can be higher, as the particle laden PCMs are expected to have lower specific heat values and latent heat as compared to pure PCM. Hence, the selection of water bath temperatures for both pure PCM and composite PCMs should be based on the results obtained from the *T-History* curves.

4.2.1.4 Experimental system for T-History curves

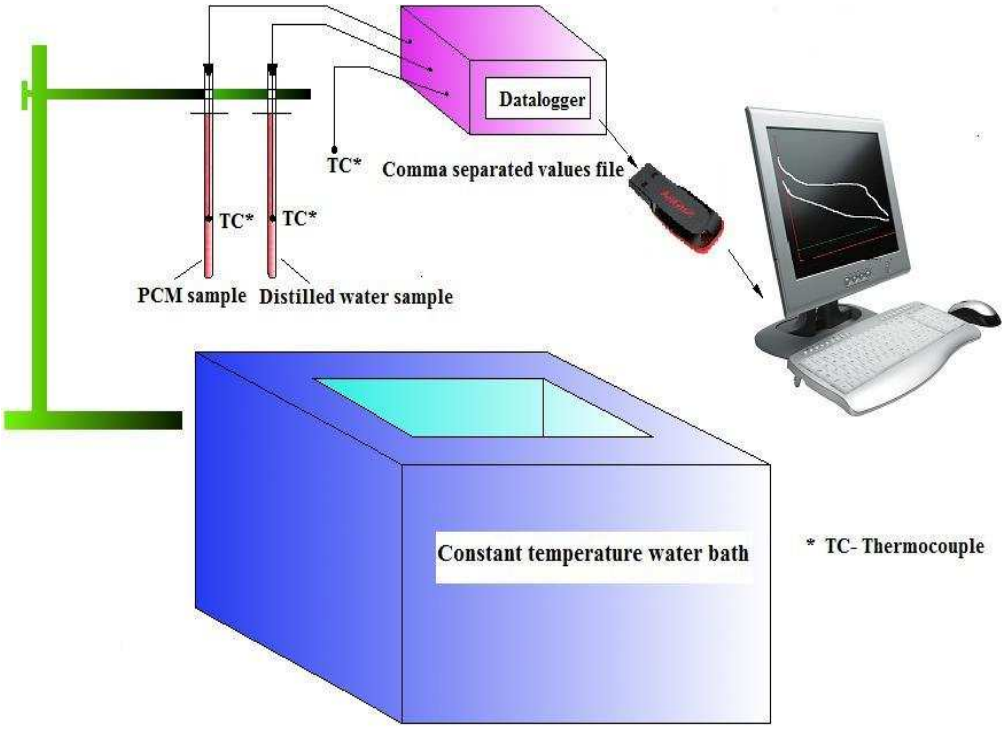

Figure 4.8 Schematic of *T-History* measurement system

To perform *T-History* measurements, a test rig was built, the schematic which is shown in Figure 4.8 and the photographic view is given in Appendix II (Figure A5). The set up comprises of,

- Two identical borosil glass tubes with inner diameter 13 mm and height 155 mm contain PCM-particles sample and distilled water (reference fluid)

- A thermostat controlled constant temperature water bath of working size 30 x 22.5 x 17.5 cm to heat the PCM-particles sample and distilled water to a same initial temperature (above melting point of PCM)
- Three k-type thermocouples of 0.2 mm diameter each to measure the temperatures of PCM-particles sample, water and atmosphere simultaneously during the cooling of PCM-particles sample
- A data logger (Model –FALCON 1600 DL with an accuracy of ± 0.5%, supplied by Scan Electronic systems, Pune) to record the temperature readings at equal time intervals

The two test tubes containing PCM-particles and water respectively were tipped into the constant temperature water bath. Two thermocouples were inserted into the test tubes centrally and along the axis and the third one was exposed to atmosphere. As soon as both the test tubes reached the same set temperature (say 10^{o}C above the melting point of PCM), the test tubes were suddenly removed from the water bath and were allowed to cool in the atmosphere. Right from the time the tubes were removed from the bath, all the three thermocouples readings at every 10 s were logged into the data logger and the data logging was continued till the samples reached the atmospheric temperature. Once the experiment was over, the temperatures data were collected from the data logger in the form of '*csv*' (comma separated values). From the collected values, the required *T-History* curves could be drawn. The experiments were repeated with different initial temperatures of samples to confirm the accuracy of the results. The obtained *T-History* curves and the subsequent results are discussed in Chapter 5.

4.2.1.5 Experimental system for thermal conductivity measurement

Initially, the PCM in the test tube was heated above its melting point using the water bath and is allowed to cool down by exposing to the atmosphere. The temperature of liquid PCM was being continuously monitored. When the temperature of sample was approximately equal to its melting point, the test tube was suddenly dipped into the constant temperature water bath, which was maintained at a temperature 2^{o}C lower than the melting point. The time taken for the complete solidification was noted down and was subsequently used to calculate the thermal

conductivity of solid PCM applying Equation (4.14b). Similarly, the solid PCM in the temperature at a temperature slightly lower (by 2^oC) than its melting point was tipped into the water bath whose temperature was just above the melting point (2^oC higher). The time taken for the complete melting was then used to calculate the thermal conductivity of liquid PCM as per Equation (4.15).

4.3 Heat transfer characteristics of PCM-micro particles composites

The numerical procedures employed to explore the phase change behavior of PCM-nano particles composites during melting and solidification are presented in the previous chapter. The thermal characteristics of micro particles dispersed PCM are also investigated numerically. However, numerical modeling technique adopted here is quite different from that one used for nano particles system. The following sections report the details of the numerical procedure applicable to micro particles dispersed PCMs.

4.3.1 Mathematical formulation

To investigate the melting and solidification heat transfer characteristics of micro particles-PCM composites, the same two dimensional computational model (Figure 3.4) employed for nano particles-PCM composites has been retained.

As discussed earlier, when nano particles are dispersed in the PCM, the uniformity of particles distribution can be ensured through ultrasonication. However, if the particles are of micro size, even the ultrasonication cannot help in obtaining the uniform distribution of particles, although it is possible initially. It is generally observed that there is migration of such micro size particles due to non-uniform shear fields in the liquid. This means that the particles migrate from higher shear rate regions to lower shear rate regions which lead to non-uniform distribution of particles in the liquid. Moreover, micro particles cannot have perfectly smooth surface like nano particles and thus, they cannot return to their original stream lines after the interactions (irreversible interactions). This results in non-uniform distribution. Hence, it becomes necessary to track the spatial variation of particle concentration at all times during the phase change processes. This is because the spatial variation of particle concentration results in mainly spatially varying effective viscosity and

thermal conductivity of liquid PCM. Therefore, the phase change heat transfer characteristics of micro particles dispersed PCM can be explored only if the changes of particle concentration and their effects are included in the formulation.

4.3.1.1 Governing equation for particle migration

To evaluate particle concentration, Phillips *et al.* (1992) have developed a constitutive equation which includes the effects of gradients of particles concentration and shear rate on particle migration. The equation is based on the following assumptions:

- The liquid in which particles are dispersed, is a Newtonian fluid
- The suspended particles are hard spheres

The constitutive equation is obviously a transport equation for particle flux which is developed by considering the two body irreversible interactions. One of the sources for particle flux is spatial variation of interaction frequency and the same is given as,

$$N_c = -K_c a^2 (e^2 \nabla \dot{\gamma} + e \dot{\gamma} \nabla e) \tag{4.16}$$

where a is the particle diameter (m) and $\dot{\gamma}$ is the strain rate (s^{-1})

The effect of shear rate gradient on particle migration, even if there is no particle concentration gradient, can be explored through the first term on the right hand side of Equation (4.16). On the other hand, the change in interaction frequency due to particle concentration gradient is described by the second term on the right hand side of Equation (4.16). Although the particle concentration in the mixture is uniform initially, due to the first term on the right hand side of Equation (4.16), there would be rise in particle flux. This would result in further flux according to the second term on the right hand side of Equation (4.16).

Apart from variation of interaction frequency, the spatial variation of viscosity which is the result of particle concentration gradient can also affect the particles interaction. This ultimately results in particle flux which is expressed as,

$$N_\mu = -K_\mu \dot{\gamma} e^2 \left(\frac{a^2}{\mu} \right) \frac{\partial \mu}{\partial e} \nabla e \tag{4.17}$$

The constants K_c and K_μ appear in Equations (4.16) and (4.17) respectively, are

experimentally evaluated values which are 0.41 and 0.62 respectively.

Now the rate of change of particle flux can be written as,

$$\frac{De}{Dt} = \nabla.(N_c + N_\mu) \tag{4.18}$$

Following the usual procedure, the material time derivative is expressed as sum of rate of change and convective terms. Thus,

$$\frac{\partial e}{\partial t} + u.\nabla e = \nabla.\left(a^2 e^2 K_c \nabla\dot{\gamma} + a^2 e K_c \dot{\gamma} \nabla e + a^2 e^2 \dot{\gamma} K_\mu \frac{1}{\mu}\frac{\partial \mu}{\partial e}\nabla e \right) \tag{4.19a}$$

Rearranging,

$$\frac{\partial e}{\partial t} + u.\nabla e = \nabla.\left[a^2 e \dot{\gamma}\left(K_c + K_\mu e \frac{1}{\mu}\frac{\partial \mu}{\partial e}\right)\nabla e \right] + K_c a^2 e^2 \nabla\dot{\gamma} \tag{4.19b}$$

The first term on the right hand side of Equation (4.19a) is the diffusive term with diffusive coefficient $\Gamma = a^2 e\dot{\gamma}\left(K_c + K_\mu e \frac{1}{\mu}\frac{\partial \mu}{\partial e}\right)$ and the second term on the right hand side of Equation (4.19a) is nothing but source term (S_e). Thus, the transport equation for particle volume fraction is expressed in general form as follows.

$$\frac{\partial e}{\partial t} + u.\nabla e = \nabla.(\Gamma \nabla e) + S_e \tag{4.19c}$$

It should be mentioned that Kim *et al.* (2008) have proposed two modifications to the original Phillips equation. However, it is also reported that the original models and the variant models are found to be qualitatively same. Moreover, Sun *et al.* (2009) have adopted original Phillips model to analyze the melting heat transfer characteristics of PCM slurry and produced reasonable valid results for dilute mixtures. Hence, the same model has been employed in this work.

4.3.1.2 Governing equations for phase change heat transfer

Following the continuum approach, the conservative equation for mass (continuity equation) is same as used for nano particles composites, i.e Equation (3.10) given in Chapter 3.

In case of nano particles system, the momentum equations are not solved and

the effect of motion of liquid PCM is simulated through effective thermal conductivity. However, for micro particles system, it becomes necessary to employ momentum equations too as particle transport equation (Equation (4.19c)) needs the solution of velocity field. Since both the pure PCM as well as composites PCM can be assumed as incompressible and Newtonian fluids, the momentum equation applicable is nothing but the well known Navier-Stokes equation and the same is expressed as,

$$\frac{\partial}{\partial t}(\rho u_i)+\frac{\partial}{\partial x_j}(\rho u_i u_j)=-\frac{\partial p}{\partial x_i}+\mu\frac{\partial^2 u_i}{\partial x_j^2}+\Delta\rho.g+S_i \tag{4.20}$$

The third term on the right hand side of Equation (4.20) is body force or buoyancy term which describes natural convection through density variation. This requires definition of density as a function of temperature. However, the Boussinesq model of natural convection allows defining the density as a constant value irrespective of temperature in all equations except for the buoyancy term in the momentum equation. Accordingly, the buoyancy term is given as,

$$\Delta\rho.g=\rho\beta(T-T_o)g \tag{4.21}$$

Using Equation (4.21), the momentum equation can now be written as,

$$\frac{\partial}{\partial t}(\rho u_i)+\frac{\partial}{\partial x_j}(\rho u_i u_j)=-\frac{\partial p}{\partial x_i}+\mu\frac{\partial^2 u_i}{\partial x_j^2}+\rho\beta(T-T_o)g+S_i \tag{4.22}$$

The momentum equation of the PCM is largely affected by the dispersion of particles as the particles addition changes the rheological behavior of the pure PCM. The change in rheological behavior of the PCM can be accounted for by defining the viscosity as a function of particle volume fraction. Accordingly, the effective viscosity of PCM is modeled by using Krieger equation (Krieger, 1972).

$$\mu_{eff}=\mu\left(1-\frac{e}{e_{\max}}\right)^{-1.82} \tag{4.23}$$

where e_{max} is the particle volume fraction when the effective viscosity tends to infinity and is found to be 0.68 for hard spherical particles.

The source term appears in the momentum equation is expressed as,

$$S_i = -Au_i \tag{4.24}$$

The above source term is introduced to allow the formulation to treat the solid and liquid phases of PCM as porous media. In a computational cell, the velocity of liquid has a finite value and it should become zero, if it full of solid. This can be formulated by defining the coefficient *A* in Equation (4.24) as a function of liquid fraction of the computational cell. i.e,

$$A(f_l) = \frac{C(1-f_l)^2}{f_l^3 + \varepsilon} \tag{4.25}$$

The constant *C* is called '*mushy zone constant'* and is set as 10,000. The other constant ε is a small computational constant taken as 0.001 to avoid division by zero arising from zero liquid fraction value.

Since momentum equation is employed here, the energy equation should have convective term too, unlike the one used for nano particles loaded PCM. The corresponding equation is given as follows.

$$\frac{\partial}{\partial t}(\rho h) + \frac{\partial}{\partial x_i}(\rho u_i h) = \frac{\partial}{\partial x_i}\left(k\frac{\partial T}{\partial x_i}\right) \tag{4.26}$$

However, the phase change process is modeled through the same enthalpy-porosity formulation as described in section 3.4.1.2 of Chapter 3.

4.3.1.3 Modeling of HTF flow and initial and boundary conditions

Since the conditions of HTF flow here in micro particles PCM system are same as those considered for nano particles PCM system, the conservation equations that describe the momentum and energy transfer of HTF are same as those described in Chapter 3, i.e, Equations (3.10) through (3.12).

Similarly, all the initial and boundary conditions defined for nano particles PCM system are retained for micro particles PCM system. However, an additional initial condition has to be applied for particle concentration. This initial condition declares that the particles of any volume fraction are uniformly distributed when $t = 0$. i.e,

$$e_{init} = e; \qquad 0 \le x \le L,\ 0 \le r \le R_i,\ t = 0;$$

4.3.2 Numerical solution

The solution of all governing equations were carried out employing the same commercial CFD software FLUENT. Hence, the computational methodology in view of geometry modeling, mesh generation, time step size, discretization scheme, under relaxation factors and convergence criteria, is same as mentioned in section 3.4. 4 of Chapter 3.

In case of nano particles PCM system, to define different thermal conductivity values for solid and liquid PCM, a UDF was written in 'C' code in such a way the thermal conductivity is a function of one of the solution variables temperature. Hence, during the solution, for any computational cell, depending on its temperature the corresponding thermal conductivity value can be applied. However, when it comes to micro particles system, the thermal conductivity is function of not only temperature but also of particle fraction which is another solution variable. This requires an altered UDF which takes into account the variation of thermal conductivity with respect to two solution variables, i.e. temperature and particle volume fraction. In addition to that, another UDF which defines the particle fraction dependent viscosity was also compiled.

The major difference between modeling of nano and micro particles systems lies in the form of particle flux equation. As far as solver is concerned, the particle flux equation is nothing but an additional transport equation for an arbitrary scalar. Hence, the particle flux has to be defined as a scalar. User defined scalar (UDS) option was executed for the same. The corresponding code is given in Appendix III. Moreover, two UDFs were also required to define the diffusion coefficient and source term of particle flux equation.

4.4 Experimental set up

An experimental test rig was built in house to verify the accuracy of the numerical model that corresponds to PCM-micro particles composites. The schematic of the experimental apparatus is shown in Figure 4.9 and the photographic view is given in Appendix II (Figure A6). The main test section was made in the form of two co-axial cylindrical tubes. The outer acrylic tube which is of inner diameter 9 cm and

outer diameter 10 cm is having sealed bottom cover and removal top cover. The removal cover facilitates the easy filling and removal of PCM. Moreover, the unsealed top cover allows the air to escape during melting of PCM. The inner tube made of copper (diameter 1.9 cm and thickness 0.1cm) allows the hot/cold water to flow downwards. The annular space between the inner and outer tubes serves as storage compartment for PCM-particles composites. The effective height of test section is 10 cm. The entire test section including the top and bottom surfaces were covered with glass wool insulating material.

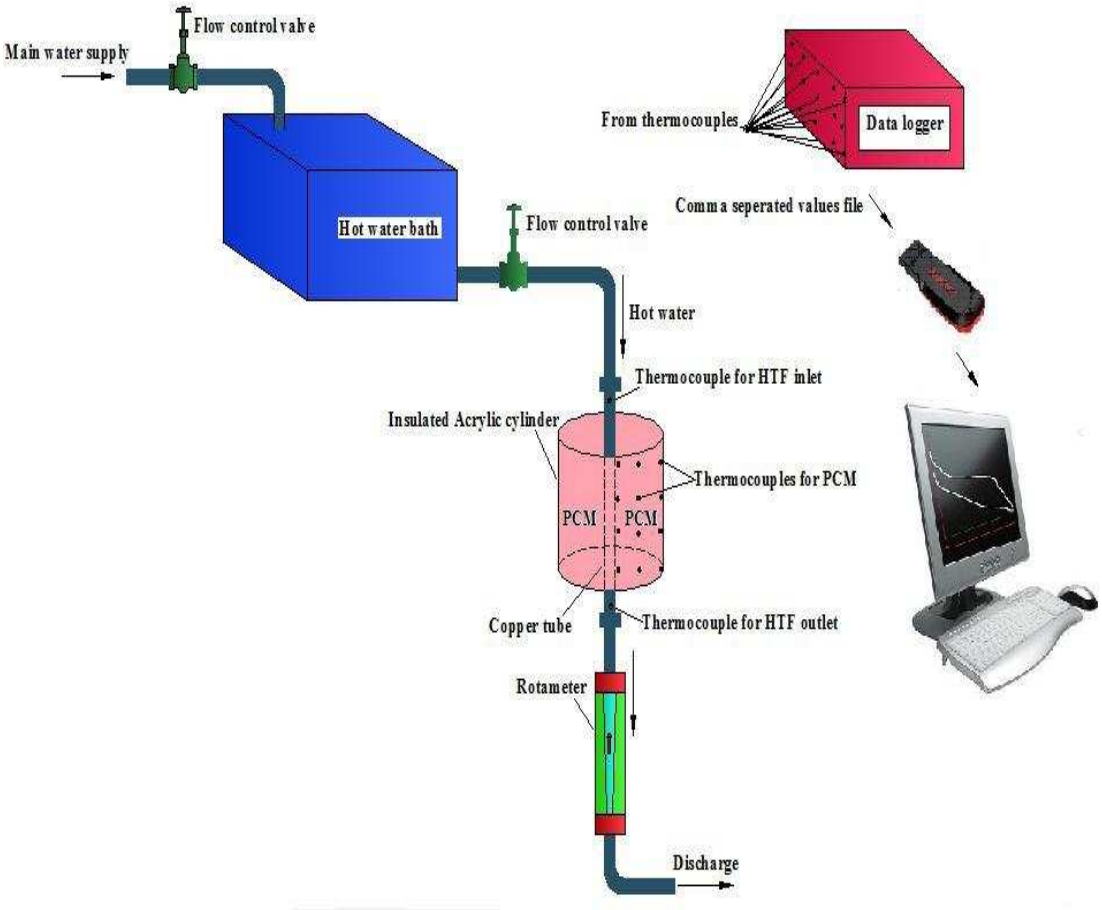

Figure 4.9 Schematic of experimental set up for melting and solidification of PCM-micro particles composites

A water bath located above the test section was used to supply water at constant temperature with an accuracy of ±2^{o}C. Two flow control valves were used at inlet and outlet of the water bath to maintain uniform supply to the test section. The copper tube discharges water freely into the atmosphere. For flow rate measurements, a

rotameter was used. During the experiments, temperatures of PCM were measured at different radial and axial locations. Nine k-type thermocouples were inserted at radial positions 0.5 cm, 3 cm and 4 cm from centre of the test section and at axial positions 3 cm, 6 cm and 9 cm from the top. Since the test section is oriented vertically, axisymmetric phase change processes are expected to occur around the inner tube. This allowed us to investigate the temperature distribution in only one half of the test section. Hence, all the nine thermocouples are placed on the right side PCM. In addition, two thermocouples were used to measure the inlet at outlet temperatures of water.

This chapter presents the results of performance characteristics of high conductive particles dispersed LHTS system. Two PCMs, one is organic material (paraffin wax) and the other is inorganic material (salt hydrate), and copper as high conductivity particles for both PCMs are selected for the analysis. The thermal performance enhancement due to the addition of nano size as well as micro size copper particles into the above PCMs is investigated to assess the influence of particle size in the heat transfer characteristics of PCMs. The energy storing and releasing capabilities of LHTS system are assessed in terms of exergy parameters employing second law of thermodynamics.

5.1 Validation of numerical modeling

Before proceeding with the present analysis, the accuracy of numerical techniques employed was verified with results of literature work and own experimental work. The model adopted for analyzing the heat transfer characteristics of pure PCMs was checked against the results of the reported experimental work by Trp (2005). Similarly, for the validity of model for PCM-micro particles composites, some experimental trials were performed in house. Since no experimental results could be traced in literature work for nano particles added PCMs or no in house experiments could be performed due to economical constraints either, the relevant model is not validated. However, one of the keys in modeling nano mixtures, i.e., the Maxwell's expression was validated as already discussed in Chapter 3.

5.1.1 Validation of model for pure PCM system

Trp (2005) has reported the heat transfer characteristics of technical grade paraffin (T_m 300.7 K) loaded in a shell and tube unit. The dimensions of the unit are:

tube inner diameter	0.033 m
tube outer diameter	0.035 m
shell inner diameter	0.128 m
shell outer diameter	0.133 m
tube length	1 m

The experiments were conducted for vertically oriented unit with water as HTF. Since the experimental set up is similar to the one considered in this work, the same unit was analyzed using present model.

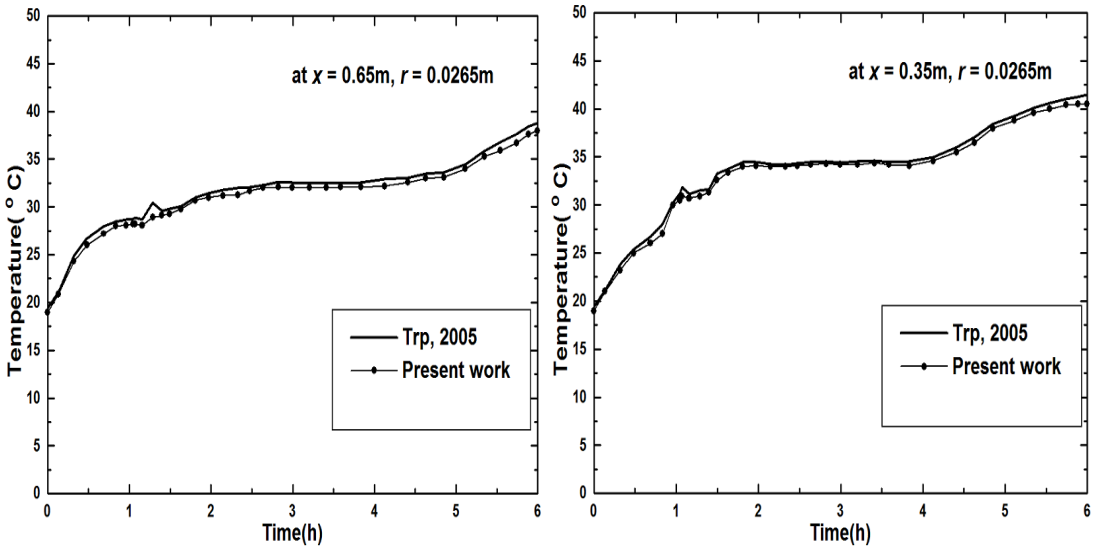

Figure 5.1 Comparison of results of numerical model employed for melting of pure PCM with those of Trp (2005)

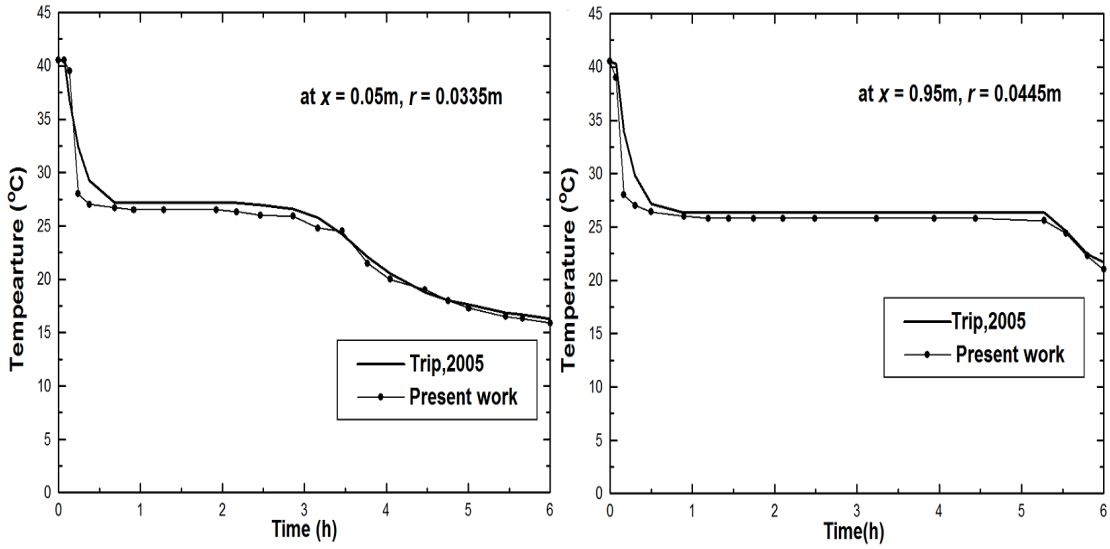

Figure 5.2 Comparison of results of numerical model employed for solidification of pure PCM with those of Trp (2005)

The temperature distribution in the PCM during melting and solidification was obtained using the present numerical model. In each case of processes, two different locations were selected, which are x = 0.35 m, r = 0.0265 m and x = 0.65 m, r = 0.0265 m for melting and x = 0.05 m, r = 0.0335 m and x = 0.95 m, r = 0.0445 m for

solidification. The numerical results of time wise variations of PCM's temperatures at the above locations were compared with the corresponding values of Trp (2005).

The comparisons are shown in Figure 5.1 and 5.2, and it is clear that the present results agree reasonably well with those of Trp (2005) with an average deviation of 2%. At one or two time instants, however, the deviation is found to be exceeding 10 %. The deviation could be due to the fact that the conditions of constant HTF inlet temperature and no heat loss from the system, which are imposed in the numerical analysis, are hard to realize exactly in the physical environment. Nevertheless, the deviation is within the acceptable limit and thus, the modeling procedure can be stated as fairly accurate.

5.1.2 Validation of model for PCM – micro particles system

For the validation of numerical results of micro particles based PCM composites, melting and solidification experiments were performed using the experimental test rig explained in Chapter 4.

During melting experiments, the PCM-particles composites were loaded at atmospheric temperature and hot water at a temperature 75^{o}C (higher than the melting temperature of paraffin wax) was supplied by the water bath continuously. The melting experiments were continued till all the thermocouple showed the same temperature. Immediately after that, cold water at room temperature was supplied directly from the main line. The supply of cold water continued till the entire PCM solidified. The temperatures were recorded by a 16-channel datalogger at every 20 s and transferred to a computer for further processing. The experiments were conducted for only paraffin wax composites of particle volume fraction 0.1 and 0.2.

The test section of same size and material was then modeled using GAMBIT and the melting and solidification of PCM-micro particles composites (10% and 20% particle volume fraction) were simulated using the numerical procedure explained in Chapter 4. The temperature variation of water entering the test section was ignored in the numerical simulation. Similarly, the heat flux through the outer surfaces was assumed to be zero.

The numerically explored transient temperature values at locations of thermocouples were then compared with the corresponding experimentally recorded

values. Figure 5.3 and Figure 5.4 presents the comparison for representative locations. As it can be seen, certain discrepancy between numerical and experimental results is observed. It can also be noticed that the deviation of numerical results from experimental measurements is relatively higher during melting.

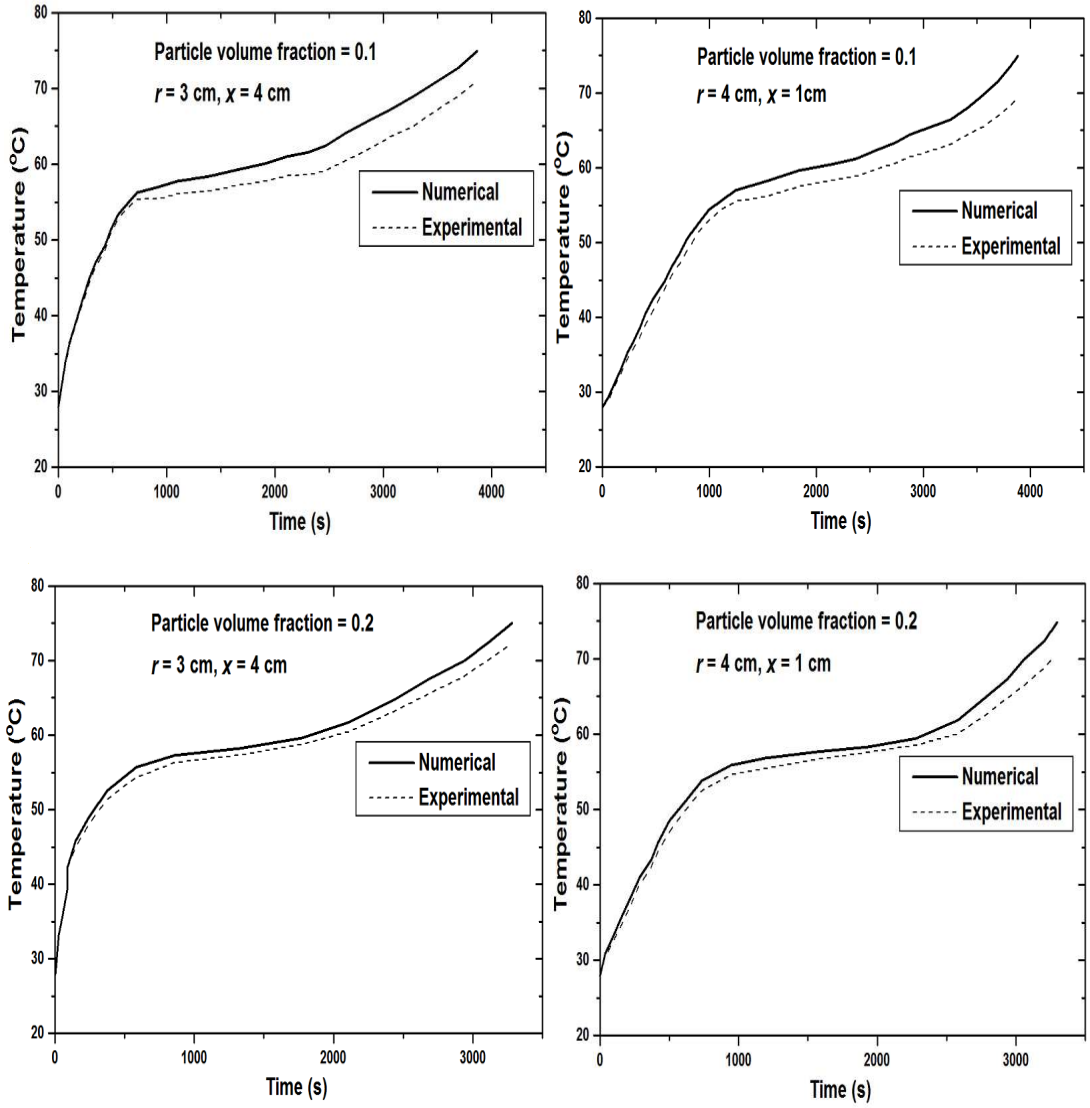

Figure 5.3 Comparison of results of numerical model employed for melting of PCM-micro particles with those of experiments

As it is discussed in the later part of this chapter, the composite PCMs suffer from uneven distribution of particles due to particle migration from one region to other regions. The non-uniform distribution of particles calls for definition of thermal properties as functions of the variable, i.e. particle volume fraction. However, the CFD code used in this work permits to define only thermal conductivity as a variable

and the specific heat and latent heat values are to be defined as constants. This limitation results in some difference between numerical and experimental results. Since the particle migration is found to be prevailing only during melting process, the definition of constant specific heat and latent heat could not affect the solidification results. Similarly, the effect of particle migration is stronger in composites of lower particle fraction and thus, the deviation of numerical results from experimental measurements is more pronounced in case of composites with 0.1 particle fraction. In general, the deviation increases as the time progresses due to stronger particle migration at later stages of melting.

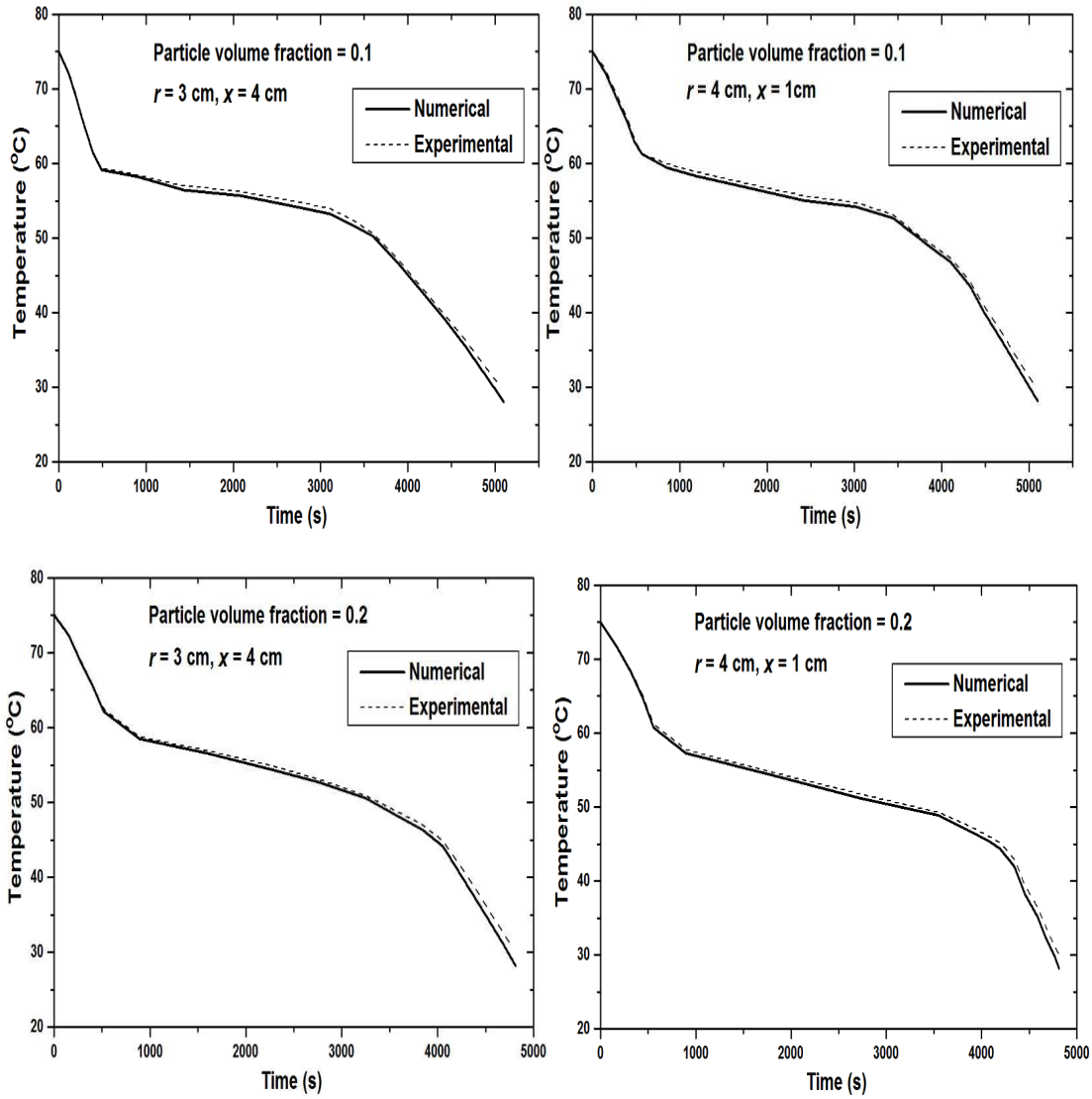

Figure 5.4 Comparison of results of numerical model employed for solidification of PCM-micro particles with those of experiments

In case of solidification, discrepancy arises due to mainly the difficulty in maintaining the adiabatic wall conditions and variation of temperature of HTF at the inlet during experimentation. Experimental uncertainties have also contributed to a certain extent. Despite the deficiency, the predicted values are qualitatively correct and the results confirm the validity of the adopted numerical model.

5.2 Heat transfer performance of LHTS unit employing PCM-nano particles

The first part of investigation focuses on the effect of nano copper particles on the transient behavior of the LHTS unit for various key operating/design conditions and amount of embedded particles. The parameters involved in the present analysis are shown in Table 5.1. A complete analysis of the LHTS unit has to consider the collective/individual influence of these on the performance of the unit. The LHTS heat exchanger unit analyzed corresponds to a solar water heater application and the simulation was carried for both charge and discharge phases.

Table 5.1 Range of input parameters

Parameter	Values	
	Solidification	Melting
Re of HTF flow	500, 2000, 10000	500, 2000, 10000
HTF inlet temperature (K)	283,287,293	340,345,350
Particle volume fraction	0,0.05,0.1,0.15,0.2	0,0.05,0.1,0.15,0.2

5.2.1 Effect of HTF mass flow rate on phase change rate

The heat transfer coefficient at HTF side is expected to play key role in determining the heat transfer performance of LHTS heat exchanger. The mass flow rate of HTF is one of the parameters that control the heat transfer coefficient, which in turn controls the phase change rate of PCM. From this perspective, different Reynolds numbers (Re = 500, 2000 and 10000) were considered to investigate the influence of mass flow rate of HTF on the melting or solidification rate. This means both laminar and turbulent flows of HTF have been taken into account. Accordingly, the influence of Re on the time required for complete solidification and complete

melting was first observed and the results are shown in Figure 5.5. Whether the system is loaded with pure PCM or with PCM-particle composites, the time for complete solidification or melting is not much affected by Re. For instance, when paraffin was used as PCM, a maximum of only 9 % decrease in time required for complete solidification could be achieved even by increasing Re from 500 to 10000. In case of melting, the benefit of increasing Re from 500 to 10000 is even less significant as the decrease in time is found to be only 5 % maximum. Similar results were also observed for the system employing hydrated salt as PCM.

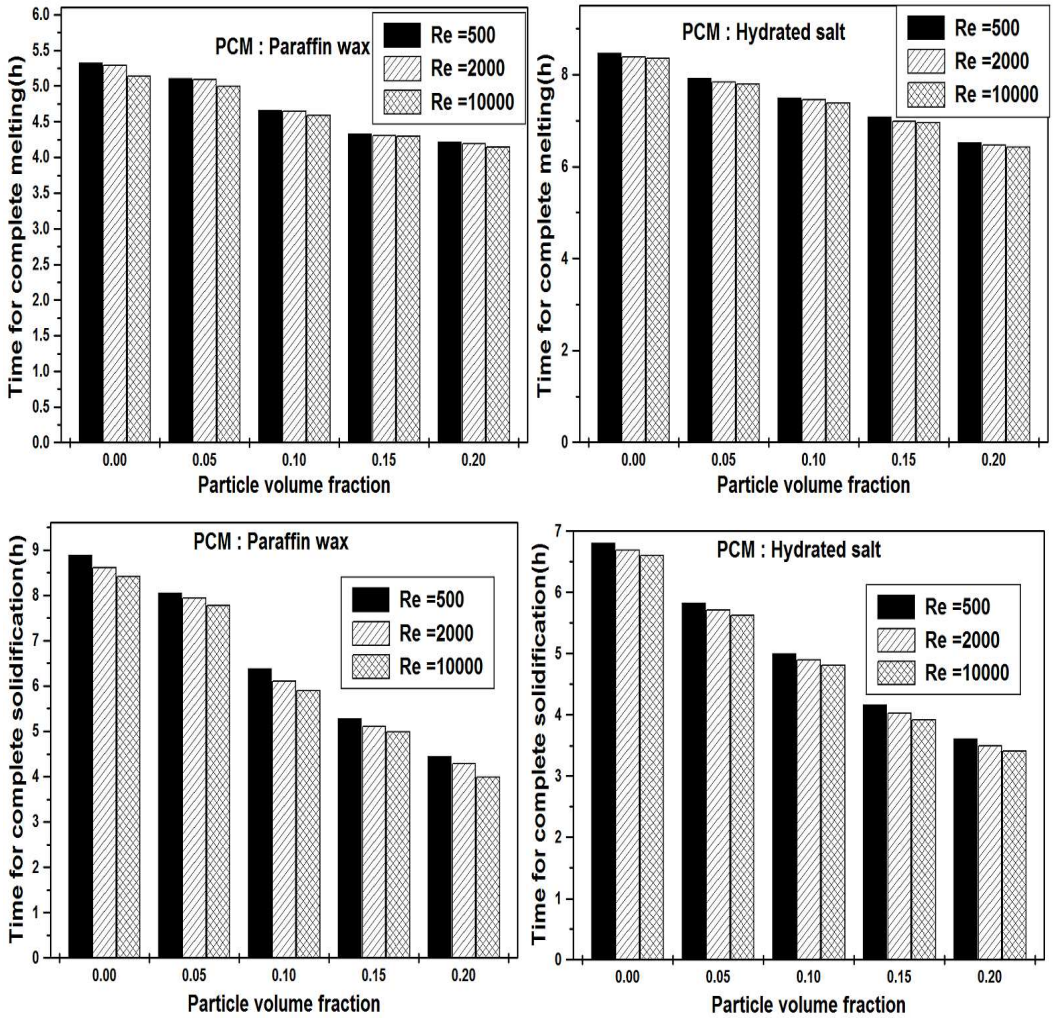

Figure 5.5 Influence of Re of HTF flow on time for complete phase change of nano particles composites

To explore further details, the values of instantaneous heat transfer rates of various Re during the phase change processes are compared and the comparison is

illustrated in Figure 5.6.

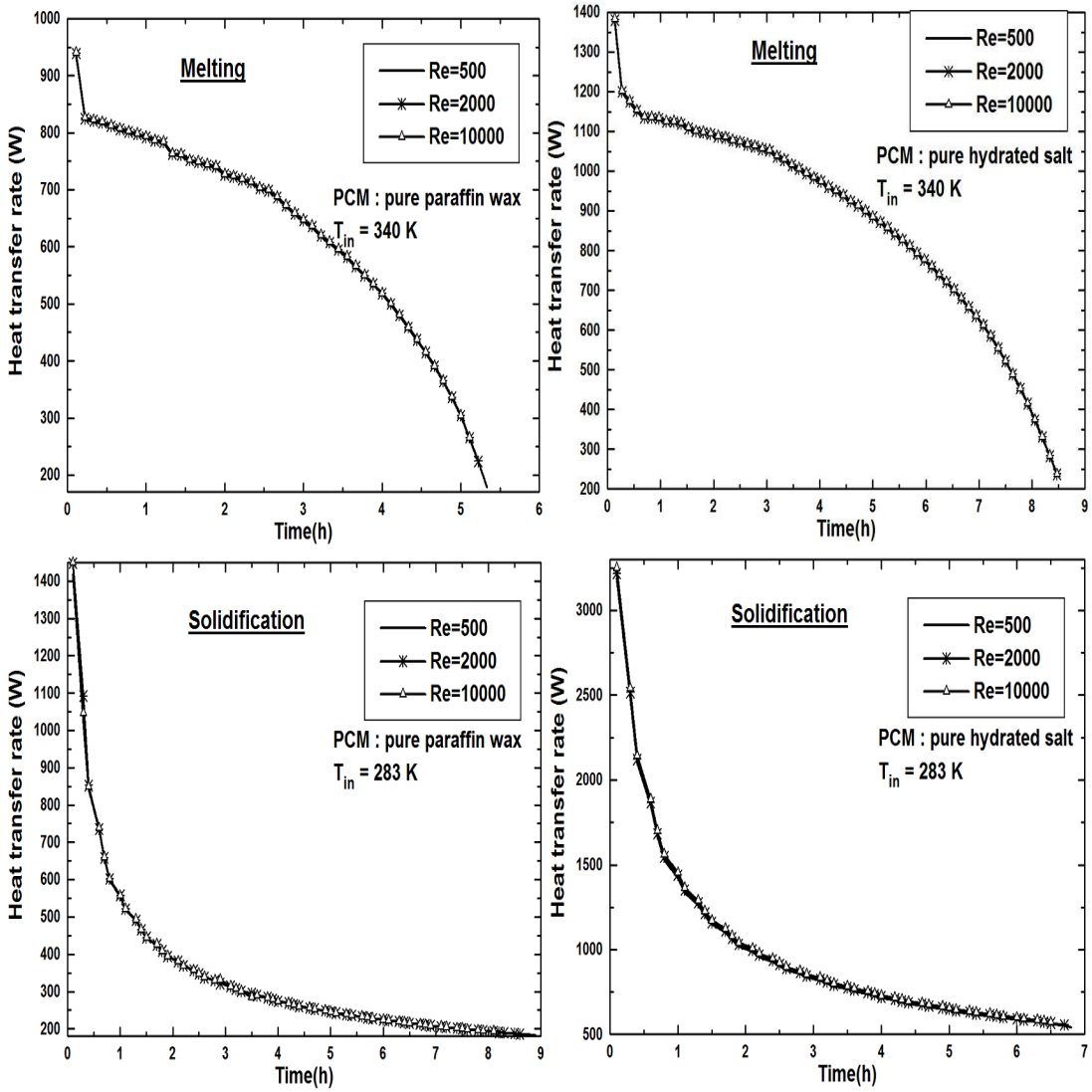

Figure 5.6 Instantaneous heat transfer rates during phase change of nano particles composites for various Re

At all Re, higher values of heat transfer rate are observed in the beginning. However, it reduces suddenly and remains at lower values as the phase change progresses. This is because of lower temperature difference between PCM and HTF that prevails as the time progresses. As it can be seen from the Figure 5.6, the increase in Re does not make much difference in the heat transfer rate. It should be mentioned that overall a maximum of only 3% increase in instantaneous heat transfer rate could be achieved even by increasing the Re from 500 to 10000. Moreover, this maximum increase is only in the initial stage of the phase change and the same decreases as the

time progresses. In other words, the solidification and melting rates cannot be enhanced significantly by increasing HTF mass flow rate despite increase in HTF side heat transfer coefficient. This indicates that the HTF side heat transfer coefficient has very small role in determining the phase change rate. Hence, it may be stated that the PCM side heat transfer coefficient is the one which has a major role to play. The PCM side heat transfer coefficient is determined by PCM's thermal resistance, which cannot be affected by Re or HTF mass flow rate. Since the dominant PCM side thermal resistance remains same despite the increased heat transfer coefficient at HTF side due to higher Re, the increase in phase change rate appears insignificant. Hence, reducing the PCM thermal resistance may be the most preferable option over increasing HTF mass flow rate for enhancing heat transfer performance of PCM. This has prompted to present further results only for Re =500.

Table 5.2 Percentage decrease in complete melting time due to nano particles addition for Re = 500

Particle fraction / T_{in} (K)	Decrease in complete melting time (%)					
	Paraffin wax			Hydrated salt		
	340	345	350	340	345	350
0.05	4.2	6.7	4.5	6.5	5	6.8
0.1	12.5	13	10	11.5	10	10
0.15	16.7	20	18	16.5	15	17
0.2	21	23	22.7	20.5	20	20.5

The decrease in thermal resistance of PCM means increase in PCM side heat transfer coefficient, which can be achieved by promoting the concerned heat transfer mechanisms at PCM side. In an attempt to enhance the PCM side heat transfer coefficient, high conductivity particles were dispersed into the PCMs. Before getting into the insight of heat transfer characteristics of particles added PCM, the immediate benefit can be verified from the already discussed graph, i.e Figure 5.5. As stated earlier, increasing Re could not shorten the time for complete phase change much. On the other hand, at any Re, particle added PCMs (both paraffin and hydrated salt) require less time for the complete phase change. This can further be clarified from Tables 5.2 and 5.3, which presents the percentage decrease in time for complete phase

change due to addition of high conductivity particles. We can also notice an increase in percentage decrease as the volume fraction of particles increases even when Re is low (HTF heat transfer coefficient is low). Moreover, this seems to be more or less consistent at all values of HTF inlet temperature. Although the reduction is considerable for both melting and solidification, it is relatively less in case of former as compared to latter. The potential reason for the same is discussed in the next section.

5.2.2 Heat transfer characteristics

To explore the insight of heat transfer characteristics of particles added PCM, the heat transfer rates during the phase change processes were first examined. Since the phase change processes are transient, the heat transfer rate values at regular time interval were tracked till the completion of phase change processes. The resultant plots corresponding to solidification and melting are presented in Figure 5.7 and 5.8, respectively. The results of instantaneous heat transfer rates obtained during solidification process (Figure 5.7) reveal that right through the solidification the heat transfer rate at any given time is higher for higher values of particle volume fraction. For instance, in case of paraffin wax a maximum of 13% increase in instantaneous heat transfer rate is possible by adding particles of 0.1 volume fraction. The percentage increase in instantaneous heat transfer rate increases with increase in volume fraction of particles. Also, for any value of volume fraction, the percentage increase in instantaneous heat transfer rate almost remains constant at all times. The increased heat transfer rates as a result of particles are pronounced also in the case of hydrated salt. This is due to the fact that high conductivity particles accelerate the conduction dominated solidification at all times till the completion of solidification.

During melting, both the PCMs show a significant change in heat transfer characteristics as revealed by Figure 5.8. A significant improvement in heat transfer rate due to increase in particle fraction can be seen especially in the earlier stages of melting. This is because of enhanced thermal conductivity of PCM. On the other hand, the heat transfer rate in the PCM-particle mix system becomes lesser than that in the pure PCM case at later stages. Since the later stages of melting are dominated by natural convection, the enhanced thermal conductivity doesn’t seem to be helpful

to improve the convection rate. In fact, the addition of particles leads to decrease in buoyancy force and increase in viscous force, which in turn dampens the natural convection. This dampening effect becomes stronger and stronger as the particle fraction increases. This is the reason why the heat transfer at later stages of melting decreases with increase in particle fraction.

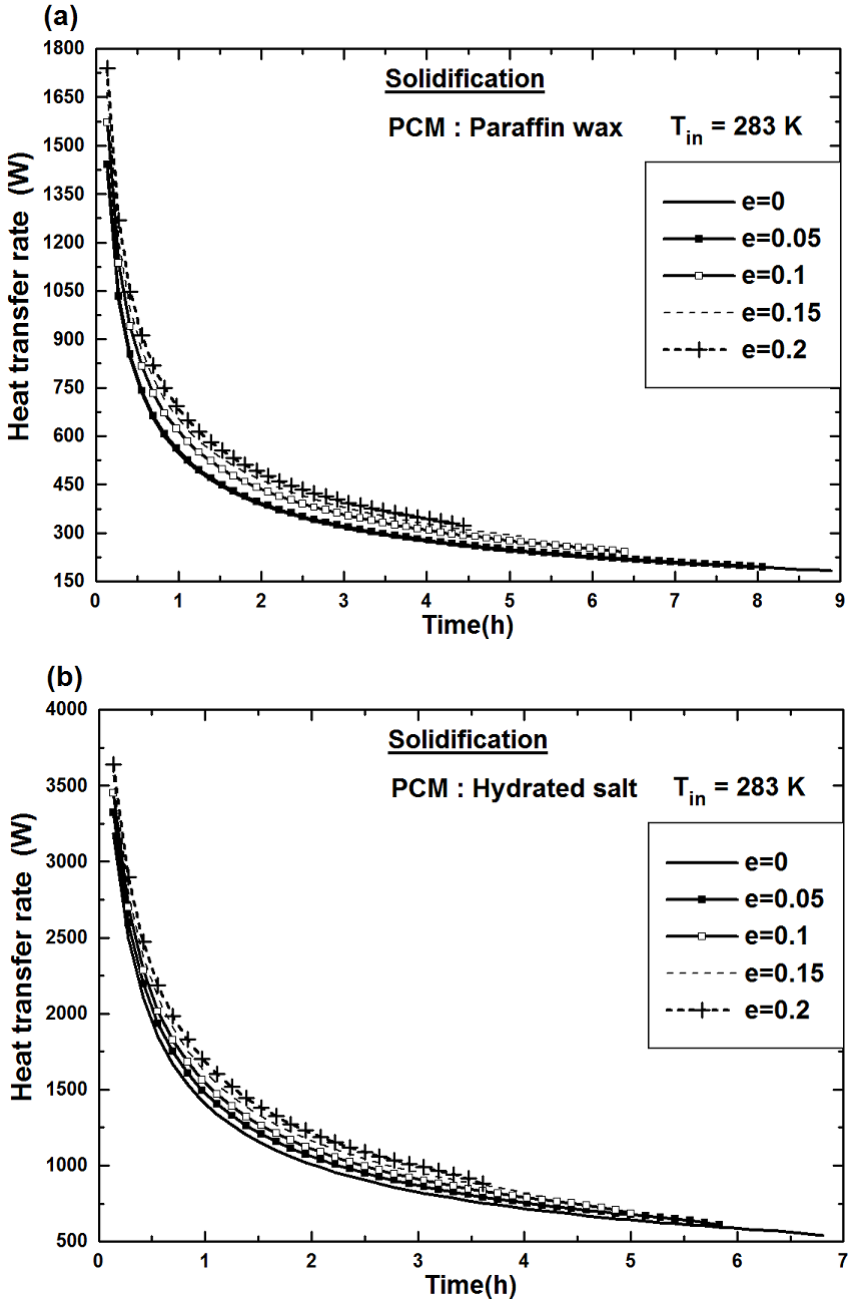

Figure 5.7 Effect of particle volume fraction on instantaneous heat transfer rate during solidification of nano particles composites (a) paraffin wax as PCM (b) hydrated salt as PCM

Although particle dispersion does not enhance the heat transfer rate all the time, the increase in heat transfer rate in the earlier stages is more significant than decrease at the later stages. Hence, the overall heat transfer rate could be enhanced even during melting by particle dispersion.

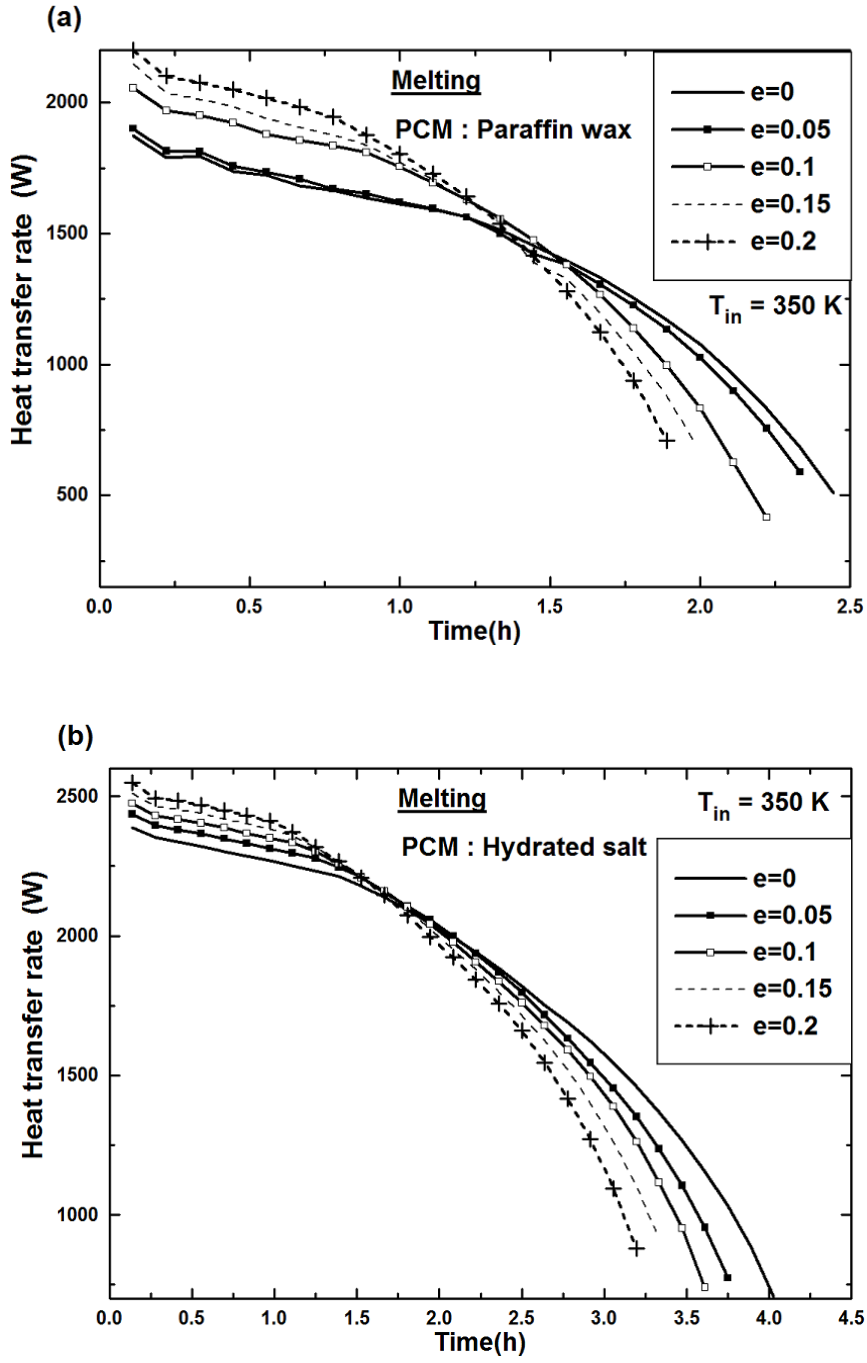

Figure 5.8 Effect of particle volume fraction on instantaneous heat transfer rate during melting of nano particles composites (a) paraffin wax as PCM (b) hydrated salt as PCM

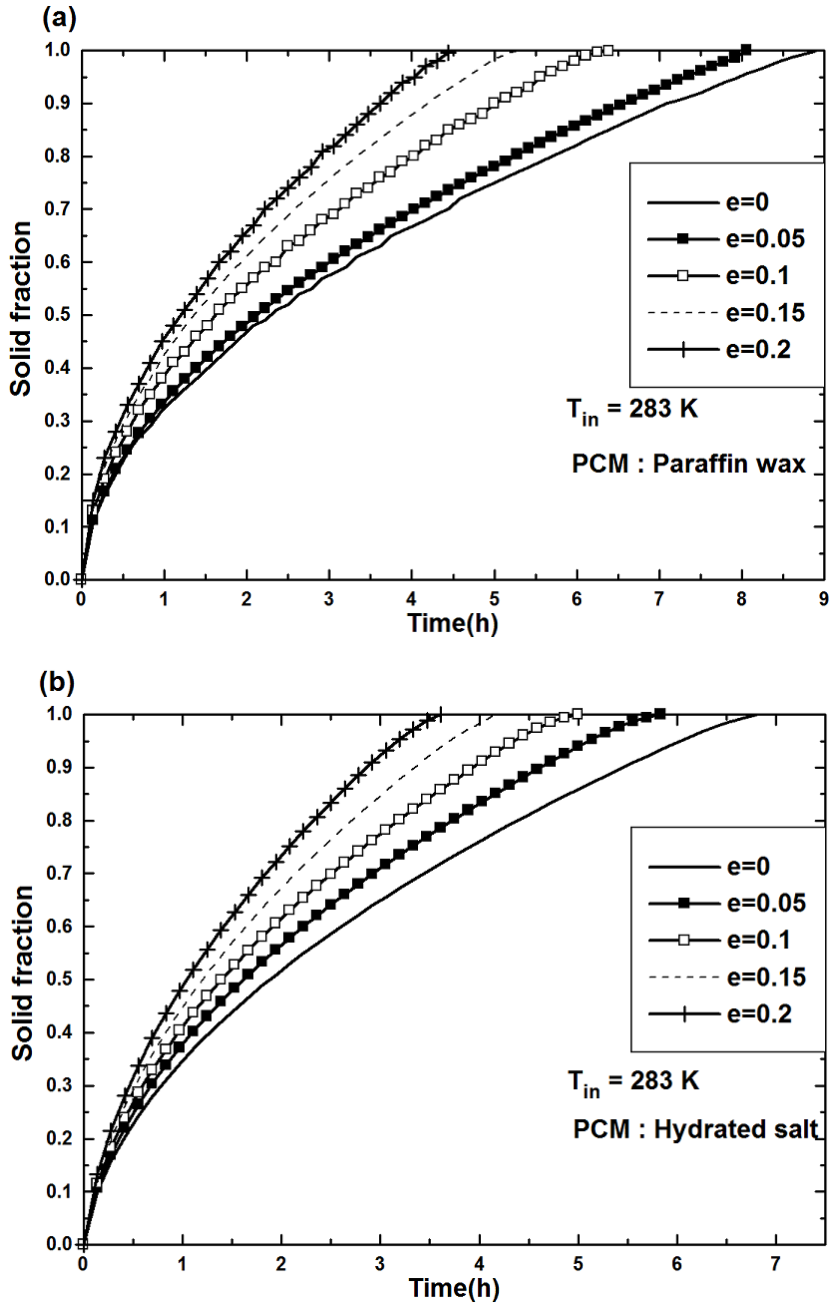

Figure 5.9 Effect of nano particles volume fraction on instantaneous solid fraction (a) paraffin wax as PCM (b) hydrated salt as PCM

The effect of higher transfer rates due to particle addition was further verified by tracking the state of PCM or phase change process at regular time intervals. The state of PCM at any instant during solidification can be visualized through the instantaneous solid fraction value (volume fraction of PCM that has been solidified). The solid fraction of 1 indicates the end of solidification process. Figure 5.9 presents the variation of solidified fraction with time. It can be seen that composite mixtures

exhibit higher solid fraction at all times as a result of high heat transfer rates. Since solid fraction is higher, it can be stated that the latent heat release is more in case of composite PCMs as compared to pure PCM. As the particle volume fraction increases, the solid fraction increases and so is the latent heat. Furthermore, due to higher values of solid fractions only, reduction in complete solidification time could be obtained as seen from Table 5.3.

Table 5.3 Percentage decrease in complete solidification time due to nano particles addition for Re = 500

Particle fraction / T_{in} (K)	Decrease in complete solidification time (%)					
	Paraffin wax			Hydrated salt		
	283	287	293	283	287	293
0.05	9	10	8	14	15	15
0.1	28	30	29.5	26.5	28.3	28.3
0.15	40	42	41	39	37.7	38.3
0.2	50	51	50	47	47.2	46.7

Similar to solid fraction, the liquid fraction can be used to examine the state of PCM during melting. Figure 5.10 shows the instantaneous liquid fraction values during melting. As it is shown earlier, in composite PCM systems, the heat transfer rate is found to be higher at the earlier stages. Hence, the liquid fraction values of composite PCM systems are also higher than that of pure PCM system. At the same time, it should be mentioned that the same remains higher throughout the melting despite lower heat transfer rates in the later stages. Since initial heat transfer rates have already increased the liquid fraction, the lower heat transfer rates afterwards could not have much impact on the same. However, the effect of lower heat transfer rate is also felt as the increase in liquid fraction due to particle addition narrows down as the time progresses. Because of this reason the percentage decrease in complete melting time due to particles is relatively less as compared to percentage decrease in complete solidification time as presented in Table 5.2.

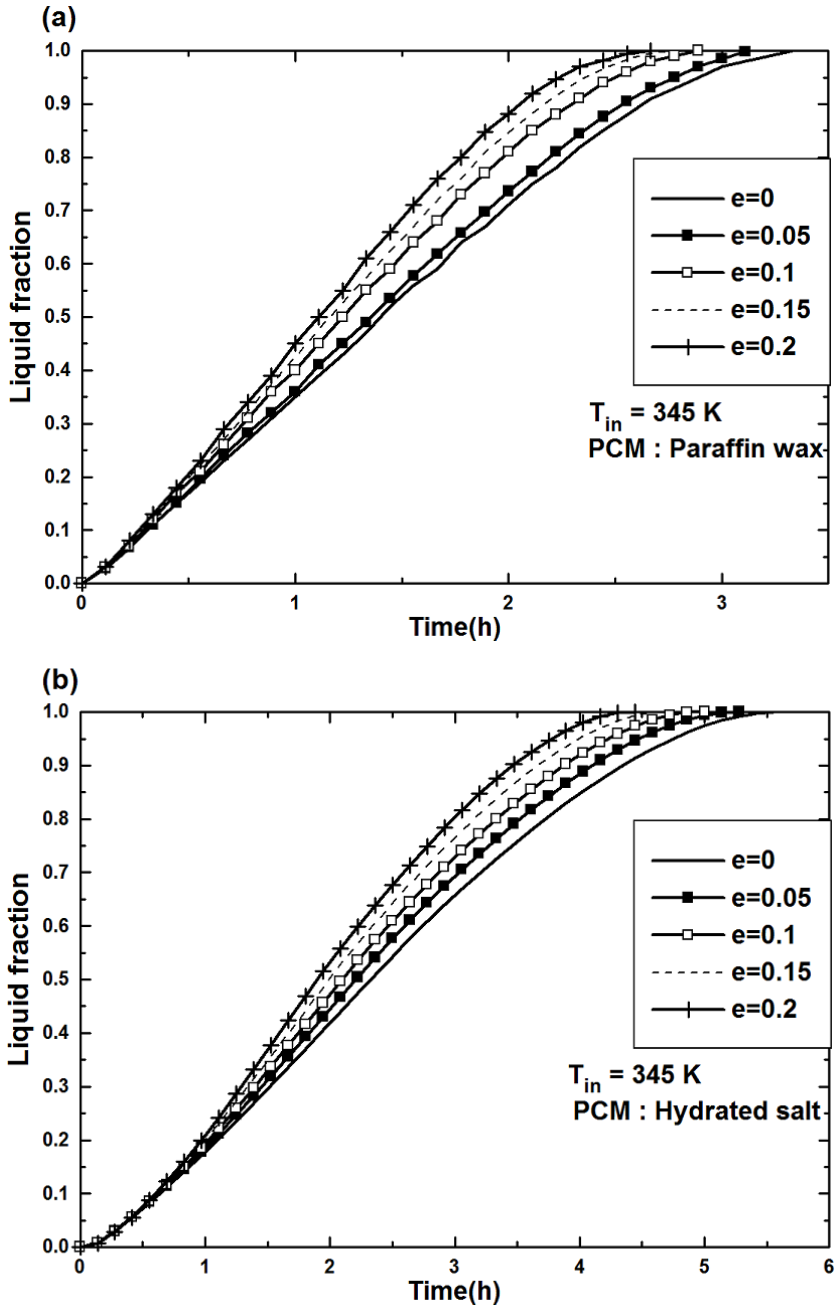

Figure 5.10 Effect of nano particles volume fraction on instantaneous liquid fraction (a) paraffin wax as PCM (b) hydrated salt as PCM

5.2.3 Paraffin wax Vs Hydrated salt

The heat transfer performance of paraffin wax composites is compared with that of hydrated salt composites to measure the relative benefit of particle addition. Although both the PCMs possess same melting points, other thermphysical properties are different and thus, different heat transfer characteristics may be expected.

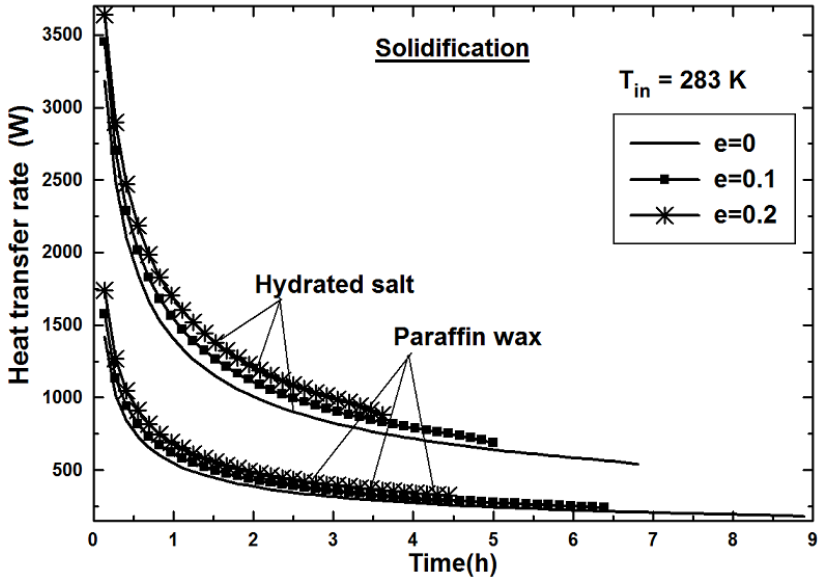

Figure 5.11 Comparison of solidification heat transfer rates of paraffin wax –nano particles PCMs with that of hydrated salt –nano particles PCMs

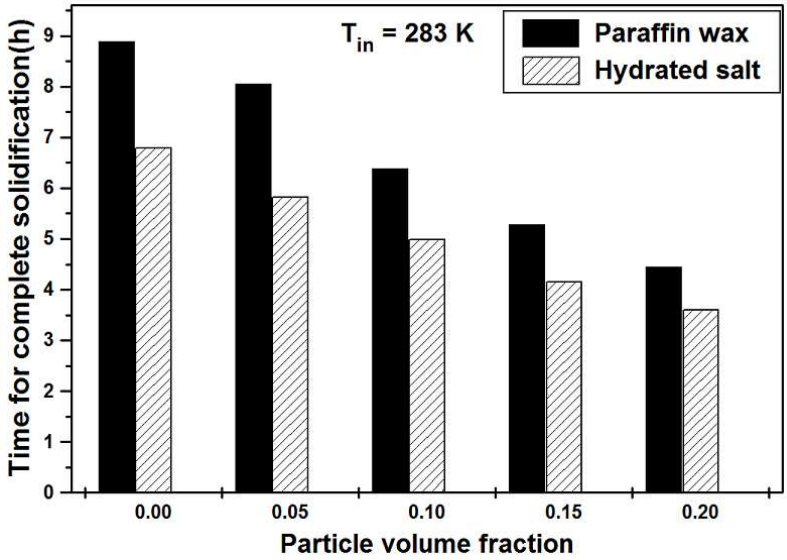

Figure 5.12 Comparison of complete solidification times of paraffin wax –nano particles PCMs with that of hydrated salt –nano particles PCMs

As far as heat transfer rate during conduction dominated solidification is concerned, the thermal conductivity is the only deciding factor under similar operating conditions. Since the thermal conductivity of pure hydrated salt is higher than that of pure paraffin wax, particles of any volume faction makes composite hydrated salts more conductive than paraffin composites. Hence, the heat transfer rates exhibited by hydrated salt composites of any particle fraction are found to be

much higher as compared to their paraffin wax counterparts. This can be seen in Figure 5.11. It should also be noted from the results that the increase in heat transfer rate due to particles addition is more in case of hydrated salt than in paraffin wax. This clears that during solidification, the effect of particles on the heat transfer performance enhancement is more pronounced if PCM of relatively high thermal conductivity is employed. Because of high transfer rates the former group needed much lesser time to solidify than the latter one as seen from Figure 5.12.

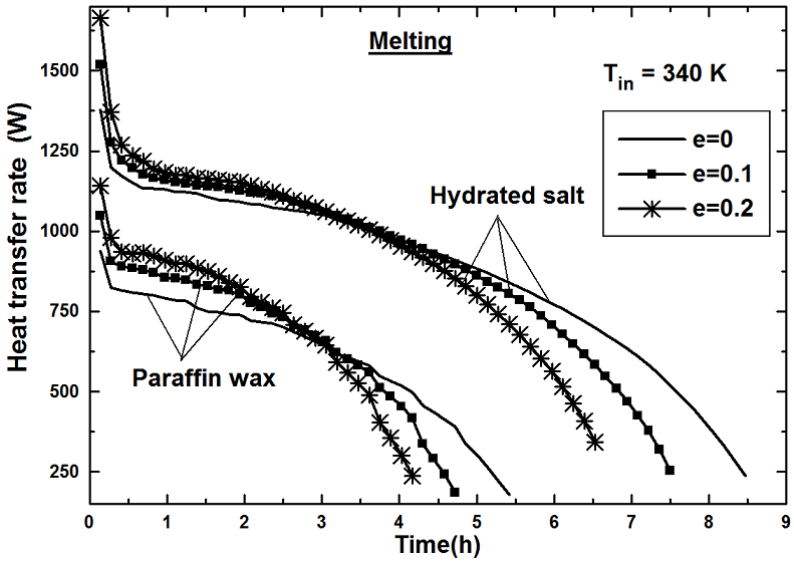

Figure 5.13 Comparison of melting heat transfer rates of paraffin wax –nano particles PCMs with that of hydrated salt –nano particles PCMs

The higher heat transfer rates are observed with pure or composite hydrated salts also during melting process as revealed by Figure 5.13. However, unlike for solidification, hydrated salt based pure or composites take more time for complete melting than their paraffin based pure or composites. This is shown by Figure 5.14. The reason for the longer melting duration despite exhibiting higher heat transfer rates can be briefed as follows:

During melting PCM transfers heat through the tube wall to the nearby layer of PCM in the shell. In the beginning, the solid hydrated salt obviously receives more heat than paraffin wax due to the former's high thermal conductivity. Even after melting, the same layer (but in liquid form) can receive more heat as the liquid hydrated salt also possess more thermal conductivity than liquid paraffin. That is why throughout the melting process, the instantaneous heat transfer rates remain higher in

case of hydrated salt PCMs. However, the rate of melting of remaining layers depending upon the heat transfer rate from one layer to another adjacent layer in the radial direction. This heat transfer rate is mainly by convection rather than conduction.

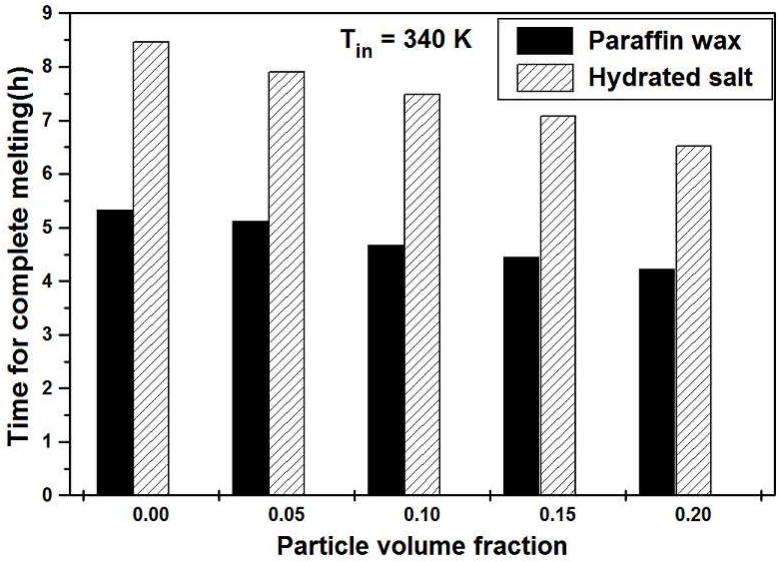

Figure 5.14 Comparison of complete melting times of paraffin wax –nano particles PCMs with that of hydrated salt –nano particles PCMs

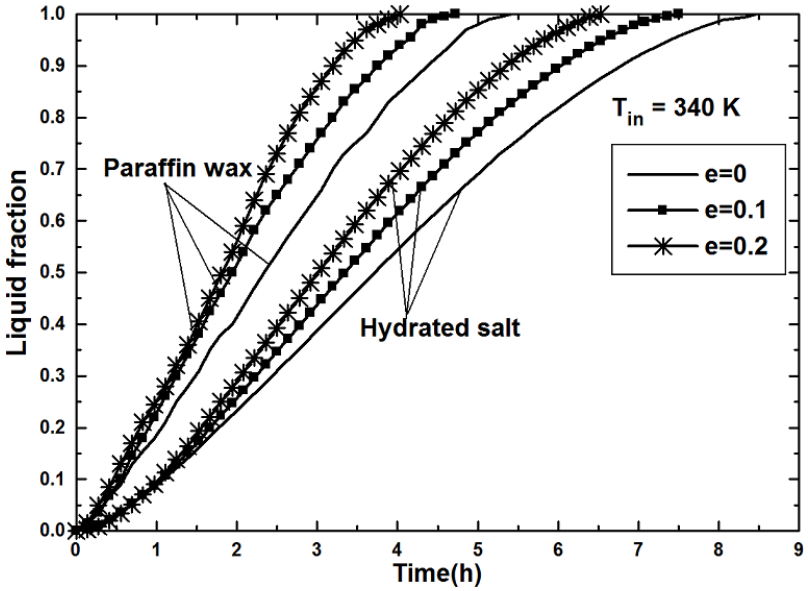

Figure 5.15 Comparison of liquid fractions of paraffin wax –nano particles PCMs with that of hydrated salt –nano particles PCMs

In case of hydrated salt PCMs, the natural convection is obviously week due to high viscosity and density and thus, the average rate of melting is lower than that in

case of paraffin PCMs. This clears that even if the PCM layers closer to the tube wall melts faster, due to the lower overall average melting rate, the liquid fraction of hydrated salt PCMs at any time remains smaller than that of paraffin PCMs. Figure 5.15 reveals the above mentioned fact. The lower liquid fraction values ultimately results in more time for complete melting.

5.2.4 HTF outlet temperature

During charging process, the HTF enters the system at a constant inlet temperature ($T_{in} > T_m$) and causes the melting of PCM. Figure 5.16 shows the effect of particle addition on the time-wise variation of HTF outlet temperature. Whether it is paraffin wax or hydrated salt, because of higher heat transfer rates in particle dispersed systems, the HTF experiences high decrease in temperature as compared to pure PCM system. At the same time, particle dispersed systems discharge HTF at relatively higher temperature at the latter stages of storage. Reduced heat transfer rates at the latter stages of melting of PCM-particles composites can be stated as a reason for this. Since the LHTS unit studied here is proposed for solar water heater, high decrease in HTF temperature (i.e. low temperature HTF at the outlet) may handicap the utilization of HTF in the application after storing the energy in the PCM. However, this problem would arise only if the storage and utilization of energy are required simultaneously. In solar water heaters, solar energy is to be stored generally during non-utilization periods as excessive energy is available mainly during those periods. Thus, the decrease in HTF temperature would not pose any utilization related problem. Moreover, as the non-utilization periods are short at most of the times, the storage process should be completed as fast as possible. As seen before, the storage process could be completed in much quicker time with particle dispersed system. From Figure 5.16, it can also be seen that for any particle fraction, there is continual drop in decrease in HTF temperature as the time progresses. This result is consistent with the drop in heat transfer rate as the melting progresses.

Whenever solar radiation is not available, the stored energy in the PCM is required to be recovered by the cold HTF by allowing the PCM to solidify. Hence, the increase in HTF temperature should be substantial in order to produce hot water at the outlet of the LHTS unit. As seen already, the heat transfer rate from PCM to HTF

during solidification remains almost same at all times irrespective of Re.

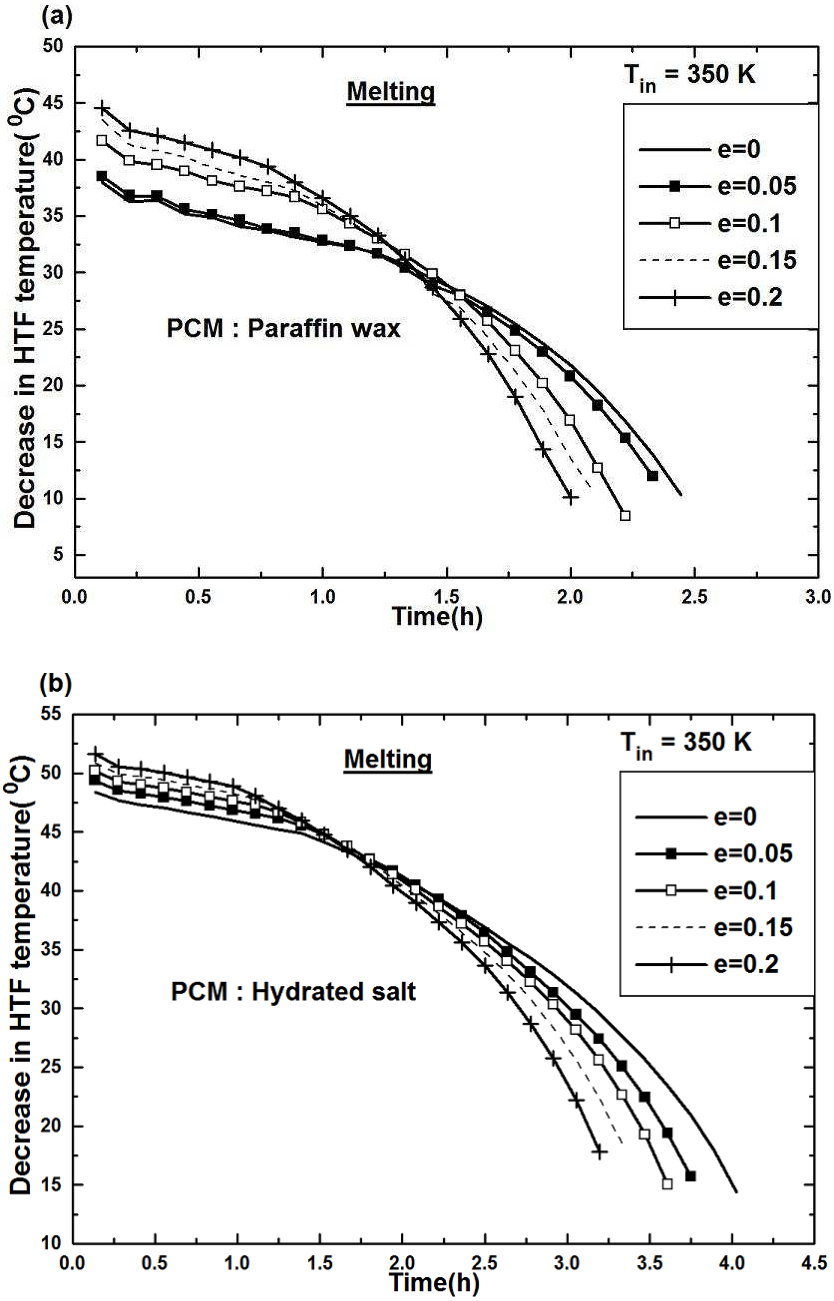

Figure 5.16 Effect of particle volume fraction on decrease in HTF temperature during melting of nano particles composites (a) paraffin wax as PCM (b) hydrated salt as PCM

Since the increase in HTF temperature depends on the heat transfer rate, the same can be expected to be indifferent, even if the Re is increased. However, the results presented in Figure 5.17, show an opposite trend. It can be seen from Figure 5.17, the increase in HTF temperature at any instant decreases as the Re increases.

This is attributed to the fact that at higher Re, the increase in mass flow rate is much higher as compared to increase in heat transfer rate. In other words, the increase in mass flow rate results in less residing time for the HTF in the tube and thus, decrease in increase of HTF temperature. Due to this reason, the lower mass flow rate for HTF should be preferred during energy recovery.

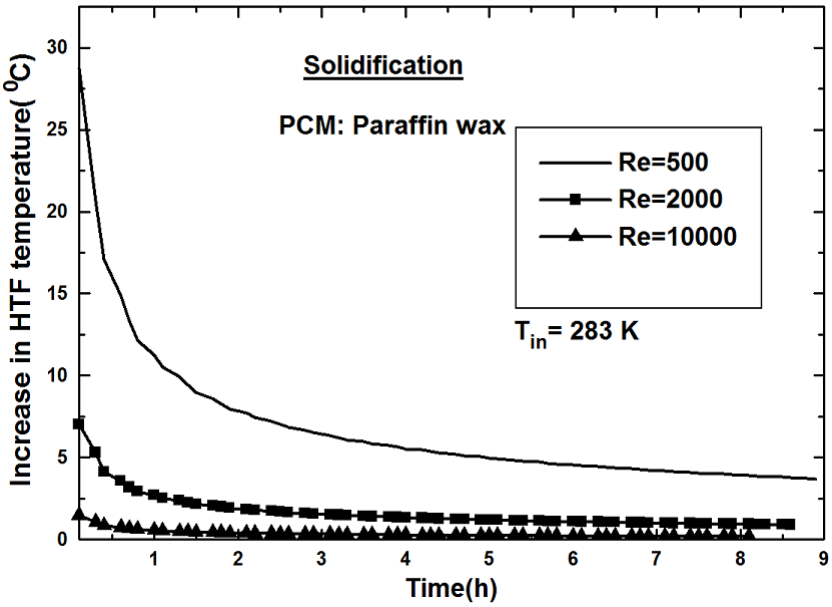

Figure 5.17 Effect of Re on increase in HTF temperature during solidification of paraffin wax

At the same time, it is also important to explore the ability of LHTS in discharging hot HTF under the influence of particles addition, when the mass flow rate of HTF is low. If high conductivity particles are added into the PCM with constant Re, then marked increase in HTF temperature can be achieved. This can be seen from Figure 5.18, in which the role of higher particle volume fractions in increasing the HTF temperature is illustrated. As shown by the previously presented results, the particle addition leads to higher heat transfer rates throughout the solidification of paraffin wax as well as hydrated salt and thus, both the composite PCMs could produce hot water at all times. However, paraffin wax composites could make considerable change in HTF temperature only when the particle fraction is 0.1 and above. On the other hand, hydrated salt composites are found to be effective even when the particle fraction is 0.5. The results also reveal that even the pure hydrated salt can discharge HTF at much high temperature than paraffin composites of 0.2 particle fraction. From this perspective, the effect of particle addition appears to be

more beneficial if PCM of relatively high thermal conductivity is employed. Similar results are obtained for all Re. However, at higher Re, the increase in HTF temperature is very less in pure PCM case and thus, the same could not be enhanced much by addition of particles. Hence, the addition of particles for higher Re cannot be justified.

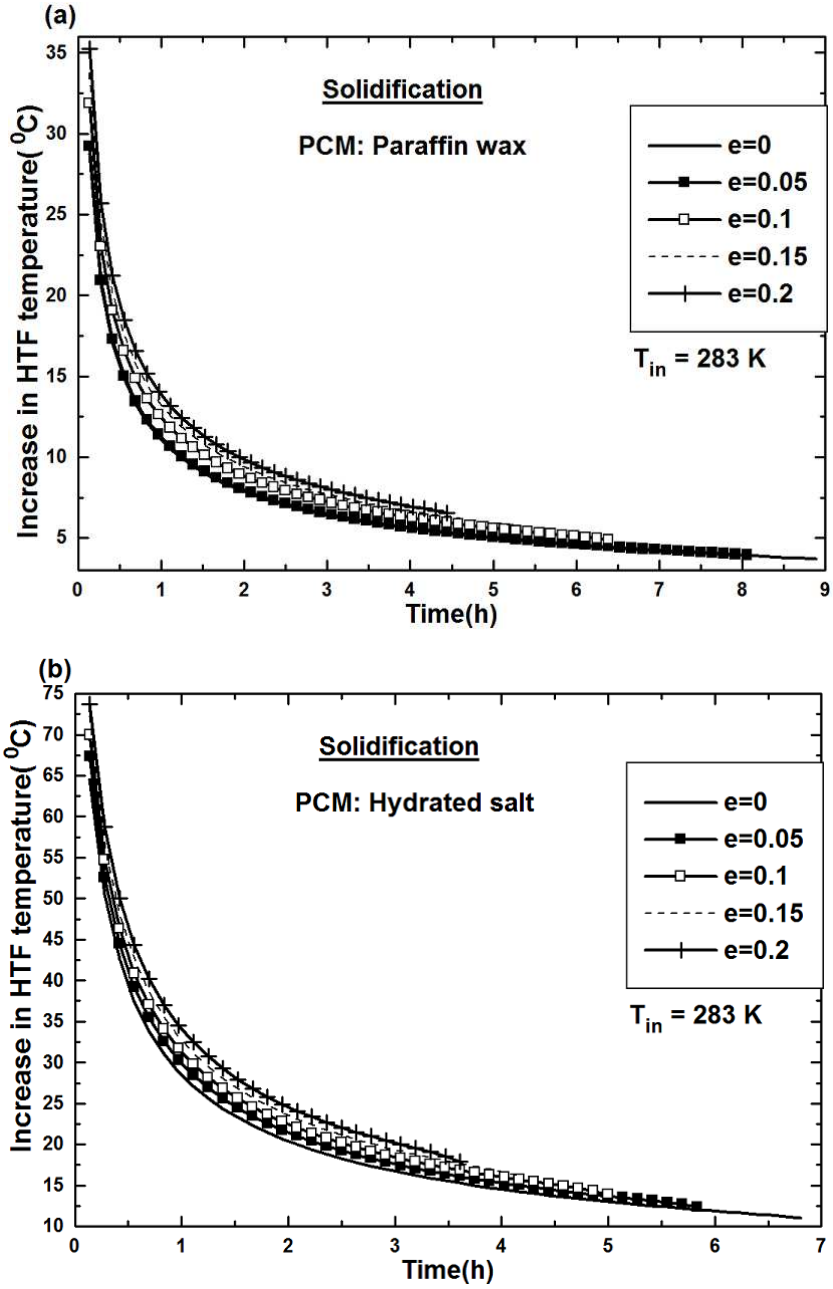

Figure 5.18 Effect of particle volume fraction on increase in HTF temperature during solidification of nano particles composites (a) paraffin wax as PCM (b) hydrated salt as PCM

5.3 Exergy performance of LHTS unit employing PCM-nano particles

This section brings out the results of exergy analysis which is carried out based on the procedure described in Chapter 3. The exergy performance of nano-particle systems is given in terms of exergy efficiency as well as total exergy stored/recovered and is compared with that of pure PCM units.

5.3.1 Exergy efficiency

During melting as well as solidification, the exergy efficiency of the system depends upon exergy rates, which in turn depend upon heat transfer rates and temperatures of PCM and HTF. During solidification, since both heat transfer rate and temperature of the PCM decrease with time, it is obvious that the rate of exergy transferred from PCM to HTF becomes less. At the same time, since the HTF outlet temperature increases as time progresses, one may expect increase in exergy efficiency. However, the relative effect of reduced heat transfer rate is stronger than that of increased HTF temperature on exergy gained by HTF and thus, exergy efficiency is found to be decreasing as the solidification progresses. The time variation of exergy efficiency during solidification is illustrated in Figure 5.19. It can also be seen that the exergy efficiency at any time can be increased by the addition of particles. The increase in exergy efficiency is consistent with the increase in particle volume fraction. This is not only because of enhanced heat transfer rate, but more importantly, the heat is transferred relatively at high temperatures in case of particle dispersed unit. The heat transfer between PCM and HTF at high temperatures results in increased exergy rate and hence, higher exergy efficiency.

Furthermore, the exergy performance of paraffin wax is compared with that of hydrated salt and it can be stated that the latter exhibits higher exergy performance in terms of exergy efficiency. For instance, the system with pure paraffin possesses a maximum exergy efficiency of only 33% against 70% by pure hydrated salt system. As seen in the earlier sections, system with hydrated salt not only displays higher heat transfer rate, but also produces higher temperature HTF. Higher exergy efficiency in case of hydrated salt system is the outcome of this combined benefit. The higher

exergy efficiency is also displayed by hydrated salt composite of any particle fraction in comparison with paraffin wax composites. As a matter of fact, the exergy efficiency of any hydrated salt composite is roughly twice that of its paraffin counterpart. The same is observed throughout the solidification.

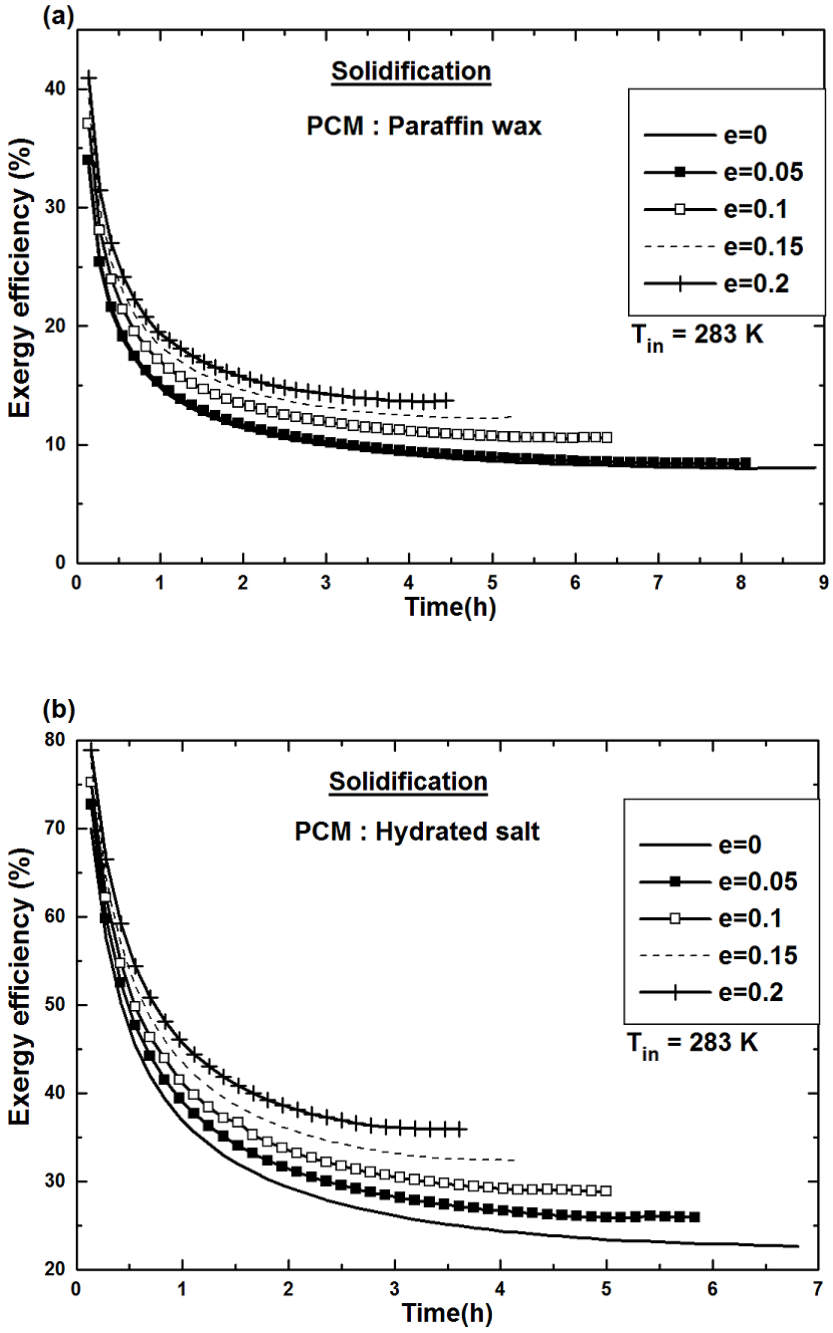

Figure 5.19 Effect of particle volume fraction on exergy efficiency during solidification of nano particles composites (a) paraffin wax as PCM (b) hydrated salt as PCM

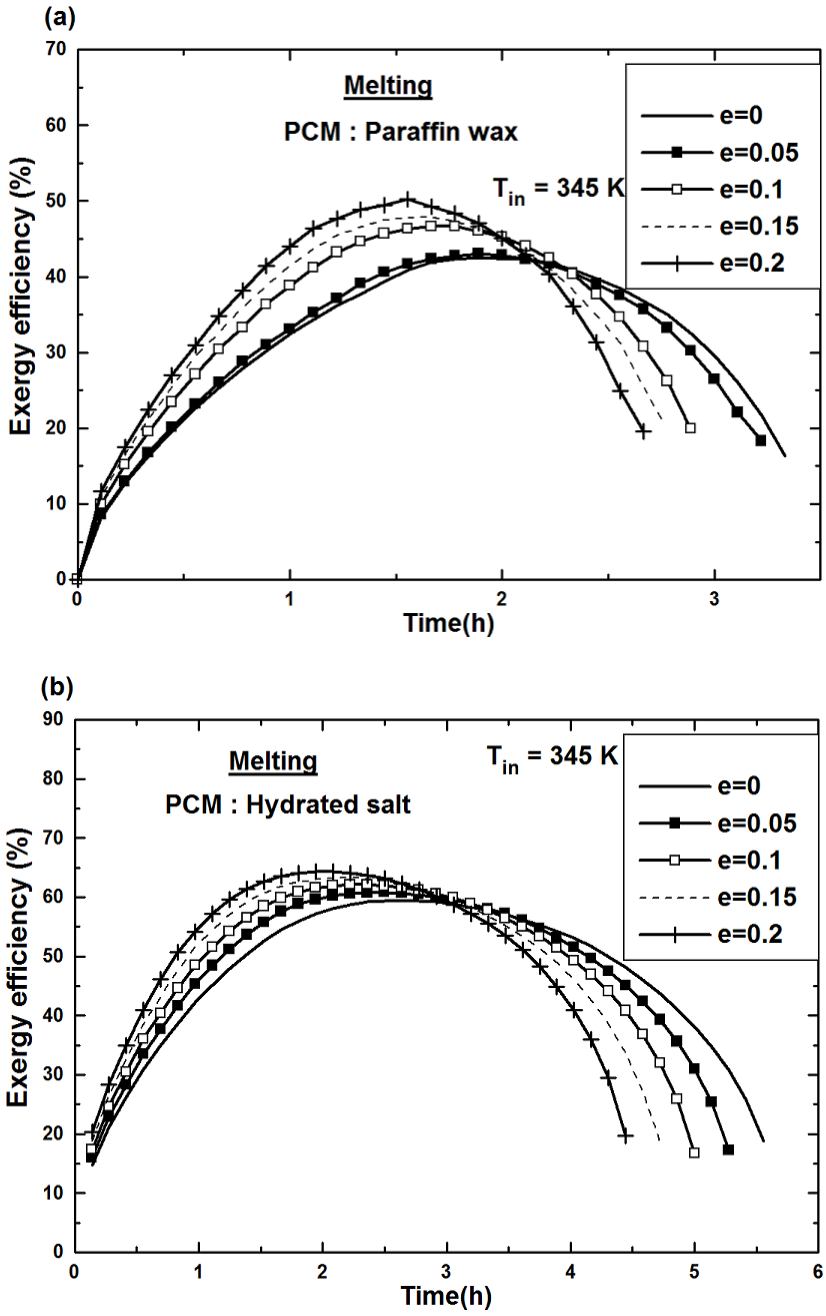

Figure 5.20 Effect of particle volume fraction on exergy efficiency during melting of nano particles composites (a) paraffin wax as PCM (b) hydrated salt as PCM

Contrary to solidification, the exergy efficiency is found to be increasing with time for some period of melting initially and the same starts decreasing thereafter. This is shown in Figure 5.20. Although heat transfer rate decreases with time since beginning, PCM temperature increases at faster rate in the early period of melting. During this period, since the exergy efficiency increases despite decreased heat transfer rate, it can be stated that the PCM temperature plays stronger role on the

variation of exergy rate than heat transfer rate. However, during later period, increase in PCM temperature becomes slower due to phase change of relatively more quantity of PCM. This reduces the role of PCM temperature on exergy rate. Whereas the heat transfer rate which is still on decreasing mode, emerges as deciding factor in controlling the exergy rate. Thus, exergy efficiency keeps decreasing during this period. During melting, the heat transfer rate in the particles added systems remain higher than that in the pure PCM system only in the earlier stages. Therefore, the exergy efficiency of composite PCM systems is higher than that of pure PCM system only during some initial period. On the other hand, pure PCM system is seen as more effective than composite PCM systems in terms of exergy during the period when pure PCM system exhibits higher heat transfer rates.

As far as exergy efficiency during melting is concerned, both paraffin wax and hydrated salt show similar trend as described earlier. However, from quantitative perspective, the hydrated salt systems appear to be relatively better one. The results also indicate that the difference between the melting exergy efficiencies of paraffin and salt is not as high as that in case of solidification. This clears that hydrated salt PCMs can be preferred over paraffin wax straightaway, if solidification alone is the matter of concern. On the other hand, when it comes to melting, since exergetic performance of hydrated salt is not well far ahead of paraffin, other performance parameters are also to be taken into account to come to a firm conclusion.

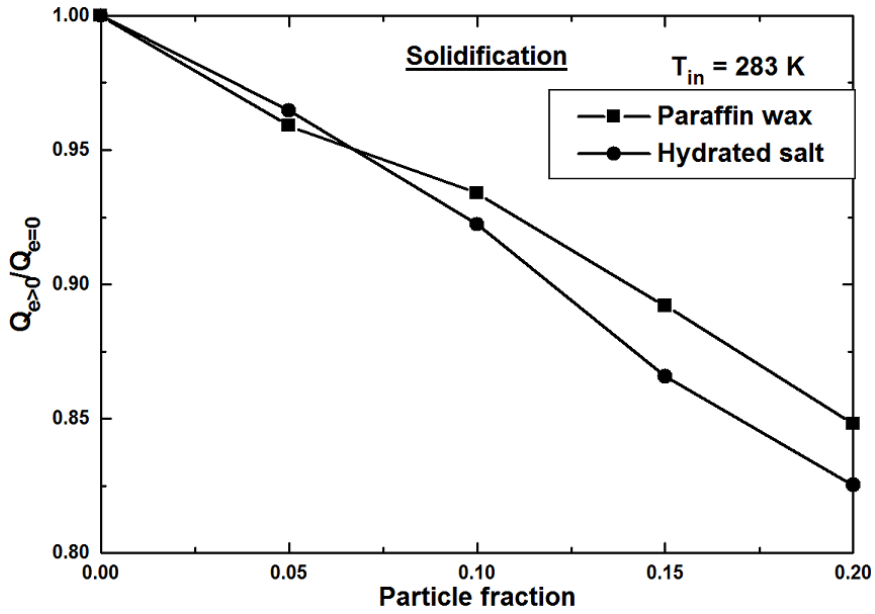

Figure 5.21 Effect of nano particles volume fraction on total energy recovered

5.3.2 Total exergy recovered

In LHTS unit, the energy storage and recovery processes can be accelerated, if the thermal conductivity of PCM is improved. Hence, it is expected that addition of high conductivity particles would accelerate the energy storage and recovery. However, as mentioned earlier, the addition of high conductivity particles leads to reduced latent heat value of PCM. Hence, in a fixed size of LHTS, the energy storage capacity becomes less as the particle volume fraction increases. This is expected to have some effect on total energy recovered too. To investigate the consequence of lower latent heat which results from particles addition, the ratio as defined by Equations (3.16) and (3.21) for charging and discharging processes, respectively have been calculated. The results of exergy recovered are shown in Figure 5.21. It is clear that the energy recovered at the end of the solidification process from particle dispersed PCM is less than that of from pure PCM. Also the reduction in the total energy recovered due to particle addition increases with increase in particle volume fraction. The particle dispersed systems behave in the similar manner even during melting. Hence, one may think that the selection of particle volume fraction is a compromise between required charging/discharging rate and total energy storage/discharge capacity.

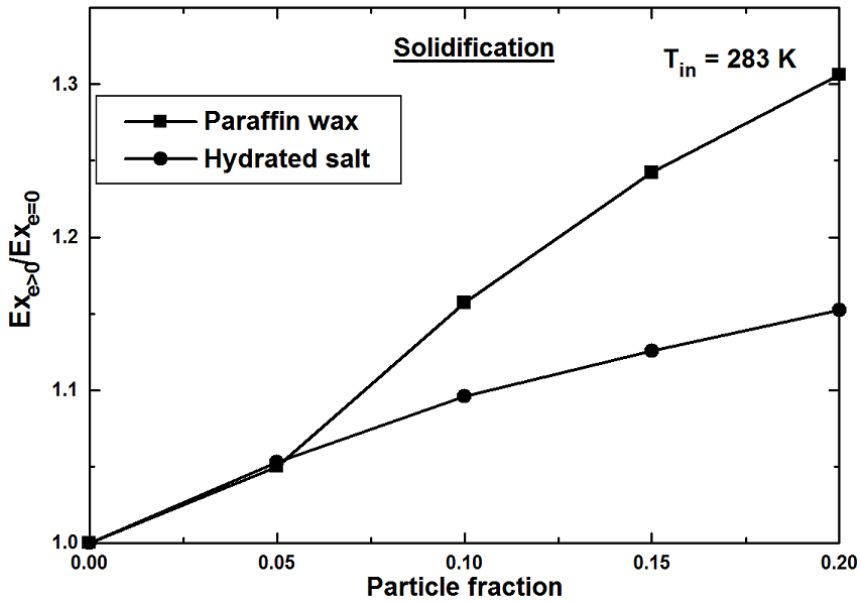

Figure 5.22 Effect of nano particles volume fraction on total exergy recovered

On the other hand, the similar ratio in terms of exergy provides a different

insight (Figure 5.22). As it can be seen from Figure 5.22, the addition of particles considerably increases the total exergy recovered from PCM. This highlights an important point that particles addition enhances the quality of recovered energy despite reducing the storage capacity of the unit. This outcome clears that the reduced latent heat has no role in determining the quality of energy recovered, although it leads to reduction in recovered energy quantity. Increase in quality of energy recovered thus, could be due to the enhanced heat transfer rate as a result of presence of particles. This is because higher heat transfer rates minimize the exergy destruction. The reduction in solidification time is also stated as a reason for better exergy performance in some previous investigations, for example Watanabe and Kanzawa (1995). The results of this work too prove the same as exergy recovered is higher in case of composite PCMs, which take lesser time to solidify. Furthermore, the exergy performance can be enhanced monotonically with increase in particle fraction.

It can also be noticed that the addition of particles is more pronounced in terms of enhancement of exergy recovered when the PCM is paraffin wax, especially when the particle fraction is above 0.05. Although both the PCMs enjoy the benefit of particle addition in terms of reduced solidification time, the reduction in solidification time is relatively higher in case of paraffin wax. Hence, the increase of exergy recovered is relatively more when paraffin wax is employed.

5.3.3 Total exergy stored

The composite PCMs also effect less storage capacity as a result of lower latent heat value. As it can be seen from Figure 5.23, the quantities of energy stored by completely melted PCM-particle composites are lower as compared to that of by completely melted PCM. Moreover, the quantity decreases more and more as the particle fraction increases. Since composite PCMs posses high heat transfer rate and could complete melting process faster, higher exergy storage capacity may be expected as in the case of discharging. However, the results shown in Figure 5.24 display a different behavior altogether, i.e, particles addition reduces not only the storage capacity, but also the quality of energy stored. In spite of higher heat transfer rate and reduced melting time, it is surprising to see aforementioned exergy

performance of composite PCMs. Unlike solidification, during melting, motion of liquid PCM is inevitable and same is included in the melting model. One of the sources for exergy destruction is the viscous force. It is evident that the presence of particles increases the viscosity of liquid PCM, which in turn leads to more exergy destruction. In this perspective, it can be stated that the effect of viscosity on exergy destruction is more dominant than that of heat transfer rate and charging time.

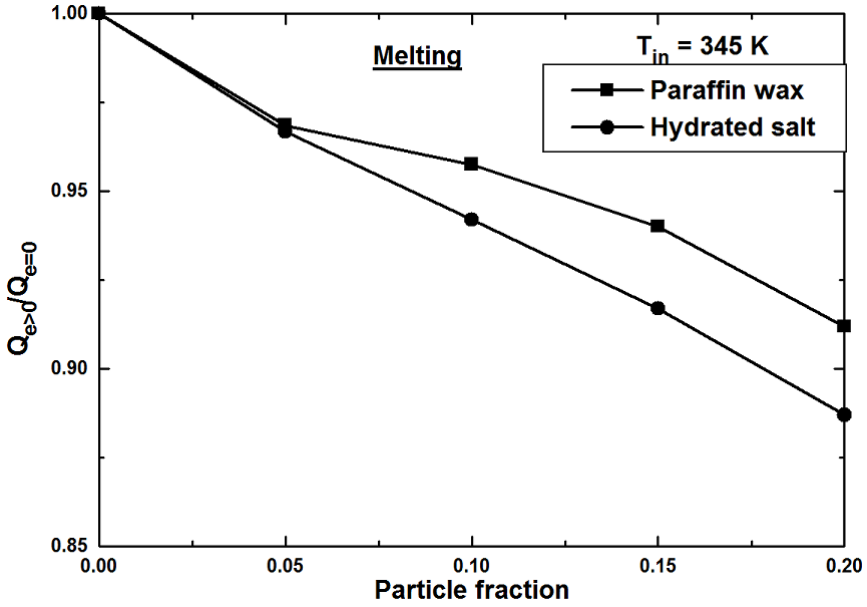

Figure 5.23 Effect of nano particles volume fraction on total energy stored

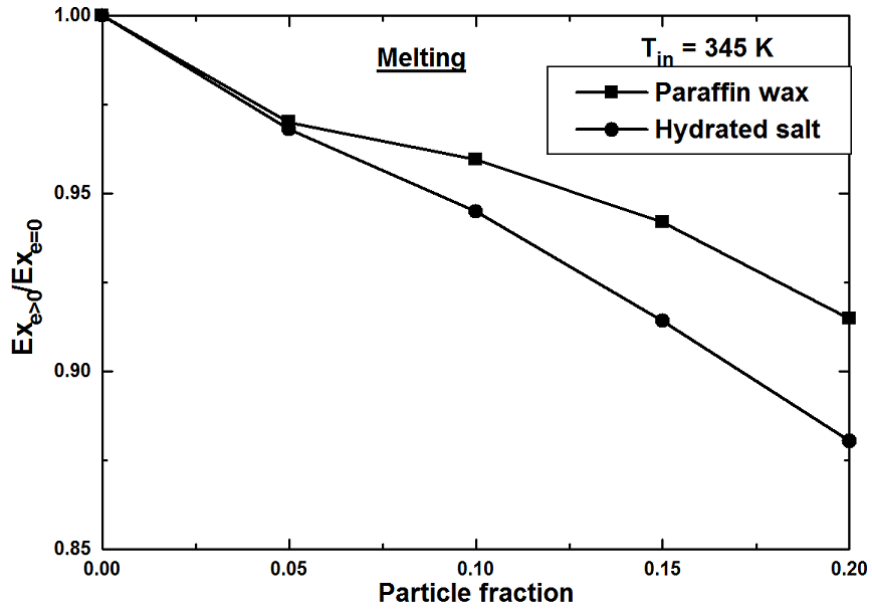

Figure 5.24 Effect of nano particles volume fraction on total exergy stored

The comparison of exergy performance of paraffin wax and hydrated salt during melting also reveals the same. For any particle fraction, since the viscosity of hydrated salt is higher than that of paraffin wax, the former encounters more exergy destruction than latter. Therefore, hydrated salt systems store less exergy than paraffin wax when particles are added.

5.4 Effect of HTF inlet temperature on heat transfer and exergy performance

In solar water heaters, whether it is charging or discharging, the LHTS system may have to deal with HTF at any temperature. From this point of view, the performance of composite PCM systems has been analyzed with different HTF inlet temperatures during charging as well as discharging.

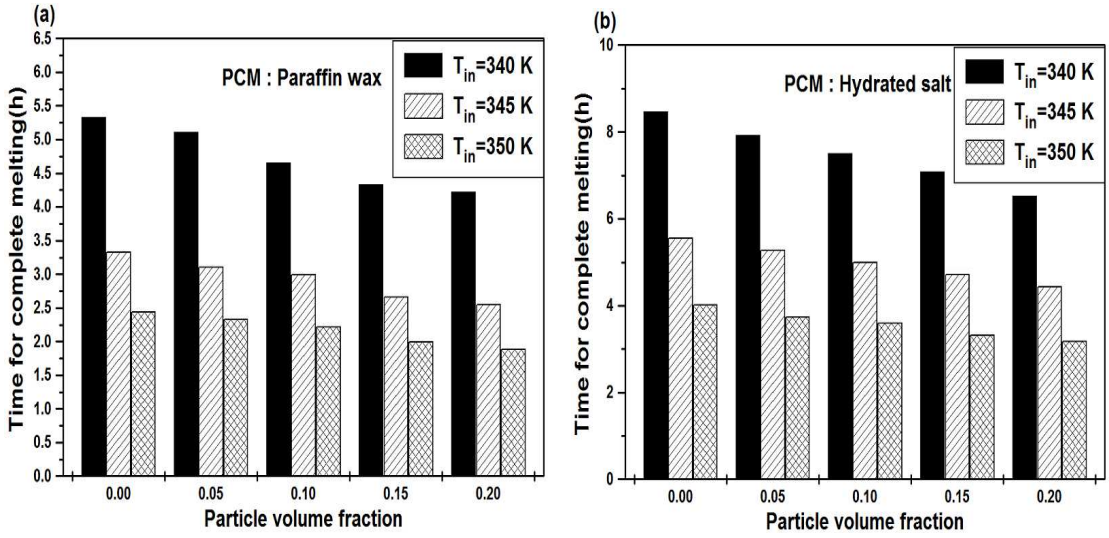

Figure 5.25 Effect of HTF inlet temperature on complete melting time of nano particles composites (a) paraffin wax as PCM (b) hydrated salt as PCM

5.4.1 Effect of HTF inlet temperature on charging process

To investigate the effect of HTF inlet temperature on charging process, three values were considered as HTF temperatures at inlet, i.e T_{in} = 340, 345 and 350 K. Higher the HTF inlet temperature, higher is the temperature difference between HTF and PCM and thus, decrease in charging time. This can be verified from Figure 5.25, which shows that for any particle fraction, composite PCMs take less time to melt completely when the HTF inlet temperature is high. These results are evident as wider

temperature difference between HTF and PCM involves high heat transfer rate at any time.

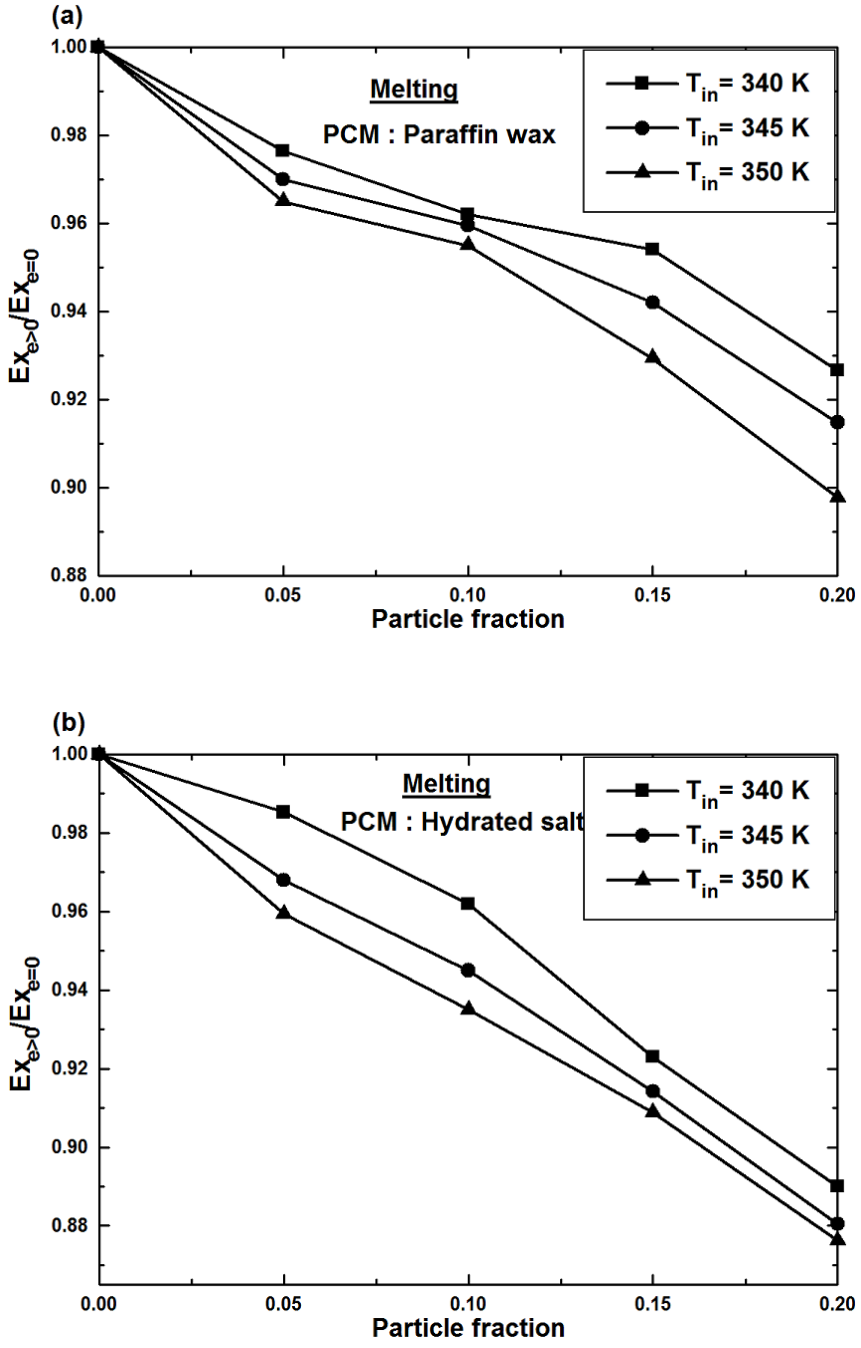

Figure 5.26 Effect of HTF inlet temperature on exergy stored in nano particles composites (a) paraffin wax as PCM (b) hydrated salt as PCM

The above discussion indicates that LHTS systems produce better heat transfer performance when the HTF inlet temperature is higher. However, the exergy performance is found to be superior with the lower temperature conditions for at HTF inlet. This is clear from Figure 5.26, which presents the ratio of exergy stored by

composite PCMs to that of pure PCM at different values of HTF inlet temperature. From thermodynamic point of view, if the heat transfer takes place at the finite temperature difference, then system irreversibility and entropy generation would be resulted in.

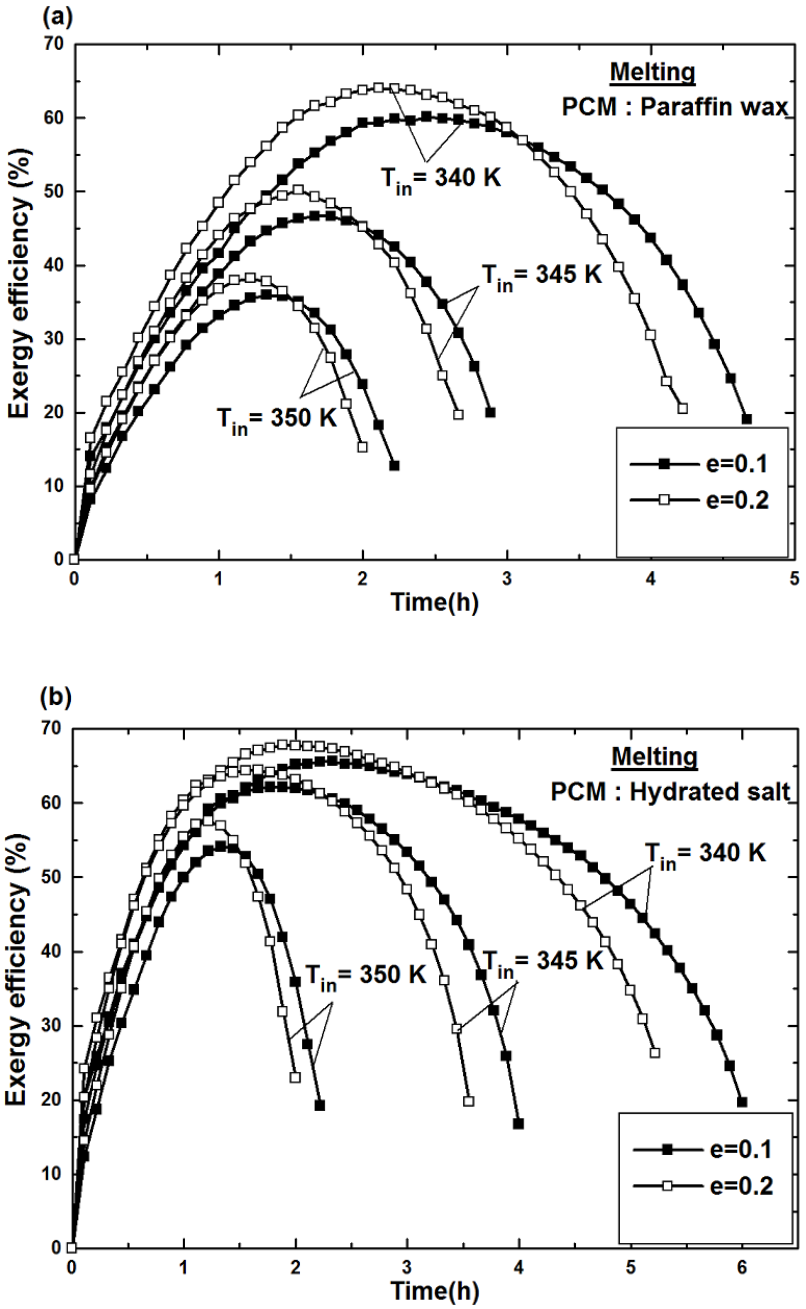

Figure 5.27 Effect of HTF inlet temperature on exergy efficiency during charging of nano particles composites (a) paraffin wax as PCM (b) hydrated salt as PCM

Accordingly, the increase of HTF inlet temperature increases the finite

temperature difference at which heat transfer occurs and thus, more irreversibility and entropy generation. More irreversibility and entropy generation indicate more exergy destruction. This is the reason why the exergy stored by composite PCM of any particle fraction is found to be less when HTF inlet temperature is high.

Due to increase in irreversibility and entropy generation, all LHTS systems utilizing either paraffin based composites or salt based composites, show lower exergy efficiency at all times throughout the charging process. This effect is shown in Figure 5.27.

5.4.2 Effect of HTF inlet temperature on discharging process

In the simulations of discharging process, the HTF inlet temperatures are taken as T_{in} = 283, 287 and 293 K. It should be noted that higher HTF inlet temperature results in lower temperature difference between HTF and PCM during discharging as against the case of charging. Hence, keeping HTF inlet temperature low (i.e, high temperature difference) seems to be effective way to improve the heat transfer characteristics of the LHTS system. Figure 5.28 reveals the superiority of LHTS systems, which deal with lower temperature HTF. Lower the HTF inlet temperature, shorter is the time required for complete solidification. Thus, the effect of higher temperature difference on discharging process is consistent with that seen during charging.

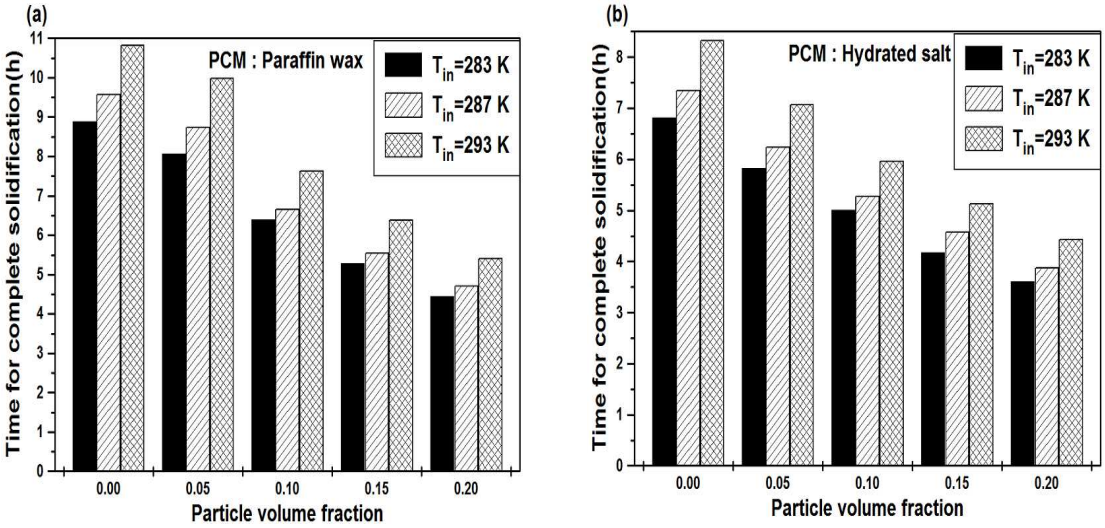

Figure 5.28 Effect of HTF inlet temperature on complete solidification time of nano particles composites (a) paraffin wax as PCM (b) hydrated salt as PCM

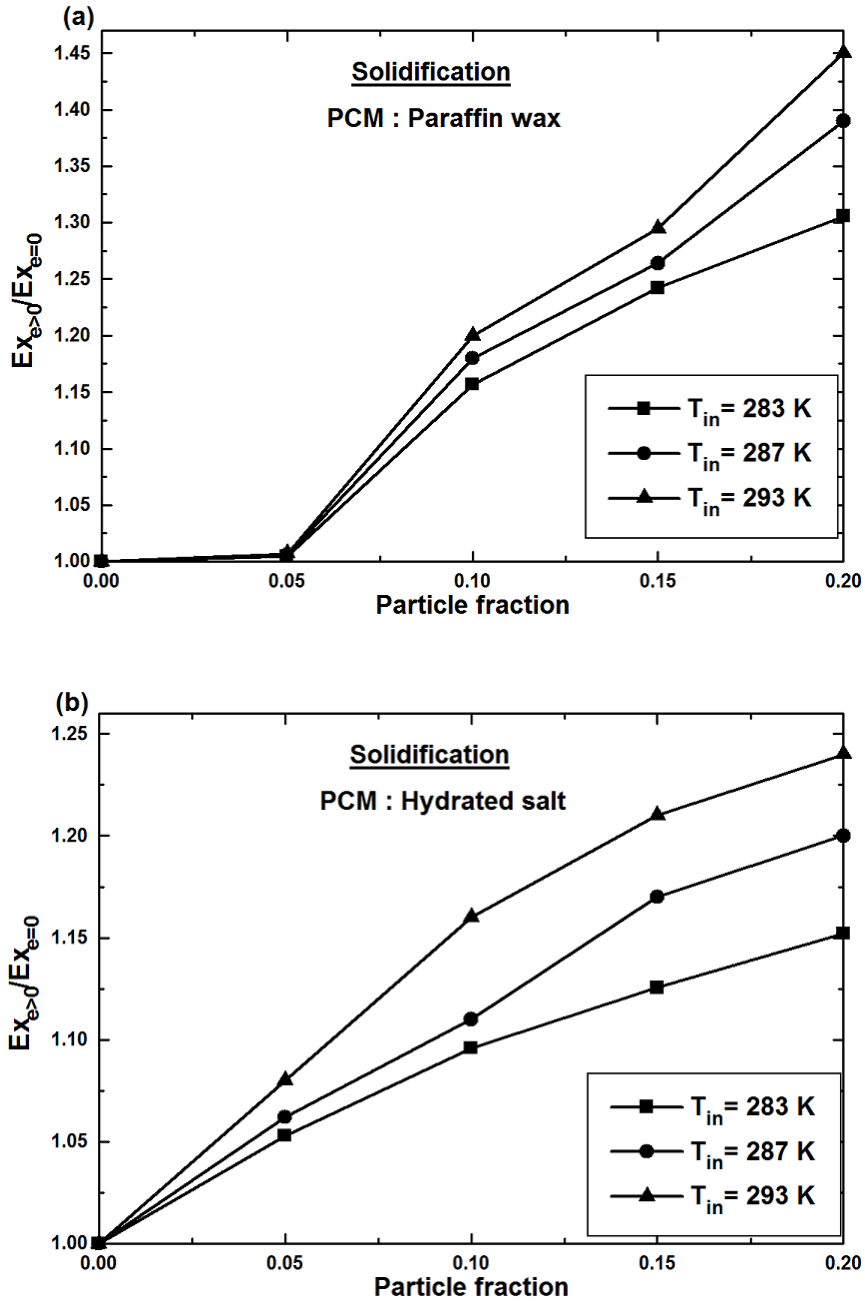

Figure 5.29 Effect of HTF inlet temperature on exergy recovered from nano particles composites (a) paraffin wax as PCM (b) hydrated salt as PCM

The same consistency is also observed with exergy results. Figure 5.29 and 5.30 present the effects of HTF inlet temperature on exergy stored and exergy efficiency respectively. As illustrated by Figure 5.29, if the systems receive HTF at lower temperature, then the benefit particles addition seems to be narrowed down. Similarly, all the cases can be seen as less effective in terms of exergy efficiency, when the HTF temperature is lowered (Figure 5.30).

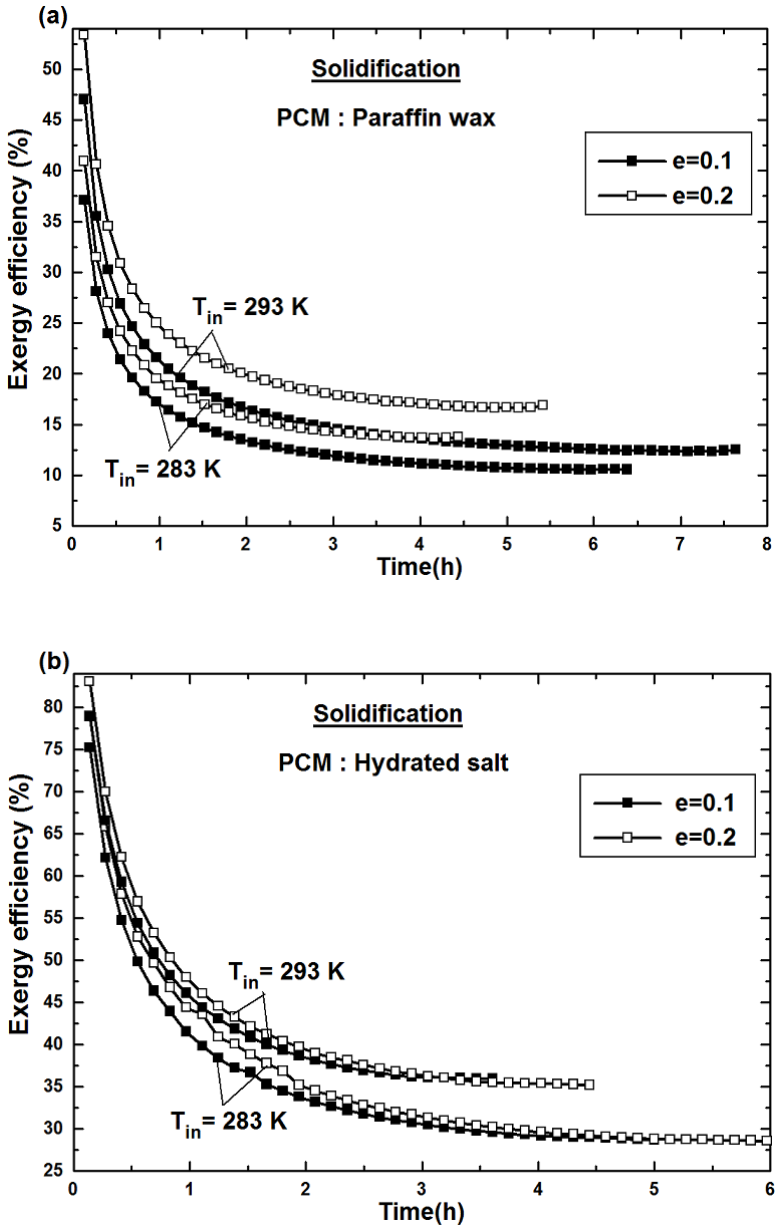

Figure 5.30 Effect of HTF inlet temperature on exergy efficiency during discharging of nano particles composites (a) paraffin wax as PCM (b) hydrated salt as PCM

5.5 Thermo-physical properties of PCM-micro particles composites

Before investigating the thermal performance of micro particles dispersed PCMs, the thermophysical properties barring density and viscosity were measured experimentally. The density was computed using the mass balance equation, the one

used for nano particles based PCM composites. The viscosity of micro particles based composites, which is time dependent during the process, has to be computed analytically as the solution progresses. Thus, as mentioned in Chapter 4, Equation (4.23) was applied for the same.

For the measurement of specific heat, latent heat and thermal conductivity, experiments were performed. Prior to the experiments, composite PCMs were prepared by mixing the copper micro particles of volume fractions 5% ,10%, 15% and 20% with pure paraffin wax / hydrated salt using the ultrasonicator (details are given in section 4.1 of Chapter 4).

5.5.1 Measurement of latent heat and specific heats

Once the composite PCMs were available, firstly the temperatures were recorded during the cooling of liquid PCMs and reference fluid (distilled water) at regular intervals (at every 10s). For each sample, the experiments were performed twice with different initial temperatures (around 10 and 30^{o}C above the melting point) to verify the accuracy of measurements.

Table 5.4 Results of *T-H* curves for different initial temperatures

PCM	Latent heat (kJ/kg)			Specific heat (kJ/kg.K)		
	A*	B*	Deviation (%)	A*	B*	Deviation (%)
HS 58 (0.1 particle fraction)	135.79	139.03	2.3	1.1817	1.212	2.5
HS 58 (0.2 particle fraction)	86.225	88.8	2.9	0.6723	0.6727	2.95
Paraffin (0.1 particle fraction)	72.74	74.74	2.4	0.595	0.61	2.4
Paraffin (0.2 particle fraction)	40.97	39.74	3	0.312	0.303	2.85

* A : $T_{init} - T_m = 10^{o}$C, B : $T_{init} - T_m = 30^{o}$C

Table 5.4 presents the comparison of results obtained from two experimental trials for some samples. In general, the difference between two set of results is not more than 3%. Similarly, to check the repeatability of measurements, the trial for any sample was conducted twice. The representative results are given in Table 5.5 and

from the results it is clear that each result differs from corresponding result of repeated trial only by less than 1%.

Table 5.5 Results of *T-H* curves from repeated trials

PCM	Latent heat (kJ/kg)			Specific heat (kJ/kg.K)		
	Trial1	Trial2	Deviation (%)	Trial1	Trial2	Deviation (%)
HS 58 (0.05 particle fraction)	180	178.38	0.9	1.5004	1.4861	0.95
HS 58 (0.15 particle fraction)	110.01	111.21	0.89	0.8151	0.8226	0.91
Paraffin (0.05 particle fraction)	108.29	109.3	0.92	0.986	0.995	0.91
Paraffin (0.15 particle fraction)	56.244	56.3	1	0.4258	0.43	0.97

Using the recorded temperature readings, the cooling curves (*T-History*) were plotted and representative cooling curves of hydrated salt composites and paraffin wax composites are presented in Figure 5.31 and Figure 5.32 respectively. First derivatives of cooling curves are also shown along with the corresponding plots. The first derivatives were used in search of inflection point to locate the end of phase change process.

In case of hydrated salt composites, the subcooling effect is consistently observed irrespective of particle volume fraction. In fact, the hydrated salts are known for their subcooling effect during solidification. It is clear from results that the addition of particles could not alleviate the subcooling. Nevertheless, the subcooling range is within 3°C, which matches with the manufacturer's data of pure PCM (www.thermalstorage.in/plussproducts.html). On the other hand, none of the paraffin wax composites has the tendency of subcooling as seen from Figure 5.32. As reported in the literature, all varieties of paraffins show no subcooling. The same effect is found with all paraffin wax composites employed here. Referring to the obtained cooling curves, it can be stated that the addition of metal particles has no role as far as subcooling phenomenon is concerned.

Further examination of cooling curves reveals that the phase change

temperature is slightly affected by the addition of particles. It is known that pure hydrated salt melts at a temperature range of 57-58°C. According to the cooling curves, the melting point range widens as the particle fraction increases. Same is true for paraffin wax PCMs. Nevertheless, the change in phase change temperature range due to particles seems to be negligible.

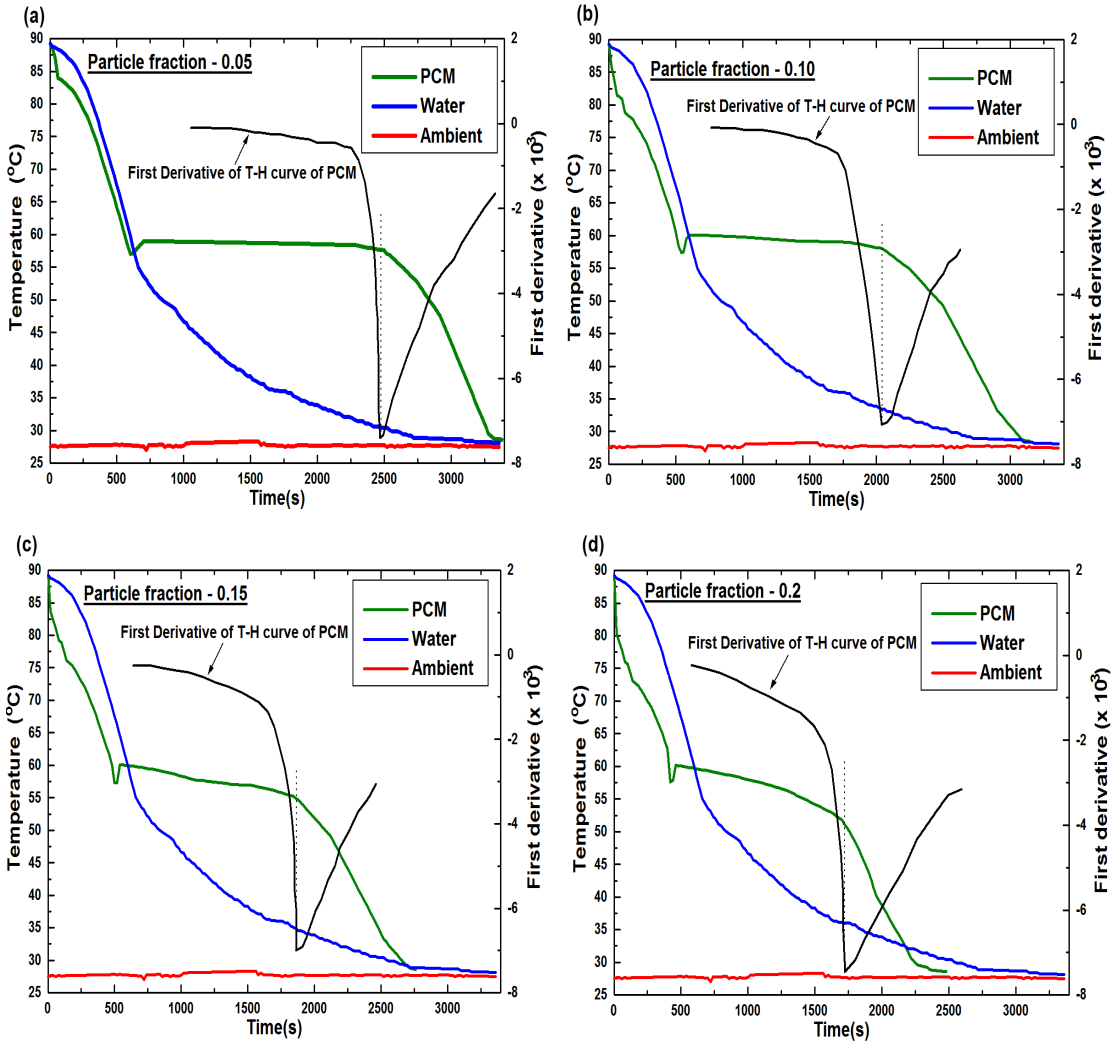

Figure 5.31 *T-H* curves of hydrated salt composites

The major objective of this experimental work is to examine the effect of particles dispersion on the latent heat of pure PCM. From the *T-H* curves, latent heat values of composites are evaluated employing the procedure explained earlier. Alongside, specific heats are also computed. The results are displayed in Table 5.6. For each composite, the values presented are the average of results obtained from various trails. Although specific heats could be obtained for solid and liquid PCMs separately, only the averages of the two values are listed as the numerical modeling

cannot deal with individual specific heats of solid and liquid PCMs.

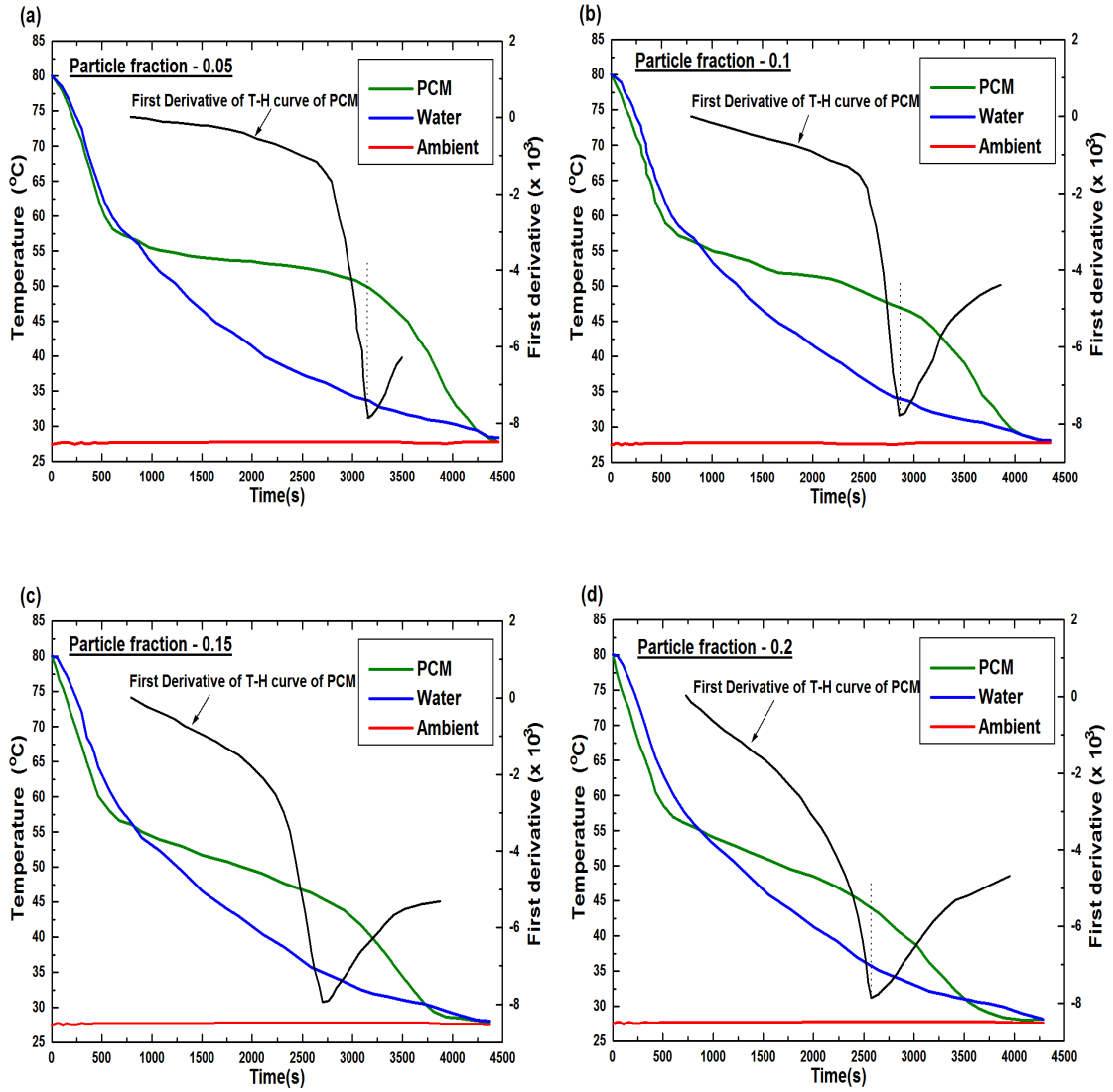

Figure 5.32 *T-H* curves of paraffin wax composites

Table 5.6 Latent heat and specific heat values obtained from *T-H* plots

Particle volume fraction	Hydrated salt composites		Paraffin wax composites	
	Latent heat (kJ/kg)	Specific heat(kJ/kg.K)	Latent heat (kJ/kg)	Specific heat(kJ/kg.K)
0.05	179.4	1.49	108.4	0.986
0.1	137.45	1.194	73.2	0.6
0.15	110	0.82	56.5	0.419
0.2	87	0.67	40.5	0.31

As expected the presence of particles reduce the latent heat value of pure PCM. Moreover, the reduction in latent heat increases as the particle fraction increases. The metal particles in the PCM are actually acting as impurities and it is proved that the presence of these impurities affects the crystallization of PCM. Since the particles in PCM accelerates heat transfer rate, the phase change region narrows down as seen from the cooling curves. The effect is more and more pronounced as the particle fraction increases. At the same time, the specific heat values are also found to be less as the particle fraction increases. This is attributed to the fact that the specific heat of copper is much lower than that of hydrated salt and paraffin wax. In fact, the cooling curves reveal that the areas below the sensible heat region become less for higher particle fractions. Hence, according to Equations (4.10) and (4.11), the specific heats of higher particle fraction composites would be higher. However, as the particle fraction increases, the mass of PCM increases substantially. The increase of mass is obviously less than the decrease of areas. This results in lower specific heat values of composites of higher particle fractions.

5.5.2 Thermal conductivity measurement

The heat transfer enhancement of LHTS system is mainly determined by the extent of thermal conductivity enhancement of PCM. In this perspective, the thermal conductivities of composite PCMs were also evaluated. The T-H curves are of no use in this regard. Hence, a different technique (as explained in Chapter 4) was employed. In order to ensure the one dimensional heat transfer (i.e Bi<0.1), melting and solidification were allowed with a temperature difference of only 5°C between source and PCM. Based on the time taken for complete melting and complete solidification, the thermal conductivities of liquid and solid PCMs are computed. To confirm the validity of perturbation method based thermal conductivity measurement, experiments were carried out for pure hydrated salt. The measured values of all trials are found to be fairly close to the data provided by the manufacturer. The thermal conductivity values obtained for composite PCMs are given in Table 5.7. It is clear from the results, thermal conductivity of PCM increases monotonically due to increase in particle volume fraction. Even with particle fraction of 0.05, it is posssible to achieve around 10% increase and the enhancement is as high as 80% with 0.2 particle

fraction. The reason is simple and straight forward. The thermal conductivity of copper is much higher than that of PCM. When micro particles are added, the particles in the PCM form conductivity networks and thus, thermal conductivity of composite PCMs are found to be higher.

Table 5.7 Experimental thermal conductivities of PCM-micro particles composites

Particle volume fraction	Hydrated salt composites		Paraffin wax composites	
	k_s (W/m.K)	k_l (W/m.K)	k_s (W/m.K)	k_l (W/m.K)
0.05	0.7768	0.476	0.231	0.1288
0.1	0.8996	0.5528	0.276	0.1503
0.15	1.03	0.632	0.324	0.1749
0.2	1.157	0.7132	0.359	0.1951

5.6 Performance of LHTS unit employing PCM-micro particles

In view of comparative evaluation, the micro particles dispersed systems are analyzed also under the same operating and design conditions those are employed for nano particles systems. Hence, the range of input parameters used for the analysis of micro particles dispersed systems are same as given in Table 5.1.

5.6.1 Heat transfer characteristics during solidification

Firstly, the effect of dispersion of micro particles on the heat transfer rate can be explored through the results in Figure 5.33. Due to the enhanced thermal conductivity by micro particles, it is obvious that the heat transfer rate is much higher throughout the solidification process. However, it is also important to examine the relative strength of micro particles in enhancing the heat transfer rate.

Before going into the heat transfer results, the thermal conductivity values of micro and nano particles composites are compared as given in Table 5.8. According to Table 5.8, the micro particles composite of any particle volume fraction show relatively higher increase in thermal conductivity as compared to nano particles composite of same particle volume fraction. In case of micro particles composites,

due to relatively larger size areas of particles, they can remain close to each other more than what is possible in case of nano particles composites. This means the particles network is stronger in micro particles composites than in their counter parts.

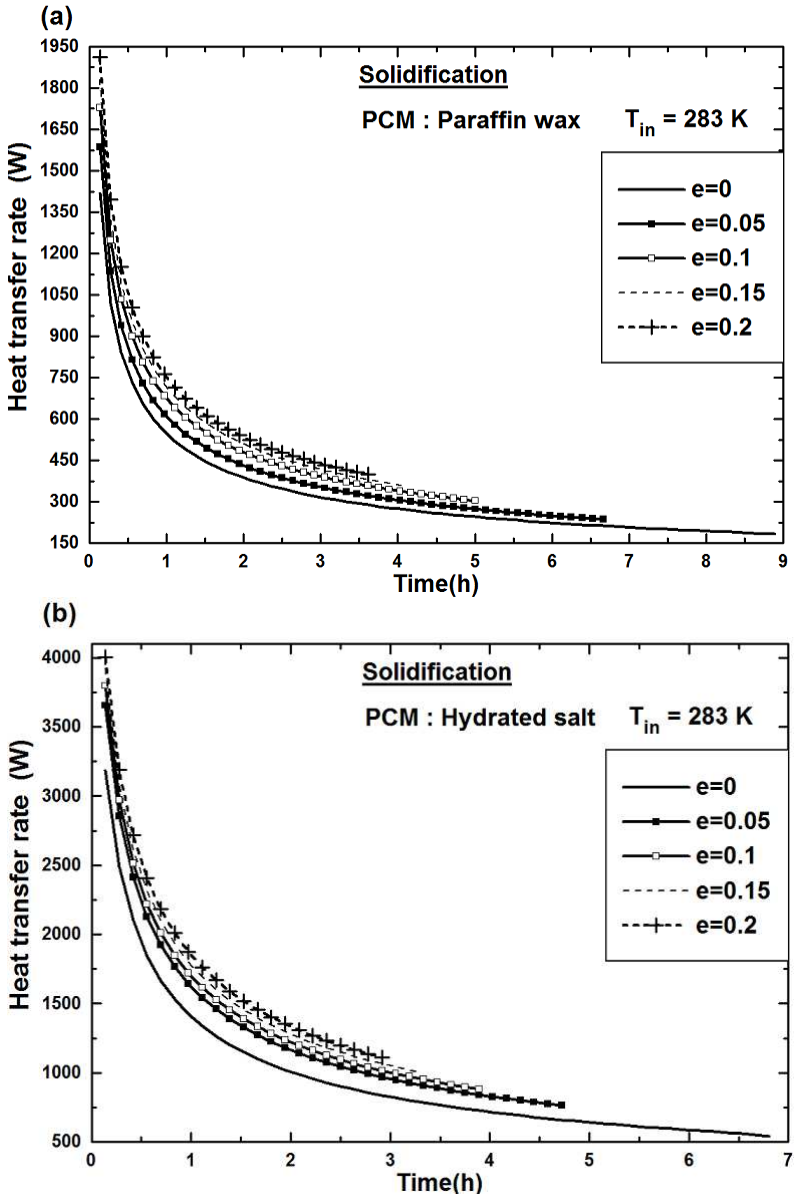

Figure 5.33 Effect of micro particles on instantaneous heat transfer rate during solidification (a) paraffin wax as PCM (b) hydrated salt as PCM

The higher thermal conductivity values suggest that the micro particles should result in more heat transfer enhancement than achieved by nano particles. However, it is known that the particles migration in micro particles composites leads to non uniform distribution of particles. Thus, the heat transfer rate may be higher only at locations

where more particles exist and there may not be much enhancement in the overall heat transfer rate. Moreover, as the particle volume fraction at any location may vary with time, the qualitative behavior of micro particles composites in terms of heat transfer rate may not be same as that of nano particles composites.

Table 5.8 Increase in thermal conductivity of pure PCM due to nano and micro particles composites

Particle volume fraction	Hydrated salt				Paraffin wax			
	Nano		Micro		Nano		Micro	
	Solid (%)	Liquid (%)	Solid (%)	Liquid (%)	Solid (%)	liquid (%)	Solid (%)	Liquid (%)
0.05	15.4	15	19.5	19	5	8	10	18
0.1	32.3	32.5	38.4	38.2	33.5	34	38	37.9
0.15	52.3	52.5	58.5	58	55.8	55	62	60.5
0.2	73.8	72.5	78	78.3	74.86	75	79	79.5

By keeping all the above mentioned points in mind, the comparison of nano and micro particles in terms of heat transfer rate enhancement is derived and the same is shown in Figure 5.34. Accordingly, the enhancement in the heat transfer rate due to micro particles dispersion is relatively higher than that of due to nano particles dispersion. As it can be seen from Figure 5.34, this is true for any value of particle volume fraction. Moreover, the higher heat transfer rates with micro particles composites maintained at all times till the end of solidification. This clears that there is no difference between micro particles and nano particles systems from qualitative perspective, although the heat transfer enhancement by the former is quantitatively higher than that by the latter.

The higher heat transfer rate at all times highlights that the initial particle volume fraction, which is uniform everywhere remains same throughout the solidification. This can be verified from Figure 5.35, in which the time variation of particles volume fraction at selected locations is shown. As it can be seen from Figure 5.35, the variation of particle volume fraction with time is negligible. Same is observed at all locations. Hence, the particle migration appears to be very weak during solidification. The reason for the insignificant particle migration is simple and

straight forward. The onset of particle migration is mainly due to strain rate gradient and the strain rate gradient depends on the strength of fluid flow. During phase change process, the only fluid flow is due to natural convection and it is known that the natural convection during solidification is incomparable. Obviously, the weaker fluid flow could not promote the particle migration. Therefore, the uniform distribution of micro particles could exhibit higher solidification rates at all times as compared to their nano counterparts.

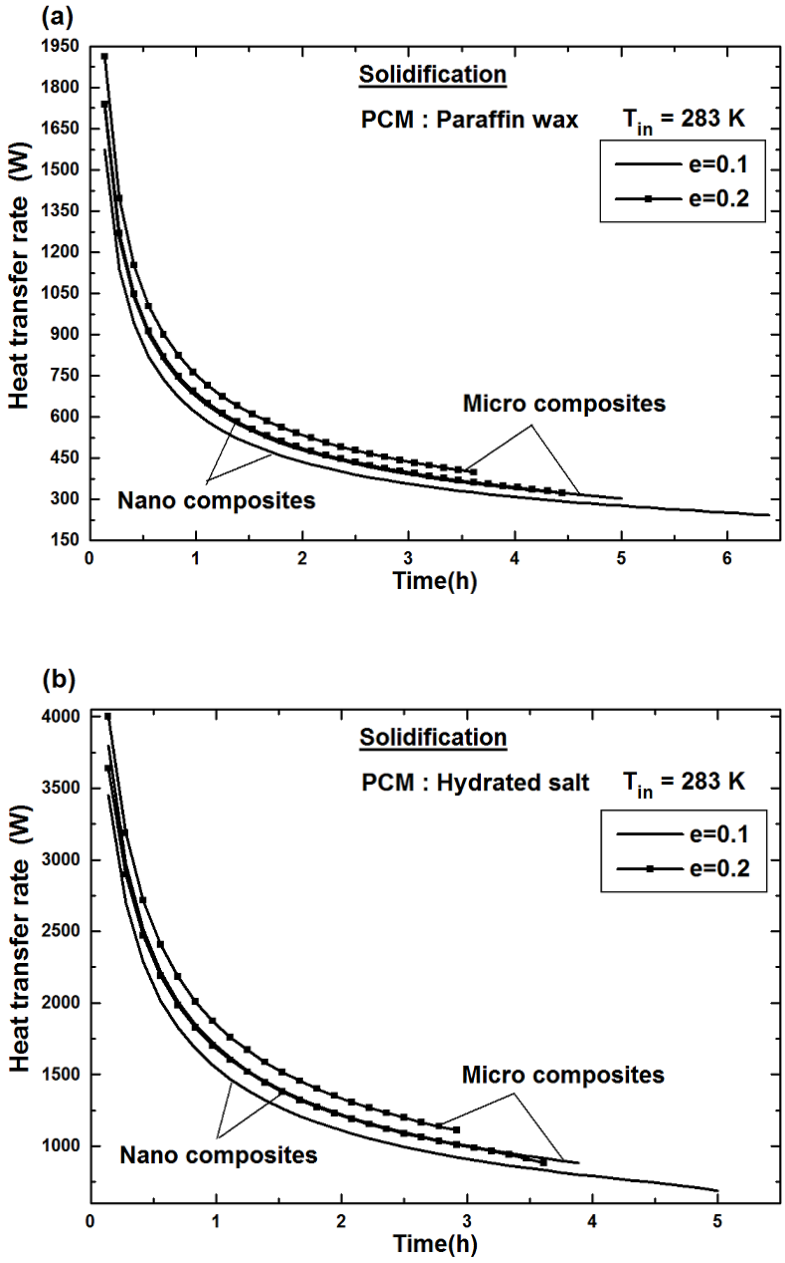

Figure 5.34 Comparison of effects of nano and micro particles on instantaneous heat transfer rate during solidification (a) paraffin wax as PCM (b) hydrated salt as PCM

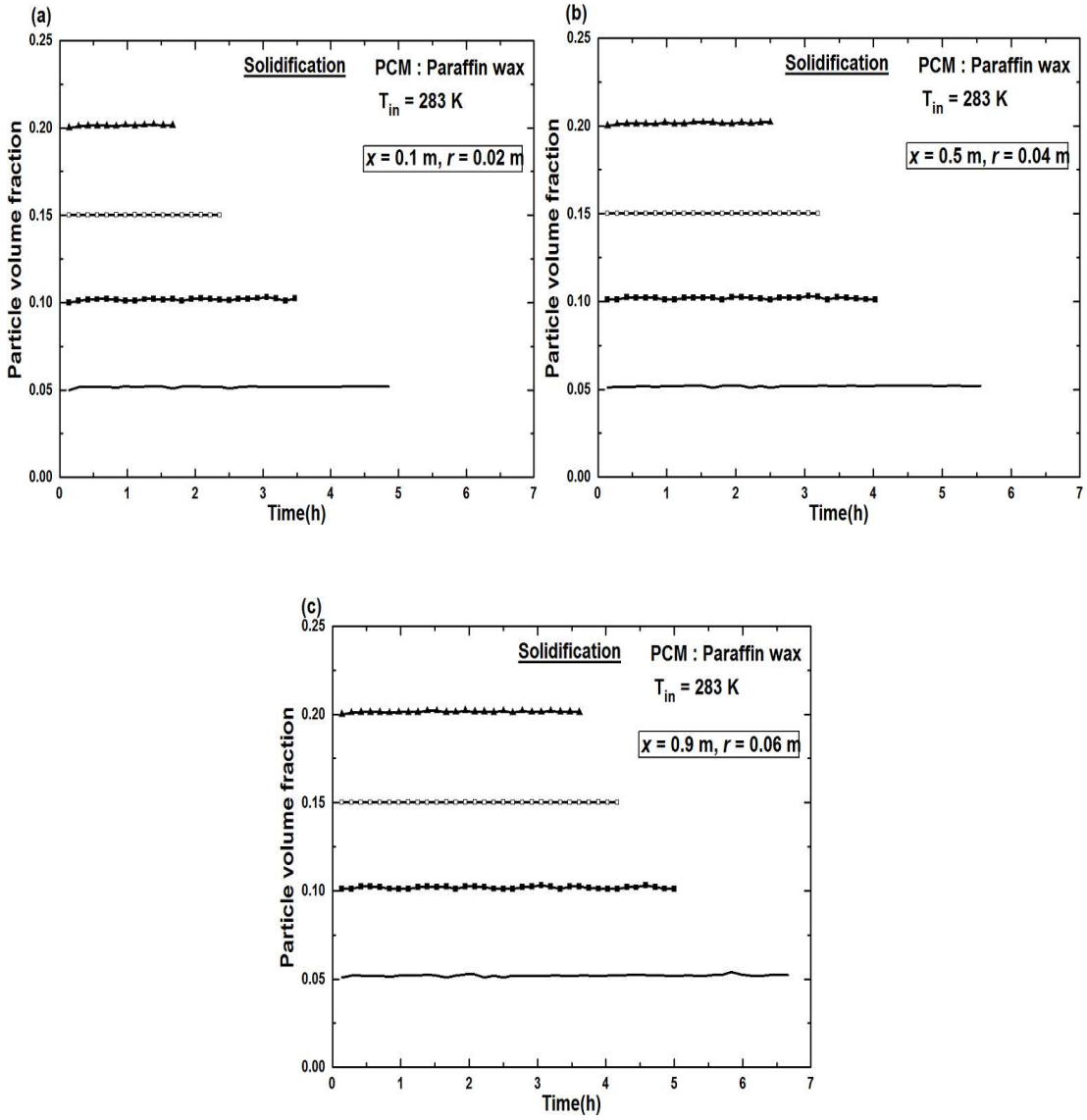

Figure 5.35 Time variation of particle volume fraction at selected locations during solidification of micro particles based composites

Table 5.9 Comparison of percentage decrease in complete solidification time due to nano and micro particles addition (Re = 500, T_{in} = 283 K)

Particle fraction	Decrease in complete solidification time (%)			
	Paraffin wax		Hydrated salt	
	Nano	Micro	Nano	Micro
0.05	9	25	14	30.6
0.1	28	43.8	26.5	43
0.15	40	53.1	39	51
0.2	50	59.4	47	57.1

To quantify the relative benefit of micro particles over nano particles, the decrease in solidification times due to micro particles are compared with that of due to nano particles. The results are presented in Table 5.9 and provide further evidence to the superiority of micro particles during solidification.

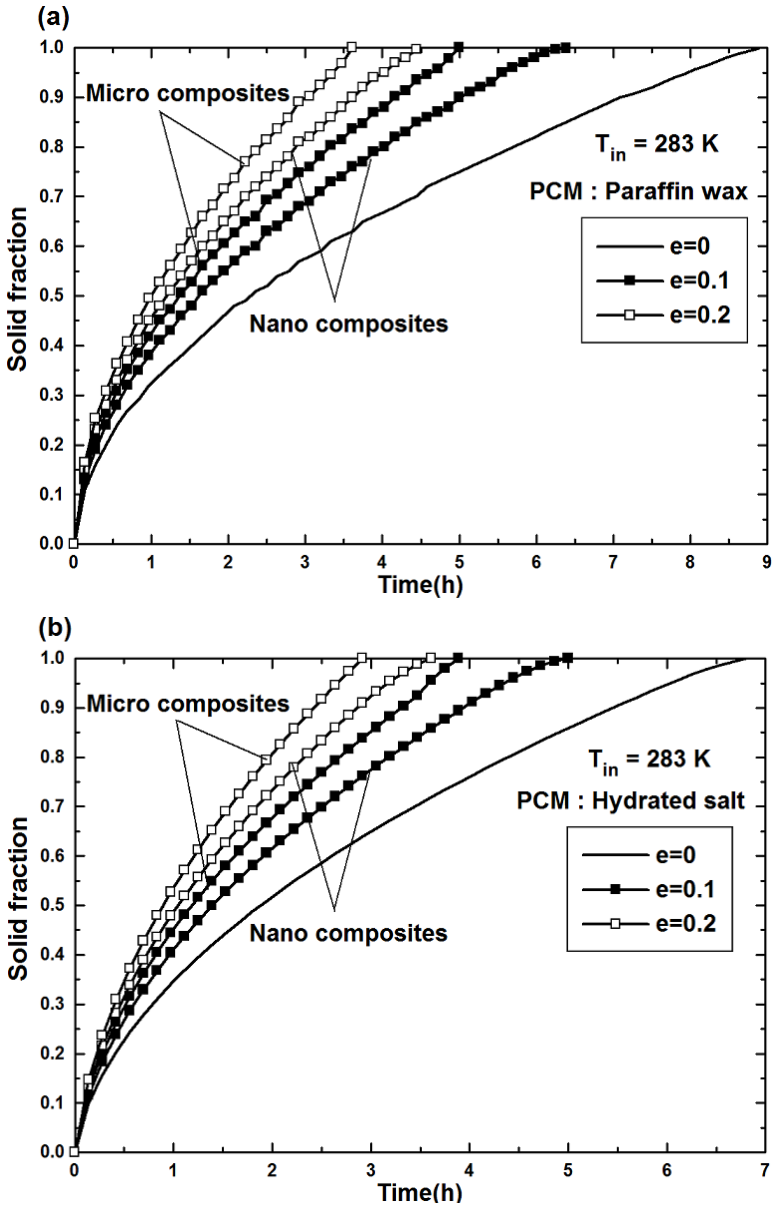

Figure 5.36 Comparison of effects of nano and micro particles on solid fraction during solidification (a) paraffin wax as PCM (b) hydrated salt as PCM

The higher solidification rate at any time obviously leads to more amount of solidified PCM. This can be seen from Figure 5.36, which displays the tracked solid fraction values till the end of solidification. According to Figure 5.36, micro particles

dispersed PCMs contain more solidified amount as compared to pure PCM at all times during solidification. Figure 5.36 also compares micro particles PCMs and nano particles PCMs and the comparison reveals that micro particles of any volume fraction help PCMs to solidify more than what could be done by nano particles of same volume fraction. As mentioned already, this is due to higher enhancement in solidification rate by micro particles.

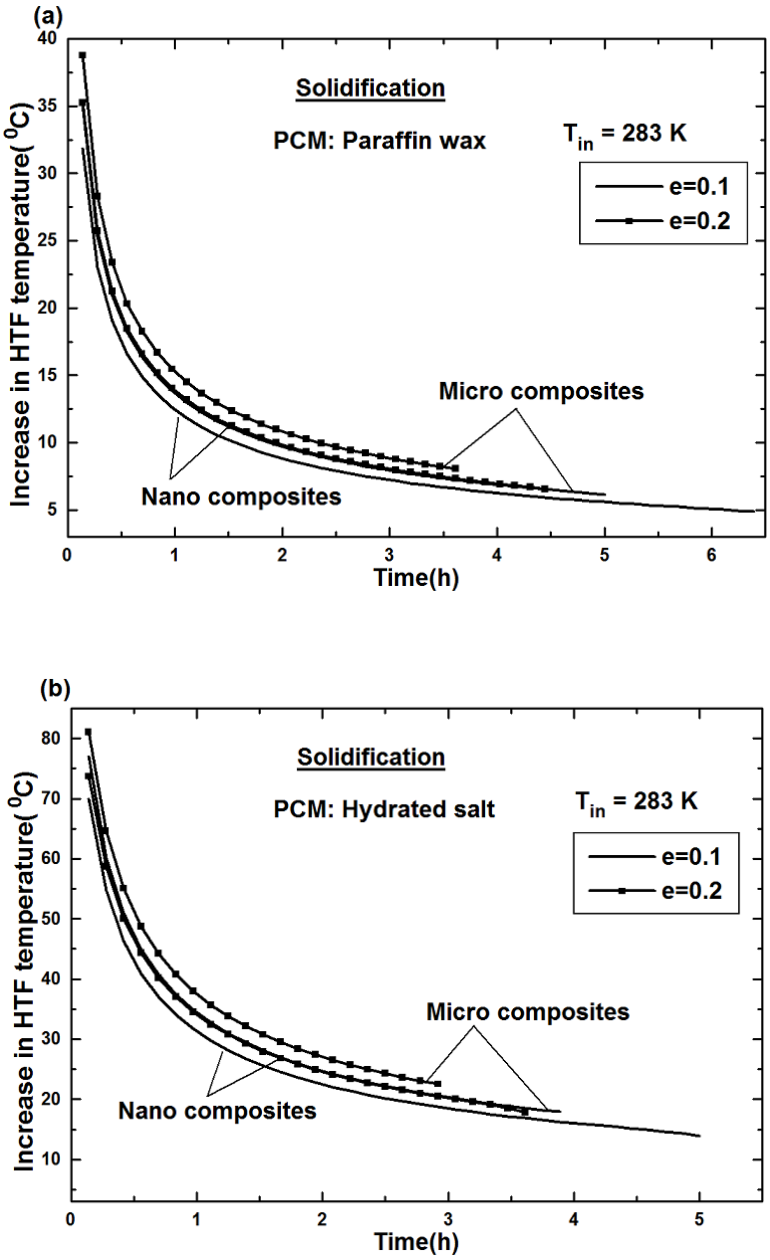

Figure 5.37 Comparison of effects of nano and micro particles on HTF out let temperature during solidification (a) paraffin wax as PCM (b) hydrated salt as PCM

5.6.2 Increase in HTF temperature

The ultimate benefit of employing micro particles rather than nano particles is revealed by Figure 5.37, which shows the time variation of HTF temperature at the outlet of micro and nano particles systems. As a result of higher heat transfer rates, micro particles systems could discharge water at relatively higher temperatures as compared to nano particles systems at all times. Therefore, from energy recovery perspective, dispersing micro particles appears to be more beneficial than employing nano particles for solar water heaters.

5.6.3 Exergy performance during solidification

As it is seen, like nano particles, micro particles also enhance the solidification rate of pure PCM significantly. Similarly, the heat transfer between PCM and HTF takes place at higher temperatures when micro particles are dispersed as observed with nano particles composites. Therefore, the exergy efficiency of micro particles dispersed PCMs should be higher than that of pure PCM. Moreover, the solidification rates and temperatures at which heat transfer occurs are found to be better with micro particles and thus, it can be predicted that systems with micro particles-PCM composites could exhibit higher exergy efficiency than that of their nano particles counter parts. The exergy efficiency results of pure PCM, nano particles-PCMs and micro particles-PCMs displayed in Figure 5.38 back the points discussed above.

As mentioned earlier, the reduction of latent heat of pure PCM is more pronounced when micro particles are added. Due to this fact, the ratio of total energy recovered from micro particles added PCM and that from pure PCM is significantly less as compared to the ratio obtained from nano particles. This can be seen from Figure 5.39. However, the micro particles appear to be superior over nano particles, if the comparison is made in terms ratio of total exergy recovered from particles and that from pure PCM. The results of ratios calculated in terms of exergy are shown in Figure 5.40. The superior exergy performance by micro particles composites is again attributed to the combined effect of higher heat transfer rates and lesser solidification time.

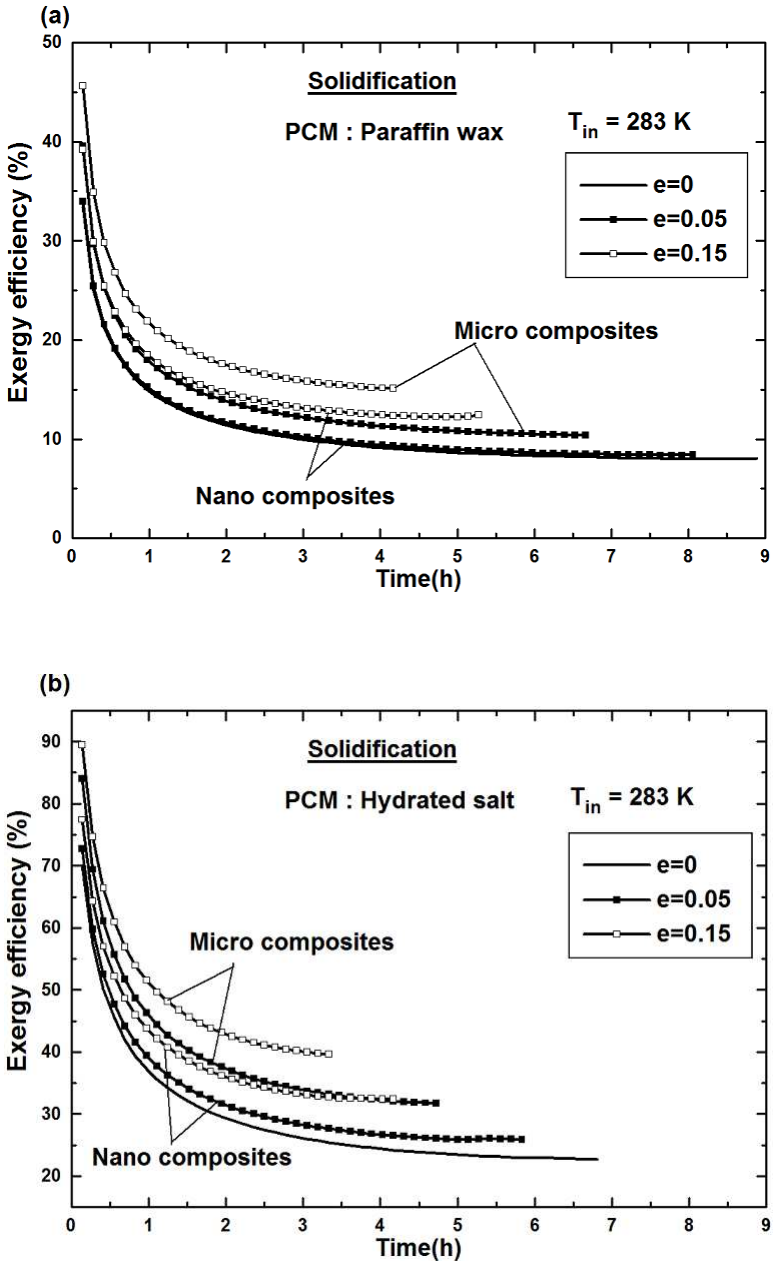

Figure 5.38 Comparison of effects of nano and micro particles on exergy efficiency during solidification (a) paraffin wax as PCM (b) hydrated salt as PCM

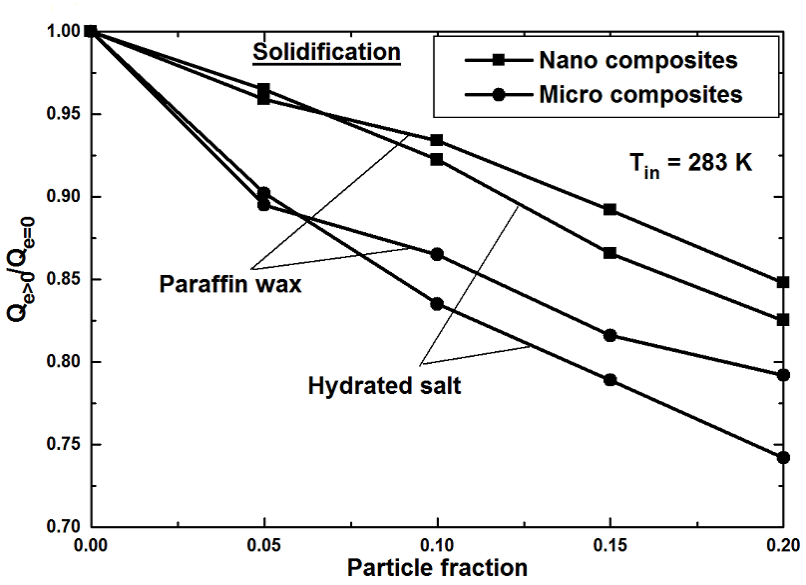

Figure 5.39 Comparison of effects of nano and micro particles on total energy recovered

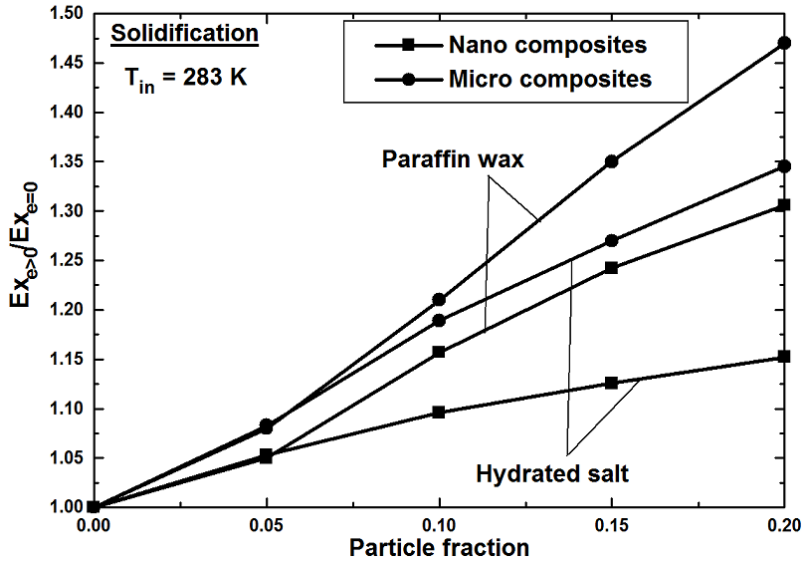

Figure 5.40 Comparison of effects of nano and micro particles on total exergy recovered

5.6.4 Particle migration during melting

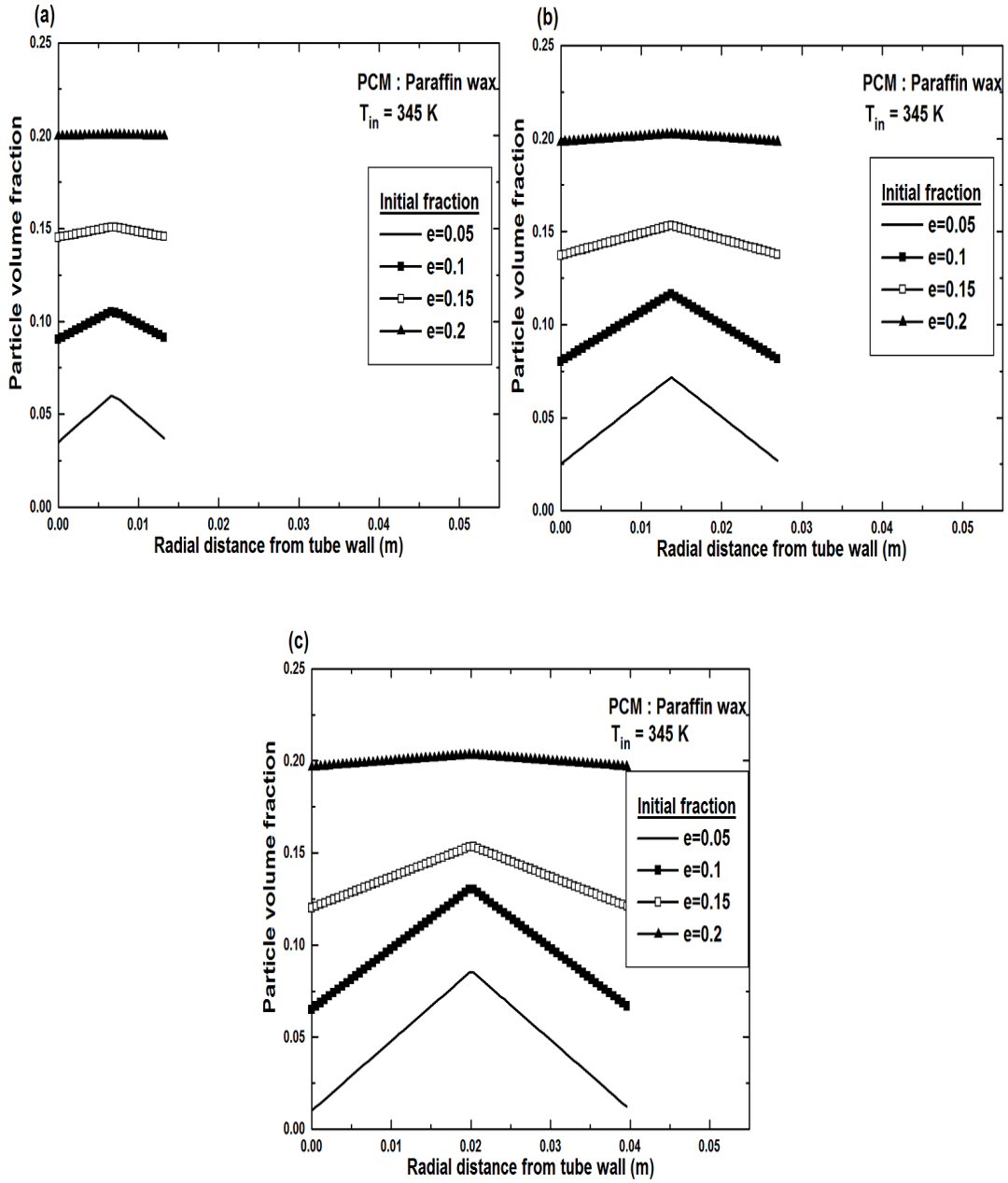

Figure 5.41 Time variation of particle volume fraction during melting of micro particles composites

Unlike the case of solidification, the flow of liquid PCM cannot be ignored during melting. This is because of existence of natural convection throughout the process. Hence, it is important to verify the potential variation of particle concentration as a result of particle migration. It is obvious that the variation of particle volume fraction can be found only in the liquid region. In order to examine the particle distribution at

various times during melting, the concentration profiles are plotted along the radial direction. Since composites of various particle volume fractions melt at different rates, in view of comparison, the profiles are obtained when the melt fractions are 0.25, 0.5 and 0.75. The corresponding graphs are shown in Figure 5.41.

In the liquid region, the distribution of particles is such that the volume fraction is found to be the lowest adjacent to the tube wall and gradually increases in the radial direction. The increase in volume fraction continues up to the middle of the liquid region and thereafter the value starts decreasing to reach the minimum value at the liquid-solid interface. As it is known, the fluid flow due to natural convection is established as the simultaneous upward and downward motions of liquid with the former along the tube wall and the latter along the interface. In such case, it can be assumed that the upward motion is bounded by the left half of the liquid region where as the downward motion exists within the second half. For the upward motion of hot fluid, the local shear rate at tube wall remains maximum and the maximum shear rate forces the particles moving to the centre region where the shear rate is zero. Similarly, maximum shear rate should be found at the interface as it acts as a wall. Hence, the particles are forced to migrate towards centre region due to the flow of cold liquid. This is the reason why the particle profiles appear as shown in Figure 5.41.

Although the above mentioned trend is observed for all values of particle volume fractions, the variation along the radius becomes less as the particle volume fraction increases. This can be attributed to the fact that higher volume fraction weakens the natural convection, which in turn dampens the particle migration. The observed particle migration in this work is consistent with the results of Phillips *et al.* (1992). As the melting progresses, natural convection becomes stronger and hence, the particle migration would be on increasing mode. This is clear from Figure 5.41 as steeper particle concentration profiles are observed at later stages of melting.

5.6.5 Variation of thermal conductivity in terms of particle fraction

For any composite PCM, the experimentally evaluated thermal conductivity can be defined as constant only for solid region. On the other hand, it is not appropriate to use constant value for liquid region as non-uniform particle concentration is observed in the melted PCM. This requires the relation between thermal conductivity of liquid

PCM and particle volume fraction. To establish such a relation, some more data were generated by performing thermal conductivity measurements with samples of different particle fraction values. The variation of thermal conductivity with particle volume fraction is presented in Figure 5.42. In the plots, symbols represent the experimental results of thermal conductivity and the curve is the generated linear regression corresponding to the experimental data. Hence, it is clear that the liquid thermal conductivities of both the PCMs establish a nearly linear relationship with particle volume fraction. The curve fitting procedure subsequently led to the following functions, which were used in the UDFs of thermal conductivities.

Paraffin wax

$$k_l = 0.10481 + 0.45725\,e$$

Hydrated salt

$$k_l = 0.39686 + 1.57022\,e$$

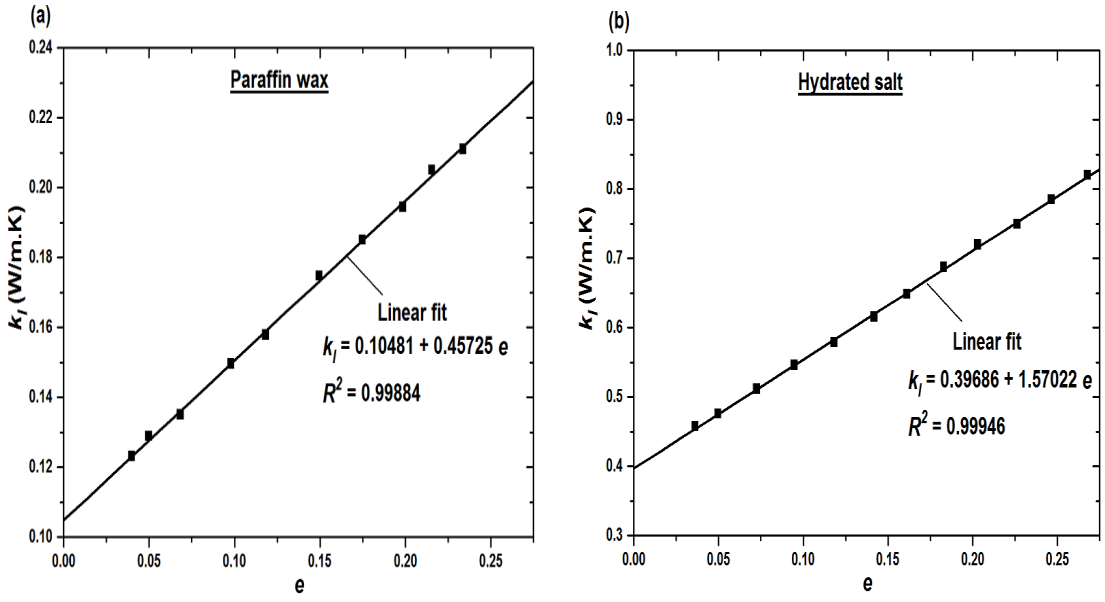

Figure 5.42 Variation of thermal conductivity of liquid micro particles composites with particle volume fraction (a) Paraffin wax composites (b) Hydrated salt composites

5.6.6 Heat transfer during melting

The time wise variation of heat transfer rates during melting of micro composites is compared with that of pure PCM in Figure 5.43. In general, heat transfer enhancement due to micro particles in the PCM is observed only for some initial period of melting. No enhancement rather decreased heat transfer rate could be seen during remaining period. In fact, enhanced heat transfer in the beginning and decreased heat transfer later are found also with nano particles composites. Hence, similar to nano particles, micro particles could enhance heat transfer only during conduction dominated period.

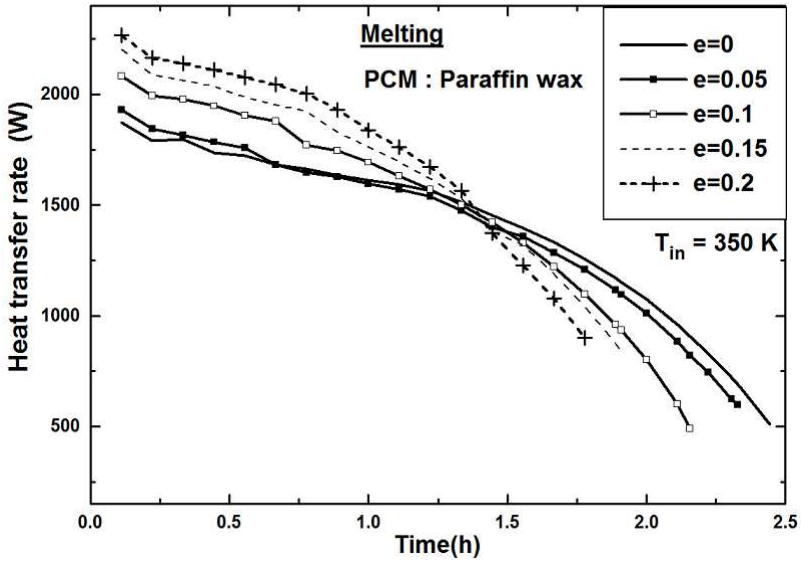

Figure 5.43 Effect of micro particles on instantaneous heat transfer rate during melting

Similarly, micro particles addition also exerts considerable dampening effect on the natural convection and thus, convection dominated melting becomes slow. However, there is significant difference between nano particles composites and micro particles composites. This is shown in Figure 5.44. First notable difference lies in the form of heat transfer enhancement period. Overall, micro particles of any fraction enhance the heat transfer rate for shorter period in comparison with its micro counterpart. However, the gap narrows down with increase in particle fraction. Due to higher thermal conductivity, micro particles PCMs are supposed to exhibit higher heat transfer rate for longer period as compared to nano particles PCMs. However, due to particle migration in the liquid PCM, particle volume fraction adjacent to heat transfer surface becomes less and keeps reducing as time progresses. Hence, effective thermal

conductivity may not be considerably high so that the reduction in heat transfer owing to dampened natural convection could be compensated. As seen earlier, particle migration is not significant when particle fraction is higher. This is the reason why higher particle fraction composites could exhibit higher heat transfer rate for longer period. Because of same reason, during enhanced heat transfer period, there is not much difference between the heat transfer rates of nano and micro composites of lower particle fractions. The difference widens as the particle fraction increases. Nevertheless, relatively higher heat transfer rates are observed with micro particles PCMs of any fraction in comparison with nano particles composites of same volume fraction.

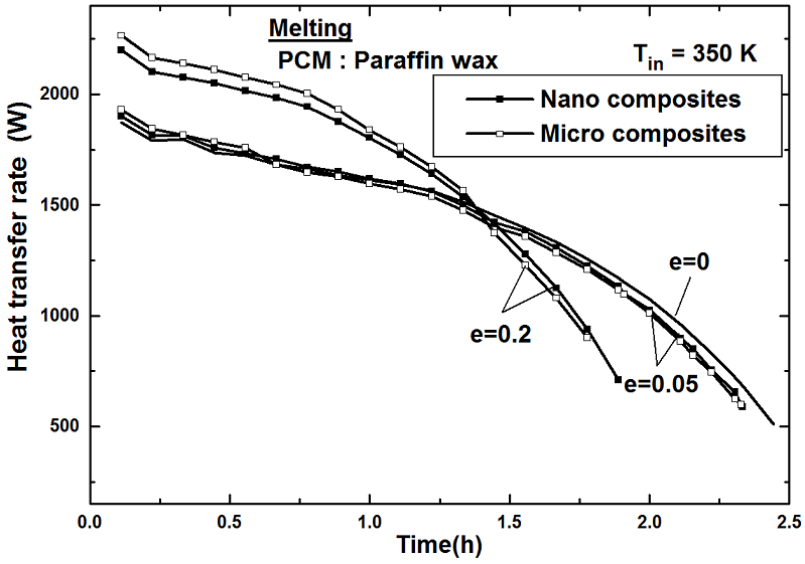

Figure 5.44 Comparison of effects of nano and micro particles on instantaneous heat transfer rate during melting

During convection dominated period, both the types of composites show poor heat transfer rates as compared to pure PCM. At the same time, micro particles composites seem to be more inferior to nano composites irrespective of volume fraction. This is due to the combined effect of higher viscosity and particle migration. In case of nano particles PCMs, first of all there is no particle migration and thus, the effective thermal conductivity remains uniform, which in turn compensates the effect of dampened natural convection to a certain extent. On the other hand, significant particle migration is observed with micro particles of all particles fractions especially at higher times. The particle migration, as it is known, cannot help in enhancing the

conduction heat transfer rate. Moreover, micro particles PCM of any particle fraction is more viscous than its nano counter parts. Table 5.10 presents the comparison of these two PCMs in terms of viscosity. The higher viscosity obviously has more impact in reducing the convection heat transfer.

Table 5.10 Comparison of viscosities of nano and micro particles composites

Particle fraction	Dynamic viscosity (kg/m.s)			
	Paraffin wax		Hydrated salt	
	Nano	Micro	Nano	Micro
0.05	0.031035	0.031371	0.035241	0.035623
0.1	0.035527	0.036466	0.040342	0.041408
0.15	0.040984	0.042968	0.046539	0.048792
0.2	0.047691	0.05146	0.054155	0.058434

Because of the higher transfer rates during first part of melting by micro composites in comparison with nano composites as well as with pure PCM, it is obvious that they could have more melted portion at any time during this period. At the same time, it should be noted that higher fraction by micro composites is maintained even during the second part of melting despite lower heat transfer rates. These characteristics are revealed by Figure 5.45.

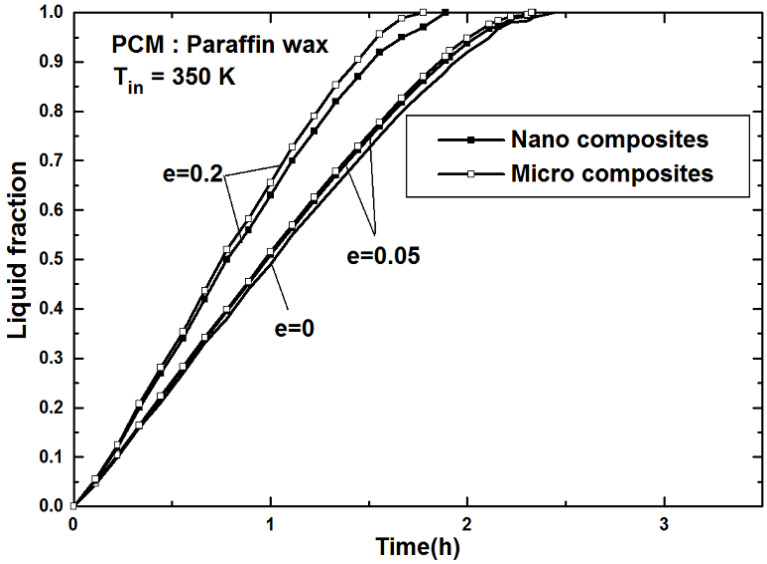

Figure 5.45 Comparison of effects of nano and micro particles on liquid fraction during melting

This means that higher melting achieved during higher heat transfer rate period helps the micro composites to dominate nano composites and pure PCM throughout the melting process and the effect of lower heat transfer rate is not pronounced in this regard. Hence, the micro particles composite of any particle fraction needs less time for complete melting as compared to nano particle composite of same particle fraction or pure PCM. The comparison of micro and nano composites in terms of reduction in melting time is given in Table 5.11.

Table 5.11 Comparison of percentage decrease in complete melting time due to nano and micro particles addition (Re = 500, T_{in} = 350 K)

Particle fraction	Decrease in complete melting time (%)			
	Paraffin wax		Hydrated salt	
	Nano	Micro	Nano	Micro
0.05	4.5	4.7	6.8	7
0.1	10	11.8	10	13
0.15	18	22	17	22
0.2	22.7	27.3	20.5	26

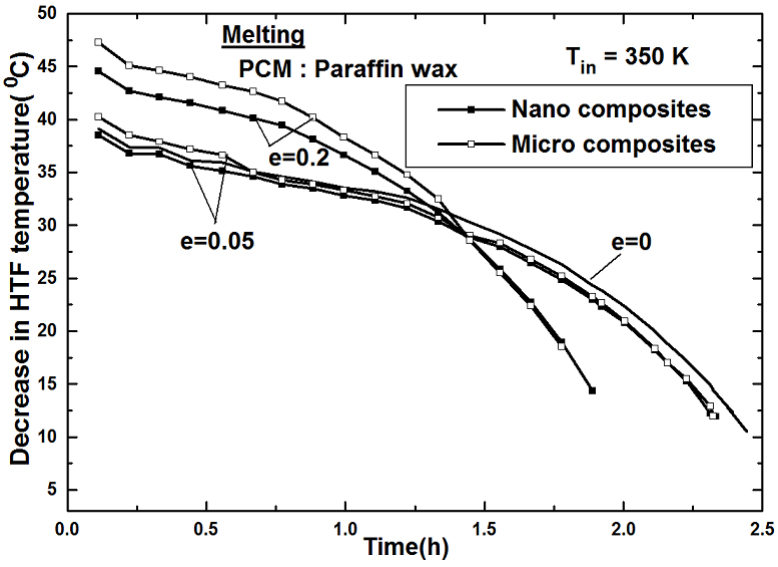

Figure 5.46 Comparison of effects of nano and micro particles on HTF out let temperature during melting

It should be mentioned that the superiority of micro particles composites in reducing the melting time is more pronounced if the particle fraction is higher. Again this is related to particle migration. As seen earlier, higher heat transfer rates are observed

for longer period when particle fraction is more because of weak particle migration. Lower heat transfer rate for a smaller period could not dampen the effect of high heat transfer rate which prevails for longer period. As a result, higher particle fraction micro composites are found to be reducing melting time significantly. On the other hand, only moderate reduction is observed when particle fraction is less as the effect of enhanced melting rate is dampened to a certain extent by lower rate of heat transfer during long period of melting. It is obvious that the effects of higher and lower heat transfer rates are directly reflected on the HTF outlet temperature. The increase in HTF outlet temperature as a result of micro particles in the PCM is in line with the heat transfer rates as shown in Figure 5.46.

5.6.7 Exergy performance during melting

To explore the exergy performance of micro particles added PCMs, the evaluated exergy efficiency of the same is compared with that of pure PCM and nano particles PCMs. The comparison is illustrated by Figure 5.47.

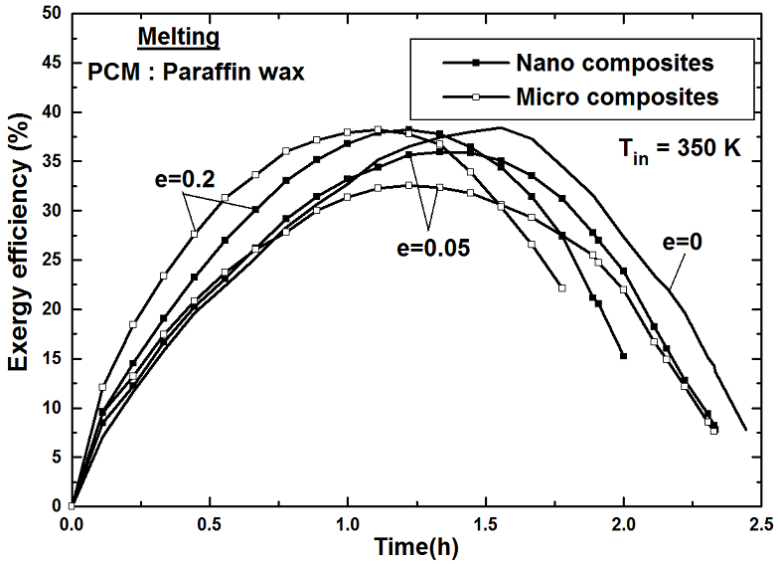

Figure 5.47 Comparison of effects of nano and micro particles on exergy efficiency during melting

As expected, micro composites possess better exergy efficiency than nano composites or pure PCM only when the heat transfer rate is enhanced by micro composites. During this period, the difference between exergy efficiencies of micro and nano composites is more significant, if the particle fraction is higher. This is

because of large gap between the heat transfer rates of those two composites. Similar behavior in terms of difference in exergy efficiencies can be seen even during the second part of melting, i.e. the period of decreased heat transfer rate by nano / micro composites. However, now the exergy efficiency of the micro composites is less in comparison with nano composites or pure PCM as the former is found to be inferior in terms of heat transfer rate during this period.

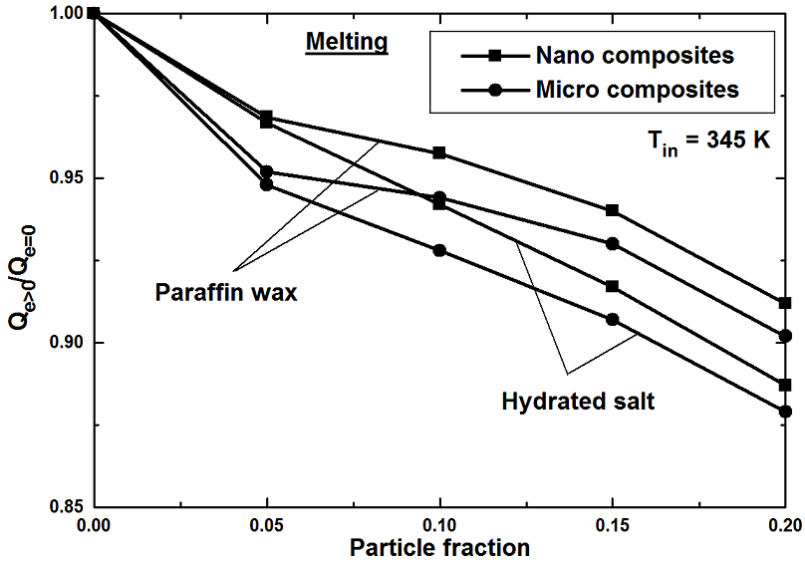

Figure 5.48 Comparison of effects of nano and micro particles on total energy stored

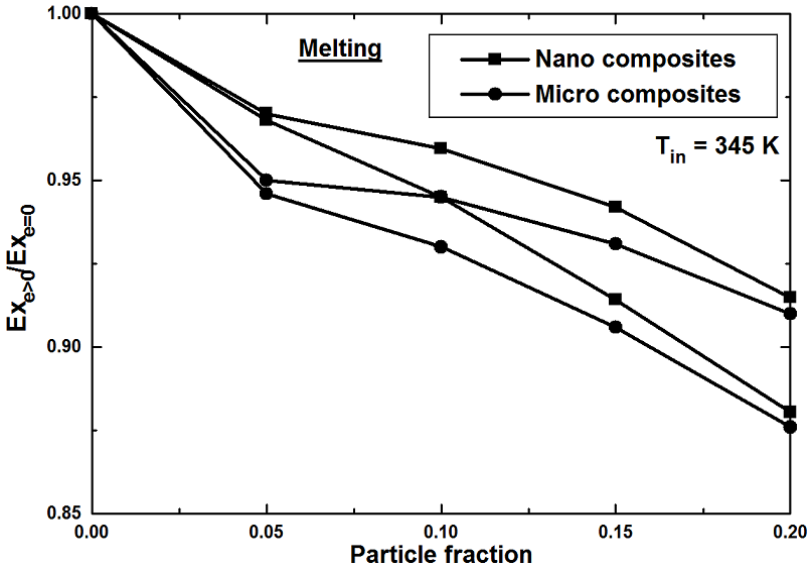

Figure 5.49 Comparison of effects of nano and micro particles on total exergy stored

As observed during solidification, the effect of reduced latent heat due to addition of micro particles is also manifested during melting. According to Figure 5.48, the ratio of total energy stored by micro particles added PCM and that by pure PCM decreases with increase in particle fraction. As far as exergy ratio is concerned, the behavior of micro particles PCMs during melting is distinct from what is observed during solidification. This is evident from Figure 5.49. Although the same trend is seen with nano particles, the decrease in energy / exergy ratio is relatively more in case of micro particles PCMs. As seen earlier, the latent heat of micro particles PCM of any particle fraction is less as compared to that of its nano counterpart. Hence, it can be stated that the reduced latent heat exerts similar effect on both the energy and exergy storage capacities. Also, this is true whether it is nano or micro particles.

For micro particles PCMs, the results presented here are based on paraffin wax. However, all the discussed points are also valid for hydrated salt based micro particles composites as they showed similar trend whether it is heat transfer behavior or exergy performance. The results of hydrated salt - micro particles composites are given in Appendix IV.

The heat transfer behavior of micro particles-PCM composites is no different from nano particles-PCM composites when it comes to response to variation of Re or variation of HTF inlet temperature. Hence, the discussion on these points is not repeated here and the results are shown in Appendix V.

Chapter 6: Summary and Conclusions

The major problem in managing energy from renewable energy sources, like solar energy is the time gap between the availability and the need. Although LHTS systems provide an attractive solution for this problem, the thermal performance has not been up to the expected level and the large scale utilization of LHTS units, remains unsuccessful. In this work, numerical studies are carried out to investigate the performance enhancement of a shell and tube storage unit applicable to solar water heaters due to the addition of high conductivity particles during charging and discharging processes. Exergy based performance evaluation is taken as a main aspect to explore both positive and adverse effects of particles dispersion on the exergy performances of conventional PCMs.

Extensive literature survey has been carried out on various proposed techniques to enhance the thermal conductivity of PCMs. The feasibility and limitations of those techniques are identified. The literature survey is also extended to address the issues related to exergy based performance evaluation of LHTS systems. The review is intended to study various exergy based evaluation techniques with their applications to a variety of LHTS systems and to come out with suitable exergy models for systems employed for solar water heaters.

Two kinds of PCMs namely, paraffin wax and hydrated salt are used to compare the relative strengths and weaknesses of organic and inorganic group PCMs. As far as particle is concerned, the influences of both nano as well as micro size copper particles are analyzed. To evaluate the thermo-physical properties of nano particles composites suitable analytical expressions are proposed whereas those of micro particles composites are measured using experimental procedure based on *Temperature-History* technique.

The melting and solidification processes are mathematically modeled with an enthalpy based method and the resulting system of conjugate governing equations are numerically solved employing commercial CFD code FLUENT. Although the numerical model for solidification process of pure PCM and nano particles

composites has neglected the natural convection in the liquid PCM, the same has been simulated using Rayleigh number (Ra) based effective thermal conductivity for liquid PCM in the modeling of melting. An additional transport equation, which is a constitutive equation for particle flux is included in the mathematical model for phase change processes of micro particles dispersed PCMs. The developed transport equation simulates the particle migration in the PCM as a result of shear rate gradient.

The numerical trails are performed for several mass flow rates and inlet temperatures of HTF. The conclusions of the evaluation derived from investigations are discussed below.

6.1 Conclusions

6.1.1 General conclusions

1. Exergy based performance evaluation of LHTS system can be stated as more perspective measure than energy based one as it reflects the true potential of the system.
2. Although it is appropriate to model the solidification as conduction dominated process, the role of natural convection during melting process cannot be ignored. For the simulation of natural convection, the effective thermal conductivity model is said to be fairly accurate and computationally inexpensive.
3. The numerical models employed for pure PCM are sufficient enough to simulate the physical conditions as the yielded results have shown good agreement with literature results.
4. Although the numerical results of micro particles dispersed PCMs during solidification have agreed well with experimental results, the results of melting have shown deviation to a certain extent especially when the particle volume fraction is less. The incapability of the CFD package in accessing the variation of latent heat and specific heat as a result of particle migration can be mentioned as a reason for this.
5. In case of micro particles dispersed PCMs, particles distribution remains

uniform during solidification as the effect of particle migration is not observed. On the other hand, because of particles migration, they tend to move away from the heat transfer surface during melting. The strength of migration effect increases as the time progresses and the particle fraction decreases.

6.1.2 Measurements of thermo-physical properties

6. The PCMs can undergo phase change almost at the same temperature range irrespective of quantity of particles dispersed.
7. If a PCM suffers from subcooling problem, the addition of particles would be of no help in alleviating the same.
8. For the measurement of latent heat and specific heats of PCMs, the *Temperature-History* technique can be preferred over other techniques such as DSC, DTA and DC methods as it is simple and cost effective technique and facilitates the testing of several samples simultaneously.
9. The thermal conductivity measurement of PCM can be realized in a fairly accurate manner through a technique based on the perturbation principle if the conditions for one dimensional heat transfer are satisfied.
10. The thermal conductivity of pure PCMs can be augmented by dispersing the high conductivity particles in the PCMs. Although both nano and micro size particles are comparable in this account, the micro size particles have edge over nano particles. In any case, thermal conductivity increases linearly with increase in particle volume fraction.
11. The short coming of particles in the PCMs is exposed in the light of reduced latent heat and specific heat capacities of composites PCMs. Moreover, reduction in heat capacities is relatively high when micro particles are added.

6.1.3 Thermal performance enhancement

12. Due to the augmentation of thermal conductivity, the discharging rate of LHTS systems loaded with composite PCMs is significantly high and micro

particles are superior to nano particles in enhancing the heat transfer performance during discharging.

13. Particles addition, however, dampens the natural convection and thus, melting rate cannot be enhanced.
14. The dampening of natural convection is more prominent when micro particles are dispersed as the viscosity of micro particles composite is higher than that of nano particles composite.
15. On the thermal performance enhancement aspect, hydrated salt PCM enjoys the benefit of particles dispersion more in comparison with paraffin wax PCM during charging rather than during discharging.
16. In solar thermal applications, heat transfer enhancement is required mainly for discharging process rather than for charging. This is because heat is available at constant rate for longer period and the same has to be removed at faster rate. Hence, the particles addition can be stated as a promising enhancement technique for LHTS system of solar water heaters as producing hot water at faster rate in the evening and night is most critical.
17. Apart from enhancing discharging rate, only particles dispersed PCMs produce water at sufficiently high temperature for longer period.

6.1.4 Exergy performance

18. Both the nano and micro size particles help in increasing the exergy efficiency of pure PCM system during discharging.
19. The exergy recovered from composites are also higher as compared to that of pure PCM.
20. From both the exergy efficiency and exergy recovered perspectives, the micro particles are superior to nano particles. However, opposite trend is disclosed by micro particles during charging.
21. In any case, hydrated salt composites can exhibit better exergy efficiency than paraffin wax composites due to their enhanced thermal performance. However, the former cannot be stated as better choice because of its inability to store /recover more exergy.

6.1.5 Influence of operating conditions

22. Increasing Re has less significant influence on performance enhancement than that of particle addition.
23. Higher Re i.e. higher mass flow rates of HTF require high pumping power. Hence, the addition of high conductivity particles is better option than increasing Re/mass flow rate of HTF.
24. On the other hand, variation in HTF inlet temperature is seen influential. The LHTS systems would produce better heat transfer performance when the difference between HTF inlet temperature and melting temperature of PCM is higher. However, the exergy performance can be superior if lower temperature difference prevails.

6.2 Specific contributions

1. The thesis is a maiden attempt to employ exergy analysis for the evaluation of performance enhancement of a LHTS system due to the dispersion of high conductivity particles.
2. The thesis contributes to the literature by reporting the information on the thermal behavior of micro particles dispersed PCMs, first time.
3. The effect of particle dispersion on natural convection during melting is critically analyzed.
4. The validation of a much simpler model for the simulation of natural convection during melting of PCM is reported.
5. Simultaneous effects of enhanced thermal conductivity and reduced latent heat as a result of particles addition are investigated.
6. The roles of nano size and micro size particles in enhancing the performance of LHTS systems are comprehensively discussed.
7. The relative strengths and limitations of an organic PCM and an inorganic PCM are also compared.

6.3 Future scope of work

1. Experimental investigations may be carried out for the validation of the numerical model employed for nano particles composites.
2. A computer code may be developed to obtain the solution for numerical formulation of micro particles composites rather than employing general purpose code. This may permit the formulation to include the variation of latent heat and specific heat which arises due to particle migration.
3. The numerical study may be extended to various geometrics and further investigations may be attempted under various geometrical parameters.

References

1. Adebiyi GA (1991). A Second-law study on packed bed energy storage systems utilizing phase- change materials. ASME Journal of Solar Energy Engineering. 113:146-156.
2. Adine HA, El-Qarnia H (2009). Numerical analysis of the thermal behavior of a shell-and-tube heat storage unit using phase change materials. Applied Mathematical Modeling. 33:2132-2144.
3. Agyenim F, Hewitt N, Eames P, Smyth M (2010). A review of materials and phase change problem formulation for latent heat thermal energy storage systems (LHTESS). Renewable and Sustainable Energy Reviews. 14:615-628.
4. Akgun M, Aydin O, Kaygusuz K (2007). Experimental study on melting/solidification characteristics of a paraffin as PCM. Energy Conversion and Management. 48:669-678.
5. Alkan C, Sari A, Karaipekli A, Uzun O (2009). Preparation, characterization, and thermal properties of microencapsulated phase change material for thermal energy storage. Solar Energy Materials and Solar Cells. 93:143-147.
6. Al-Naglah MA (1997). Second-law-based thermoeconomic analysis and optimization of thermal-energy-storage systems. M.S thesis. Faculty of the College of Graduate Studies. King Fahd University of Petroleum and Minerals. Dhahran. Saudi Arabia.
7. Azzouz K, Leducq D, Gobin D (2010). Enhancing the performance of household refrigerators with latent heat storage: An experimental investigation. International Journal of Refrigeration. 32:1634-1644.
8. Badar MA, Zubair SM (1995). On thermoeconomic of a sensible heat thermal energy storage system. ASME Journal of Solar Energy Engineering. 117:225-259.
9. Badar MA, Zubair SM, Al-Farayedhi AA (1993). Second-law-based thermoeconomic optimization of a sensible heat thermal energy storage system. Energy. 18:641-649.
10. Badescu V (2007). Optimal control of flow in solar collectors for maximum exergy extraction. International Journal of Heat and Mass Transfer. 50**:** 4311-4322.

11. Bahrami PA (1990). Natural melting within a spherical shell. NASA Technical Memorandum. 102822.
12. Bayón R, Rojas E, Valenzuela L, Zarza E, León J (2010). Analysis of the experimental behaviour of a 100 kW^{th} Latent heat storage system for direct steam generation in solar thermal power plants. Applied Thermal Engineering. 30: 2643-2651.
13. Bejan A (1978). Two thermodynamic optima in the design of sensible heat units for energy storage. Journal of Heat Transfer. 100:708-712.
14. Bejan A (1989). Analysis of melting by natural convection in an enclosure. International Journal of Heat and Fluid Flow. 10:245-252.
15. Bejan A (1996). Entropy generation minimization. London: CRC press.
16. Bejan A (2004). Convection heat transfer. New York: Wiley.
17. Bellecci C, Conti M (1994). Phase change energy storage: entropy production, irreversibility, and second law efficiency. Solar Energy. 53:163-170.
18. Bi Y, Guo T, Zhang L, Chen L, Sun F (2010). Entropy generation minimization for charging and discharging processes in a gas-hydrate cool storage system. Applied Energy. 87:1149-1157.
19. Buddhi D, Sawhney RL, Sehgal PN, Bansal NK (1987). A simplification of the differential thermal analysis method to determine the latent heat of fusion of phase change materials. Journal of Physics D: Applied Physics. 20:1601-1605.
20. Cabeza LF, Castellon C, Nogues M, Medrano M, Leppers R, Zubillaga O (2007). Use of microencapsulated PCM in concrete walls for energy savings. Energy Buildings. 39:113-119.
21. Cabeza LF, Ibanez M, Sole C, Roca J, Nogues M (2006). Experimentation with water tank including a PCM module. Solar Energy Materials and Solar Cells. 90:1273-1282.
22. Caldwell J, Kwan YY (2003). On the perturbation method for the Stefan problem with time-dependent boundary conditions. International Journal of Heat and Mass Transfer. 46:1497-1501.
23. Caldwell J, Kwan YY (2009). A brief review of several numerical methods for one-dimensional Stefan problems. Thermal Science. 13:61-72.
24. Canbazoglu S, Sahinaslan A, Ekmekyapar A, Aksoy YG, Akarsu F (2005).

Enhancement of solar thermal energy storage performance using sodium thiosulfate pentahydrate of a conventional solar water-heating system. Energy Buildings. 37:235-242.

25. Cerón I, Neila J, Khayet M (2011). Experimental tile with phase change materials (PCM) for building use. Energy and Buildings. 43:1869-1874.
26. Challis RE, Povey MJW, Mather ML, Holemes AK (2005). Ultrasound techniques for characterizing colloidal dispersions. Reports on Progress in Physics. 68:1541-1637.
27. Chan ALS (2011). Energy and environmental performance of building façades integrated with phase change material in subtropical Hong Kong. Energy and Buildings. 43:2947-2955.
28. Charach Ch (1993). Second-law efficiency of an energy storage-removal cycle in a phase-change material shell-and-tube heat exchanger. ASME Journal of Solar Energy Engineering. 115:240-243.
29. Charach Ch, Zemel A (1992). Thermodynamic analysis of latent heat storage in a shell-and-tube heat exchanger. ASME Journal of Solar Energy Engineering. 114:93-99.
30. Cheng W, Mei B, Liu Y, Huang Y, Yuan X (2011). A novel household refrigerator with shape-stabilized PCM (Phase Change Material) heat storage condensers: An experimental investigation. Energy. 36:5797-5804.
31. Cherkasova AS (2009). Thermal conductivity enhancement in micro- and nano-particle suspensions. Doctoral Dissertation. Graduate School-New Brunswick Rutgers. The State University of New Jersey. New Jersey. USA.
32. Choi SUS, Zhang ZG, Yu W, Lockwood FE, Grulke EA (2001). Anomalous thermal conductivity enhancement in nanotube suspensions. Applied Physics Letters. 79:2252-2254.
33. Cui H, Yuan X, Hou X (2003). Thermal performance analysis for a heat receiver using multiple phase change materials. Applied Thermal Engineering. 23:2353-2361.
34. Date AW (1992). Novel strongly implicit enthalpy formulation for multidimensional Stefan problems. Numerical Heat Transfer Part B. 21:231-251.
35. Demirbas MF (2006). Thermal energy storage and phase change materials: an

overview. Energy Sources Part B. 1:85-95.

36. Demirel Y (2007). Heat storage by phase changing materials and thermoeconomics. *In* Paksoy HO (Editor). Thermal energy storage for sustainable energy consumption. Dordrecht: Springer. p 133-151.
37. Demirel Y, Ozturk HH (2006). Thermoeconomics of seasonal latent heat storage systems. International Journal of Energy Research. 30:1001-1012.
38. Devahastin S, Pitakusuriyarat S (2006). Use of latent heat storage to conserve energy during drying and its effect on drying kinetics of a food product. Applied Thermal Engineering. 26:1705-1713.
39. Dincer I, Cengel YA (2001). Energy, entropy and exergy concepts and their roles in thermal engineering. Entropy. 3:116-149.
40. Domanski R, Fellah G (1996). Exergy analysis for the evaluation of a thermal storage system employing PCMs with different melting temperatures. Applied Thermal Engineering. 16:907-919.
41. Dutil Y, Rousse DR, Salah NB, Lassue S, Zalewski L (2011). A review on phase-change materials: Mathematical modeling and simulations. Renewable and Sustainable Energy Reviews. 15:112-130.
42. Eastman JA, Phillpot SR, Choi SUS, Keblinski (2004). Thermal transport in nanofluids. Annual Review of Materials Research. 34:219-246.
43. El Qarnia H (2009). Numerical analysis of a coupled solar collector latent heat storage unit using phase change materials for heating the water. Energy Conversion and Management. 50:247-254.
44. El-Dessouky H, Al-Juwayhel F (1997). Effectiveness of a thermal energy storage system using phase-change materials. Energy Conversion and Management. 38:601-617.
45. Elgafy A, Lafdi K (2005). Effect of carbon nanofiber additives on thermal behavior of phase change materials. Carbon. 43:3067-3074.
46. Erek A, Dincer I (2008). An approach to entropy analysis of a latent heat storage module. International Journal of Thermal Sciences. 47:1077-1085.
47. Erek A, Dincer I (2009). A New approach to energy and exergy analyses of latent heat storage unit. Heat Transfer Engineering. 30:506-515.
48. Ettouney H, Alatiqi I, Al-Sahali M, Al-Ali SA (2004). Heat transfer enhancement by metal screens and metal spheres in phase change energy

storage systems. Renewable Energy. 29:841-860.

49. Ettouney H, Alatiqi I, Al-Sahali M, Al-Hajirie K (2006). Heat transfer enhancement in energy storage in spherical capsules filled with paraffin wax and beads. Energy Conversion and Management. 47:211-228.

50. Ettouney H, El-Dessouky H, Al-Ali A (2005). Heat transfer during phase change of paraffin wax stored in spherical shells. ASME Journal of Solar Energy Engineering. 127:357-365.

51. Ettouney H, El-Dessouky H, Al-Kandari E (2004). Heat transfer characteristics during melting and solidification of phase change energy storage process. Industrial and Engineering Chemical Research. 43:5350-5357.

52. Fan J, Wang L (2011). Review of heat conduction in nanofluids. ASME Journal of Heat Transfer. 133:040801-1-14.

53. Fan L, Khodadadi JM (2011). Thermal conductivity enhancement of phase change materials for thermal energy storage: A review. Renewable and Sustainable Energy Reviews. 15:24-46.

54. Fang M, Chen G (2007). Effects of different multiple PCMs on the performance of a latent thermal energy storage system. Applied Thermal Engineering. 27:994-1000.

55. Farid M, Kim Y, Honda T, Kanzawa A (1989). The role of natural convection during melting and solidification of PCM in a vertical cylinder. Chemical Engineering Communications. 84:43-60.

56. Farid MM, Kanzawa A (1989). Thermal performance of a heat storage module using PCM's with different melting temperatures: mathematical modeling. ASME Journal of Solar Energy Engineering. 111:152-157.

57. Farid MM, Khudhair AM, Razack SAK, Al-Hallaj S (2004). A review on phase change energy storage: materials and applications. Energy Conversion and Management. 45:1597-1615.

58. Fiedler T, Ochsner A, Belova IV, Murch GE (2008). Thermal conductivity enhancement of composite heat sinks using cellular materials. Defect and Diffusion Forum. 273-276:222-226.

59. Frusteri F, Leonardi V, Vasta S, Restuccia G (2005). Thermal conductivity enhancement of a PCM based storage syatem containing carbon fibers.

Applied Thermal engineering. 25:1623-1633.

60. Fukai J, Hamada Y, Morozumi Y, Miyatake O (2002). Effect of carbon-fiber brushes on conductive heat transfer in phase change materials. International Journal of Heat and Mass Transfer. 45:4781-4792.

61. Fukai J, Hamada Y, Morozumi Y, Miyatake O (2003). Improvement of thermal characteristics of latent heat thermal energy storage units using carbon-fiber brushes: experiments and modeling. International Journal of Heat and Mass Transfer. 46:4513-4525.

62. Fukai J, Hamada Y, Morozumi Y, Miyatake O (2003). Improvement of thermal characteristics of latent heat thermal energy storage units using carbon-fiber brushes: experiments and modeling. International Journal of Heat and Mass Transfer. 46:4513-4525.

63. Fukai J, Kanou M, Kodama Y, Miyatake O (2000). Thermal conductivity enhancement of energy storage media using carbon fibers. Energy Conversion and Management. 41:1543-1556.

64. Gharebaghi M, Sezai I (2008). Enhancement of heat transfer in latent heat storage modules with internal fins. Numerical Heat Transfer Part A. 53:749-765.

65. Gil A, Medrano M, Martorell I, Lázaro A, Dolado P, Zalba B, Cabeza LF (2010). State of the art on high temperature thermal energy storage for power generation. Part 1—Concepts, materials and modellization. Renewable and Sustainable Energy Reviews. 14:31-55.

66. Goel M, Roy SK, Sengupta S (1994). Laminar forced convection heat transfer in microencapsulated phase change material suspensions. International Journal of Heat and Mass Transfer. 37:593-604.

67. Gong ZX (1996). Time-dependent melting and freezing heat transfer in multiple phase change materials. PhD thesis. Department of Chemical Engineering. McGill University. Mantreal. Canada.

68. Gong ZX, Devahastin S, Mujumdar AS (1999). Enhanced heat transfer in free convection-dominated melting in a rectangular cavity with an isothermal vertical wall. Applied Thermal Engineering. 19:1237-1251.

69. Gong ZX, Mujumdar AS (1996a). Thermodyanamic optimization of the thermal process in energy storage using multiple phase change materials.

Applied Thermal Engineering. 17:1067-1083.

70. Gong ZX, Mujumdar AS (1996b). Finite element analysis of a multistage latent heat thermal storage system. Numerical Heat Transfer Part A. 30:669-684.

71. Gumus M (2009). Reducing cold-start emission from internal combustion engines by means of thermal energy storage system. Applied Thermal Engineering. 29:652-660.

72. Haillot D, Py X, Goetz V, Benabdelkarim M (2008). Storage composites for the optimization of solar water heating systems. Chemical Engineering Research and Design. 86:612-617.

73. Hamada Y, Fukai J (2005). Latent heat thermal energy storage tanks for space heating of buildings: comparison between calculations and experiments. Energy Conversion and Management. 46:3221-3235.

74. Hamada Y, Ohtsu W, Fukai J (2003). Thermal response in thermal energy storage material around heat transfer tubes: effect of additives on heat transfer rates. Solar Energy. 75:317-328.

75. Hamada Y, Otsu W, Fukai J, Morozumi Y, Miyatake O (2005). Anisotropic heat transfer in composites based on high-thermal conductive carbon fibers. Energy. 30:221-233.

76. Hasan A, McCormack SJ, Huang MJ, Norton B (2010). Evaluation of phase change materials for thermal regulation enhancement of building integrated photovoltaics. Solar Energy. 84: 1601-1612.

77. Hasnain SM (1998). Review on sustainable thermal energy storage technologies, part I: Heat storage materials and techniques. Energy Conversion and Management. 39:1127-1138.

78. Hawlader MNA, Uddin MS, Zhu HJ (2002). Encapsulated phase change materials for thermal energy storage: experiments and simulation. International Journal of Energy Research. 2002; 26:159-171.

79. He B (2004). High-Capacity Cool Thermal Energy Storage for Peak Shaving. Doctoral Thesis Department of Chemical Engineering and Technology. KTH Chemical Engineering and Technology. Stockholm. Sweden.

80. Heine MC, Vicente J, Klingenberg DJ (2006). Thermal transport in sheared electro-and magnetorheological fluids. Physics of Fluids. 18:023301-11.

81. Hepbasli A (2008). A key review on exergetic analysis and assessment of renewable energy resources for a sustainable development. Renewable and Sustainable Energy Reviews. 12:593-661.
82. Ho CJ, Gao JY (2009). Preparation and thermophysical properties of nanoparticle-in-paraffin emulsion as phase change material. International Communications in Heat and Mass Transfer. 36:467-470.
83. Hong H, Kim SK, Kim YS (2004). Accuracy improvement of T-history method for measuring heat of fusion of various materials. International Journal of Refrigeration. 27: 360-366.
84. Hong H, Park CH, Choi JH, Peck JH (2003). Improvement of the T-history method to measure heat of fusion for phase change materials. International Journal of Air-Conditioning and Refrigeration. 11: 32-39.
85. Huang CL, Shih YP (1975). A perturbation method for spherical and cylindrical solidification. Chemical Engineering Science. 30:897-906.
86. Huang MJ, Eames PC, Norton B, Hewitt NJ (2011). Natural convection in an internally finned phase change material heat sink for the thermal management of photovoltaics. Solar Energy Materials and Solar Cells. 95:1598-1603.
87. Incropera FP, Dewitt DP, Bergman TL, Lavine AS (2007). Introduction to heat transfer. New Jersey: John Wiley & Sons.
88. Jang JL, Choi SUS (2007). Effects of various parameters on nanofluid thermal conductivity. Journal of Heat Transfer. 129:617-623.
89. Jang SP, Choi SUS (2007). Effects of various parameters on nanofluid thermal conductivity. ASME Journal of Heat Transfer. 129: 617-623.
90. Jaworski M (2011). Thermal performance of heat spreader for electronics cooling with incorporated phase change material. Applied Thermal Engineering. 10.1016/j.applthermaleng.2011.10.036.
91. Jellouli Y, Chouikh R, Guizani A, Belghith A (2007). Numerical study of the moving boundary problem during melting process in a rectangular cavity heated from below. American Journal of Applied Sciences. 4:251-256.
92. Jones BJ, Sun B, Krishnan S, Garimella SV (2006). Experimental and numerical investigation of melting in a cylinder. International Journal of Heat and Mass Transfer. 49:2724-2738.
93. Kaizawa A, Kamano H, Kawai A, Jozuka T, Senda T, Maruoka N, Akiyama T

(2008). Thermal and flow behaviors in heat transportation container using phase change material. Energy Conversion and Management. 49:698-706.

94. Kaygusuz K (2003). Phase change energy storage for solar heating systems. Energy Sources. 25:791-807.

95. Kaygusuz K, Ayhan T (1993). Exergy analysis of solar-assisted heat-pump systems for domestic heating. Energy. 18:1077-1085.

96. Kenisarin M (2010). High temperature phase change materials for thermal energy storage. Renewable and Sustainable Energy Reviews. 14:955-970.

97. Kenisarin M, Mahkamov K (2007). Solar energy storage using phase change materials. Renewable and Sustainable Energy Reviews. 11:1913-1965.

98. Khillarkar DB, Gong ZX, Mujumdar AS (2000). Melting of a phase change material in concentric horizontal annuli of arbitrary cross-section. Applied Thermal Engineering. 20:893-912.

99. Khodadadi JM, Hosseinizadeh SF (2007). Nanoparticle-enhanced phase change materials (NEPCM) with great potential for improved thermal energy storage. International Communications in Heat and Mass Transfer. 34:534-543.

100. Kim DJ (2010). A new thermoeconomic methodology for energy systems. Energy. 35:410-422.

101. Kim JM, Lee SG, Kim C (2008). Numerical simulations of particle migration in suspension flows: Frame-invariant formulation of curvature-induced migration. Journal of Non-Newtonian Fluid Mechanics. 150:162-176.

102. Kim S, Drzal LT (2009). High latent heat storage and high thermal conductive phase change materials using exfoliated graphite nanoplatelets. Solar Energy Materials and Solar Cells. 93:136-142.

103. Koca A, Oztop HF, Koyun T, Varol Y (2008). Energy and exergy analysis of a latent heat storage system with phase change material for solar collector. Renewable Energy. 33:567-674.

104. Kousksou T, El Rhafiki T, Arid A, Schall E, Zeraouli Y (2008). Power, efficiency, and irreversibility of latent energy systems. Journal of Thermophysics and Heat Transfer. 22:234-239.

105. Kousksou T, Jamil A, El Rhafiki T, Zeraouli Y (2010). Paraffin wax mixtures as phase change materials. Solar Energy Materials and Solar Cells. 94:2158-

2165.

106. Kousksou T, Strub F, Lasvignottes JS, Jamil A, Bedecarrats JP (2007). Second law analysis of latent thermal storage for solar system. Solar Energy Materials and Solar Cells. 91:1275-1281.

107. Krane RJ (1987). A second law analysis of the optimum design and operation of thermal energy storage systems. International Journal of Heat and Mass Transfer. 30:43-57.

108. Kravvaritis ED, Antonopoulos KA, Tzivanidis C (2010). Improvements to the measurement of the thermal properties of phase change materials. Measurement and Science technology.21: 045103 (9 pages).

109. Krieger IM (1972). Rheology of monodisperse lattices. Advances in Colloid and Interface Science. 3:111-136.

110. Krishnan S, Murthy JY, Garimella SV (2005). A two-temperature model for solid-liquid phase change in metal foams. ASME Journal of Heat Transfer. 127:995-1004.

111. Krishnan S, Murthy JY, Garimella SV (2007). Analysis of solid-liquid phase change under pulsed heating. ASME Journal of Heat Transfer. 129:395-400.

112. Kuznik F, David D, Johannes K, Roux JJ (2011). A review on phase change materials integrated in building walls. Renewable and Sustainable Energy Reviews. 15:379-391.

113. Kuznik F, Virgone J, Johannes K (2011). In-situ study of thermal comfort enhancement in a renovated building equipped with phase change material wallboard. Renewable Energy. 36:1458-1462.

114. Lacroix M (1993). Study of the heat transfer behavior of a latent heat thermal energy storage unit with a finned tube. International Journal of Heat and Mass Transfer. 36:2083-2092.

115. Lacroix M, Benmadda M (1998). Analysis of natural convection melting from a heated wall with vertically oriented fins. International Journal of Numerical Methods in Heat and Fluid Flow. 8:465-478.

116. Laing D, Bauer T, Lehmann D (2010). Development of a thermal energy storage system for parabolic through power plants with direct steam generation (2010). ASME Journal of Solar Energy Engineering. 132:021011 (8 pages).

117. Lamberg P (2003). Mathematical modeling and experimental investigation of melting and solidification in a finned phase change material storage. Doctoral Dissertation. Department of Mechanical Engineering. Helsinki University of Technology. Espoo. Finland.

118. Lamberg P, Lehtiniemi R, Henell AM (2004). Numerical and experimental investigation of melting and freezing processes in phase change material storage. International Journal of Thermal Sciences. 43:277-287.

119. Lamberg P, Siren K (2003). Analytical model for melting in a semi-infinite PCM storage with an internal fin. Heat and Mass Transfer. 39:167-76.

120. Liu Z, Sun X, Ma C (2005). Experimental investigations on the characteristics of melting processes of stearic acid in an annulus and its thermal conductivity enhancement. Energy Conversion and Management. 46:959-969.

121. Lu S, Pugh RJ, Forssberg E (2005). Dispersion of particles in liquids. Studies in Interface Science. 20:517-558.

122. MacPee D, Duncer I (2009). Thermodynamic analysis of freezing and melting processes in a bed of spherical PCM capsules. ASME Journal of Solar Energy Engineering. 131:031017 (11 Pages).

123. Malvi CS, Dixon-Hardy DW, Crook R (2011). Energy balance model of combined photovoltaic solar-thermal system incorporating phase change material. Solar Energy. 85:1440-1446.

124. Marcus Y, Minevich A, Ben-Dor L (2003). Differential drop calorimetry for the determination of enthalpy of fusion. The Journal of Chemical Thermodynamics. 35:1009-1018.

125. Marin J, Zalba B, Lazaro (2005). New installation at the University of Zaragoza (Spain) of T-history method to measure the thermal properties. 8th Workshop Annex 17. ECES. IEA.

126. Marin JM, Zalba B, Cabeza LF, Mehling H (2003). Determination of enthalpy-temperature curves of phase change materials with the temperature-history method: improvement to temperature dependent properties. Measurement and Science technology.14: 184-189.

127. Mawire A, McPherson M (2008). Experimental characterization of a thermal energy storage system using temperature and power controlled charging. Renewable Energy. 33:682-693.

128. Maxwell JC (1954). A treatise on electricity and magnetism. New York: Dover.

129. Mehling H, Hiebler S, Ziegler F (2000). Latent heat storage using a PCM-graphite composite material. *In* Proceedings of 8th International Conference on Thermal Energy Storage. Stuttgart.

130. Mesalhy O, Lafdi K, Elgafi A, Bowman K (2005). Numerical study for enhancing the thermal conductivity of phase change material (PCM) storage using high thermal conductivity porous matrix. Energy Conversion and Management. 46:847-867.

131. Mettawee EBS, Assassa GMR (2006). Experimental study of a compact PCM solar collector. Energy. 31:2958-2968.

132. Mettawee ES, Assassa GMR (2007). Thermal conductivity enhancement in a latent heat storage system. Solar Energy. 81:839-845.

133. Michels H, Pitz-Paal R (2007). Cascaded latent heat storage for parabolic trough solar power plants. Solar Energy. 81:829-837.

134. Modal S (2008). Phase change materials for smart textiles. Applied Thermal Engineering. 28: 1536-1550.

135. Murshed SMS, Leong KC, Yang C (2005). Enhanced thermal conductivity of TiO2-water based nanofluids. International Journal of Thermal Sciences. 44:367-373.

136. Nakaso K, Teshima H, Yoshimura A, Nogami S, Hamada Y, Fukai J (2008). Extension of heat transfer area using carbon fiber cloths in latent heat thermal energy storage tanks. Chemical Engineering and Processing: Process Intensification. 47:879-885.

137. Ng KW, Gong ZX, Mujumdar AS (1998). Heat transfer in free convection-dominated melting of a phase change material in a horizontal annulus. International Communications in Heat and Mass Transfer. 25:631-640.

138. Ozilgen M (2011). Transport phenomena models. *In* Handbook of food process modeling and statistical quality control, Florida:CRC Press. p 39-185.

139. Ozisik MN (1994). Finite difference methods in heat transfer. *In* Phase change problem, Florida:CRC Press. p 275-306.

140. Ozonur Y, Mazman M, Paksoy HO, Evliya H (2006). Microencapsulation of coco fatty acid mixture for thermal energy storage with phase change material.

International Journal of Energy Research. 30:741-749.

141. Ozturk HH (2005). Experimental evaluation of energy and exergy efficiency of a seasonal latent heat storage system for green house heating. Energy Conversion and Management. 46:1523-1542.

142. Pandiyarajan V, Chinna Pandian M, Malan E, Velraj R, Seeniraj RV (2011). Experimental investigation on heat recovery from diesel engine exhaust using finned shell and tube heat exchanger and thermal storage system. Applied Energy. 88:77-87.

143. Parameshwaran R, Harikrishnan S, Kalaiselvam S (2010). Energy efficient PCM-based variable air volume air conditioning system for modern buildings. Energy and Buildings. 42:1353-1360.

144. Parang M, Crocker DS, Haynes BD (1990). Perturbation solution for spherical and cylindrical solidification by combined convective and radiative cooling. International Journal of Heat and Fluid Flow. 11:142-148.

145. Peck JH, Kim JJ, Kang C, Hong H (2006). A study of accurate latent heat measurement for a PCM with a low melting temperature using T-history method. International Journal of Refrigeration. 29: 1225-1232.

146. Phillips RJ, Armstrong RC, Brown RA, Graham AL, Abbott ALG (1992). A constitutive equation for concentrated suspensions that accounts for shear-induced particle migration. Physics of Fluids. 4:30-40.

147. Pincemin S, Olives R, Py X, Christ M (2008a). Highly conductive composites made of phase change materials and graphite for thermal storage. Solar Energy Materials and Solar Cells. 92:603-613.

148. Pincemin S, Py X, Olives R, Christ M, Oettinger O (2008b). Elaboration of conductive thermal storage composites made of phase change materials and graphite for solar power plant. ASME Journal of Solar Energy Engineering. 130:11005(5 pages) .

149. Pinelli M, Casano G, Piva S (2000). Solid-liquid phase change heat transfer in a vertical cylinder heated from above. International Journal of Heat and Technology. 18:61-67.

150. Pinelli M, Piva S (2003). Solid/liquid phase change in presence of natural convection: a thermal energy storage case study. ASME Journal of Energy Resources Technology. 125:190-197.

151. Pokhrel R, Gonzalez JE, Hight T, Adalsteinsson T (2010). Analysis and design of a paraffin/graphite composite PCM integrated in a thermal storage unit. ASME Journal of Solar Energy Engineering. 132:041006 (8 pages).
152. Rady MA, Arquis E, Bot CL (2010). Characterization of granular phase changing composites for thermal energy storage using T-history method. International Journal of Energy Research. 34: 333-344.
153. Reddy KS (2007). Thermal modeling of PCM-based solar integrated collector storage water heating system. ASME Journal of Solar Energy Engineering. 129:458-464.
154. Regin AF, Solanki SC, Saini JS (2006). Latent heat thermal storage using cylindrical capsule: numerical and experimental investigations. Renewable Energy. 31:2025-2041.
155. Rosen MA (1992). Appropriate thermodynamic performance measures for closed systems for thermal energy storage. ASME Journal of Solar Energy Engineering. 114:100-105.
156. Rosen MA (2001). The exergy of stratified thermal energy storages. Solar Energy. 71:173-185.
157. Rosen MA, Dincer I (2003). Exergy methods for assessing and comparing thermal storage systems. International Journal of Energy Research. 27:415-430.
158. Rosen MA, Pedinelli N, Dincer I (1999). Energy and exergy analyses of cold thermal storage systems. International Journal Energy Research. 23:1029-1038.
159. Salaun F, Devaux E, Bourbigot S, Rumeau P (2010). Development of phase change materials in clothing part I: Formulation of microencapsulated phase change. Textile Research Journal. 80:195-205.
160. Sanchez P, Sanchez-Fernandez MV, Romero A, Rodriguez JF, Sanchez-Silva L (2010). Development of thermo-regulating textiles using paraffin wax microcapsules. Thermochimicia Acta. 498:16-21.
161. Sari A, Karaipekli A (2007). Thermal conductivity and latent heat thermal energy storage characteristics of paraffin/expanded graphite composite as phase change material. Applied Thermal Engineering. 27:1271-1277.
162. Sari A, Kaygusuz K (2000). Energy and exergy calculations of latent heat

energy storage systems. Energy Sources. 22:117-126.

163. Sari A, Kaygusuz K (2004). First and second laws analyses of a closed latent heat thermal energy storage system. Chinese Journal of Chemical Engineering. 12:290-293.

164. Schossig P, Henning HM, Gschwander S, Haussmann T (2005). Micro-encapsulated phase change materials integrated into construction materials. Solar Energy Materials and Solar Cells. 89:297-306.

165. Schramm LL (2005). Emulsions, foams and suspensions: fundamentals and applications. Weinbeim: Wiley-VCH.

166. Schramm LL, Stasiuk EN, Marongoni DG (2003). Surfactants and their applications. Annual Reports on the Progress of Chemistry; Section C: Physical Chemistry. 99:3-48.

167. Seeniraj RV, Narasimhan NL (2008). Performance enhancement of a solar dynamic LHTS module having both fins and multiple PCMs. Solar Energy. 82:535-542.

168. Seeniraj RV, Velraj R, Narasimhan NL (2002). Heat transfer enhancement study of a LHTS unit containing dispersed high conductivity particles. ASME Journal of Solar Energy Engineering. 124:243-249.

169. Seeniraj RV, Velraj R, Narasimhan NL (2002). Thermal analysis of a finned-tube LHTS module for a solar dynamic power system. Heat and Mass Transfer. 38:409-417.

170. Sharma A, Tyagi VV, Chen CR, Buddhi D (2009). Review on thermal energy storage with phase change materials and applications. Renewable and Sustainable Energy Reviews. 13:318-345.

171. Sharma SD, Iwata T, Kitano H, Sagara K (2005). Thermal performance of a solar cooker based on an evacuated tube solar collector with a PCM storage unit. Solar Energy. 78:416-426.

172. Sharma SD, Sagara K (2005). Latent heat storage materials and systems: a review. International Journal of Green Energy. 2:1-56.

173. Shatikian V, Ziskind G, Letan R (2005). Numerical investigation of a PCM-based heat sink with internal fins. International Journal of Heat and Mass Transfer. 48:3689-3706.

174. Shatikian V, Ziskind G, Letan R (2008). Numerical investigation of a PCM-

based heat sink with internal fins: constant heat flux. International Journal of Heat and Mass Transfer. 51:1488-1493.

175. Shiina Y, Inagaki T (2005). Study on the efficiency of effective thermal conductivities on melting characteristics of latent heat storage capsules. International Journal of Heat and Mass Transfer. 48**:**373-383.

176. Shmueli H, Ziskind G, Letan R (2010). Melting in a vertical cylindrical tube: Numerical investigation and comparison with experiments. International Journal of Heat and Mass Transfer. 53:4082-4091.

177. Siegel (1977). Solidification of low conductivity material containing dispersed high conductivity particles. International Journal of Heat and Mass Transfer. 20:1087-1089.

178. Smith MC, Farid MM, Easteal AJ (2006). Microencapsulated phase change materials for thermal energy storage applications. *In* Proceedings of IIR/IRHACE Conference. Auckland.

179. Song YW (1981). On the solution of heat conduction in a cylindrical body undergoing solidification by the method of singular perturbation. Journal of Engineering Thermophysics. 2:359-365. (In Chinese and Abstract in English).

180. Stritih U (2004). An experimental study of enhanced heat transfer in rectangular PCM storage. International Journal of Heat and Mass Transfer. 47:2841-2847.

181. Strub F, Bedecarrats JP (1999). Numerical second law analysis of a refrigeration phase-change storage. International Journal of Thermodynamics. 2:133-138.

182. Strub F, Bedecarrats JP (2000). Thermodynamics of phase-change energy storage: the effects of undercooling on entropy generation during solidification. International Journal of Thermodynamics. 3:35-42.

183. Sun D, Annapragada SR, Garimella SV (2009). Experimental and numerical study of melting of particle-laden materials. International Journal of Heat and Mass Transfer. 52:2966-2978.

184. Tadros TF (1991). Some industrial applications of surfactants. Lecture Notes in Physics. 386:349-360.

185. Tadros TF (2005). Applied surfactants: principles and applications. Weinbeim: Wiley-VCH.

186. Tan FL (2008). Constrained and unconstrained melting inside a sphere. International Communications in Heat and Mass Transfer. 35:466-475.

187. Trp A (2005). An experimental and numerical investigation of heat transfer during technical grade paraffin melting and solidification in a shell and tube latent heat thermal energy storage unit. Solar Energy. 79:648-660.

188. Tyagi VV, Buddhi D (2007). PCM thermal storage in buildings: a state of art. Renewable and Sustainable Energy Reviews. 11:1146-1166.

189. Vaisman L, Wagner HD, Margom G (2006). The role of surfactants in dispersion of carbon nanotubes. Advances in Colloid and Interface Science. 128-130:37-46.

190. Vand V (1945). Theory of viscosity of concentrated suspensions. Nature. 155:364-365.

191. Vasiliev LL, Burak VS, Kulakov AG, Mishkinis DA, Bohan PV (2000). Latent heat storage modules for preheating internal combustion engines: application to a bus petrol engine. Applied Thermal Engineering. 20:913-923.

192. Velraj R, Seeniraj RV, Hafner B, Faber C, Schwarzer K (1997). Experimental analysis and numerical modeling of inward solidification on a finned vertical tube for a latent heat storage unit. Solar Energy. 60:281-290.

193. Velraj R, Seeniraj RV, Hafner B, Faber C, Schwarzer K (1999). Heat transfer enhancement in a latent heat storage system. Solar Energy. 65:171-180.

194. Venkataramayya A, Ramesh KN (1998). Exergy analysis of latent heat storage systems with sensible heating and subcooling of PCM. International Journal of Energy Research. 22:411-426.

195. Verma P, Varun, Singal SK (2008). Review of mathematical modeling on latent heat thermal energy storage systems using phase-change material. Renewable and Sustainable Energy Reviews. 12:999-1031.

196. Versteeg HK, Malalasekera (1995). An introduction to computational fluid dynamics: the finite volume method. London: Pearson Education.

197. Voller VR, Swaminathan CR (1991). Generalized source-based method for solidification phase change. Numerical Heat Transfer Part B. 19**:**175-189.

198. Wang J, Ouyang Y, Chen G (2001). Experimental study on charging processes of a cylindrical heat storage capsule employing multiple-phase-change materials. International Journal of Energy Research. 25:439-447.

199. Wang N, Yang S, Zhu D, Ju X (2010). Preparation and heat transfer behavior of paraffin based composites containing nano-copper particles. *In* Proceedings of 7th International Conference on Multiphase Flow. USA.

200. Wang W, Yang X, Fang Y, Ding J, Yan J (2009). Enhanced thermal conductivity and thermal performance of form-stable composite phase change materials by using β –Aluminum Nitride. Applied Energy. 86:1196-2000.

201. Wang Y, Yang Y (2011). Three-dimensional transient cooling simulations of a portable electronic device using PCM (phase change materials) in multi-fin heat sink. Energy. 36:5214-5224.

202. Watanabe T, Kanzawa A (1995). Second law optimization of a latent heat storage system with PCMs having different melting points. Heat Recovery Systems and CHP. 15:641-653.

203. Xia L, Zhang P, Wang RZ (2010). Numerical heat transfer analysis of the packed bed latent heat storage system based on an effective packed bed model. Energy. 35:2022-2032.

204. Xue L, Keblinski P, Phillpot SR, Choi SUS, Eastman JA (2004). Effect of liquid layering at the liquid-solid interface on thermal transport. International Journal of Heat and Mass Transfer. 47:4277-4284.

205. Yang Y, Wang Y (2012). Numerical simulation of three-dimensional transient cooling application on a portable electronic device using phase change material. International Journal of Thermal Sciences. 51:155-162.

206. Yin H, Gao X, Ding J, Zhang Z (2008). Experimental research on heat transfer mechanism of heat sink with composite phase change materials. Energy Conversion and Management. 49:1740-1746.

207. Yingqiu Z, Yinping Z, Yi J, Yanbing K (1999). Thermal storage and heat transfer in phase change material outside a circular tube with axial variation of the heat transfer fluid temperature. International Journal of Solar Energy Engineering. 121:145-149.

208. Yinping Z, Yi J, Yi J (1999). A simple method, the T-history method, of determining the heat of fusion, specific heat and thermal conductivity of phase-change materials. Measurement and Science Technology.10: 201-205.

209. Zalba B, Marin JM, Cabeza LF, Mehling H (2003). Review on thermal energy storage with phase change: materials, heat transfer analysis and applications.

Applied Thermal Engineering. 23:251-283.

210. Zeng JL, Sun LX, Xu F, Tan ZC, Zhang ZH, Zhang J, Zhang T (2007). Study of a PCM based energy storage system containing Ag nanoparticles. Journal of Thermal Analysis and Calorimetry. 87:369-373.

211. Zhang Y, Chen Z, Wang Q, Wu Q (1993). Melting in an enclosure with discrete heating at a constant rate. Experimental Thermal and Fluid Science. 6:196-201.

212. Zhang Y, Faghri A (1996). Heat transfer enhancement in latent heat thermal energy storage system by using an external radial finned tube. Journal of Enhanced Heat Transfer. 3:119-127.

213. Zhong Y, Guo Q, Zi S, Shi J, Liu L (2010). Heat transfer enhancement of paraffin wax using graphite foam for thermal energy storage. Solar Energy Materials and Solar Cells. 94:1011-1014.

214. Zubair SM, Al-Naglah MA (1999). Thermoeconomic optimization of a sensible heat thermal storage system: a complete cycle. ASME Journal of Energy Resources Technology. 121:286-294.

Appendix I: Domination of conduction / convection heat transfer during phase change processes

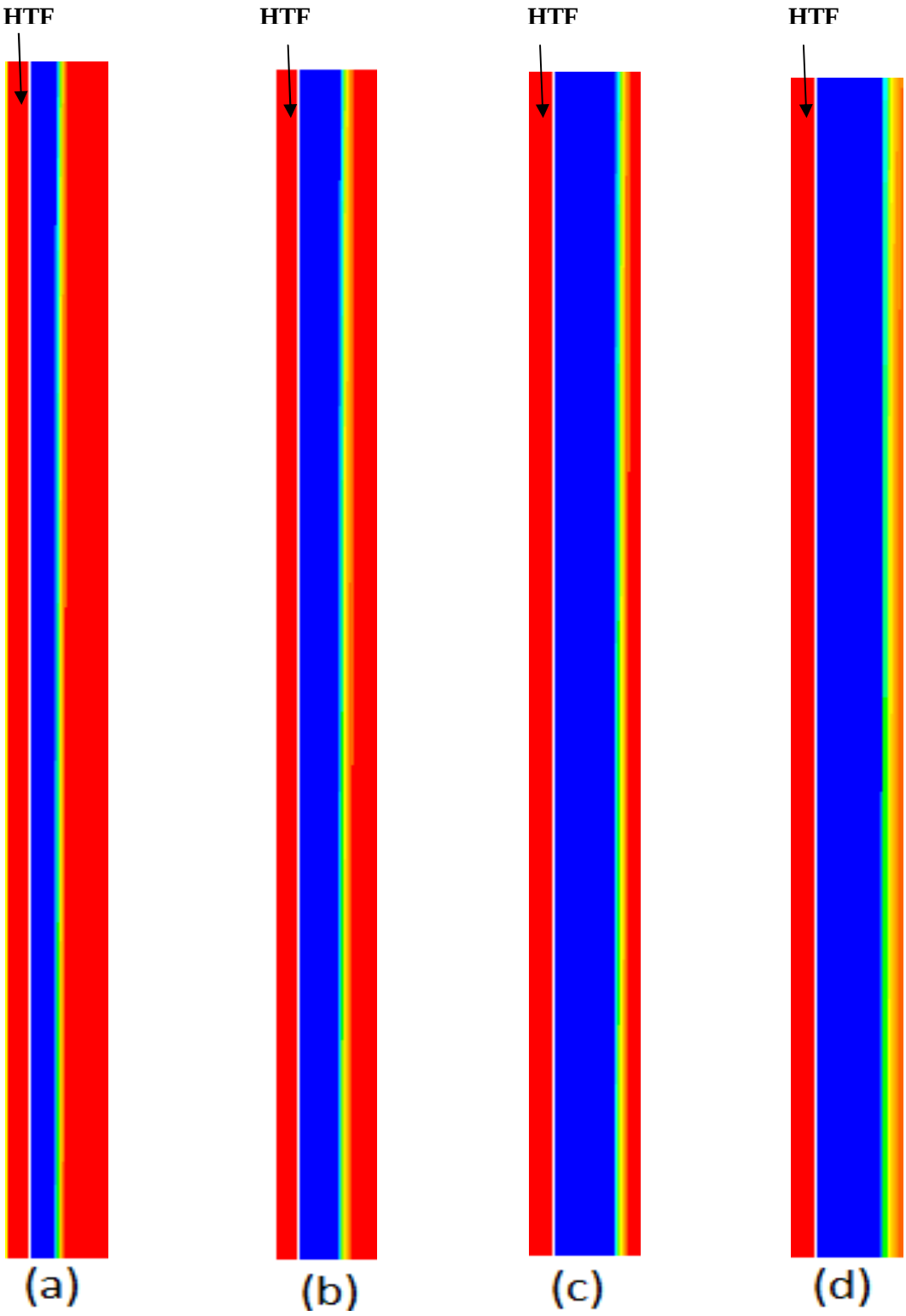

Figure A1 Interface locations during solidification of hydrated salt –nano particles composites (e =0.05) (a) at 1 h (b) at 2 h (c) at 3 h (d) at 4 h

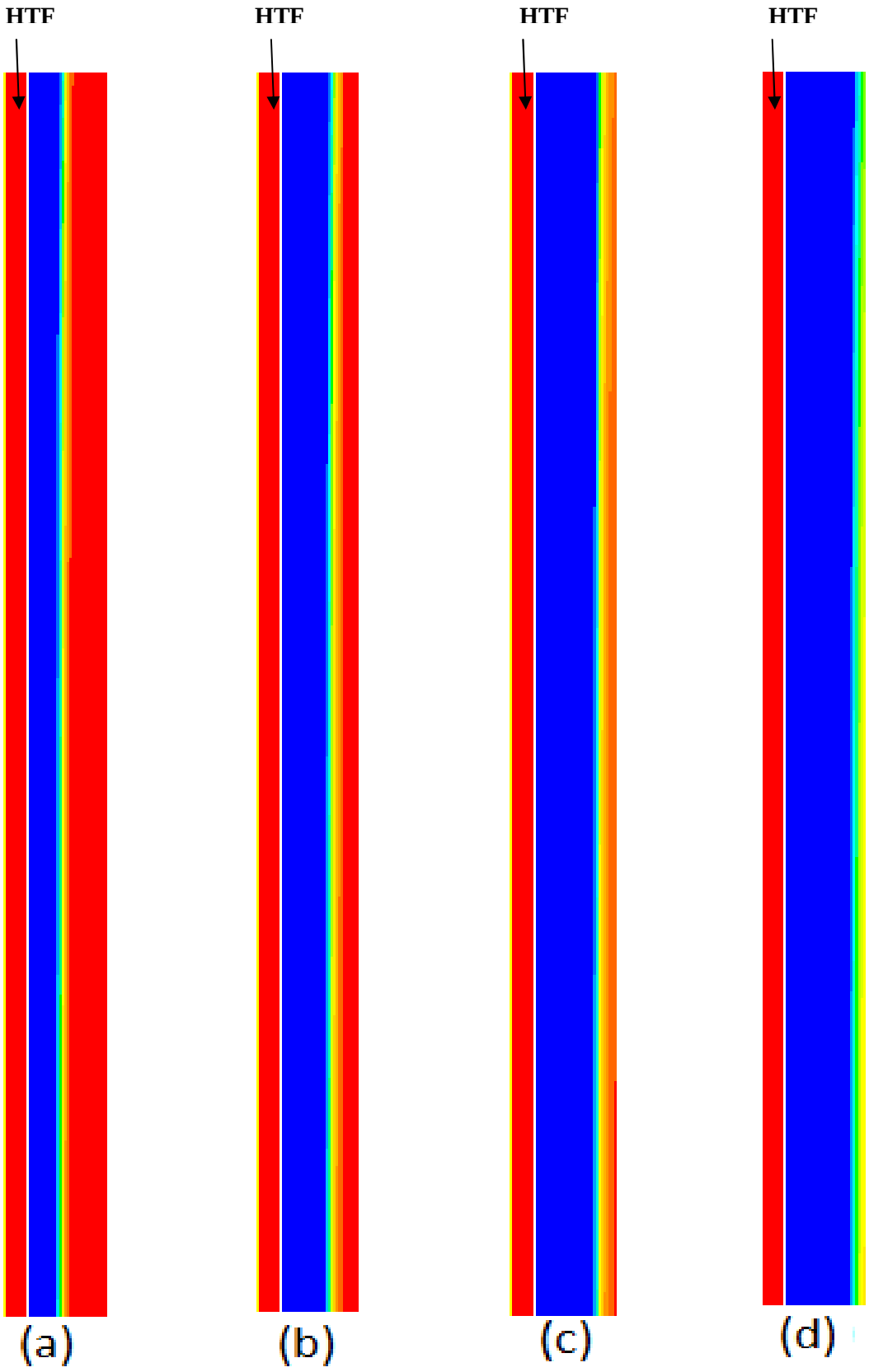

Figure A2 Interface locations during solidification of paraffin wax –nano particles composites (*e* =0.2) (a) at 1 h (b) at 2 h (c) at 3 h (d) at 4 h

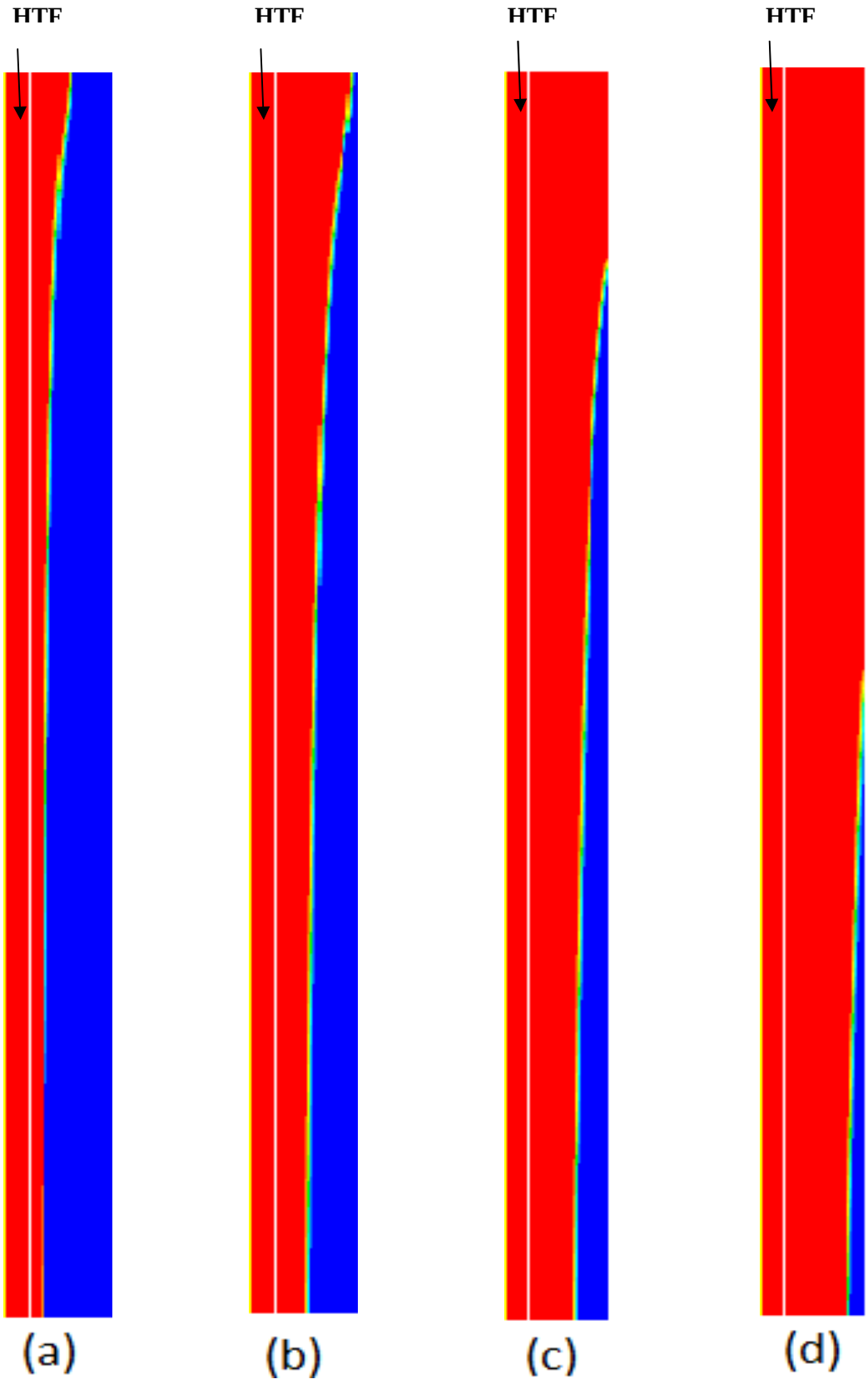

Figure A3 Interface locations during melting of paraffin wax –nano particles composites (*e* =0.05) (a) at 30 min (b) at 60 min (c) at 90 min (d) at 120 min

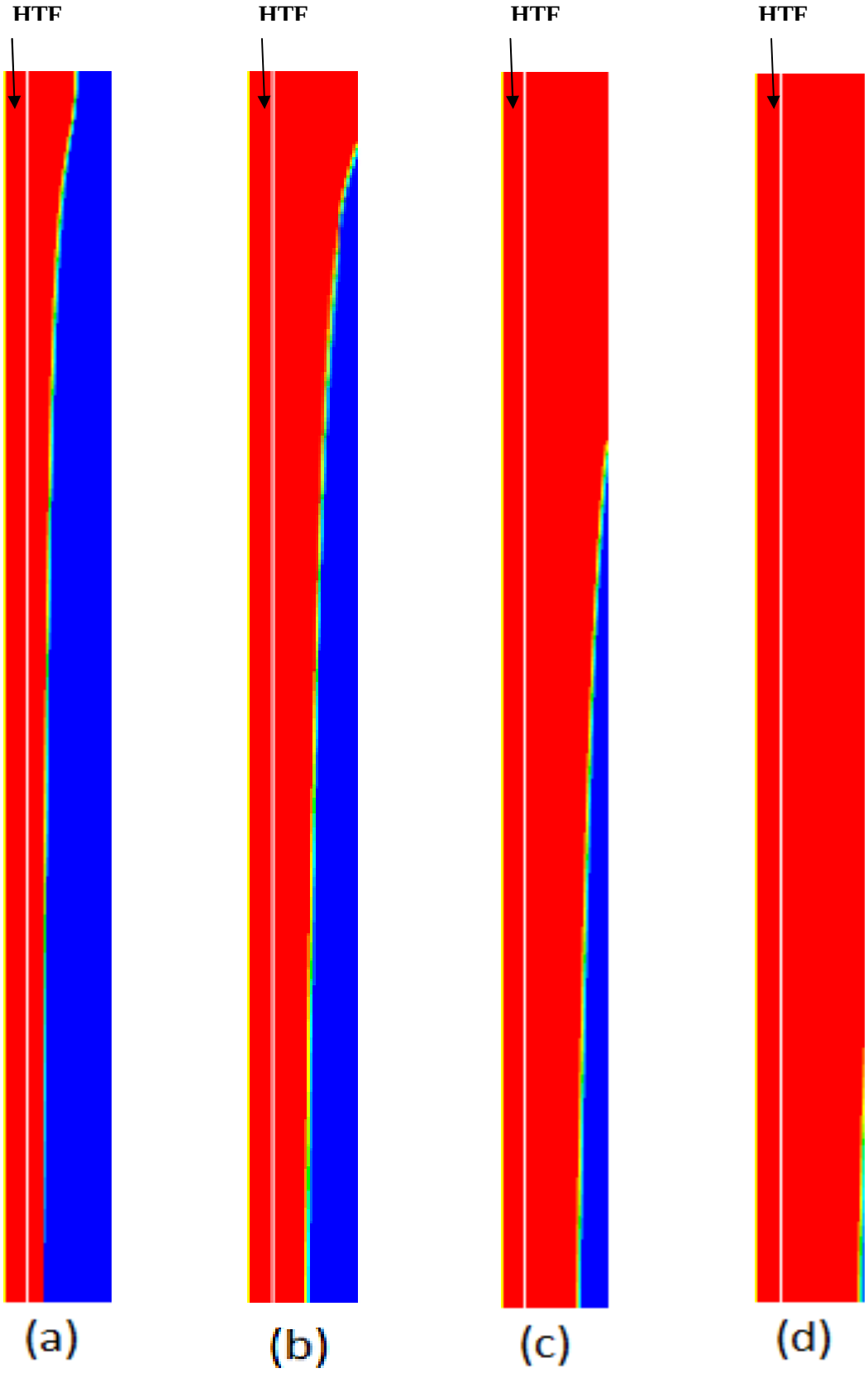

Figure A4 Interface locations during melting of hydrated salt –nano particles composites (e =0.1) (a) at 30 min (b) at 60 min (c) at 90 min (d) at 120 min

Appendix II: Experimental set ups

Figure A5 Photographic view of experimental apparatus of *T-History* measurement

Figure A6 Photographic view of experimental apparatus for melting and solidification of PCM-micro particles composites

Appendix III: Sample UDF and UDS

UDF used to define thermal conductivity of paraffin wax composites of particle fraction 0.2

```
#include "udf.h"

 /* Thermal conductivity - Paraffin wax-nano composites (e=0.2)  */

#define e  0.2

DEFINE_PROPERTY(cell_thermalconductivity, cell, thread)
{
 real ksolid = 0.2*((400.+(2.*0.2)-2.*e*(0.2-400.))/(400.+(2.*0.2)-e*(0.2-400.)));
 real rho = C_R(c,t);
 real cp = C_CP(c,t);
 real mu = C_MU_L(c,t);
 real kliquid = 0.109*((400.+(2.*0.109)-2.*e*(0.109-400.))/(400.+(2.*0.109)-
                e*(0.109-400.)));
 real Ra = (power(rho,2)*cp*9.81*0.000815*(350.-332))/mu*kliquid;
 real ktc_therm;
 real temp = C_T(cell, thread);

 if (temp >= 332)
   ktc_therm = kliquid*0.18*power(Ra,0.25);
 else if (temp <= 328)
   ktc_therm = ksolid;
 else
   ktc_therm = 0.99999*ksolid;

   return ktc_therm;
}
```

UDS used to execute particle concentration equation

```
/* Particle concentration*/
#include "udf.h"

enum
{
  pc,
  stg,
  N_REQUIRED_UDS
};

/* Viscosity as a function of particle concentration-paraffin wax*/

DEFINE_PROPERTY(cell_viscosity, cell, thread)

#define mu_pure          0.0273
{
  real mu_lam;
  real temp = C_T(cell, thread);
  if (temp > 332.)
    mu_lam = mu_pure*power(1-(C_UDSI(c,t,pc)/0.68),-1.82);
  else
    mu_lam = 1.;
  return mu_lam;
}
/* Calculation of gradient of strain rate */

DEFINE_ADJUST(pc_adjust, domain)
{
  /* to make sure  enough uds*/
  if (n_uds < N_REQUIRED_UDS)
    Internal_Error("not enough user-defined scalars allocated");
}
```

```
DEFINE_ADJUST(adjust_fcn, d)
{
 Thread *t;
 cell_t c;

 /* Do nothing if gradient isn't allocated yet. */
 if (! Data_Valid_P())
  return;

 thread_loop_c (t,d)
  {
  if (FLUID_THREAD_P(t))
    {
     begin_c_loop_all (c,t)
        {
         C_UDSI(c,t,stg) +=
                  C_STRAIN_RATE_MAG(c,t);
        }
     end_c_loop_all (c,t)
    }
  }
}
DEFINE_SOURCE(pc_source, c, t, dS, eqn)
{
 dS[eqn] = 2.0*0.41*power(0.00025,2)*C_UDSI(c,t,pc)*C_UDSI_G(c,t,stg);
 return 0.41*power(0.00025,2)*power(C_UDSI(c,t,pc),2)*C_UDSI_G(c,t,stg);
}

DEFINE_DIFFUSIVITY(pc_diffusivity, c, t, i)
{
return
power(0.00025,2)*C_UDSI(c,t,pc)*C_STRAIN_RATE_MAG(c,t)*(0.41+(0.62*C_U
DSI(c,t,pc)*2.6765*mu_pure*(mu_pure-(mu_pure*C_UDSI(c,t,pc)/0.68))));
}
```

Appendix IV: Melting results of hydrated salt based micro particles composites

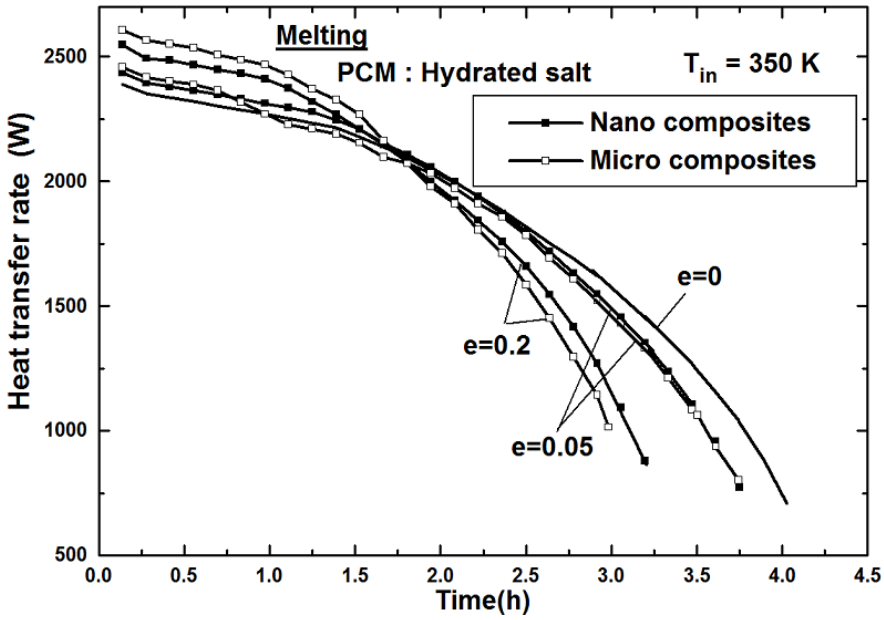

Figure A7 Comparison of effects of nano and micro particles on instantaneous heat transfer rate during melting of hydrates salt micro composites

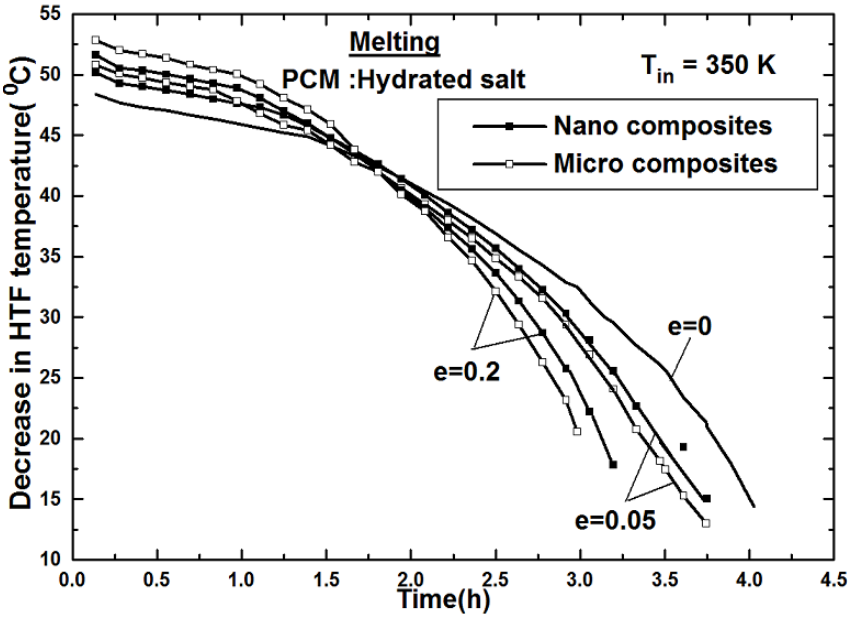

Figure A8 Comparison of effects of nano and micro particles on HTF out let temperature during melting of hydrates salt micro composites

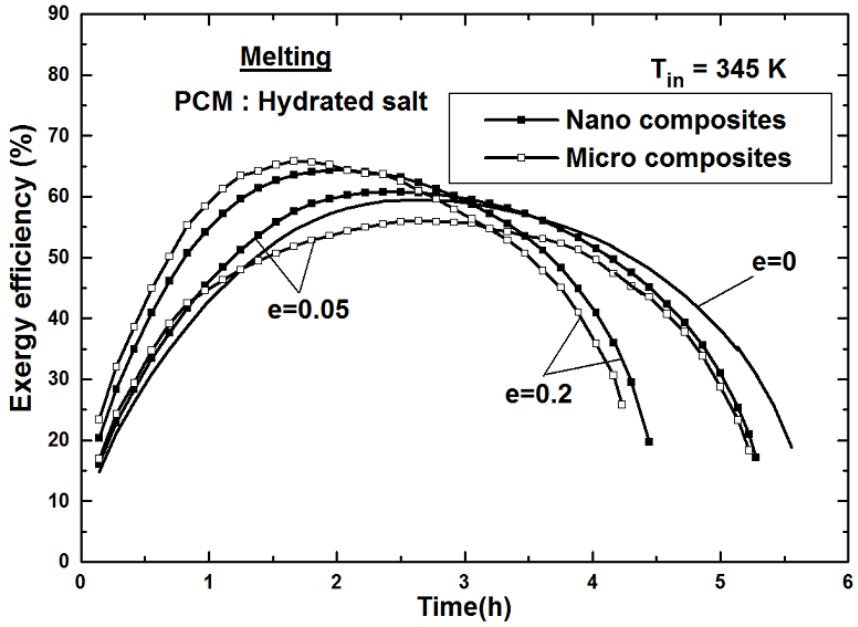

Figure A9 Comparison of effects of nano and micro particles on exergy efficiency during melting of hydrates salt micro composites

Appendix V: Behavior of micro particles composites under the variation of Re and HTF inlet temperature

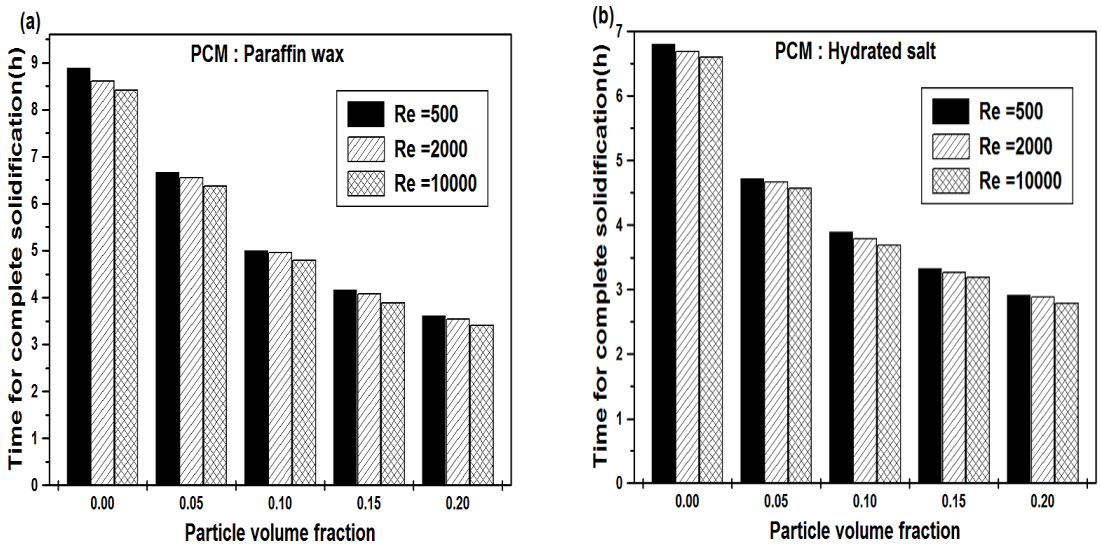

Figure A10 Influence of Re of HTF flow on time for complete solidification of micro particles composites (a) Paraffin wax as PCM (b) Hydrated salt as PCM

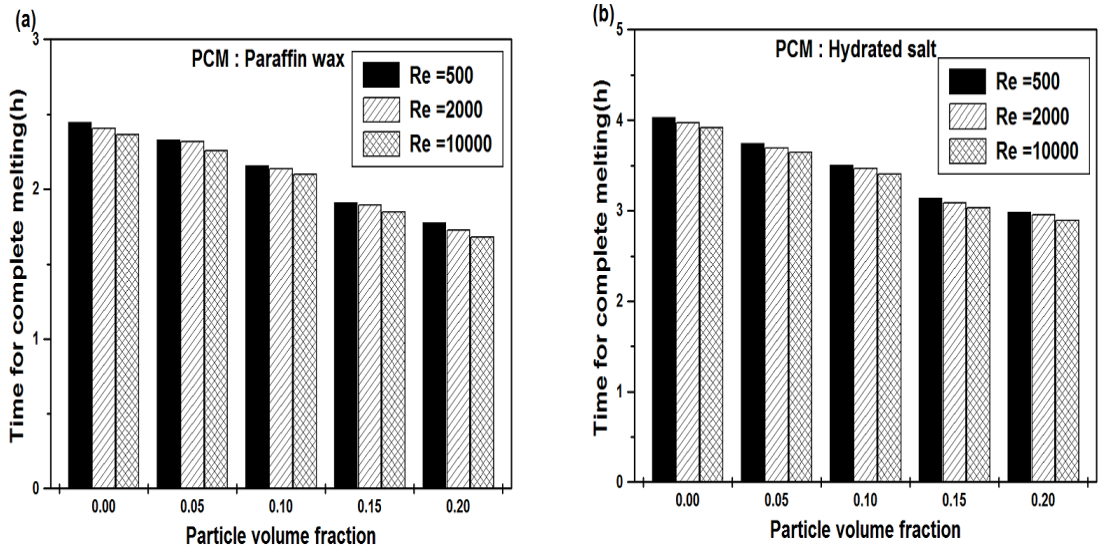

Figure A11 Influence of Re of HTF flow on time for complete melting of micro particles composites (a) Paraffin wax as PCM (b) Hydrated salt as PCM

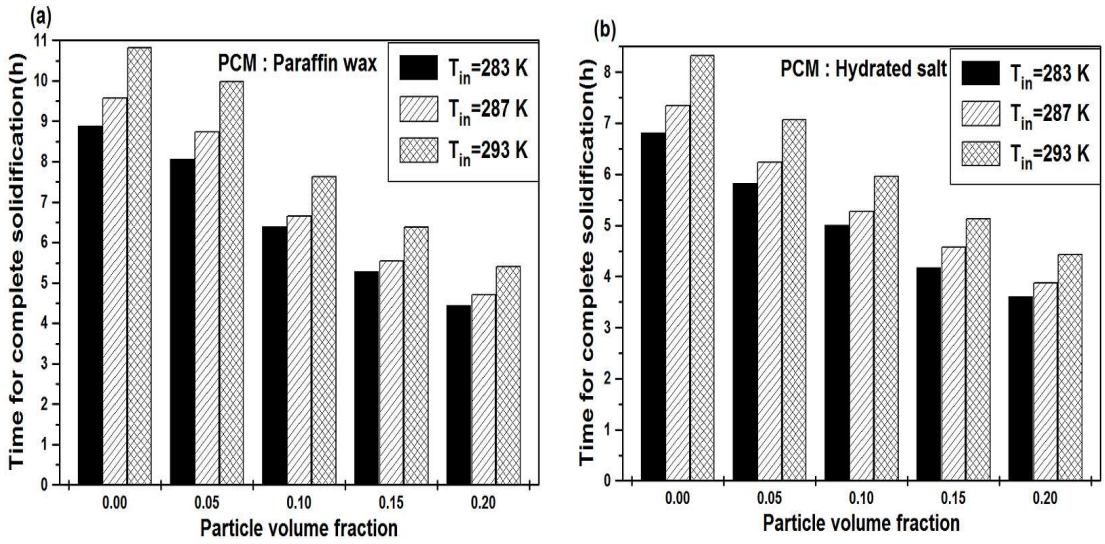

Figure A12 Effect of HTF inlet temperature on complete solidification time of micro particles composites (a) paraffin wax as PCM (b) hydrated salt as PCM

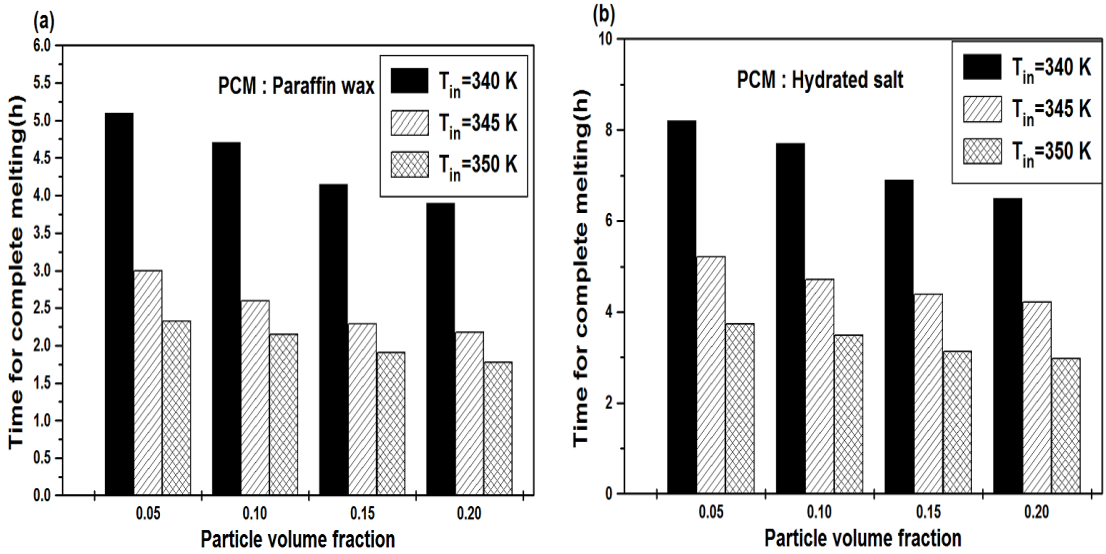

Figure A13 Effect of HTF inlet temperature on complete melting time of micro particles composites (a) paraffin wax as PCM (b) hydrated salt as PCM

List of publications and presentations

I: International Journals

1. Jegadheeswaran S, Pohekar SD (2009). Performance enhancement of latent heat thermal storage system: a review. Renewable and Sustainable Energy Reviews. 13: 2225-2244.
2. Jegadheeswaran S, Pohekar SD (2010). Energy and exergy analysis of particle dispersed latent heat storage system. International Journal of Energy and Environment.1: 445-458.
3. Jegadheeswaran S, Pohekar SD (2010). Exergy analysis of particle dispersed latent heat thermal storage system for solar water heaters. Journal of Renewable and Sustainable Energy. 2: 023105-1-17.
4. Jegadheeswaran S, Pohekar SD, Kousksou T (2010). Exergy based performance evaluation of latent heat thermal storage system: A review. Renewable and Sustainable Energy Reviews. 14: 2580-2595.
5. El Rhafiki T, Kousksou T, Jamil A, Jegadheeswaran S, Pohekar SD, Zeraouli Y (2011). Crystallization of pcms inside emulsion: supercooling phenomenon. Solar Energy Materials & Solar cells. 95: 2588-2597.
6. Jegadheeswaran S, Pohekar SD, Kousksou T (2011). Performance enhancement of solar latentheat thermal storage system with particle dispersion — an exergy approach. Clean-Soil, Air, Water. 39: 964-971.
7. Jegadheeswaran S, Pohekar SD, Kousksou T (2012). Conductivity particles dispersed organic and inorganic phase change materials for solar energy storage– an exergy based comparative evaluation. Energy Procedia. 14: 643-648.
8. Jegadheeswaran S, Pohekar SD, Kousksou T. Investigations on thermal storage system containing micro size conductivity particles dispersed phase change material. International Journal of Thermal Sciences (Communicated, under review).

II: National Journals

1. Jegadheeswaran S, Pohekar SD (2008). Latent heat thermal energy storage for solar water heaters. Bulletin of Marine Science and Technology. 4: 28-33.
2. Jegadheeswaran S, Pohekar SD (2009). Numerical investigation on heat transfer enhancement in latent heat thermal storage system. Bulletin of Marine Science and Technology. 5: 1-5.
3. Rajvanshi U, Singh AK, Jegadheeswaran S, Pohekar SD (2010). Latent heat thermal storage system for fuel oil pre-heating. Bulletin of Marine Science and Technology. 6: 60-65.

III: Conference Proceedings

1. Jegadheeswaran S, Pohekar SD (2008). Numerical studies on performance enhancement of latent heat thermal energy storage systems. *In* Proceedings of 2nd National Conference on Advances in Energy Conversion Technologies. Manipal.
2. Jegadheeswaran S, Pohekar SD (2009). Numerical Investigations on the Performance Enhancement of a Latent Heat Thermal Storage Unit with Particle Laden Phase Change Material. *In* Proceedings of 6th International Conference on Computational Heat and Mass Transfer. Ghongzhou.
3. Jegadheeswaran S, Pohekar SD, Anbudurai K (2010). Performance Enhancement of Latent Heat Thermal Storage System through High Conductivity Particles. *In* Proceedings of International Conference on Emerging Trends in Energy and Environment. Chennai.

1. Brief Biography of the Candidate

S Jegadheeswaran obtained bachelor degree in Automobile engineering from Institute of Road and Transport Technology, Erode of Bharathiyar University, Coimbatore in 1993. He received his master degree in Thermal engineering from Karunya Institute of Technology, Coimbatore of Anna University, Chennai in 2004. He took up the research in heat transfer characteristics of latent heat thermal storage systems at Birla Institute of Technology and Science, Pilani (Rajasthan) from 2008. His primary research interest focuses on performance enhancement and exergy analysis of latent heat thermal storage systems. His research contributions are also extended to computational heat transfer and fluid flow in general and numerical modeling of free surface flow around ship in particular. His research contributions have been recognized in the form of publications in international and national journals. Apart from journal publications, he has presented several papers at international conferences held at various parts of India as well as China and Thailand.

He has been in teaching for more than sixteen years and currently, is associated with Tolani Maritime Institute, Pune. Besides teaching for undergraduate students, he is also involved in Staff up-gradation programme of Bharat Forge Ltd, Pune and Eaton Corporation Ltd, Pune in collaboration with BITS, Pilani. His contribution to academic field is extended to presentation of seminars, lectures, short courses, workshops etc in energy storage and exergy analysis of thermal systems.

2. Brief Biography of the Supervisor

Dr. Sanjay Pohekar graduated in Mechanical Engineering in 1989, did Master of Technology in Energy Management in 1994 and MBA (HR) in 2000. He obtained his doctorate degree in Mechanical Engineering in 2004 from Birla Institute of Technology and Science Pilani, India. He has 20 years of experience in teaching and industry. He has taught in Amravati, Nagpur and Pune University affiliated institutions for 5 years. He has also taught in various capacities at BITS, Pilani for 8 years and Tolani Maritime Institute, Pune (Off Campus Center for BITS, Pilani) for 5 years. He was also looking after the entire Ph.D programme of BITS, Pilani. He has taught in various continuing education programmes of National Thermal Power Corporation, Bharat Forge, Reliance Energy, Eaton Corporation etc.

He has conducted management development programmes for the officers of Ministry of New and Renewable Energy Sources, India and process steam engineers. He has also convened two national level conferences on energy management at Pilani and Pune. He has organized workshops on passive solar architecture, patent awareness and convergence of technologies.He has 15 international journal publications to his credit in addition to several conference proceedings. He was on reviewer board of Elsevier Science, Inder-science, Interscience, IACSIT, Desalination Society USA and Wiley-VCH, UK. He was guest editor for Energy and Fuel Users Journal in 2004 and is editor for Bulletin of Marine Science and Technology. He was referee for scientific awards of Turkish and Japanese governments.

He has guided two National Renewable Energy fellowships and is guiding four Ph. D candidates in the areas of energy engineering, heat transfer and computational fluid dynamics. He was examiner for Ph. D. theses in Amravati and Manipal University and BITS, Pilani for Mechanical, Chemical and Electrical Engineering areas. He is member of Indian Society of Tech Education, Solar Energy Society of India, Fellow of Institution of Engineers (India), International Society on Multiple Criteria Decision Making, Senior Member of International Association of Computer Science and Information Technology and Fellow Maritime Research Network, Singapore. Dr. Pohekar is presently Professor of Mech. Engineering at Tolani Maritime Institute, Induri, Pune.